University of Nottingham
UK | CHINA | MALAYSIA

Novel Power Electronic Systems with Embedded Energy Storage and Renewable Energy Generation

Shangkun Li (MSc)

Submitted to the University of Nottingham for the degree of Doctor of Philosophy,

June 2024

Abstract

To advance the "net zero" target by 2050, residential solar energy applications have gained significant traction. This study aims to design a cost-effective residential PV embedded energy storage system. Battery energy storage and thermal energy storage are prominent technologies in residential sectors. Given the widespread use of hot water tanks in British homes, storing excess PV energy in these tanks appears economically favourable.

Additionally, differential electricity tariffs, like Economy-7, offer potential savings by shifting energy usage to off-peak hours or storing energy for peak demand periods. Optimizing the design of the PV utilization system involves avoiding oversizing components by leveraging historical data or models. This approach ensures efficient PV utilization, cost-effectiveness, and supports the transition to net-zero energy goals.

Additionally, conventional electric water heaters using relays or TRIACs struggle to accurately utilize excess solar power, often resulting in unnecessary power import or export. With the increasing adoption of power electronic appliances in households, which employ diode bridge front ends, concerns about grid power quality, such as grid harmonics, arise. Therefore, this thesis proposes a novel power electronic water heater to precisely consume excess PV energy and mitigate grid harmonics caused by household non-linear loads. This approach is validated through both simulation and experimentation. Furthermore, the performance of the PV-battery-power electronic water heater system is evaluated in the experimental setup.

Acknowledgement

"Why do I do the PhD?" This was a difficult question for me to answer four years ago when I was nearing the end of my master's course. Initially, the answer seemed simple: it was an opportunity to work in a field I was interested in. Now, I realize that the process of earning a PhD has significantly enhanced my ability to overcome obstacles, both in life and work, especially in unfamiliar environments.

During my PhD research, I was constantly reminded of the gap between theory and practical application. While something might perform perfectly in a computer simulation, the results can often be quite disappointing in practice, which has frequently driven me crazy and annoyed me. This experience has taught me valuable lessons about the realities of translating theoretical knowledge into practical solutions.

I deeply appreciate both of my supervisors, Dr. Christian Klumpner and Dr. Rishad Ahmed. With their guidance and immense knowledge, I successfully developed my research capabilities in the field of power electronics from an almost zero level. Additionally, I extend my gratitude to my friends and colleagues in the Power Electronics, Machines, and Control group (PEMC). Without their help, it would be difficult for me to construct the experimental setup and complete my practical work.

Lastly, I would like to thank my family for their continuous support, both financially and emotionally, through their encouragement, consolation, and blessings. Special thanks to my girlfriend Jiaing, who has been by my side with

a positive attitude, helping me overcome all the difficulties over the past four years, especially during the challenging times of the pandemic.

Contents

Chapter 1: Introduction 1

1.1. Research objectives 7

1.2. Main contributions 9

1.3. Thesis outline 10

Chapter 2: Literature review 12

2.1. PV household power system configuration 14

2.2. An overview of energy storage technologies 17

2.2.1. Review of mechanical storage 17

2.2.2. Review of hydrogen 18

2.2.1. Review of thermal storage 19

2.2.2. Review of electro-chemical storage 21

2.3. Review of Power conversion systems topologies 25

2.3.1. Review of PV inverter topologies for PV power generation 25

2.3.2. Review of bidirectional DC/DC converter topologies for battery energy storage 32

2.3.3. Review of electric water heater system 37

2.4. Review of optimal components sizing procedure 41

2.4.1. Input data 42

2.4.2. Design constraints 43

2.4.3. Control and energy management strategies 44

2.4.4. Review of optimization methodologies 46

2.4.5. Objective functions 52

2.5. Challenges for the household PV power system optimization 54

2.6. The gap aiming to be improved by this study 55

2.7. Summary 56

Chapter 3: Sizing procedure for the domestic PV energy application 57

3.1. Common limitations for all scenarios/cases 58

3.2. Steps of the optimal sizing procedure 62

3.3. Identifying different study scenarios/cases 63

3.3.1. PV self-consumption scenario 64

3.3.2. PV-battery energy storage scenario 67

3.3.3. PV-power electronic water heater power system scenario 70

3.3.4. PV-battery-power electronic water heater power system scenario 74

3.4. Input data 80

3.4.1. Imported PV generation, loads demand, hot water consumption and room space temperature profile 80

3.4.2. Grid electricity price tariffs 81
3.4.3. Device price 82
3.5. Modelling for system components 84
3.5.1. Modelling converters 84
3.5.2. Modelling battery 90
3.5.3. Modelling water cylinder 94
3.6. Overnight charging algorithm 103
3.7. Objective functions 104
3.8. Examining scenarios/cases and processing optimization simulation 106
3.9. Summary 107
Chapter 4: Single house application 109
4.1. Scenarios examination 109
4.1.1. PV self-consumption scenario 110
4.1.2. PV-battery energy storage scenario 112
4.1.3. PV-power electronic water heater scenario 117
4.1.4. PV-battery-power electronic water heater scenario 121
4.2. Different overnight charging level of battery stack 126
4.2.1. Different *SOCpre* for PV- battery energy storage scenario 127
4.2.2. Different *SOCpre* for PV-battery-power electronic water heater energy storage scenario 129
4.3. Impact of complex modelling factors 133
4.3.1. Battery model 133
4.3.2. Cut-off power for all converters 136
4.4. Different input data impact 139
4.4.1. Different house occupants 140
4.4.2. Different sample resolution 141
4.5. Optimal sizing 144
4.5.1. Sizing for PV self -consumption scenario 145
4.5.2. Sizing for PV-battery energy storage scenario 147
4.5.3. Sizing for PV-power electronic water heater scenario 151
4.5.4. Sizing for PV-battery-power electronic water heater scenario 155
4.5.5. Comparison of these four scenarios 159
4.6. Summary 162
Chapter 5: Modelling PV-battery-novel power electronic water heater power system 164
5.1. The proposed power electronic water heater 166
5.1.1. The topology of the power electronic water heater 166
5.1.2. Switching patterns of simplified circuit. 168

5.1.3. Harmonics compensation capability limitations exploration 171
5.1.4. Comparison with conventional electric water heater and another filter respectively 175
5.1.5. Harmonics compensation control schemes 177
5.2. PV inverter 181
5.2.1. Topology of PV inverter 181
5.2.2. Control schemes of PV inverter 182
5.2.3. PR controllers design for PV inverter 183
5.3. Battery DC/DC converter 189
5.3.1. Topology of battery DC/DC converter 189
5.3.2. The control scheme of the battery DC/DC converter 190
5.4. Excess PV power consumption demonstration 197
5.5. Simulation 197
5.5.1. Harmonics compensation capability simulation validation 198
5.5.2. PV inverter and battery charging system performance 204
5.6. Summary 207
Chapter 6: Experimental results 208
6.1. Experimental evaluation of the power electronic water heater 209
6.1.1. Power consumption tests 212
6.1.2. Harmonics compensation capability tests 214
4.2.1 Determining the limitations of the harmonics compensation capability 218
6.2. Experimental tests of PV inverter and battery DC/DC converter 222
6.2.1. Grid-connected PV inverter experimental tests 223
6.2.2. Battery DC/DC converter experimental tests 226
6.3. The performance of PV-battery-power electronic water heater power system 228
6.3.1. Performance of PV-battery power system 228
6.3.2. Performance of the entire PV-battery-power electronic water heater power system 231
6.4. Summary 235
Chapter 7: Conclusion and future work 237
7.1. Conclusion 237
7.2. Contributions 239
7.3. Future work 241
7.4. Publication 242
Reference 243
Appendix A: CREST model demonstration 251

Appendix B: DSP controlling platform 254

List of Acronyms and Nomenclature

PV-Photovoltaic

AC-Alternating current

DC- Direct current

PFAC-Power frequency AC-coupled

HFAC-High frequency AC-coupled

PHS-Pumped hydro storage

CAES-Compressed air energy storage

FES-Flywheel energy storage

TES-Thermal energy storage

PCM-Phase change materials

EDLCs- Electrostatic double-layer capacitors

DOD-Depth of discharge

SOC-State of charge

NPC-Neutral point clamped

IEEE- Institute of Electrical and Electronics Engineers

PWM-Pulse-width modulation

LF-Low frequency

HF-High frequency

MPPT- Maximum power point track

CM-Common mode

DM-Differential mode

EMI-Electromagnetic interference

VSI-Voltage source inverter

BDC-Bidirectional DC/DC converter

UDC-Unidirectional DC/DC converter

IUDC-Isolated unidirectional DC/DC converter

ZVS-Zero-voltage-transition

ZCS-Zero-current-transition

DNO-Distribution Network operator

DOD-Depth of discharge

ToU-Time of use

EST-Energy saving trust

DWH-Domestic hot water consumption

Rin-Resistance capacitor circuit

SAP-Standard assessment procedure

VF-Cylinder volume factor

TF-Appropriate temperature factor

PLL-Phase locked loop

THD-Total harmonics distortion

FFT-Fast Fourier transform

V_{oc}-Open circuit voltage of battery

R_{bat}-Inner resistance of battery

$V_{terminal}$-Battery terminal voltage

I_{bat}-battery current

P_{bat_los}-battery ohmic power loss

Vol- Average litres of daily hot water consumption

E_m-Daily hot water energy consumption

ρ-Density of water

c_w-Specific heat capacity of water

θ_m-Required temperature rise

E_{tank_loss}-Cylinder energy storage loss

Vol_{usenew}-Transferred hot water usage amount

T_{win}-Inlet cold water temperature

T_{wout}-Outlet hot water temperature

H_{loss}-Cylinder heat loss coefficient

SOC_{pre}-Pre-charge level of battery stack

C_{ele}-Electricity cost for one week

E_{ope}-Amount of electricity bought form grid during off-peak time

E_{pe}- Amount of electricity bought form grid during peak time

E_{ele}-Total electricity amount bought from grid

δ_{PV}-PV utilization rate

E_l-Household loads demand

E_{losses}-energy losses of the system

C_{total}-Total costs of the system for 10-year period

C_{fixed}-Installation fee

η_{PV}-PV utilization rate

R_{non}-Nonlinear load resistor

C_{non}-Nonlinear load capacitor

R_{non_in}-Nonlinear load input resistor

L_{non_in}-Nonlinear load input inductor

i_{non_in}-Nonlinear load input current

i_{non_fund}-Nonlinear load fundamental input current

i_{non_har}-Nonlinear load input current harmonics

L_{grid}-Grid side inductor

L_{HR_in}-Power electronic water heater input inductor

C_{HR_in}-Power electronic water heater input capacitor

R_{HR}-Heating resistor

L_{HR}-Parasitic inductance of heating resistor

v_{grid}-Grid voltage

i_{grid}-Grid current

P_{grid}-PV inverter output power or grid power imported

f_{sw}-Switching frequency

T-Grid voltage fundamental period

V_{dc}-DC bus voltage

V_{bat}-Battery stack voltage

I_{bat}-Battery stack current

P_{bat}-Battery stack power

v_{HR_in}-Water heater input voltage

i_{HR_in}-Water heater input current

i_{HR}-Heater resistor current

P_{HR}-Water heater power consumption

L_{bat}-Battery side inductor

C_{bat}-Battery side inductor

C_{DC_bus}-DC link capacitor

L_{boost}-Inverter side inductor

L_{ac}-Grid side inductor

R_{LCL}-Dumping resistor

C_{LCL}-*LCL* filter capacitor

List of Figures

Figure 1.1. The share of global electricity production from renewables from 2000 to 2023. 1

Figure 2.1. Schematical diagram of a DC-coupled residential PV power system. 14

Figure 2.2. Schematical diagram of a simplified AC-coupled residential PV power system. 16

Figure 2.3. Ragone diagram of energy density and number of cycles of EDLCs, lead-acid and lithium-ion battery. 22

Figure 2.4. The theoretical structure of a typical rechargeable battery cell. 23

Figure 2.5. 6 types of common string PV inverters. 29

Figure 2.6. 3 examples of central inverters. 30

Figure 2.7. Two examples of muti-string PV inverters. 31

Figure 2.8. Two examples of AC module PV inverters. 31

Figure 2.9. Examples of various non-isolated BDCs. 34

Figure 2.10. Examples of isolated BDCs. 37

Figure 2.11. The diagram of three types of electric water heater system. 38

Figure 2.12. The demonstration of relay control electric water heater. (a) The topology of relay control circuit. (b) Relay switched on at voltage zero-crossing points. 40

Figure 2.13. The summary of sizing optimization procedure diagram [97]-[99]. 42

Figure 2.14. The summary of the schematic diagram of centralized, distributed and hybrid control. 45

Figure 3.1. Steps of the optimal sizing procedure. 63

Figure 3.2. The schematic diagram of residential PV self-consumption scenario. 65

Figure 3.3. The schematic diagram of residential PV-battery power system. 69

Figure 3.4. The schematic diagram of residential PV power electronic water heater system. 72

Figure 3.5. The schematic diagram of residential PV-battery and power electronic water heater system. 79

Figure 3.6. Typical efficiency characteristics of bidirectional converter. (a) converter efficiency. (b) converter power losses. (taken from [145]) 87

Figure 3.7. Comparison between data collected and curve fitting. 89

Figure 3.8. The power loss as a function of processing power level (a) Battery charger. (b) DC/AC inverter. (c) converter for electric water heater. 90

Figure 3.9. The converter efficiency as a function of processing power level charger (300V battery stack, 400V DC bus and 240V grid) (a) Battery charger. (b) DC/AC inverter. (c) converter for electric water heater. 90

Figure 3.10. Rin model and the modified Rin model used. 92

Figure 3.11. The relationships between Voc and SOC for three different lithium-ion battery. (a) 2Ah battery. (b) 2.8Ah battery. (c) 3.35Ah battery. 93

Figure 3.12. Two methods for modelling daily hot water consumption. 96

Figure 3.13. The configuration for a typical hot water cylinder. 97

Figure 3.14. Hot water cylinder model [125]. 101

Figure 3.15. The thermal model of hot water cylinder validation. 102

Figure 4.1. Battery energy storage operation for PV-battery & overnight charging scenario during a spring week. 114

Figure 4.2. Battery energy storage operation for PV-battery & overnight charging scenario during a summer week. 115

Figure 4.3. Battery energy storage operation for PV-battery & overnight charging scenario during an autumn week. 115

Figure 4.4. Battery energy storage operation for PV-battery & overnight charging scenario during a winter week. 116

Figure 4.5. The power electronic water heater system operation for PV-power electronic water heater energy storage scenario-spring. 118

Figure 4.6. The power electronic water heater system operation for PV-power electronic water heater energy storage scenario-summer. 119

Figure 4.7. The power electronic water heater system operation for PV-power electronic water heater energy storage scenario-autumn. 119

Figure 4.8. The power electronic water heater system operation for PV-power electronic water heater energy storage scenario-winter. 120

Figure 4.9. The power process of battery stack and power electronic water heater system during a spring week. 123

Figure 4.10. The energy process of battery stack and power electronic water heater system during a spring week. 123

Figure 4.11. The power process of battery stack and power electronic water heater system during a winter week. 124

Figure 4.12. The energy process of battery stack and power electronic water heater system during a winter week. 124

Figure 4.13. The battery capacity changing behaviour at 0.1,0.5,0.9 overnight charging level-spring and summer. 127

Figure 4.14. The battery capacity changing behaviour at 0.1,0.5,0.9 overnight charging level-spring and summer. 130

Figure 4.15. Weekly average electricity cost as the function of different battery stack. 134

Figure 4.16. The comparison of different battery model with different battery stack size in the PV-battery-power electronic water heater scenario (summer week). 136

Figure 4.17. The comparison of the charging/discharging of battery stack with/without cut-off power in the summer. 138

Figure 4.18. The comparison of the weekly average total energy losses and the purchased electricity cost with/without cut-off power considered for all converters. 139

Figure 4.19. The weekly average purchased electricity cost for different house occupants at different converters power size and different battery stack energy rating. 141

Figure 4.20. The battery stack charging pattern for different occupants at different input datasets sample resolution in summer. 143

Figure 4.21. The weekly average purchased grid energy for different house occupants for 1-minute (solid) and 5-minute (dash) power sample resolution. 143

Figure 4.22. Financial benefits of the overall system for 10-year period at different PV peak power and PV inverter size. 147

Figure 4.23. Series number of the battery stack and the combination of PV inverter and battery charger. 148

Figure 4.24. Financial benefits of PV-battery energy storage scenario for 10-year period at 0.1 pre-charge. 150

Figure 4.25. Financial benefits of PV-power electronic water heater scenario at different PV and converters combination installation for 10-year period. 154

Figure 4.26. Series number of the battery stack and the combination of PV inverter, battery charger, and electric water heater converter. 157

Figure 4.27. Financial benefits of PV-battery-power electronic water heater scenario for 10-year period at 0.2 pre-charge. 159

Figure 5.1. Schematic diagram of PV-battery-novel power electronic water heater integrated system. 165

Figure 5.2. Topology of the proposed power electronic water heater. 167

Figure 5.3. Simulation results of input voltage and current at different switch combinations with (a) DC input voltage and (b) AC input voltage. 168

Figure 5.4. Theory waveform of proposed system. 170

Figure 5.5. Demonstration of limitations of the power electronic water heater used for grid harmonics compensation. (a) Overall household nonlinear input current inon_in, which is a sum of its fundamental current inon_in_fund and all current harmonics inon_in_har. (b) Harmonics compensated and uncompensated power electronic water heater input current iHR_in. 173

Figure 5.6. The curves of $fA(mwid)$, $fB(mwid)$, and $fC(mwid)$ as the function of $mwid$. 174

Figure 5.7. Control diagrams. (a) General PLL control diagram. (b) Orthogonal generation system of grid voltage. 178

Figure 5.8. Direct harmonics compensation method. 179

Figure 5.9. The diagram of PI control harmonics compensation method. 179

Figure 5.10. PV inverter topology. 181

Figure 5.11. The control scheme of the PV inverter. 183

Figure 5.12.Control loop for fundamental PR controller design. 184

Figure 5.13.Equivalent control diagram. 184

Figure 5.14.Bode diagram of the original and simplified inverter plant. 186

Figure 5.15.Bode diagram of the open loop. 187

Figure 5.16.Bode diagram of the closed loop. 188

Figure 5.17.Step response diagram. 188

Figure 5.18. The topology of the battery stack charger. 190

Figure 5.19. Control diagram of the battery DC/DC converter. 191

Figure 5.20. Bode diagram of the current open loop. 193

Figure 5.21. Bode diagram of the current closed loop. 194

Figure 5.22. Step response diagram of the current closed loop. 194

Figure 5.23. Bode diagram of the voltage open loop. 195

Figure 5.24. Bode diagram of the voltage closed loop. 196

Figure 5.25. Step response diagram of the voltage closed loop. 196

Figure 5.26. The diagram of surplus PV consumed by the power electronic water heater. 197

Figure 5.27. The grid harmonics compensation simulation validation topology. 199

Figure 5.28. An example of harmonics compensation capability limitation. (a) d_{act} =0.35. (b) d_{act} =0.05. 200

Figure 5.29. Simulation results of full harmonics compensation using direct harmonics compensation method. 201

Figure 5.30. Simulation results of full harmonics compensation using PI control-based harmonics compensation method. 202

Figure 5.31. Simulation results of a part of harmonics compensation using direct harmonics compensation method. 203

Figure 5.32. Simulation results of a part of harmonics compensation using PI-based harmonics compensation method. 204

Figure 5.33. Performance of PV inverter at different output power with the PR controller. 205

Figure 5.34. Transient performance of battery charger’s current loop. 206

Figure 5.35. Transient performance of battery charger’s double loop controller (current and voltage loop). 206

Figure 6.1. The entire established experimental prototype. 209

Figure 6.2. The hardware figure of the proposed power electronic water heater and non-linear load. 210

Figure 6.3. The pictures of the practical immersion heater and coil winding resistors. (a) Practical immersion heater which has three individual resistors. (b) Coil winding resistors used in the experiment. 211

Figure 6.4. Experimental results (vgrid, iHR_in, and iHR) with sudden duty cycle change. Yellow-grid voltage, purple-grid current, and green-heater resistor current.212

Figure 6.5. Experimental results of respond speed for two harmonics compensation methods. (a) The direct harmonics compensation method. (b) The PI control harmonics compensation method. Grid voltage vgrid (yellow line), grid current igrid (purple line), non-linear load input current inon_in (blue line), and power electronic water heater input current iHR_in (green line). 215

Figure 6.6. Experiment validation results at full harmonics compensation condition. (a) Uncompensated. (b) Direct harmonics compensation method. (c) PI control harmonics compensation method. Grid voltage vgrid (yellow line), grid current igrid (purple line), non-linear load input current inon_in (blue line), and power electronic water heater input current iHR_in (green line). 217

Figure 6.7. FFT analysis of grid current igrid at full harmonics compensation. (a) The value of each harmonic order. (2) The magnitude of each harmonic order compared with grid current fundamental component. 218

Figure 6.8. Experiment validation results at part harmonics compensation condition. (a) Uncompensated. (b) Direct harmonics compensation method. (c) PI control harmonics compensation method. Grid voltage vgrid (yellow line), grid current igrid (purple line), non-linear load input current inon_in (blue line), and power electronic water heater input current iHR_in (green line). 220

Figure 6.9. FFT analysis of grid current igrid at part harmonics compensation. (a) The value of each harmonic order. (2) The magnitude of each harmonic order compared with grid current fundamental component. 221

Figure 6.10. Battery DC/DC converter and PV inverter hardware figure. 223

Figure 6.11. FFT of output voltage of autotransformer. 224

Figure 6.12. Experimental results of PV inverter grid connection test with/without low order harmonics compensation. Yellow-grid voltage, blue-grid current, and green-DC bus voltage. 224

Figure 6.13. FFT analysis of grid current. 225

Figure 6.14. Experimental results of the power transferred changing. Yellow-grid voltage, purple-grid current, and green-DC bus voltage. 226

Figure 6.15. The inner current loop experimental test of battery DC/DC converter during a battery current step experimental test. Yellow-battery voltage, blue battery current, and green-DC bus voltage. 227

Figure 6.16. The double loops experimental tests of the battery DC/DC converter nested controller test to a DC-link reference voltage step change from 400 V to 370V. Yellow-battery voltage, blue-battery current, and green-DC bus voltage. 228

Figure 6.17. Topology of PV-battery power system. 229

Figure 6.18. Experimental results of battery charging/discharging process from the grid. Green-DC bus voltage, yellow-grid voltage, purple-grid current, blue battery current. 230

Figure 6.19. Experimental results of battery charging/discharging process from the grid under varying PV generation and loads consumption. Green-DC bus voltage, yellow-grid voltage, purple-grid current, blue battery current. 231

Figure 6.20. Topology of the entire PV-battery-power electronic water heater system when power electronic water heater is connected to AC grid. 232

Figure 6.21. Topology of the entire PV-battery-power electronic water heater system when power electronic water heater is connected to AC grid. 232

Figure 6.22. Experimental results of power electronic water heater and battery under varying loads demand and PV generation. Green-input current of power electronic water heater, yellow-grid voltage, purple-grid current, blue battery current. 233

Figure 6.23. Experimental results of power electronic water heater and battery under varying PV generation. Green-input current of power electronic water heater, yellow-grid voltage, purple-grid current, blue battery current. 234

List of Tables

Table 2.1 The classification of various energy storage technologies based on the form of energy stored. 17

Table 3.1. The annual average electricity prices for the standard and Economy-7. 82

Table 3.2. Typical percentage contribution of each type of loss in a power converter. 86

Table 3.3. The curve fitting parameters for three types of converters' power loss model. 89

Table 3.3. The factor for calculating the average litres per day in each individual month and annual level. 98

Table 3.4. The required temperature rise (℃) in each month and annual level. 98

Table 3.5. Modelling results as a function of the number of occupants 99

Table 4.1. The input date and model selection for these examined scenarios ('-' means not applied). 110

Table 4.2. Outcome of PV self-consumption with two meters scenario on one week basis. 111

Table 4.3. Outcome of PV-battery with overnighting charging with two meters scenario over a one-week basis. 116

Table 4.4. Outcome of PV-power electronic water heater power system (2-occupant) with two meters scenario on one week basis. 120

Table 4.5. Outcome of PV-battery and power electronic water heater system (2 occupants) on a per weekly basis. 125

Table 4.6. The input data and model selection for two examined scenarios ('-' means not applied). 126

Table 4.7. Outcomes of different SOCpre for PV-battery energy storage scenario (20 Ah/5.98kWh battery). 128

Table 4.8. Weekly average outcome for different overnight charging levels. 129

Table 4.9. Outcomes of different SOCpre for PV-battery-power electronic water heater power system scenario (20 Ah/5.98kWh battery). 131

Table 4.10. Average weekly outcome for different overnight charging levels. 132

Table 4.11. The input date and model selection for researching different DOD impacts. 133

Table 4.12. The input date and model selection for researching Ohmic losses impacts. 135

Table 4.13. The input data and model selection for researching cut-off power impacts. 137

Table 4.14. The input data and model selection for researching different house occupants impacts. 140

Table 4.15. The input data and model selection for researching different sample resolution impacts. 142

Table 4.16. The input data and model selection in the PV self-consumption scenario optimization ('-' means not applied). 145

Table 4.17. Financial benefits and PV utilization rate at optimal point for different occupants applications for 10-year period. 147

Table 4.18. Input data and model selection in the PV-battery scenario optimization ('-' means not applied). 148

Table 4.19. Optimal devices design for PV-battery energy storage scenario for different house applications for 10-year period. 151

Table 4.20. Input data and model selection in the PV-power electronic water heater scenario optimization ('-' means not applied). 152

Table 4.21. Optimal devices design for PV-power electronic water heater scenario for different house applications for 10-year period. 155

Table 4.22. Input data and model selection in the PV-battery-power electronic water heater scenario optimization. 157

Table 4.23. Optimal devices design for PV-battery-power electronic water heater scenario for different house applications for 10-year period. 159

Table 4.24. The comparison between financial benefits and PV utilization rate for different scenario for different occupants applications ('×' represents the stuff is not applied). 161

Table 5.1. 5 types of heating resistance at different switching combinations (0-switching off, 1-swicthing on). 168

Table 5.2 The maximum and minimum values of fA(mwid), fB(mwid), fC(mwid).175

Table 5.3 Comparison with conventional electric water heater. 176

Table 5.4 Comparison with another filters. 177

Table 5.5. Knr for different harmonic PR controller. 189

Table 5.3. Parameters used in the simulation and experimental setup. 198

Table 6.1. The measurement inductance of one immersed heater and one coil winding resistor. 211

Table 6.2. THD of grid current $igrid$ at full harmonics compensation. 218

Table 6.3. THD of grid current $igrid$ when the harmonics compensation capability is limited by the current envelope ($vgrid/RHR$). 221

Chapter 1: Introduction

Energy is an integral part of modern human life. Nowadays, around 80% [1] of our energy demand is sourced from fossil fuels, and simultaneously the rapid growth of population and increasing industrialization are placing considerable pressure on the world's finite fossil fuels resource, leading to energy shortage [2]. Furthermore, those energy resources utilization is closely associated with significant greenhouse gas emissions that cause climate change and environment degradation [3]-[5], which adversely affect wildlife and human wellbeing. The most effective ways to tackle this situation are to significantly increase the renewable energy share in global energy consumption and to make the energy utilization more eco-friendly and efficiently through technological advancement [6]. As depicted in Figure 1.1, the proportion of electricity generated from renewables has steadily risen, climbing from 18.71% in 2000 to 30.24% in 2023 [7], and continues to progress towards achieving "net zero." This crucial milestone entails striking a balance between greenhouse gas emissions and their removal from the atmosphere.

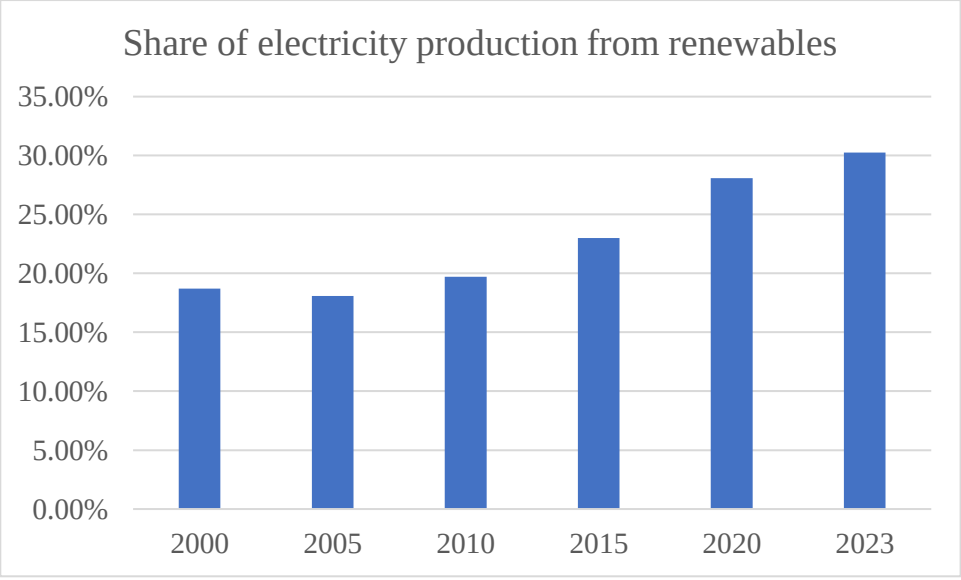

Figure 1.1. The share of global electricity production from renewables from 2000 to 2023.

Hence, the exploit of renewables and utilization approaches have increased in recent years. For example, by the end of 2020 the UK has already reduced its CO2 emissions by 50% below the 1990 levels [8], and around 33% of electricity is generated from renewables in 2022 [9] but this is not sufficient to limit climate change. This is why, in 2019, the UK government agreed to an ambitious net-zero emissions target to be achieved by 2050 [10] and to successfully implement that, it is necessary to understand and assess the potential and limitations of the relevant technologies that can help the reduction of CO2 emission in all energy intensive sectors.

Based on data from the Department for Business, Energy & Industrial Strategy (BEIS), residential energy consumption in the UK fluctuates annually but generally represents about 25-30% of the nation's total energy usage [11]. In the urban residential sector, solar power generation in the form of photovoltaics (PV) is an excellent and popular renewable energy generation option where the solar panels can be installed on the roof of houses which prevent occupying land that could be used by wildlife or agriculture. Also due to this solar energy being predominantly consumed locally, it means that the infrastructure investment for connecting the PV installations to grid are minimum compared to a large-scale solar farm. Thus, the household energy bill can be significantly reduced as the photovoltaic (PV) energy is utilized locally. However, due to the PV generation being easily affected by the weather condition as clouds are limiting sunlight radiation captured by PV panels which is very common in UK, the intermittent PV power hardly matches with the local loads demand, which may result in the excess PV power being exported in the distribution grid by the households. This situation, in conjunction to a pricing scheme not designed to maximise PV

generation would typically have a detrimental effect on the finances, discouraging some homeowners to install or further increase the size of their PV system. To address this problem, employing energy storage to prevent export of excess PV power rewarded at low price that is later in the evening imported at expensive price may be considered. Different means of storing energy such as compressed air energy storage, battery energy storage, thermal storage can be considered. Due to the limitations of space and cost, the battery energy storage which currently is very efficient but expensive and thermal energy storage which is cheap but less efficient seem to be the feasible choices in residential PV application [12]. Practically, a significant amount of energy is used for generating heat (cold/hot) in residential applications. According to the UK government data, most of the domestic energy is used to heat homes (space heating) (62%) with the second largest energy being used to heat water (18%) [13]. Hot water can be produced instantly in gas boilers or can be produced using electricity by high power resistive heaters integrated in instant hot water taps and showers or inside washing machines, and the advantage is that heating only as much water as is consumed, it limits heat losses. The other alternative is to utilize smaller heaters that operate for a longer time that work in conjunction with a thermal insulated water cylinder which would act as a thermal energy storage, and this is a technology that was very popular in the past in UK with many households still having installed a hot water cylinder. This is why the alternative to the expensive battery energy storage exist, to store the excess PV energy in the hot water tank at virtually no added equipment cost. Besides, early in 1978, a new off-peak tariff known as Economy-7 was introduced [14]. It features a seven-hour night rate some pennies per unit cheaper than the rest of day, made

possible for residents to save electricity bill by moving some household loads to this period or storing some energy from the grid during off-peak hours for peak-hour usage. Thus, in the past, the strategy of heating hot water during the off-peak hours was adopted by many British family. There is however a potential problem, with the hot water heater which is traditionally design to consume constant power which may not always match the available PV excess power, which may be sensed by the energy meter. Therefore, in order to store only the excess PV energy in the hot water tank, the heating resistor needs to be able to consume at any time the variable excess PV power exactly and respond quickly to any changes needing an advanced controller. Conventional commercial electric water heaters exist [15][16] to control the dissipated power in a water heater by employing simple circuits relying on relays/TRIACs but these may result in unwanted power import/export and in addition, may further degrade the power quality.

Furthermore, as more non-linear loads relying on a diode bridge front end are widely employed in the domestic power network, a significant level of current harmonics are injected causing a significant increase of power quality issues, such as additional heat losses, and failure in sensitive electronic devices [17]. To eliminate the harmonics detrimental influence on sensitive consumers, traditional solutions are used such as the implementation of filters (passive filter, active filter, and hybrid harmonics filter) or equipping appliances with an active front end [18] but all these solutions will increase costs. A grid connected PV inverter would have the capability to perform also active filtering functionality for the household and this feature was reported in research literature [19][20] but the authors are not aware of any manufacturer that actually embedded this

function in their PV inverter and the reason is that the controller and bandwidth of the grid current sensors need increasing which impacts cost and also there is the additional resonance with the grid side PWM filters using LCL topologies [21]. Hence, it is an interesting and meaningful topic to incorporate grid current harmonics compensation capability into the power electronic controlled water heater.

Therefore, it is feasible to utilize the battery energy storage or thermal energy storage (hot water cylinder) in the residential sector. Some of the excess PV power can be stored in a battery stack and released to satisfy the household (electronic) load demand when PV generation is too small or during evening reducing energy imports. It is also possible to reduce the electricity bill by heating water in the tank overnight at cheap off-peak electricity price and/or store any excess PV power when battery is full. This means that compared with battery only energy storage installation, it is possible to reduce the size of the battery stack in an installation comprising of a PV-battery-hot water tank. However, there is a challenge of how to choose the size and configure all the system components, such as, PV panels, converter rated power and rated battery energy. Due to the expensive capital cost of these components, especially of the battery, using an inappropriate method could lead to oversizing these components increasing significantly costs and limit financial benefits which will discourage the motivation of residents to employ more PV generation.

Presently, there is a lot of research effort directed at how to optimally design household PV power system components [22][23]. Nevertheless, most research focuses on PV with single energy storage technology utilization, like PV-battery or PV-heat pump. More complicated power systems such as PV-battery-thermal

storage power system, is rarely researched. Simultaneously, there are not many comparisons of PV interfaced with different energy storage technology scenarios which is essential for consumers to choose a suitable PV utilization scheme.

Therefore, the aim of this thesis is to propose and investigate a power electronic circuit and associated control that is able in addition to controlling accurately the power dissipation in a hot water tank to match the exact available excess PV power, to also achieve significant reduction of overall household current harmonics which is then validated by simulation and experimentally. The optimization design procedure and associated simulation models to size the battery is also implemented four different PV application scenarios (only PV self-consumption scenario, PV- battery energy storage scenario, PV-power electronic water heater scenario, and PV-battery-power electronic water heater scenario) to provide recommendations for consumers to optimally design their own PV power system.

1.1. Research objectives

There are two main tasks in this project: the one is to propose a novel power electronic water heater which can be used to compensate the grid harmonics and consume the excess PV energy exactly. The other is to build the optimization procedure to provide the recommendation for consumers to design the optimal PV utilization power system.

The following objectives are considered:

- Clarify the optimal sizing PV power system routines/procedure by the research/papers investigation. In this section, the steps for optimising the PV power system components are defined and illustrated individually.
- Construct the models, collect the input data, specify the constraints and requirements for the optimization procedure. For example, battery stack, converter, and hot water cylinder are modelled. The PV generation, household loads consumption profiles, electricity tariff, and device price, etc. are collected. Besides, there are various constraints and requirements also should be defined in advance.
- Compose optimization MATLAB codes for four design scenarios (only PV self-consumption scenario, PV- battery energy storage scenario, PV-power electronic water heater scenario, and PV-battery-power electronic water heater scenario), followed by the examination of each scenario. To explore how different values of an independent variable affect the optimisation procedure, sensitive analysis is done. Lastly, the optimal procedure of each scenario is processed.

- Different input data and power size converter models applied, like PV generation size and power converter power size, it aims to capture the optimal size design for each scenario.
- Propose and investigate the novel power electronic water heater topology and control schemes and analyse the harmonics compensation capability limitations, and then validate the concept on an experimental prototype.
- Build a PV-battery-power electronic water heater power system experimental prototype to validate the stability and transient performance. Besides, some practical problems are also done in this part, like the elimination of low order grid harmonics caused by the distortion of grid voltage.

1.2. Main contributions

There are two main contributions in this thesis as follows.

- Propose a novel type of the power electronic water heater. Distinguished from the conventional relay based electric water heater, it can accurately match the amount of excess PV power by PWM technology and compensate the grid current harmonics caused by the household appliances. The simulation and experimental prototype are established to validate these functionalities.
- Provide schemes and recommendations on how to maximise the financial benefits for a residential PV application. There are four different types of PV applications are researched and compared.

1.3. Thesis outline

To document how these research objectives have been achieved, the thesis is structured in seven chapters as follows.

Chapter 1 This chapter provides the introduction of this work and highlights the major contributions.

Chapter 2 The literature review of the structure of PV-battery-power electronic water heater power system is shown firstly, including the demonstration of current available energy storage technologies, PV inverter, battery charger, and electric water heater topologies. Then, the optimization procedure used in another research is reviewed.

Chapter 3 The demonstration of each scenario is shown in this chapter, including different scenario demonstration, system components models, main constraints, input data collection, and objective functions definition.

Chapter 4 In this chapter, the optimization codes for four residential PV application scenarios are examined and processed for the study case to design the optimal system components size to maximum the financial benefits for 10-year period.

Chapter 5 A novel power electronic water heater is proposed, including the topology demonstration, harmonics compensation capability analysis, and control schemes. To construct a PV-battery-power electronic water heater power system, the topology and control methods of each subsystem are described respectively. Besides, the simulation validation of the proposed power electronic water heater used for grid current harmonics compensation and the excess PV power consumption is done in the PLECS software.

Chapter 6 At the beginning, the experimental validation of the proposed electronic water heater used for grid harmonics compensation is done. The

harmonics compensation capability limitations are also experimentally validated. Then, the stability and transient performance of the entire power system are validated and analysed under different PV generation/loads consumption.

Chapter 7 Conclusions and future works are discussed.

Chapter 2: Literature review

To realize the ‘‘zero carbon’’ target by 2050, a more attractive solution is the decentralised energy system deployment which generates green power close to the point of use [24]. In the UK, the increasing use of decentralised energy forms is also essential to achieve this ambitious target. Traditionally, the power producers and consumers in a centralised power system structure were strictly separated and distinguished which caused significant energy losses during transmission and distribution, leading to inefficiencies and increased environmental impact. Nowadays, due to the widespread distribution characteristics of some renewable energies, like PV energy, it is possible to integrate the energy production, consumption, and storage together at the small or medium power scale [25]. For instance, a growing field of renewable energy application is the millions of British private houses that installed roof-top PV generation, lowering the dependence of consumers on the power grid with noticeable implication in cost of electricity. Consequently, the large-scale PV generation is integrated following a traditional power system approach.

This chapter aims to provide a good comprehension of PV household power system with integrated PV generation, in view of making it more applicable and cost effective. The framework consists of certain key components which include the topology of PV system, as well as the key load devices which are important from the point of view of power consumption and potential energy storage capacity that will be relevant for the size optimisation procedure.

Driven by the reduction of PV panel cost [26], the PV market and manufacturing experienced a rapid growth over the last decade. However, deciding on the right choice of PV system configuration and size, including also

the energy storage technology/component and the associated power conversion systems, for meeting given load requirements has great influence on the PV power system cost and performance.

To optimally select the appropriate system devices, this literature review focuses on state of the art on optimally sizing PV power system components—primarily PV generation, energy storage capacity, and converter capacity—through mathematical analysis and software-based computations.

In this thesis, the battery energy storage and power electronic water heater is integrated into PV power system. Thus, the configuration of this power system should be reviewed, including the selection and design of each subsystem, such as energy storage technologies, power conversion systems, and electric water heaters. Following this, the optimization procedure for sizing residential PV power systems is presented, along with the available software tools and associated challenges. Finally, the chapter concludes by outlining the aims of this study.

2.1. PV household power system configuration

Firstly, it is essential to define the structure of the PV power system. There are primarily two approaches to integrating PV power generation into the power system [27]-[30]. In the first approach, PV generation is coupled with the DC bus through a DC/DC converter (DC coupled). In the second approach, PV generation is coupled with the AC bus through a DC/AC converter (AC coupled). The differences between DC-coupled and AC-coupled systems are described as follows.

- **DC coupled system:** As shown in Figure 2.1, PV panels are linked to the DC bus either through a dedicated DC/DC power converter or directly connected with the DC bus in certain configurations. In households with DC loads, accessing power directly from the DC bus is straightforward. The bidirectional DC/AC inverter allows power converted from the DC side to the AC side or vice versa. Thus, this simple scheme of DC-coupled has more potential to reduce costs from the shared components (PV inverter).

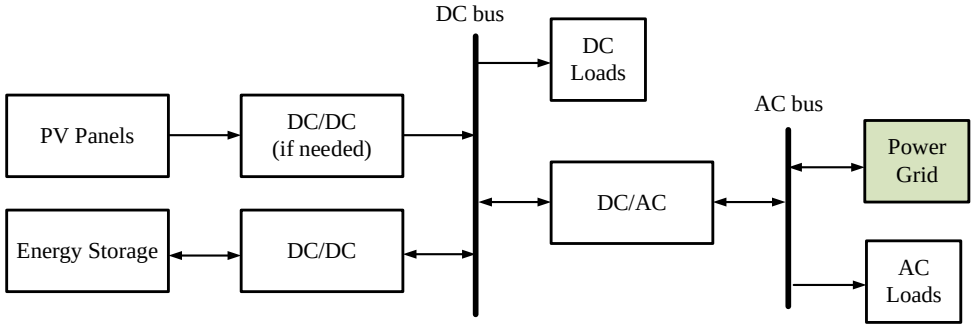

Figure 2.1. Schematical diagram of a DC-coupled residential PV power system.

- **AC-coupled system**: Figure 2.2 illustrates a simplified AC-coupled residential PV power system. In this AC-coupled configuration, both the photovoltaic power generation unit and the energy storage unit are typically connected to an AC bus via converters. Each DC subsystem

within the AC-coupled system must synchronize with the common AC bus frequency. For grid-tied power systems, isolation is often crucial for ensuring safety, compatibility, and regulatory compliance. In this residential PV power setup, two primary isolation methods are commonly employed. The first utilizes transformer-less inverters, such as switched-capacitor inverters [31] and neutral point clamped (NPC) inverter [32]. These inverters enhance safety and reduce leakage currents without the need for a bulky transformer. Although they offer high efficiency, they must adhere to stringent safety standards to prevent leakage and ensure secure operation. The second method employs transformers to provide galvanic isolation, effectively separating the PV array and energy storage components from the grid. This approach prevents direct electrical connections, thereby eliminating the risk of fault currents transferring between the grid and household circuits. There are two main approaches to implementing galvanic isolation. The first involves using a transformer before the inverter to isolate the power grid from the PV array and energy storage device. However, this grid-frequency transformer can be quite large. Alternatively, another solution entails splitting the DC/AC converter into two stages: DC/DC and DC/AC [33], with a high-frequency transformer positioned in the DC/DC stage [34]. This high-frequency transformer is smaller than a grid-frequency transformer, providing a more efficient and compact isolation solution.

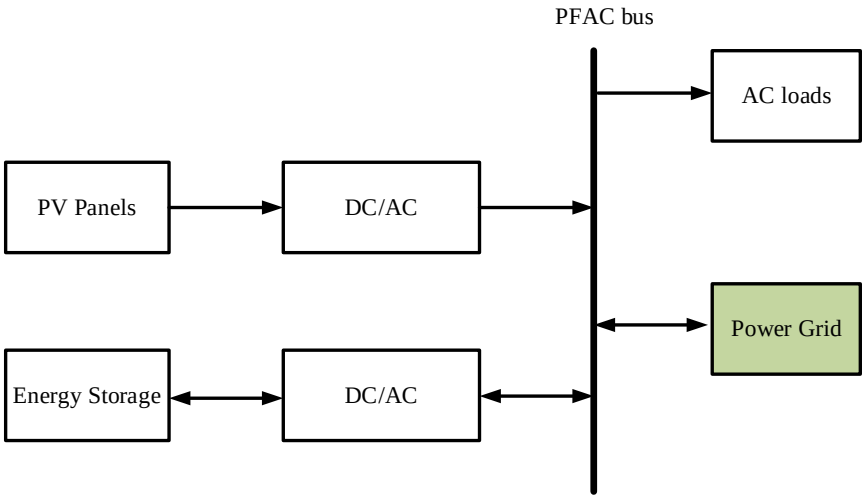

Figure 2.2. Schematical diagram of a simplified AC-coupled residential PV power system.

2.2. An overview of energy storage technologies

As renewable energy penetration increases in the power grid, the utilization of energy storage devices has become increasingly prevalent, serving various purposes such as storing surplus PV energy, grid frequency/voltage support, and saving electricity bills [35]. Energy storage technologies are typically categorized based on storage duration, response time, and function [36]. Additionally, they can be classified according to the form of energy stored, including mechanical, chemical, thermal, and electrochemical energy [37][38]. Table 2.1 provides an overview of different energy storage technologies categorized by the form of energy stored. This chapter presents currently applicable storage technologies to select the proper energy storage technology in household PV applications.

Table 2.1 The classification of various energy storage technologies based on the form of energy stored.

Classification	Examples
Mechanical	Pumped hydro storage
	Compressed air storage
	Flywheel
Chemical	Hydrogen
Thermal	Sensible heat
	Latent heat
	Thermochemical
Electro-chemical	Supercapacitor
	Battery (lithium-ion, lead-acid, etc.)

2.2.1. Review of mechanical storage

Among mechanical storage technologies, capacity-oriented pumped hydro storage (PHS) and compressed air energy storage (CAES) typically feature long discharge duration and cycle life, making them suitable for long-term energy storage or bulk energy applications, especially for managing slow load variations. Pumped hydro storage remains the most widely adopted and commercially developed storage technology, with a global energy installation capacity reaching up to 3.4 GW by the end of 2020 [39]. While CAES is experiencing rapid development, its energy efficiency is relatively lower. CAES can be

categorized as conventional and adiabatic. The first conventional CAES plant was constructed in Germany in 1978 with 290 MW power level [40] while an adiabatic CAES plant in Australia, costing around $30 million, aims to provide 5 MW of backup power for up to 2 hours [39].

In contrast, the flywheel energy storage system offers high response speed, efficiency (80%-90%), and a long lifetime, making it favourable for use in renewable/hybrid energy systems. Notably, the United Kingdom hosts the world's largest short term flywheel project, capable of supplying 400 MW for 30 seconds every 20-30 minutes, primarily utilized for frequency regulation [39].

2.2.2. Review of hydrogen

Hydrogen is a clean, highly abundant, and non-toxic energy vector that can be directly produced by electrolyzing water with renewable energy. Conversely, electrical energy is directly produced through the chemical reaction between hydrogen and oxygen. Compared to other hydrocarbon fuels, hydrogen contains much higher chemical energy per mass (142 MJ), nearly three times that of gasoline yet it releases no pollution into the environment as its only byproduct is water when burned. However, it is 3.2 times less energy dense than natural gas and 2700 times less energy dense than gasoline, leading to hydrogen being identified as an energy carrier rather than an energy source [41]. Nevertheless, hydrogen faces a range of safety, economic, and environmental challenges that affect its widespread adoption [42]. The primary safety concern with hydrogen fuel relates to its safe usage and handling [43]. Hydrogen’s properties—including its tendency to leak easily, low ignition energy, broad range of combustible fuel-air mixtures, and its ability to cause metal embrittlement—necessitate careful management to ensure safe operation.

Additionally, most hydrogen is currently produced using fossil fuels or renewable energy, which remains costly and slows its adoption. According to the United States Department of Energy (DOE) database, the world's largest plants (at 6 MW) are located in Germany, with a capital expenditure of $19 million [39].

Finally, hydrogen production from fossil fuels generates substantial CO_2 emissions, while hydrogen leakage can indirectly impact the atmosphere by extending the lifespan of greenhouse gases such as methane or altering the ozone layer. This is particularly concerning if large-scale hydrogen adoption results in significant leakage.

2.2.1. Review of thermal storage

Thermal energy storage is a viable technology that can reduce dependence on fossil fuels. Following pumped hydro systems, thermal energy storage (TES) accounted for the second-largest share (up to 1.2 GW) of global installed energy storage capacity in 2020. Typically, thermal energy storage can be divided into sensible heat, latent heat, and thermochemical storage. Sensible heat storage involves the temperature of the storage material varying with the amount of energy stored, such as in water or refractory bricks. Conversely, latent heat storage utilizes phase change materials (PCMs), allowing for much more energy to be stored in a relatively small volume compared to bulk water storage tanks [44]. When solar irradiation is available, the charging process involves high heat of fusion materials melting to store PV output energy by changing the phase of the PCM from solid to liquid. Subsequently, the PCM freezes, and the stored heat is recovered to drive a steam turbine when there is a need for electricity consumption during the discharge process. Unlike sensible and latent heat

storage methods, the principles of thermochemical heat storage are based on materials' chemical reactions, as shown in (2.1) [45]. During the charging process, thermochemical substance A absorbs heat to synthesize substance C and B, where the heat can be stored in different substance separately. The reverse reaction occurs when energy is needed, and substance A is formed. Thus, the storage capacity of thermochemical storage is the heat of reaction when substance A is formed.

$$A + \text{heat} \leftrightarrow C + B \tag{2.1}$$

Thermochemical heat storage stands out as a highly promising option due to its exceptional energy density, efficiency, and operating temperature flexibility. Sensible heat storage operates within a temperature range spanning from ambient temperatures up to the upper limit suitable for the material, such as in hot water energy storage, which typically ranges from room temperature (approximately 25°C) to boiling temperature (100°C). In latent heat storage, the operational temperature range is specific to the material's phase change properties, for example, paraffin wax typically operates between 20°C and 60°C.

Thermochemical heat storage, however, involves temperatures dictated by specific chemical reactions and the materials used. For instance, zinc oxide (ZnO) reacts with water (H_2O) at elevated temperatures, typically over 100°C, producing zinc hydroxide ($Zn(OH)_2$) and hydrogen gas (H_2). Unlike sensible and latent storage methods, thermochemical energy storage theoretically allows for the storage of reactants at ambient temperatures indefinitely, without time limitations on storage duration.

Nevertheless, it is important to note that thermochemical energy storage systems are more complex compared to other thermal storage methods and are currently in the laboratory research and pilot-scale testing phase [46].

2.2.2. Review of electro-chemical storage

Like conventional capacitors, supercapacitors operate based on the same fundamental equations. To achieve high capacitance values, supercapacitor electrodes are designed with high specific surface areas and thinner dielectrics. Various organic and inorganic nanostructured materials, such as carbon nanotubes, metal oxides, graphene nanosheets, and conducting polymers, are utilized to fabricate high-performance devices [47].

2.2.2.1. Review of supercapacitors

Supercapacitors are primarily divided into electrostatic double-layer capacitors (EDLCs), electrochemical pseudo capacitors, and hybrid capacitors [48]. EDLCs use activated carbon electrodes or derivatives with significantly higher electrostatic double-layer capacitance than electrochemical pseudo capacitance. Meanwhile, metal oxides or conducting polymers are applied for electrochemical pseudo capacitor electrodes to achieve a high amount of electrochemical pseudo capacitance in addition to the double-layer capacitance. Hybrid capacitors combine battery-like electrodes with capacitor-like electrodes in the same cell to achieve both the good cyclic stability of EDLCs and the greater specific capacitance of electrochemical pseudo capacitors. Supercapacitors has lower energy density but accepts much faster and more round-trip cycles than rechargeable batteries [49], as shown in Figure 2.3. Consequently, in many scenarios requiring rapid charging/discharging rates,

such as buses, cranes, and elevators [50], supercapacitors can provide short-term compact energy storage or burst-mode power delivery for the entire system.

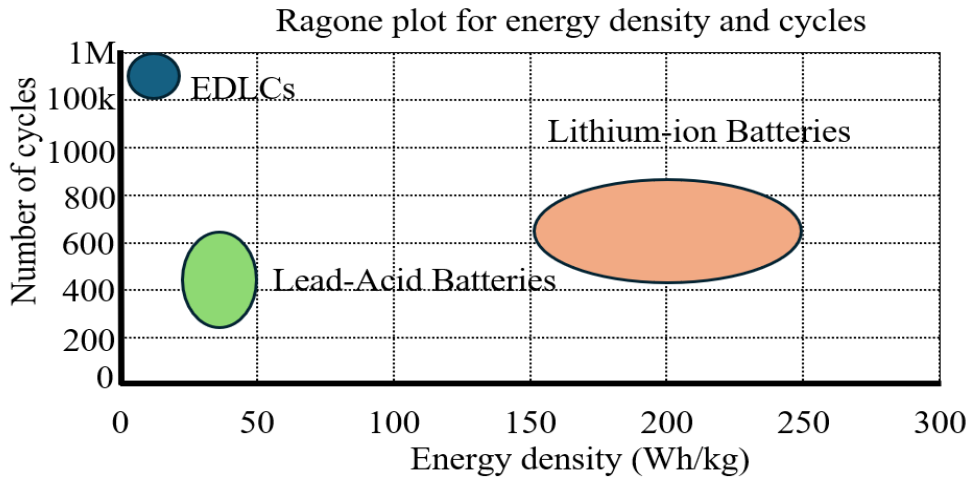

Figure 2.3. Ragone diagram of energy density and number of cycles of EDLCs, lead-acid and lithium-ion battery.

2.2.2.2. Review of battery

In recent years, with the proliferation of renewable energy sources and advancements in electrified transportation and smart grids, batteries have become essential components of the large-scale energy storage market. The charging/discharging process of a battery involves the bidirectional transformation of chemical energy into electrical energy and vice versa. Figure 2.4 illustrates the theoretical structure of a typical rechargeable battery, primarily consisting of positive/negative electrodes, electrolyte, and current collectors [51]. Electrochemical reactions occur at the positive and negative electrodes to store electric charges and serve as current density vectors. The electrolyte medium provides a high-resistance path for transferring ions (charge-carrying particles) back and forth between the two electrodes, enabling battery charging and discharging. The current collector, typically made of highly conductive metal, adheres the electrodes and interfaces with the outer circuit. Two battery

technologies: lead-acid and lithium-ion, have been in use long enough to be considered mature technologies.

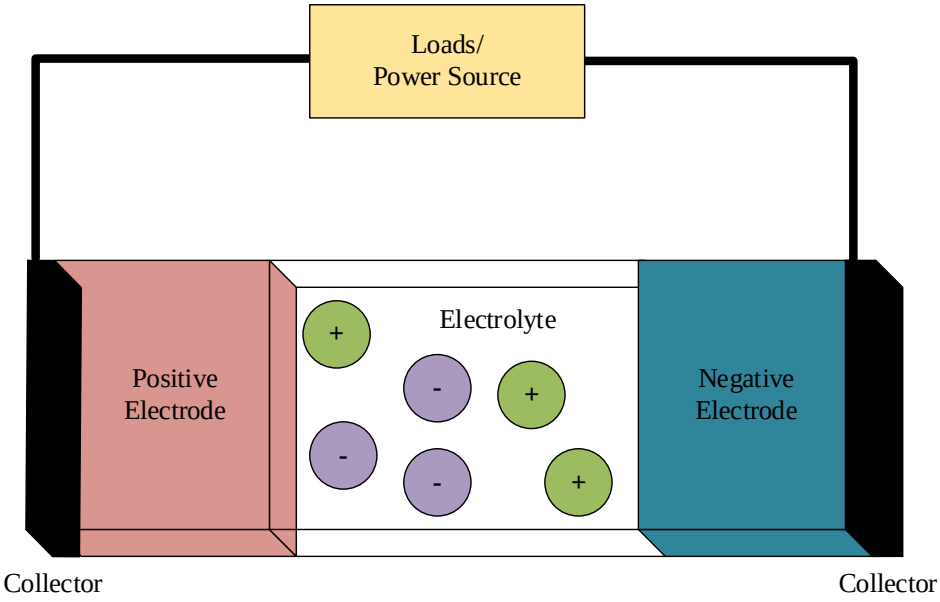

Figure 2.4. The theoretical structure of a typical rechargeable battery cell.

The first rechargeable lead-acid battery was invented in 1895 by Gaston Planté, with a unit voltage of 2 volts. By the end of the 19th century, lead-acid batteries had quickly evolved to serve multiple applications, such as lighting, bulk energy storage, and spinning reserve. Recently, the largest lead-acid battery storage project, with a capacity of 10 MW, is located in Phoenix, Arizona, USA [39]. Lead-acid batteries generally have relatively high efficiency (70%-80%) and low capital costs. However, their operational temperature and depth of discharge (DOD) significantly limit their lifespan and maintenance frequency. Advances in lead-acid technology, such as the development of valve-regulated lead-acid batteries, have been made to address the short lifespan of conventional lead-acid batteries [52].

Lithium-ion batteries offer better characteristics than lead-acid batteries, such as higher efficiency (85% to 95%), greater power density (200-2000W/kg), and longer lifecycle (500-1000). These advantages have made lithium-ion batteries

increasingly dominant in the renewable energy storage market [53] and popular among automotive manufacturers and consumers. However, the high initial investment cost remains a significant barrier for stationary energy storage applications. Additionally, various new electrode materials to lower cost, such as sodium-sulfur (Na-S) [55] and nickel-cadmium (Ni-Cd) [56], are being explored. Different battery structures, such as flow batteries [57] and bipolar batteries [58], are also being designed to meet the growing demand in the energy storage market.

2.3. Review of Power conversion systems topologies

In the DC-coupled PV power system, there are main two types of power converter used: DC/AC inverter and DC/DC converter. However, various topologies for these converters have been proposed. To select the appropriate converter topologies, this study reviews the available DC/AC inverters and DC/DC converters.

2.3.1. Review of PV inverter topologies for PV power generation

PV inverter converts DC electricity generated by solar panels into AC electricity. The rapid growth of PV renewables in the electricity market has led to a constant evolution of the PV conversion stage. In the past two decades, the demands placed on PV inverters have undergone significant development to meet increasingly stringent specifications, including performance requirements and legal regulations [59].

1. Performance requirements

The conversion efficiency of a PV inverter at its rated power level is the most critical criterion. Even a 1% improvement in efficiency can result in approximately a 10% reduction in inverter costs [60] due to higher energy conversion rates and a decreased need for additional components to compensate for efficiency losses. Presently, the efficiency of the transformer-less inverters is up to 98% in series products and in research 99% efficiency has been reached. Such extreme high efficiencies can be achieved with three level or multilevel inverter topologies and new power semiconductors like Silicon Carbide (SiC) and Gallium Nitride (GaN). [61][62]. Another consideration is power density, particularly for domestic and commercial applications. It should not be extremely big since it impacts the design, cost, and efficiency of the inverter. To

address this, solutions such as the neutral point clamped (NPC) topology and the use of high-frequency transformers instead of bulk low-frequency transformers have been implemented. Additionally, due to the high parasitic capacitance between PV panels and the ground, minimizing leakage current is essential. This can be achieved through accessible approaches like galvanic isolation transformers and specially designed power converter topologies with low common mode voltage generation. The cost of installation and manufacturing is also crucial in inverter configuration selection. Besides, the power quality, like PQ (active and reactive power) capability, is another important factor since it ensures grid compatibility, optimizes energy conversion and system performance, supports grid stability, and enhances cost-effectiveness. Typically, higher inverter performance entails higher device costs, necessitating a trade-off between power quality and cost that warrants thorough investigation.

2. Legal regulations

For safety, high quality, and standardized operation, legal requirements for PV systems include galvanic isolation, anti-islanding detection, and the need to comply to grid codes and standards defined by committees and governments. Anti-islanding detection is a mechanism for the inverter to halt the feeding of PV power to the grid when the power grid experiences a trip [63]. International standards proposed by committees like the Institute of Electrical and Electronics Engineers (IEEE) form the basis for these requirements, with additional regulations defined by local governments. For instance, in some countries, the use of an isolating transformer in PV systems is mandatory according to local regulations.

Driven by the increasing installed capacity of PV systems and efforts to enhance PV inverters, various inverter topologies have emerged at the practical

level. Recently, these topologies have been categorized based on the connection or arrangement of PV modules as string, central, multi-string, and AC module PV inverters [66]. These topologies can be utilized in both single-phase and three-phase power systems.

- **String PV inverters**

Typically, multiple PV modules are connected in series to generate a string voltage ranging from 150 to 450V, producing a few kilowatts of output power. The most common method of connecting PV panels to the power system is through string PV inverters.

Common-mode (CM) noise is a significant concern in photovoltaic (PV) inverters. This issue primarily arises from the high-frequency switching of inverters, which generates fluctuating voltages and currents relative to ground. High levels of CM noise can result in various problems, including safety risks due to elevated leakage currents, electromagnetic interference (EMI), degradation of power quality, and erroneous ground detection. To mitigate these common-mode issues, PV inverter manufacturers and system designers employ several strategies. Figure 2.5 compares and analyses six types of typical and modified PV inverters.

Firstly, filters can be installed on either the DC or AC side to attenuate high-frequency components and limit leakage currents. For instance, the H-bridge configuration paired with a grid-frequency transformer, as shown in Figure 2.5 (a), is a straightforward solution in which the transformer provides both voltage step-up and galvanic isolation for the PV system. The galvanic isolation offered by the transformer enables the use of unipolar pulse-width modulation (PWM) control without the risk of leakage currents. However, employing a bulky low-frequency (LF) transformer can reduce circuit power density and efficiency. An

alternative approach involves incorporating a high-frequency transformer on the DC side, as illustrated in Figure 2.5 (b). This configuration significantly improves inverter size and system power density compared to the LF transformer topology [64].

Secondly, common-mode chokes can be installed on power lines to mitigate common-mode currents. Figure 2.5 (c) demonstrates the use of geometrically symmetrical filters on both the grid phase and neutral lines, effectively suppressing common-mode currents and reducing the conversion of common-mode (CM) noise to differential-mode (DM) noise [65].

Thirdly, adopting inverter topologies [66] specifically designed to minimise common-mode effects, such as H6 topologies (Figure 2.5 (d)), 5-level NPC configurations (Figure 2.5 (e) [67]), and 3-level half-bridge NPC (Figure 2.5 (f)), can help reduce leakage currents and EMI. Additionally, advanced control techniques, including various PWM modulation schemes, can further diminish common-mode voltage and its adverse effects.

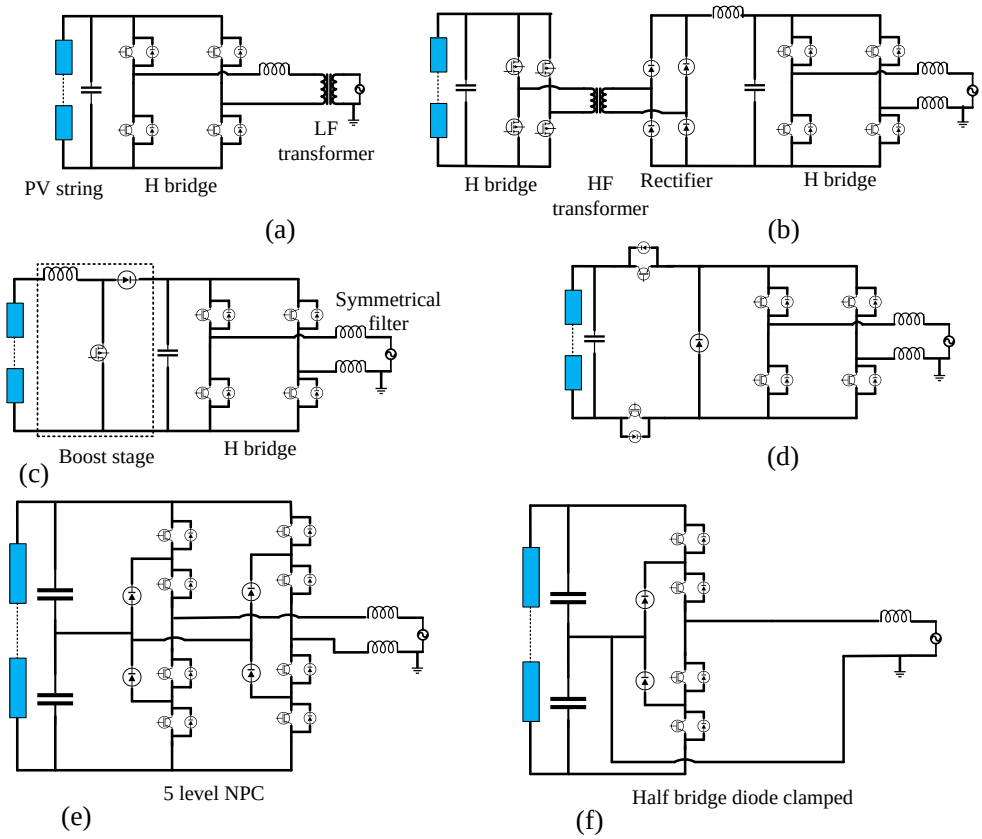

Figure 2.5. 6 types of common string PV inverters.

- **Central PV inverters**

Central PV inverter topologies involve connecting a large number of PV modules to a single inverter, as illustrated in Figure 2.6. Typically, central PV inverter topologies are utilized in large-scale PV system applications ranging from a few hundred kilowatts to several megawatts. The maximum power point tracking (MPPT) function for the PV output power is achieved by the central inverters.

The 2-level voltage source inverter (2L-VSI), depicted in Figure 2.6 (a), is a fundamental topology of central inverters that comprises three half-bridge converters. It is connected to the medium voltage 3-phase grid (A, B, C phase) through a voltage step-up transformer. Additionally, similar to the string PV inverter topologies, other topologies are also utilized in central inverters, such as

the neutral point clamped (NPC) and T-type inverters, shown in Figure 2.6 (b) and (c) respectively [59].

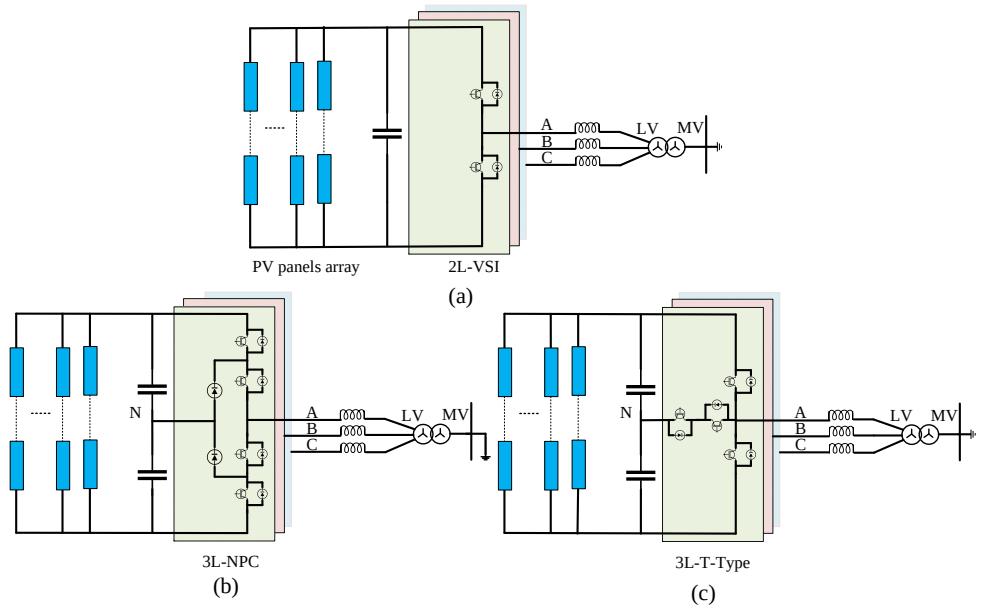

Figure 2.6. 3 examples of central inverters.

- **Muti-string PV inverter**

Multi-string PV inverter topologies combine features of central and string PV inverters to ensure each PV string sector operates at its maximum power point (MPP) by incorporating a DC-DC stage for each PV string. Figure 2.7 illustrates two examples of multiple string PV inverters. The basic multi-string inverter utilizes the 2-level voltage source inverter (2L-VSI) topology shown in Figure 2.7 (a), which can also be replaced by a 3-level neutral point clamped (3L-NPC) converter to improve efficiency. The multi-string inverter with galvanic isolation using a high-frequency (HF) transformer shown in Figure 2.7 (b), is a more complex topology and results in higher losses. Typically, all topologies with two-stage conversion can be used to construct multi-string inverters [69].

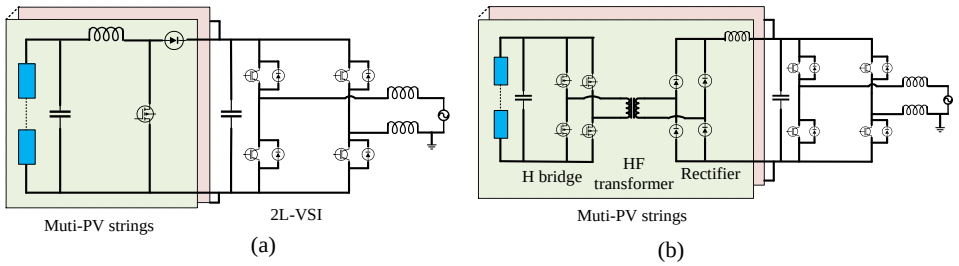

Figure 2.7. Two examples of muti-string PV inverters.

- **AC module PV inverters**

Each PV module is connected to a micro-inverter, resulting in what is known as an AC module inverter. The primary advantage of these topologies is the elimination of losses caused by I-V and MPP mismatch between PV modules, leading to higher energy yield. However, the use of multiple inverters significantly increases costs compared to conventional inverters. Two examples of AC module inverters are depicted in Figure 2.8.Figure 2.8 (a) shows an AC module inverter employing an H-bridge with a high-frequency (HF) transformer [70]. This topology is a commercial module offered by Enecsys company. Figure 2.8 (b) depicts an inverter embedded with interleaved flyback converters [71], which is another commercial module offered by Siemens.

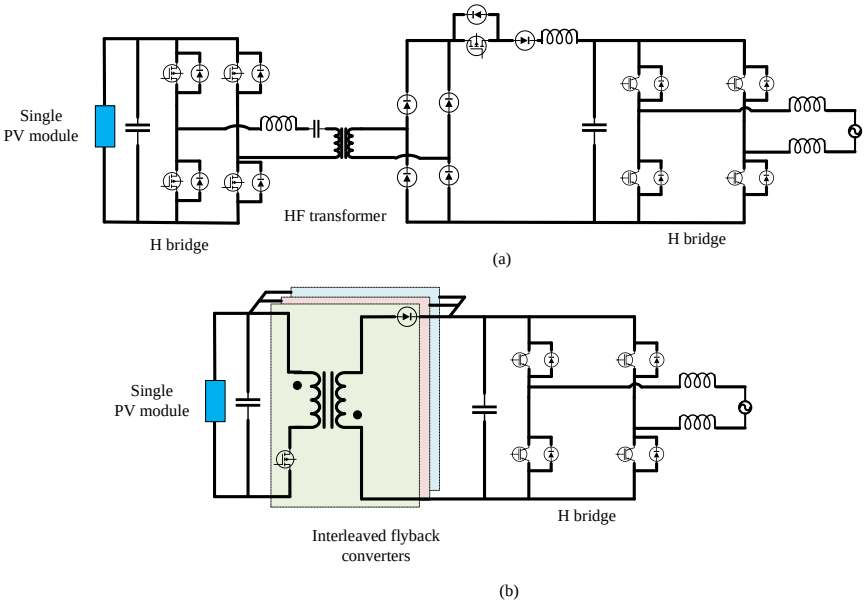

Figure 2.8. Two examples of AC module PV inverters.

2.3.2. Review of bidirectional DC/DC converter topologies for battery energy storage

According to the investigation [72], lithium-ion batteries are a more suitable and cost-effective choice for low and medium-sized stationary energy storage applications. In this PhD thesis, a DC/DC converter equipped with bidirectional power flow capability is necessary for power and energy exchange between the batteries and the rest of the system. Bidirectional DC/DC converters (BDCs) can typically be classified into non-isolated and isolated types [73].

- **Non-isolated BDCs**

Generally, by replacing diodes with controllable switches in conventional buck/boost DC/DC converters, a unidirectional DC/DC converter gains the ability for reverse power flow. Non-isolated bidirectional DC/DC converters (BDCs) do not use high-frequency transformers, leading to improvements in system efficiency, power/energy density, and cost [74]. This section reviews some basic converter topologies, the single phase, soft switching, and interleaved converters, shown in Figure 2.9.

The most common non-isolated BDC topology made of two half-bridge inverter structures consists of a boost (power/inductor current from right to left) combined with a buck converter (power/inductor current left to right) connected in parallel as depicted in Figure 2.9 (a) [75]. It can operate in either buck or boost mode to transfer power in both directions by selecting the proper switching patterns. However, its main drawback is the battery voltage needs to be lower than DC bus voltage and the relatively high value of the output inductor needed to limit current ripple, which may damage batteries.

Building upon the half-bridge BDC topology, the flexible 4-quadrant converter is proposed as shown in Figure 2.9 [76], which has the capability of

voltage step-up and step-down operations in both directions which means voltage transfer ratio is no longer a limitation. However, more switches lead to higher losses and a more complicated control algorithm.

The modified BDC topology (Figure 2.9 (c)) with a tapped inductor has a higher step-up ratio and lower step-down ratio, resulting in higher power density due to an additional inductor magnetically coupled with the original inductor on the same core [77].

To further improve the efficiency of hard-switching converters, soft-switching technologies such as zero-voltage-transition (ZVT) and zero-current-transition (ZCT) are introduced into non-isolated topologies. Figure 2.9 (d) [78] shows a type of ZVT converter with an auxiliary circuit ensuring that the main switches work at ZVT mode regardless of the converter's operation mode.

In high-power applications, interleaved converters have become more attractive. Several (N) half bridges are connected in parallel, as shown in Figure 2.9 (e) [79]. With the phase shift (360°/N) of control for each leg, the output current has minor ripple due to ripple cancellation, facilitating optimized inductor design. Interleaving converters achieve high efficiency in a wider power range and fault tolerance by splitting the current into N paths, leading to lower conduction losses whilst switching losses can be reduced at light loads by deactivating some of the channels.

Based on the conventional interleaved converter, the modified multi-stage interleaved converter topology is explored to minimize filter size/weight by coupling inductors, as depicted in Figure 2.9 (f) [80]. The high mutual inductance of the coupled inductor provides high impedance to the differential mode (DM) PWM voltage to suppress the DM component. However, an extra

inductor (stage 3) may be installed to limit common-mode (CM) noise by supplementing the lack of leakage inductance derived from previous stage coupled inductors (stage 2).

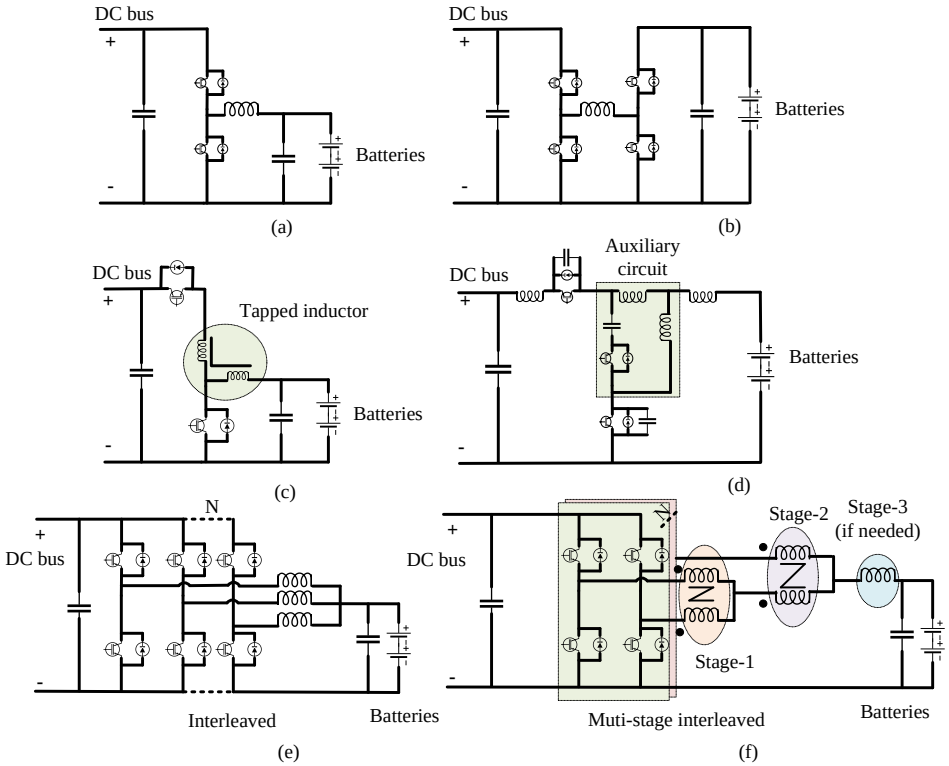

Figure 2.9. Examples of various non-isolated BDCs.

- **Isolated BDCs**

Galvanic isolation between multiple sources is a requirement mandated by many standards and regulations for safety, noise reduction, and proper operation of system protection devices [73]. Compared to LF transformers, HF transformers offer higher power density, lighter weight, and lower noise without compromising efficiency, cost, and reliability. Therefore, replacing traditional LF transformers with HF transformers is considered more attractive in the next-generation power conversion field. HF transformers also serve as key high-frequency link devices in isolated bidirectional DC/DC converters (BDCs).

Most traditional isolated unidirectional DC/DC converters (UDCs) can be used to compose isolated BDCs [81]. For instance, a half-bridge-push-pull

isolated BDC is composed of a half-bridge UDC and a push-pull UDC, with the half-bridge and push-pull structures capable of withstanding high- and low-source voltages. Isolated BDC topologies are diverse, with the transmission power capability typically proportional to the number of switches. Isolated BDCs can range from the simplest dual-switch topology to more complex structures [81], as shown in Figure 2.10.

The simplest hard-switched BDC topology is shown in Figure 2.10 (a) [82], which operates in both forward and reverse modes. By replacing the diode in the standard flyback converter, bidirectional power flow capability is enabled. However, the relatively high switching frequency required to reduce the weight and size of inductors can increase switching losses.

Figure 2.10 (b) shows a five-switch isolated BDC with zero-voltage switching (ZVS) characteristics for all switches achieved through phase shift control strategy [83]. The optimized performance and increased efficiency of the converter are observed when coupled inductors are applied.

Leandro proposed a full-bridge-forward DC/DC converter, as depicted in Figure 2.10 (c) [84], for interfacing the energy storage system with the DC bus in a residential microgrid application. Since the energy storage system in a residential microgrid is infrequently used due to low electric energy supply interruption indices, there are extended periods of inactivity between successive operations. This allows the charging process to take place over a longer duration. Consequently, the converter is designed to deliver higher power during discharging compared to charging. The full-bridge structure is not employed during the charging process. A passive clamping circuit is added to avoid voltage

spikes caused by interruption of current through the transformer leakage inductance during the turn-off process of the forward converter active switch.

K. Wang [85] achieved an extremely high voltage conversion ratio from a 12 V battery stack to a 288 V DC bus through a six-switch BDC converter as depicted in Figure 2.10 (d). A clamping circuit is added to limit the peak voltage of the battery stack, enabling the use of smaller voltage-rated switches on the low voltage side.

Figure 2.10 (e) shows a typical eight-switch dual full-bridge BDC topology proposed in [86] commonly seen in hybrid electric vehicles and energy storage systems. However, this topology exhibits high switching losses in high-power scale applications. Enhanced topologies have been developed, such as the dual full bridge BDC with auxiliary circuit shown in Figure 2.10 (f) as proposed in [87], which enables the low voltage side switches to operate under soft-commutating conditions during boost mode operation.

Figure 2.10 (g) [88] illustrates the topology of a dual active bridge (DAB) converter. This converter employs a compact high-frequency transformer and operates at a high switching frequency, enabling it to achieve high power density. This design significantly reduces the overall size and weight while providing galvanic isolation. However, the DAB converter requires a greater number of active components, which increases its cost. Additionally, it exhibits high input and output current ripple, and its soft-switching capability is limited to a specific operational range.

Figure 2.10 (h) [89] depicts a bidirectional isolated LLC converter. The LLC converter maintains soft switching across a wide load range, ensuring consistent efficiency and performance. This converter features two distinct resonant frequencies: one determined by the resonant inductor L_r and resonant capacitor C_r, and another

determined by the combination of the magnetizing inductance L_m, resonant inductor L_r, and resonant capacitor C_r.

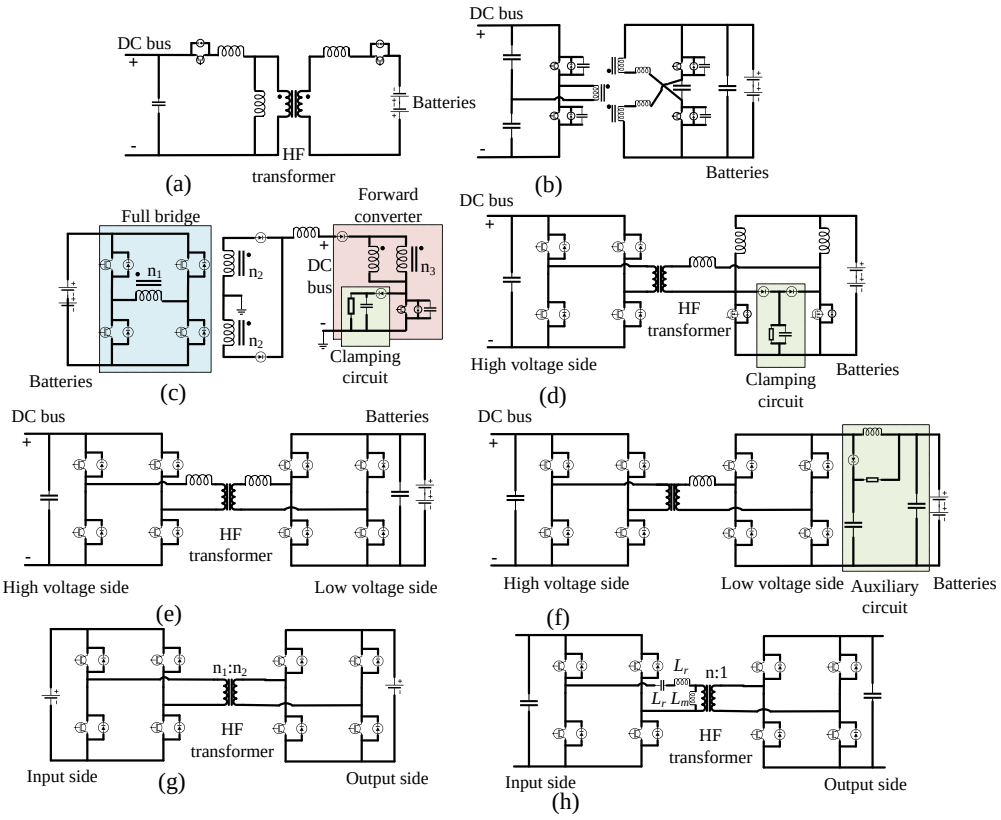

Figure 2.10. Examples of isolated BDCs.

2.3.3. Review of electric water heater system

According to the investigation conducted by the Association of Plumbing & Heating Contractors Ltd [91], there are currently three main types of water heater systems in use in the UK: open vented, unvented, and instantaneous, as depicted in Figure 2.11.

1. Open vented water heater system: This system comprises a hot water cylinder, a cold-water storage cistern (tank), special pipework, and a boiler (heat resistor) serving as the heat source. The hot water cylinder is typically located in an airing cupboard or loft space. Cold water is heated by the gas boiler and stored in the cylinder until needed. The electric heater resistor is integrated in the tank. This system is characterized by its reliance on gravity to deliver hot water to taps and showers.

2. Unvented water heater system: Unlike the open vented system, the unvented system utilizes only one water tank to heat cold water and provide hot water to various outlets. Due to the higher working pressure, an expansion vessel is integrated to remove pressure from the system. An additional immersion heater serves as a backup to the main boiler or is used independently, especially during summer months, ensuring continuous hot water supply in case of boiler failure or when higher power heating is required.

3. Instantaneous water heater system: This system is designed to rapidly heat cold water to a usable temperature without the need for water storage. In the electric version, cold water is typically heated using a high-power immersion heater or other similar electric heating method. The hot water is then immediately diverted to the hot water outlets throughout the home.

Each of these water heater systems has its own advantages and considerations, depending on factors such as household size, water usage patterns, and available space for installation.

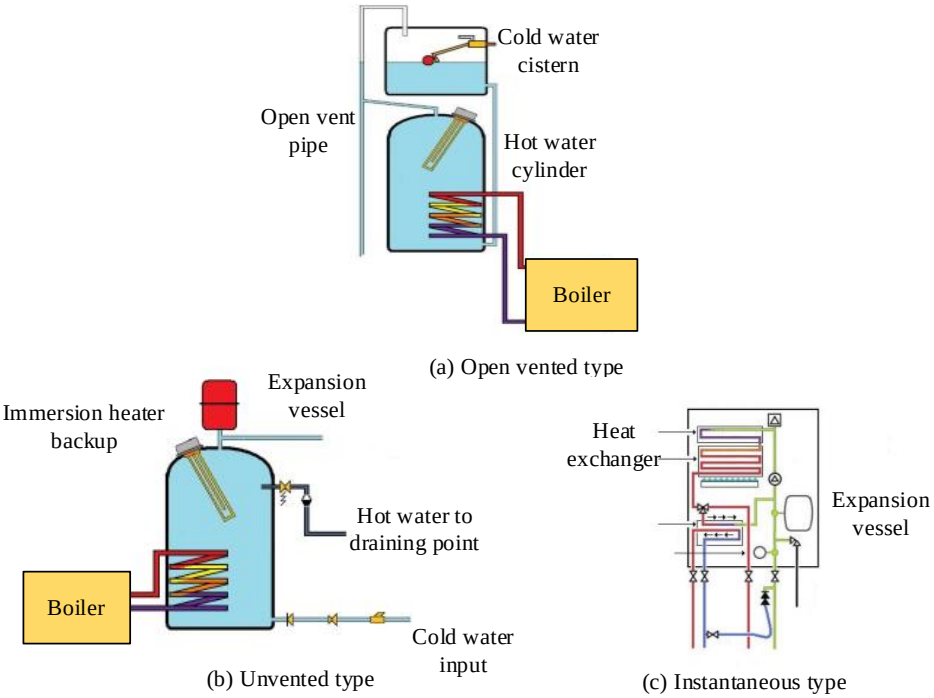

Figure 2.11. The diagram of three types of electric water heater system.

To improve the PV self-consumption rate, a controllable water heater working in conjunction with a hot water cylinder to implement heat energy storage has become a very popular approach, proven also by the availability of commercial products on the market [92] [93]. A conventional electric hot water boiler consists of a plunger resistive heating element connected to the AC supply via a thermostat to control the temperature inside the hot water [94]. To meet higher power demands, additional resistive loads (such as three resistors) are connected in parallel, with each resistor requiring a dedicated switch for control. However, this needs a more complex control to connect all 3 resistors to the AC supply usually using electronic sensing and relays. It is possible to control the connection/disconnection of each of the three resistors individually which would offer a possibility to vary the dissipated power in steps but this would involve an even more complex control circuitry but these products need to be specially programmed to initiate the process of heating of water when excess PV power is available and even then, will frequently result in mismatch between dissipated power into the water cylinder and PV excess with only a minimal financial gain for the user.

When a solid-state switch is turned on at points other than the zero-crossing of the voltage waveform, it can generate voltage spikes. To smooth the AC voltage, two methods are employed. (i) Zero-Crossing Switching: At the zero-crossing point of an AC waveform, the voltage is at or near zero. Switching the relay at this point minimizes abrupt voltage changes, significantly reducing the likelihood of arcing across relay contacts. While this method effectively minimizes voltage distortion, as illustrated in Figure 2.12, it has certain limitations. Relay can only be switched on at grid voltage zero-crossing points,

and power dissipation is calculated based on integer multiples of the half-cycle voltage [95]. This can lead to mismatches between the energy produced by PV generation and the energy consumed, which may be recorded differently by utility energy meters, potentially affecting billing accuracy. (ii) Pulse Width Modulation (PWM): This method uses semiconductor switches to connect and disconnect the heating element multiple times within each cycle [96]. To smooth the resulting voltage and current fluctuations, filtering components are required.

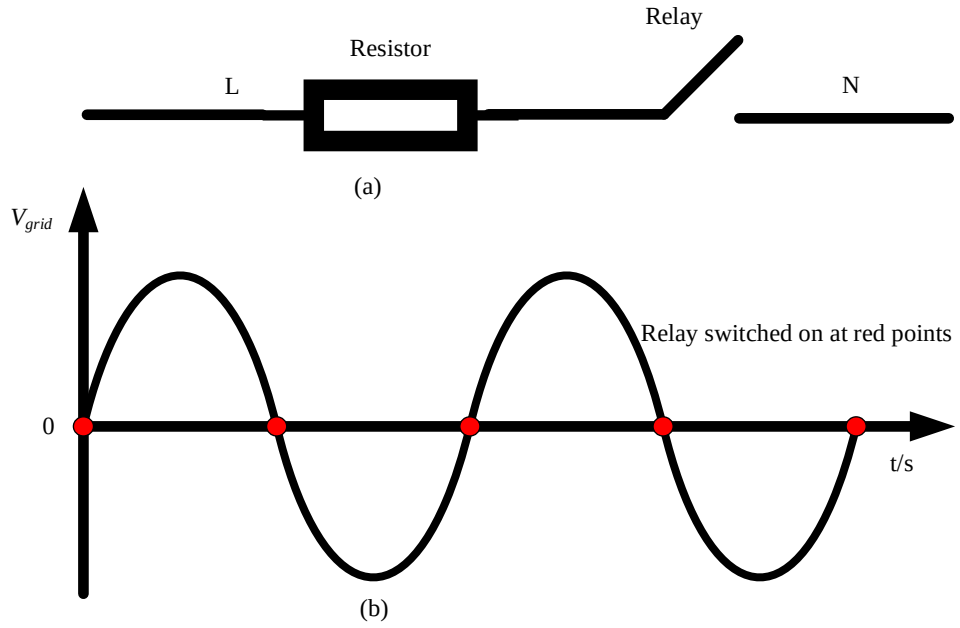

Figure 2.12. The demonstration of relay control electric water heater. (a) The topology of relay control circuit. (b) Relay switched on at voltage zero-crossing points.

2.4. Review of optimal components sizing procedure

In a domestic PV power system, ensuring reliability and cost-effectiveness is crucial for benefiting inhabitants and promoting the growth of household PV energy adoption. Apart from selecting appropriate system technologies and topologies, sizing system components plays a significant role in enhancing the overall system efficiency and cost-effectiveness. Numerous efforts have been made to explore how to optimize system components in various applications [97]-[99]. These studies typically outline an optimization procedure, as depicted in Figure 2.13, which includes input data, constraints, control and energy management strategies, optimization methodologies, and objective functions.

It's evident that various factors influence the optimization results. To select the optimal size for system components, each part of the sizing procedure needs to be analysed in detail in the following sections. This analysis typically involves considering factors such as system constraints, economic considerations, and performance objectives. By thoroughly examining these factors, it becomes possible to optimize the sizing of system components to meet the specific requirements of the domestic PV power system while maximizing cost-effectiveness and efficiency.

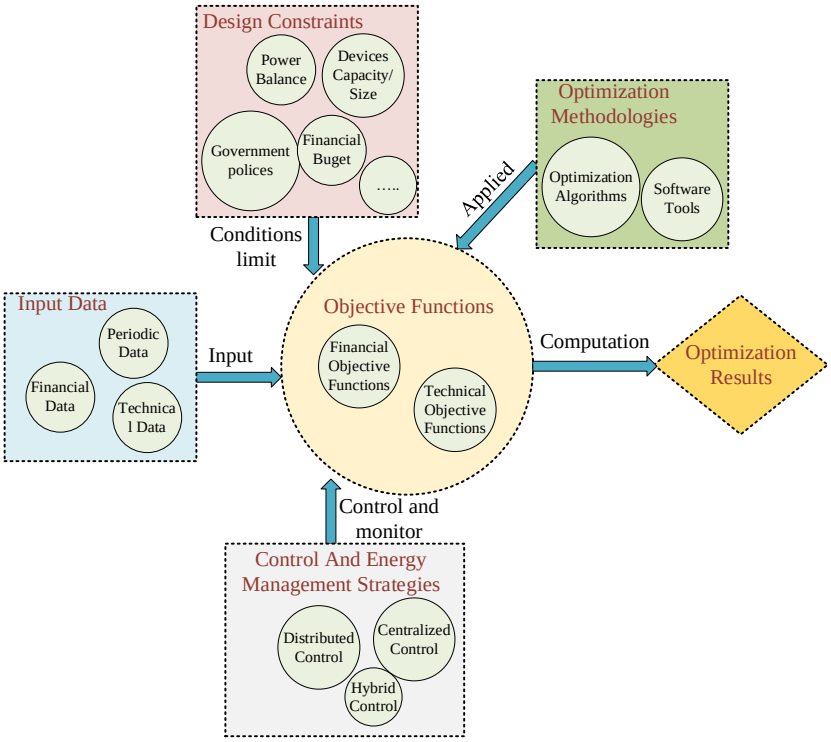

Figure 2.13. The summary of sizing optimization procedure diagram [97]-[99].

2.4.1. Input data

In the sizing process, various data categories are essential for making informed decisions and optimizing the design of the PV power system. These categories include financial data, periodic data, and technical data [98], each sourced from different documents and resources:

- **Financial data**

Financial data encompasses costs associated with device purchase and installation, as well as electricity price rates. These costs can vary significantly depending on factors such as location, government policies, and energy subsidies. Device purchase and installation costs may differ between countries and regions due to varying market conditions and regulations. Similarly, grid electricity prices can vary based on usage periods, tariffs, and government policies.

- **Periodic data**

Periodic data includes information that varies over time, such as load consumption, solar irradiation, and ambient temperature changes. This data can

be collected at various intervals, ranging from short periods (minutes, hours, and days) to longer periods (months and years). Accurate and reliable periodic data is crucial for modelling system performance and optimizing system sizing. In cases where real-time data is lacking, probabilistic methods can be employed to generate realistic data.

- **Technical data**

Technical data is derived from the technical specifications of system components and operational regulations. For example, PV cells and battery cells manufactured using different materials and technologies exhibit varying characteristics such as lifetime and efficiency. Additionally, factors such as ambient temperature can impact the performance of devices and may need to be considered during system design and optimization.

By incorporating these three categories of data into the sizing process, it becomes possible to conduct comprehensive analyses and make informed decisions regarding the design and optimization of the domestic PV power system.

2.4.2. Design constraints

In ensuring the safety and reliability of the power system, several design constraints are employed for the selection and operation of system components. These constraints help maintain a balanced and stable system operation while adhering to regulatory requirements and practical limitations:

1. Power Balance: The power balance between sources (such as PV panels) and loads (such as household appliances) is a crucial design constraint [100]. In distributed networks, there may be restrictions on the level of exported/imported power based on local grid regulations. Domestic PV applications are often

constrained by factors such as available roof space for PV panel installation, roof shapes, and surrounding obstructions like trees, which can impact PV generation capacity.

2. Battery Constraints: Constraints associated with batteries include parameters such as state of charge (SOC) and charging/discharging rates [101]. Managing these constraints effectively ensures the optimal utilization and longevity of battery storage systems.

3. Financial Budget: Financial considerations play a significant role in system optimization. Higher installation capacities of PV panels, larger battery storage capacities, and increased power sizes of converters can impose a heavier financial burden on residents [102]. Optimizing system components within budgetary constraints is essential for ensuring cost-effectiveness and affordability.

4. Device Ratings: The maximum power transferred by circuit devices such as converters and inductors must remain below their rated power levels to avoid hazards and damage. Adhering to device ratings ensures safe and reliable operation of the power system under various operating conditions.

By considering and adhering to these design constraints, engineers and designers can develop PV power systems that are safe, reliable, and cost-effective, meeting both technical requirements and financial considerations.

2.4.3. Control and energy management strategies

Proper control of a PV household power system with multiple energy sources (such as solar and grid) and energy storage (including batteries and a power electronic water heater system) is essential for achieving system reliability and improving operational efficiency. Maintaining a balance between energy/power

generation and consumption is critical, necessitating an effective power control or energy management strategy that allocates active and reactive power appropriately across the system components while ensuring that voltage and frequency levels are maintained within specified ranges.

The energy management structure typically consists of three main approaches: centralized control, distributed control, and hybrid control, as depicted in Figure 2.14 [103].

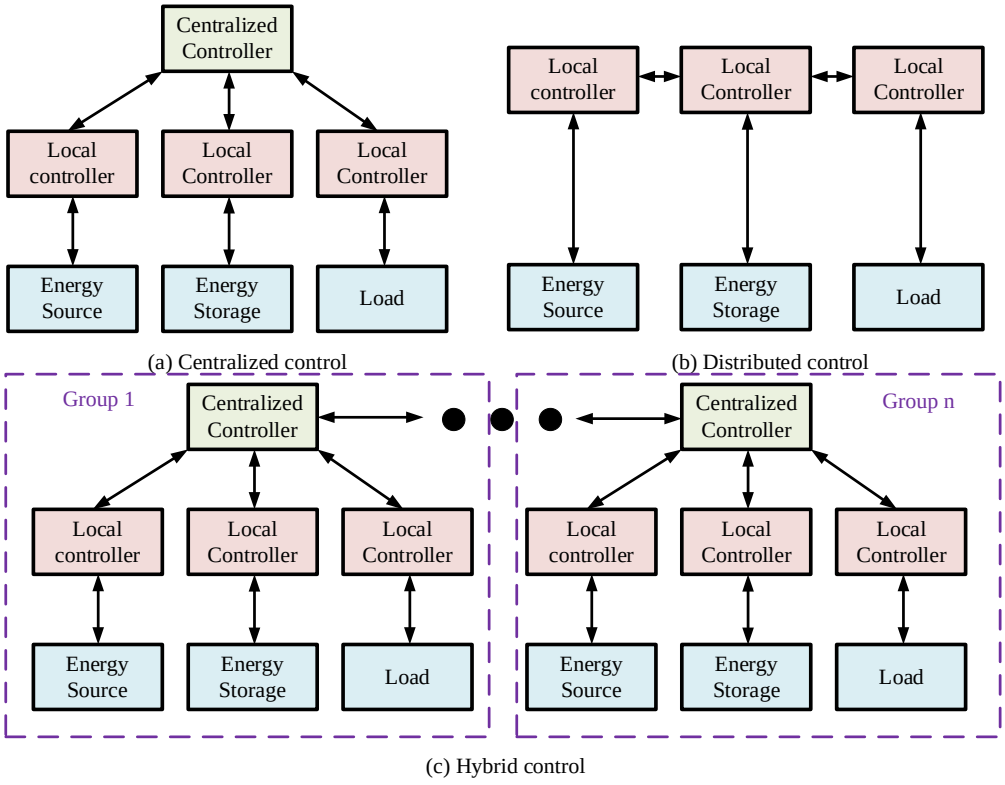

Figure 2.14. The summary of the schematic diagram of centralized, distributed and hybrid control.

- **Centralized control**

In centralized control [104][105], a single centralized controller is responsible for managing the operation of the entire power system. This controller receives data from various system components and makes decisions regarding power generation, distribution, and consumption based on predefined algorithms and control strategies. Centralized control offers a high level of coordination and optimization but may be less flexible and scalable than other approaches.

- **Distributed control**

Distributed control involves delegating control functions to individual components or subsystems within the power system. Each component or subsystem has its own controller, which makes localized decisions based on local measurements and communication with neighbouring components. Distributed control offers greater flexibility and scalability compared to centralized control, as it can adapt to changes in system conditions and accommodate diverse operating scenarios more effectively [106][107].

- **Hybrid control (the combination of centralized and distributed)**

Hybrid control combines elements of both centralized and distributed control approaches, leveraging the strengths of each to achieve optimal system performance [108]. In a hybrid control system, certain control functions may be centralized for coordination and optimization purposes, while others are decentralized to enhance flexibility and responsiveness. Hybrid control allows for a tailored approach that balances the need for centralized oversight with the benefits of distributed decision-making.

2.4.4. Review of optimization methodologies

In this research, the sizing of system components primarily focuses on PV generation, converter power size, and battery stack capacity. While a simple approach to component selection involves oversizing all components to provide a safety margin for system requirements, this method often results in unnecessary waste in terms of device capital costs. To improve cost-effectiveness while meeting design requirements, optimization methodologies can be employed based on available statistical data about generation, load consumption, financial parameters, system reliability, and other specific information [110].

Optimization methodologies aim to streamline computation while addressing the complexity of multi-objective optimization. A variety of optimization algorithms and accessible software tools are available for optimizing component sizes, as analysed in [111]. These optimization algorithms can be broadly categorized into intuitive, numerical, analytical, and intelligent methods [111]. Additionally, the reference [111] demonstrates various analysis software tools that facilitate the optimization process.

By leveraging optimization methodologies and software tools, designers and engineers can systematically optimize the sizing of system components, achieving cost-effective solutions that meet design requirements.

- **Optimization algorithms**

In sizing system components, various methods are employed, each offering different levels of simplicity, accuracy, and computational complexity.

1.Intuitive Methods: These are the simplest methods, often relying on basic equations or the designer's experience to calculate component sizes. For example, the size of the PV array and battery capacity can be determined based on the given load demand profile, without considering the randomness of solar irradiation or the interaction among subsystems [112]. However, intuitive methods tend to oversize or undersize systems due to the use of average monthly or annual data, leading to either high investment costs or suboptimal system designs.

2.Numerical Methods: Numerical methods use simulation-based programs to compute component sizes based on varying time-scale input data, typically ranging from minutes to hours. These methods employ the rule of energy balance to propose optimal sizes at the hourly input data level [113]- [115]. While numerical methods require heavy computations, they improve accuracy by using

smaller time intervals as input. They can be categorized into stochastic numerical methods, which use smaller time interval data, and deterministic numerical methods, which use daily averaged data.

3.Analytic Methods: Analytic methods are simple and accurate, utilizing empirical relationships and mathematical models to achieve optimal sizing of the entire system. However, computing coefficients for these equations can be challenging as they are site-specific [116]. For example, sizing PV systems can be conducted using empirical relationships and fitting functions derived from time-series solar radiation data.

4. Intelligent Methods: Intelligent methods, such as artificial neural networks, genetic algorithms, and fuzzy logic, are employed to solve complex optimization problems. These methods can handle incomplete data while exhibiting high accuracy and reliability, albeit requiring significant computational resources. Artificial intelligence methods [118] efficiently overcome the nonlinearities of optimization models and can be used to achieve global optimum results with relative computational simplicity. For instance, genetic algorithms [119] have been applied to optimally size stand-alone hybrid solar-wind systems.

Each method has its advantages and limitations, and the choice depends on the specific requirements of the project, including accuracy, computational resources, and available data.

- **Software tools**

Software tools play a crucial role in analysing operations, conducting techno-economic assessments, and optimizing the sizing of PV and energy storage systems. Several simulation software tools are available for sizing PV power systems, including HOMER, RETScreen, HYBRID2, iHOGA, as well as simulation environments like TRNSYS and MATLAB.

1. HOMER: It is a sophisticated software platform designed to facilitate the design, optimization, and simulation of microgrids and distributed energy systems. Initially developed at the National Renewable Energy Laboratory (NREL) in the United States, HOMER (Hybrid Optimization of Multiple Energy Resources) is now widely used across industries for assessing energy systems that integrate various energy sources such as solar, wind, batteries, and conventional generators. The key features include: (1) **Hybrid system optimization**: HOMER models hybrid systems that combine renewable and non-renewable energy sources. It evaluates the technical and economic feasibility of integrating these sources. (2) **Simulation and sensitivity analysis**: HOMER simulates the operation of energy systems over a defined time period (e.g., a year) and performs sensitivity analysis to examine how uncertainties like fuel prices, load demand, and resource availability affect performance. (3) **Economic Analysis**: The software calculates key financial metrics such as net present cost (NPC), levelized cost of energy (LCOE), and return on investment (ROI), enabling stakeholders to make informed investment decisions. (4) **Flexibility**: HOMER supports various configurations, from isolated off-grid systems to grid-connected setups, allowing users to design tailored solutions for different environments and objectives.

2. RETScreen: It is a powerful clean energy management software tool developed by the Government of Canada, under the leadership of Natural Resources Canada (NRCan). It assists decision-makers in assessing the financial viability, energy performance, and environmental impact of energy projects. RETScreen is widely recognized for its user-friendly interface and robust

analytical capabilities, making it a global standard in clean energy feasibility analysis.

3. HYBRID2 is an advanced simulation tool designed for modelling and analysing hybrid renewable energy systems. Developed by the University of Massachusetts at Amherst Renewable Energy Research Laboratory, HYBRID2 provides detailed insights into the performance and economics of systems that integrate multiple energy sources, such as wind turbines, solar panels, diesel generators, and battery storage. HYBRID2 emphasizes system performance under real-world conditions by incorporating stochastic (random) variability in its modelling, making it particularly suited for assessing hybrid systems in dynamic environments.

4. iHOGA (Intelligent Hybrid Optimization by Genetic Algorithms) is a specialized software tool developed for the design, simulation, and optimization of hybrid renewable energy systems. Created by the University of Zaragoza, Spain, iHOGA leverages advanced genetic algorithms to optimize system performance and minimize costs. Its ability to handle complex, multi-objective optimization problems makes it a preferred choice for researchers and engineers aiming to design cost-effective and environmentally friendly hybrid systems.

5. TRNSYS (Transient System Simulation Tool) is a versatile software suite for simulating and analysing transient systems, particularly in the fields of energy systems and building performance. Developed originally by the Solar Energy Laboratory at the University of Wisconsin-Madison, TRNSYS is widely used in academic research, engineering design, and consulting for projects involving renewable energy systems, HVAC systems, and building energy performance. It uses a modular approach, with each component (e.g., solar

panels, wind turbines, HVAC units, or buildings) represented as a separate "Type." Users can combine these components to create custom system configurations. TRNSYS also allows users to modify or create new components using programming languages like Fortran or Python, ensuring flexibility for specialized applications.

6. MATLAB: MATLAB (short for Matrix Laboratory) is a high-level programming environment and computing platform developed by MathWorks. It is widely used for numerical computation, data analysis, visualization, and algorithm development. MATLAB provides a comprehensive, flexible, and efficient environment for conducting economic analyses of renewable energy systems. Its ability to combine technical simulations with financial modelling, optimize system performance, and present results clearly makes it an invaluable tool for researchers, engineers, and policymakers.

A review conducted by Sunada Sinha and S.S. Chandel [120] assessed 19 software tools, highlighting their main features, status, and areas for further research. This review provided valuable insights for researchers to select and utilize the appropriate software tool for their needs. For example, HOMER is widely used and user-friendly, offering quick prefeasibility, optimization, and sensitivity analysis across various system configurations. However, it has limitations such as allowing only a single objective function, disregarding battery depth of discharge, intra-hour variability, and variations in bus voltage.

Additionally, software environments like MATLAB-Simulink provide the flexibility to develop personalized optimization tools tailored to specific research requirements [121]. By leveraging such platforms, researchers can

create customized optimization tools that address specific system constraints and objectives.

While simulation software tools offer valuable capabilities for system analysis and optimization, it is essential to consider their limitations and areas for improvement. Continued research and development efforts are necessary to enhance the functionality and accuracy of these tools, ensuring they meet the evolving needs of the renewable energy industry.

2.4.5. Objective functions

Objective functions play a crucial role in optimization algorithms, guiding them to either maximize or minimize specific criteria. These functions can vary depending on the goals of the optimization problem and can be categorized into financial and technical objectives [98].

- **Financial objective functions**

Financial objective functions focus on the economic aspects of the renewable energy system. They typically involve factors such as the purchase, installation, and maintenance costs of devices, as well as potential profits generated from selling excess energy back to the grid [122]. Subsidies and feed-in tariffs may also be considered to evaluate the overall cost-effectiveness of the system over its lifetime.

- **Technical objective functions**

Technical objective functions are concerned with system performance and efficiency. These functions may include metrics such as the grid-independence rate, total losses during system operation, dumped energy, and carbon emissions. The grid-independence rate reflects the system's ability to meet its energy demands without relying heavily on the utility grid. Efficiency can be assessed by calculating the ratio of total losses to total imported energy. Dumped energy

refers to unused renewable energy that could not be stored or utilized efficiently [123]. Lastly, carbon emissions are evaluated to understand the environmental impact of the system, particularly in comparison to grid-supplied energy generated from fossil fuels.

By defining and optimizing these objective functions, researchers and system designers can effectively evaluate and improve the performance, cost-effectiveness, and environmental sustainability of renewable energy systems.

2.5. Challenges for the household PV power system optimization

Indeed, optimizing PV and energy storage systems for residential use poses several challenges, as outlined in recent papers [98][111]. Firstly, local weather conditions significantly impact PV generation, while household loads profiles vary among different houses/families. Obtaining accurate data for each house on an annual scale is challenging, often leading to the use of hourly or daily data for simulations. Developing accurate simulation methods that balance simplicity and accuracy is crucial for optimization.

Secondly, the characteristics of electronic devices vary between brands, making it difficult to create accurate models for power system components. Models must closely reflect real-world performance while balancing calculation time and convergence [124].

Thirdly, varying electricity price tariffs necessitate new energy management strategies to optimize power flow among subsystems. For instance, charging batteries during low-price periods and discharging during high-price periods requires determining optimal pre-charge levels.

Moreover, changes in government policies, local regulations, and electricity prices can significantly impact optimal system designs. Reductions or cancellations of renewable energy subsidies may increase costs for residents, requiring adjustments to financial objective functions.

Addressing these challenges requires interdisciplinary approaches, incorporating advanced modelling techniques, innovative energy management strategies, and adaptive optimization algorithms. By overcoming these hurdles, researchers can develop more robust and cost-effective residential PV and energy storage systems.

2.6. The gap aiming to be improved by this study

The author highlights several gaps and areas for improvement in existing research on residential PV power systems. Firstly, most studies focus on one PV application scenario without comparing them to other scenarios, limiting the understanding of system performance across different setups. Secondly, the impacts of various parameters, such as charging/discharging patterns, and technical constraints, on optimization results are not thoroughly explored. Therefore, in this thesis, four types of PV application scenarios are compared.

Additionally, the water tank serves the purpose of storing excess PV energy and a novel power electronic system to provide fine-tuned voltage to the power resistor is accommodated. This innovative power electronic system is designed to allow the transfer of the excess PV energy into the hot water cylinder for storage and to cancel/compensate for current harmonics produced by nonlinear household appliances to result in a harmonic free current drawn from the grid. The effectiveness of this system is verified through an experimental prototype.

To address these gaps, the author built a comprehensive residential PV power system integrated with battery storage and the power electronic water heater experimental prototype. This system will undergo experimental and simulation validation to verify its performance and effectiveness.

By addressing these areas, the research aims to provide valuable insights into the optimization and design of residential PV power systems with integrated energy storage, facilitating their widespread adoption and enhancing their efficiency and cost-effectiveness.

2.7. Summary

In this chapter, the topology of the entire PV power system is outlined, starting with a thorough review of each subsystem: energy storage technologies, PV inverters, battery chargers, and electric water heaters. Following this, the optimization procedure for proposing a cost-effective household PV power system is detailed, including a step-by-step description of each stage. Lastly, the research identifies gaps that this thesis aims to address.

Chapter 3: Sizing procedure for the domestic PV energy application

The main objective of this chapter is to design a procedure to determine and optimize a cost-effective domestic photovoltaic (PV) power system with embedded storage. The optimization components include the capacity of PV generation (peak output power), converter rated power which in this study may be smaller than the peak power of PV string and the energy capacity of the battery. A rule-based approach integrated with numerical data processing (called as hybrid method) is employed to formulate the optimization problem. To identify which scenario can provide the maximum financial benefits, a case study of a domestic PV power system situated in UK and evaluated under different operation scenarios is researched in this thesis. The case study utilizes the PV generation and load consumption dataset, the electricity tariff input, the power loss models of the converter and battery, and a thermal model of the hot water tank to produce the optimized component selection results.

In this chapter, each scenario is first described, followed by presentation of the input data collection. Then, the power loss models for the battery and converters, as well as the thermal model of the hot water tank, are estimated. Finally, the optimization objective functions (the financial benefits and PV utilization rate) are presented to produce the optimal design results for the study case.

3.1. Common limitations for all scenarios/cases

There are some system limitations considered for all scenarios/study cases, as follow:

- All examined scenarios consider a **British domestic grid-connected power system**. In this study, the PV generation and loads consumption profiles are collected from the CREST demand model version 2.2 [125] which is established and validated by the Loughborough University. It is an integrated thermal-electrical demand model based on a bottom-up activity-based structure, using stochastic programming techniques to represent dwelling diversity, producing calibrated and validated output profiles at high-resolution. More details can be seen in Appendix A. Thus, any findings may not be applicable to systems outside the UK or to standalone power systems, although the design principles and procedures could be extrapolated if a representative input dataset would be available
- The design methodology is used for **the single residential house case only**, and the results are not representative for commercial or public facilities, like supermarkets, schools, and hospitals, etc, although with a representative input dataset and application specific rules, it should be possible to extend the findings also to these cases.
- Typically, the **DC/DC converter** implementing the maximum power point tracking (MPPT) function is designed with a hard limit for the maximum current it can draw from the PV string and a given voltage range for both the PV string and the inverter DC link which means that indirectly the power is also limited. The DC/DC converter for the MPPT control is not optimised in this thesis.

- The **PV inverter** assuming it delivers power to a constant AC voltage grid, is limited by its rated power.
- **The roof surface for domestic PV installation capacity** is limited. To expand PV installation capacity, permission is needed from the Distribution Network Operator (DNO) for residential PV systems with export power over 3.6 kW. However, this aspect is not considered in this study.
- **The demand side management** concept is not applied in the study. Hence, the everyday habits of occupants remain unchanged. Instead, dedicated energy management strategies or energy storage technologies are employed to satisfy the electricity consumption behaviour of residents.
- **The only available renewable energy source is the solar energy** which is produced from the roof-top PV panels. The electrical power grid is used only in last instance when the battery and the hot water tank are fully charged, or electricity is imported when PV power and battery energy are not available.
- **Batteries and hot water tank** are considered as the energy storage devices in this study. As the most developed energy storage technology, batteries are widely used in renewable energy storage applications, including at the residential level. Additionally, hot water tanks are commonly used to store hot water for household use. The water in the tank can be heated by PV-generated electricity, grid electricity, or natural gas.

- This study considers only the **lithium-ion battery** as the only considered battery energy storage technology.
- The **Economy-7** is the only ToU (time of use) tariff applied in this study. It is a pricing plan that distinguishes between peak and off-peak hours for electricity use. This plan is designed to encourage consumers to use electricity during times when it is more abundant and cheaper. In the future it is expected that more complex ToU tariff schemes will be developed, or the prices may be changing more dynamically as a result of excess large-scale renewables.
- The size of the **hot water tank** is predetermined and selected to accommodate the number of occupants in a single household: 86 liters for 2 occupants, 111 liters for 3 occupants, and 161 liters for 5 occupants.
- **Any subsidy or financial support** from the public or government is ignored in this study since the future of new similar projects will likely not benefit from any government incentives.
- **The excess PV energy sold to the grid via the feed-in tariff is not considered in this study**. There are several reasons for this: 1) Policy effects: The UK government cancelled electricity feed-in tariff scheme for the new built PV household applications in 2019 [126]. Instead, the price of electricity sold into grid depends on the market which causes the returns more unpredictable. 2) The grid capacity constraints: The grid has a limited capacity to handle power inflows, especially for distributed grid. the curtailment of PV generation may be necessary to avoid overloading the grid. 3) The grid balancing requirements: Grid operators need to balance supply and demand in real-time. During periods of low demand

and high PV generation, curtailment helps maintain this balance and ensures a stable and reliable electricity supply. 4) Market conditions: The price of electricity sold to the grid is often significantly lower than the price of electricity purchased from the grid, making selling excess PV energy less attractive. For example, according to the Ofgem data [127], in the early of 2024, the feed-in tariff is about 7.14 p/kWh while the average price of electricity bought from the grid is 24.5 p/kWh. 5) Additional energy meter needed: An extra energy meter is needed to record how much energy sold which increases the capital cost. 6) Energy storage system applied: Energy storage can help mitigate PV generation curtailment.

- The effects of **DC bus voltage variations and grid frequency fluctuations** on the optimization are not considered.
- In this study, the main energy losses considered are the losses associated with **converters and battery Ohm losses**. Transmission losses caused by line distribution resistance are excluded due to the relatively short transmission distances involved. For converter losses, simplified energy loss models are used, including standby losses, switching losses and conduction losses, magnetic losses, and copper losses. Regarding battery losses, only Ohmic losses caused by the battery charging/discharging are considered.

3.2. Steps of the optimal sizing procedure

The detailed steps of the optimization procedure are illustrated in Figure 3.1. These include:

1. Identification of Study Scenarios/Cases: This step involves identifying the different scenarios or cases to be studied. It includes defining the aims and objectives, power system topology structure, power flow, action priority, and any additional constraints necessary to meet the requirements and specifications.

2. Input Data Collection: Input data is primarily collected from CREST model, websites and current research materials.

3. Modelling of System Components: Models for each system component are built. For each device model, constraints such as power and voltage limits and efficiency are derived from technical datasheets and design requirements.

4. Definition of Objective Functions: The objective functions are defined to encompass both technical and financial aspects of the system.

5. Monitoring and Analysis: The proper functioning of each study case is validated by monitoring and analysing the outcomes.

6. Programming and Simulation: Optimization codes are programmed, and simulations are processed on the MATLAB platform. In the study case, this step provides optimised results for customers to purchase a specific set of PV panels, battery stacks, and converters to achieve the financial benefits.

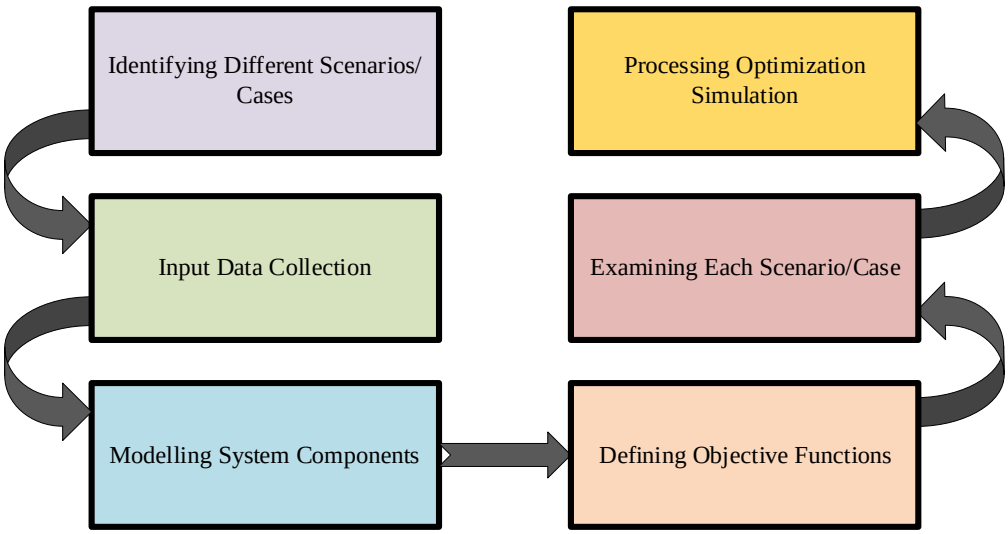

Figure 3.1. Steps of the optimal sizing procedure.

3.3. Identifying different study scenarios/cases

The initial capital investment in devices, a system fixed cost (like installation fee) and the cost of electricity from the utility grid are the main financial cost for end-users when solar energy is applied at the domestic level. This study investigates four scenarios:

1. PV Self-Consumption Scenario: In this scenario, the focus is on using PV-generated electricity directly for household consumption, while the hot water energy consumption is not considered here.

2. PV-Battery Storage System Scenario: This scenario examines the use of a battery storage system alongside the PV system to store excess PV energy for later use or the PV generation is limited if the battery is fully charged.

3. PV-Power Electronic Water Heater System Scenario: This scenario involves using PV-generated electricity to power an electronic water heater during peak hours, while the grid electricity can be used to heat water in the water tank during off-peak hours.

4. PV-Battery-Power Electronic Water Heater System Scenario: This scenario combines PV generation, battery storage of a smaller size than that in scenario 2, and a power electronic water heater to maximize financial benefits.

Each scenario has some common and specific constraints, specifications, and requirements. To quantify the financial benefits of each scenario for a single household, the detail of each scenario is described individually.

3.3.1. PV self-consumption scenario

Due to the closure of the electricity feed-in tariffs scheme for newly built PV household applications by the UK government in 2019, which was paying the prosumer households significantly more for the kWh exported in the grid, it is more economically convenient for the generated PV energy to be consumed locally by household load in this scenario and minimise exports by matching the size of the PV system with the load profile.

a) The aim of this scenario

The main aim of this scenario is to optimize the size of PV generation (peak PV power output) and PV inverter rated power size to build a cost-effective domestic PV power system.

b) Basic structure and power flow

The system block diagram of this power system scenario is shown in Figure 3.2. It consists of PV panels, DC/DC boost stage (not optimised in this thesis), and PV inverter. The PV panels are interfaced with grid through the DC/DC boost stage and PV inverter. The DC/DC boost stage is applied for extracting maximum power point (MPP) of PV generation or outputting a specific power [128] [129] to satisfy the household loads consumption. As the interface port between DC bus and AC grid, the PV inverter transfers the PV power to the house loads and synchronized with power grid. However, due to the randomness

of PV generation especially in countries like UK where cloud cover changes very dynamically during the day, and the custom variations of end-user electricity consumption, the PV generation sometimes can only supply a proportion of loads demand where the remaining power deficit of loads demand can be imported from grid. Commonly, there are two essential parameters used to describe the characteristics of this scenario: self-consumption rate and self-sufficiency rate [130]. The self-consumption rate (also called PV utilization rate in this thesis) is the self-consumed part relative to the total production while the self-sufficiency rate is the degree to which the on-site generation is sufficient to fulfil the energy needs of the building. In this thesis, the PV utilization rate for one week is calculated to evaluate how much of PV energy is consumed.

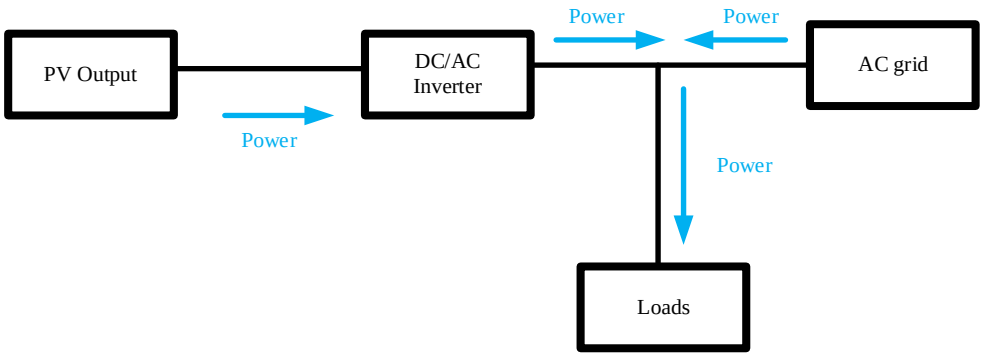

Figure 3.2. The schematic diagram of residential PV self-consumption scenario.

c) Constraints

Additionally, given that feed-in tariffs are significantly lower than the grid electricity price, it is preferable to store excess PV energy in a battery stack or water tank rather than selling it to the grid once the load demand is met. Thus, in this thesis, excess PV energy is considered to be consumed by loads, stored in a battery or water tank, or curtailed (which should happen rarely).

To align with other scenarios, there is no energy storage device, and no PV energy is sold to the grid in this scenario. The only constraint limiting the PV power transmission capability is the rated power of the PV inverter.

1. Converter power rating: There are two converters that are considered in this scenario: the DC/DC boost converter that performs MPPT and the PV inverter delivering the DC power to the AC grid. However, due to varying conditions such as imperfect inclination of the roof, cloud movements, sunlight irradiation, and temperature changes, the output power of PV panels rarely reaches its peak power. This can lead to inefficiencies, which happen when a larger rated converter processes lower power levels but also has financial implications since the larger rated power converter costs more. In this study, only the PV inverter rated power is subject to optimization, while the power of the DC/DC boost and MPPT stage is always selected to match the PV panels' peak output power level to always be able to capture all PV power generation.

2. Relative Sizes of PV Generation and Load Demand: The PV self-consumption rate (PV utilization rate) is not proportional to PV generated energy/power. As PV power generation increases relative to demand, the self-consumption rate tends to decrease, even when the total PV energy produced is high. This is because there are more instances when PV production exceeds immediate household demand, leading to potential excess PV generation that cannot be utilized without storage leading to PV excess power to be exported to grid or lost. Therefore, the PV peak power generation should be designed in close connection to the actual power demand profile.

3. Time Resolution: In many studies, discrete data series of average power generation and demand are used as input data for optimization, typically hourly values. Low-resolution data tends to overestimate self-consumption, as transient mismatches between generation and loads are averaged out and not be captured [131]. Therefore, optimal time resolution of the input data should be considered.

3.3.2. PV-battery energy storage scenario

A significant limitation to improving the residential PV self-consumption rate is the power mismatch between load demand and PV generation. Two methods are commonly used to enhance the PV self-consumption rate: energy storage and load management. Energy storage devices can store excess PV power and energy making possible for loads to use stored PV energy in periods of time with no PV power availability, while load management can shift the timing of load power/energy use to periods when PV generation is sufficient. This combination helps to better match power and energy PV production with load consumption, thereby enhancing the PV self-consumption rate and reducing reliance on grid electricity.

In this scenario, a lithium-ion battery is used as the preferred energy storage device. The battery can store energy from excess PV power generation (daytime) or purchased from the grid during night/low off-peak tariff periods. This stored energy can then be released to supply household loads when needed during peak time, thereby improving the PV utilization rate or lowering electricity costs.

a) The aims of this scenario

The main aim of this scenario is to optimize three key components: PV generation capacity (peak power of PV string), PV inverter rated power, and lithium-ion battery stack stored energy rating. This optimization is focused on maximizing the economic profits of the domestic PV-battery power system. By efficiently sizing these components, the system aims to minimize grid electricity purchases during peak tariff periods and enhance overall economic benefits for the household, such as highest return for lowest investment by maximizing the savings on the electricity bills.

b) Basic structure and power flow

The schematic diagram of this scenario is depicted in Figure 3.3. Building upon the residential PV system shown in Figure 3.2, an additional battery energy storage system is integrated, consisting of a bidirectional DC/DC converter connecting the battery stack to the DC link of the PV inverter. Here is how the system operates:

1. Daytime Operation:

1) PV generation initially supplies power to meet part or full household load consumption.

2) Any surplus PV power not immediately consumed by loads is stored in the battery stack.

3) The battery can discharge stored energy to cover PV-load power deficit during periods when PV generation reduces or to meet additional household load power demand, as needed.

2. Grid Interaction:

If the combined PV-battery system cannot fully meet household energy demands, any shortfall is supplemented by importing grid electricity.

3. Off-Peak Charging:

During off-peak hours when electricity tariffs are lower, the battery stack can be recharged to a preset state of charge (SOC) level. This stored energy is then available for use early next day during peak tariff periods, before PV generation rises to a suitable level to facilitate more energy cost savings.

4. PV Generation Control:

The PV generation is primarily used to meet the load demand. Any excess PV generation is then stored in the battery stack, which can be used when PV generation is insufficient to meet the load consumption during peak hours.

Finally, if the load demand is met and the battery stack is fully charged, the PV generation is curtailed.

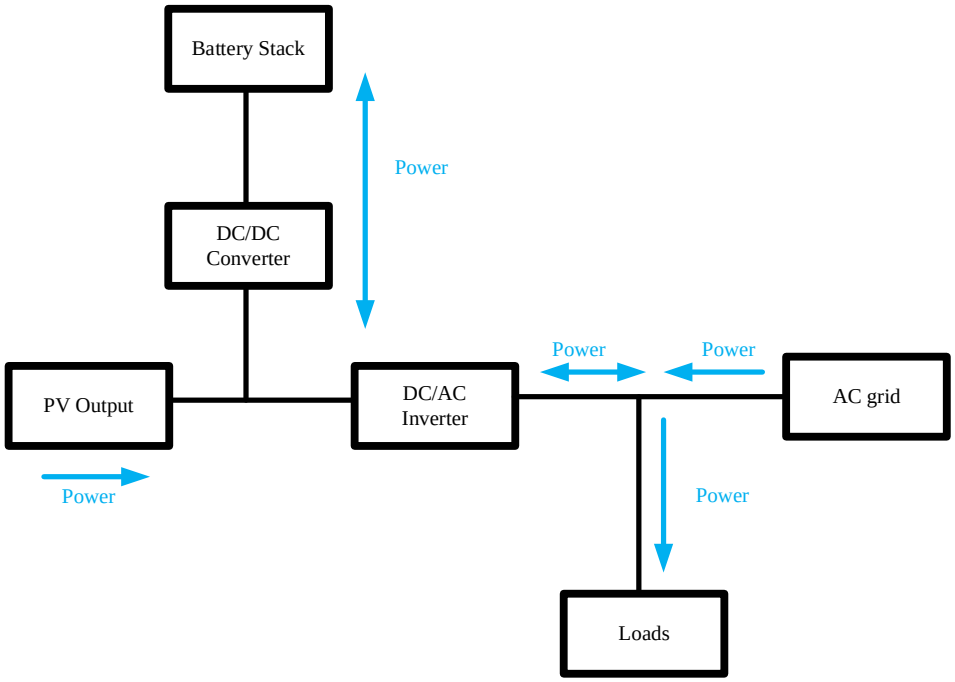

Figure 3.3. The schematic diagram of residential PV-battery power system.

c) Constraints

Based on the constraints in the only PV self-consumption scenario, the extra constraints caused by battery energy storage system are proposed in this scenario.

1) The maximum current rating of bidirectional DC/DC converter and the stack voltage range. The bidirectional DC/DC converter has a hard limit for the maximum battery current that it can process which in conjunction with a given voltage range, will limit the power flow between DC bus and battery stack.

2) The battery charging and discharging current rates and the state of charge (SOC). To avoid damaging the battery or reducing its lifetime, the battery asymmetric charging and discharging current (typically I_{charge}=0.5-2 C; $I_{discharge}$=1-5 C) [132] is always limited. In many types of batteries, the full energy stored in the battery cannot be fully used without causing serious and irreparable damage to the battery. As battery SOC depends on the actual battery

stack voltage and nominal capacity in amp-hours, the relative capacity will be used which represents the percentage of actual capacity (Ah) relative to the nominal Ah of the battery.

These constraints are pivotal in designing and implementing a battery energy storage system that optimizes self-consumption of PV-generated electricity while ensuring the longevity and reliability of the storage system.

3.3.3. PV-power electronic water heater power system scenario

Domestic water heating represents a significant portion of total household electricity consumption that places considerable strain on the utility grid. This is primarily due to high power demands and the unpredictable nature of hot water usage patterns among users. Therefore, storing surplus PV energy in a hot water cylinder proves to be a crucial and effective strategy whilst requiring negligible investment.

a) The aims of this scenario

In this study, the primary objective of the scenario is to optimize PV generation, PV inverter power size and determine the optimal power size for the converter used to adjust the power dissipation of the electric water heater. The overarching goal is to maximize financial benefits through increased self-utilization of solar energy. Key aspects of this aim include:

1. Selecting the Optimal Converter Power Rating: The converter, which interfaces the PV system and the electric water heater resistor, plays a crucial role in managing this additional power flow. Determining the optimal converter power size involves balancing factors such as the maximum power output of the PV system, the heating requirements of the water heater, and power control accuracy.

2. Maximizing Economic Benefits: By effectively utilizing PV-generated electricity to meet the heating demands of the water heater, economic benefits are realized in several ways:

1) Reduced Energy Costs: Minimizing the purchase of grid electricity at peak tariff by using solar energy directly for heating water reduces utility bills.

2) Increased Self-Consumption: Enhancing the self-consumption rate of PV energy ensures that more of the electricity generated on-site is utilized rather than exported for a low rate or wasted.

3) Improve Return on Investment (ROI): Increased use of solar energy can improve the return on investment in PV systems, as savings from reduced energy costs accumulate over time.

b) Basic structure and power flow

In the schematic diagram illustrated in Figure 3.4, A converter is connected to the DC bus to transfer excess PV power to the electric heating resistor. This allows for effective utilization of surplus PV energy to heat water in the tank without incurring energy losses from the PV inverter.

Research conducted by P. Armstrong [133] highlighted significant energy losses in both stainless steel and copper hot water tanks over a 24-hour period, despite the use of effective thermal insulation materials. Moreover, the introduction of cold water into the tank during hot water to replace usage of hot water can cause a rapid drop in water temperature. Therefore, managing heat loss dissipation from the tank and heating water during periods of excess PV energy availability are crucial to maintain adequate hot water temperatures.

In this study, the operational strategy involves:

1. Off-Peak Hours Operation: During off-peak hours, cheap grid electricity is directed via the PV inverter to main DC link and from there via the DC/DC

converter into the heating resistor, to heat the water in the cylinder. This ensures cost effective use of grid energy when electricity rates are lower.

2. Peak Hours Operation: Excess PV generated power available during peak sunlight hours is stored in the water tank. This surplus energy is utilized to heat or ensure the temperature of the water for usage, reducing reliance on grid-supplied electricity and maximizing self-consumption of PV generated energy.

3. Priority on PV Energy Utilization: The power electronic water heater system prioritizes consuming excess PV energy over limiting PV generation through the DC/DC MPPT boost stage. This approach minimizes energy waste and ensures more efficient utilization of available PV power.

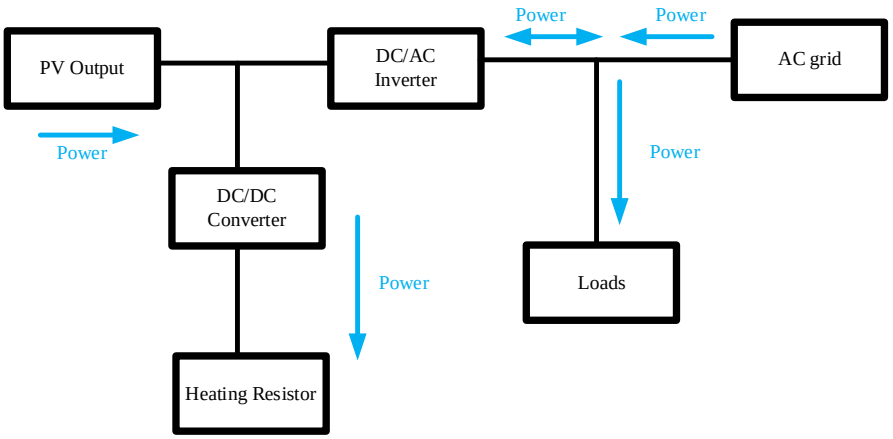

Figure 3.4. The schematic diagram of residential PV power electronic water heater system.

c) Constraints

In this scenario, compared to a basic PV self-consumption setup, several additional constraints are imposed by the power electronic water heater system. These constraints are critical for ensuring effective operation and maximizing the benefits of integrating PV energy with water heating:

1. Converter Power Size: The DC/DC converter plays a critical role in regulating the power delivered to the electric heater for water heating. In this thesis, the power rating of this converter is designed to be equal to or greater than the power rating of the PV inverter. This is because a significant amount of

grid electricity is used to heat water from a low temperature (15°C) to a high temperature (90°C) in the water cylinder at low electricity tariffs during off-peak hours. Thus, the power transmission capability of the PV inverter can be adequately utilized. Additionally, commercial electric heaters typically integrate three individual resistors, allowing for easy adjustment of the power rating of the electric heater to match the power rating of the converter. Therefore, the power rating of electric heater is not considered in this thesis.

2. Daily Hot Water Consumption and Tank Size: The amount of hot water used daily depends on the number of occupants in the household. This parameter directly influences the required size of the hot water tank. For instance, households with 2, 3, or 5 occupants would require different hot water tank size to meet their daily hot water demands satisfactorily. This consideration is crucial for sizing the system appropriately to avoid shortages or installing excess capacity that has higher losses.

3. Safety Regulations: Installation and operation of the hot water cylinder must comply with safety regulations. For instance, there are specific requirements, such as limiting the maximum temperature of stored water to 90°C to prevent boiling. This allows the cold inlet water to be heated at a lower grid electricity price during off-peak hours. Consequently, as hot water is consumed and cold water is injected, the temperature of the hot water in the tank will remain high and not drop prematurely, ensuring appropriate hot water usage for an extended period. Adherence to these regulations ensures safe operation and reduces risks associated with exploitation of hot water systems.

4. Cylinder Insulation Specifications: The thermal insulation of the hot water tank's external cladding significantly affects heat dissipation. The material and

thickness of the insulation determine the heat loss coefficient of the tank. This parameter is crucial for accurately modelling the thermal performance of the water heater system and optimizing energy efficiency.

In summary, these additional constraints highlight the complexity involved in integrating PV powered water heating systems. Addressing these factors effectively ensures that the power electronic water heater system operates effectively, maximizes self-consumption of PV energy, complies with safety standards, and meets the hot water demands of the household economically. Each constraint plays a crucial role in designing and implementing a sustainable and effective PV-integrated water heating solution tailored to specific household requirements.

3.3.4. PV-battery-power electronic water heater power system scenario

Since the hot water tank only stores PV energy as thermal energy and cannot release electric energy to satisfy the household loads demand during evenings and that a high investment cost applies to installing a large battery stack, the combination of a smaller battery energy storage and thermal storage in the household PV system may be a more economically convenient compared with implementing only one of energy storage technologies individually.

Here are some key reasons why this combined approach can be beneficial:

1. Complementary Storage Capabilities: Batteries excel at directly storing and discharging electric energy for immediate use, providing flexibility in managing fluctuating PV generation and household electricity demand. On the other hand, thermal storage in a hot water tank stores surplus PV energy in the form of heated water, which can only be used later for domestic hot water needs. This complementary storage capability allows for a more balanced and efficient

utilization of excess PV energy throughout the day. However, the hot water energy consumption is necessary each day. To avoid using the expensive peak hours grid electricity, the hot water tank has the priority than battery stack to consume excess PV energy or off-peak grid electricity.

2. Cost Effectiveness: Battery storage systems often entail high upfront costs due to the high price of batteries and associated electronics. By integrating thermal storage with batteries, the overall investment cost can be optimized as the size of the battery is reduced. Thermal storage systems, like hot water tanks, are typically more cost-effective per unit of stored energy compared to batteries and many households have these already installed. This combined approach allows for leveraging the cost-effectiveness of thermal storage while still benefiting from the flexibility and rapid response of battery storage.

3. Maximized Self-Consumption: The integration of both storage technologies enhances the PV system's ability to maximize self-consumption of generated solar energy. To ensure the appropriate hot water temperature for usage, a significant amount of energy is used to heat the water in the tank, especially when hot water is consumed, and cold water is injected during peak hours. To ensure sufficient PV energy to heat water, excess PV energy can first be stored in the hot water tank during sunny periods. If the hot water temperature in the water tank reaches the upper limit (80°C -90°C), the surplus PV power can then be directed to the battery storage system. This ensures that as much solar energy as possible is consumed on-site, as it is produced or later via the battery, reducing reliance on peak priced grid electricity and potentially lowering overall energy costs.

3. Environmental Benefits: Utilizing both battery and thermal storage in a PV system contributes to reducing overall carbon emissions by maximizing the use of renewable energy. By storing and utilizing solar energy more effectively, households can decrease their reliance on fossil fuel-based electricity from the grid.

In conclusion, integrating battery energy storage with thermal storage in a household equipped with a PV power generation system, offers a holistic approach that balances cost-effectiveness, operational efficiency, and sustainability. This combined strategy can maximize the economic benefits of PV self-consumption while addressing the challenges of energy storage and load management in residential settings.

a) The aims of this scenario

In this scenario, the aim is to optimize the integration of PV generation, thermal energy storage (in the form of a hot water tank), and battery energy storage within a power electronic water heater system. The goal is to design an economical household PV power system that maximizes self-consumption of PV generation and its economic benefits. Here are the key components that are optimized in this integrated approach:

1. PV Generation peak power: The goal is to maximize the financial benefits of the entire system while ensure a high PV utilization rate.

2. PV Inverter Power rating: The PV inverter converts DC electricity as extracted by the DC/DC MPPT controller from the PV panels into AC electricity usable by household appliances and the grid. Optimizing the inverter power rating ensures efficient conversion and utilization of solar energy as larger inverters will operate less efficient at lower powers and smaller inverters will

not deliver enough power to feed loads causing unnecessary import of peak priced electricity.

3. Battery Stack energy rating: The energy rating of the battery storage system determines the amount of energy that can be stored and discharged as needed. It is optimized based on household electricity consumption patterns, and PV generation variability.

4. DC/DC converter power rating of battery stack and water heater: Two different DC/DC converter that regulates the power flow between the PV system, battery storage, and the power electronic water heater system.

b) Basic structure and power flow

The block diagram illustrated in Figure 3.5 depicts an integrated household PV power system that combines PV generation, battery storage, and a power electronic water storage heater system connected at the DC side. Here's a breakdown of the operational strategy and optimization considerations outlined in this scenario:

1. Integration of Components: The system integrates a PV array, a battery storage system, and a power electronic water heater. These components operate together to maximize self-consumption of PV power and the financial benefits.

2. Power and Energy Management:

1) Off-Peak Hours: Both the battery stack and the power electronic water heater system can draw power and energy from the grid during off-peak hours. However, the initial temperature of hot water in the water tank is quite low after a day of hot water consumption. Therefore, the water heater system prioritizes charging during the limited 7 hours of off-peak hours. This ensures that the water heater has sufficient power and energy to meet hot water demand while minimizing grid energy usage during peak times.

2) Peak Hours: During peak solar generation hours, excess PV power is prioritized for heating water in the tank rather than the battery. It ensures that the hot water temperature drop caused by energy losses from the hot water tank, hot water consumption, and cold-water injection can be compensated for first.

3. Optimized Battery Energy Rating: Since excess PV power is primarily used for heating water, the battery stack's required energy rating can be reduced. The hot water tank serves as a buffer for surplus PV power and energy, reducing the reliance on the battery for energy storage during periods of high solar generation. However, the battery stack can be charged at low electricity tariffs during off-peak hours and then release the stored energy to reduce the expensive grid electricity purchased during peak hours. This optimization approach lowers the overall investment cost of the battery storage system while still maintaining system flexibility and resilience.

In conclusion, the integrated approach illustrated in Figure 3.5 optimizes the sizing and operation of a household PV power system by effectively combining PV generation, battery storage, and thermal energy storage for water heating. This strategy enhances energy utilization effectively and reduces electricity costs.

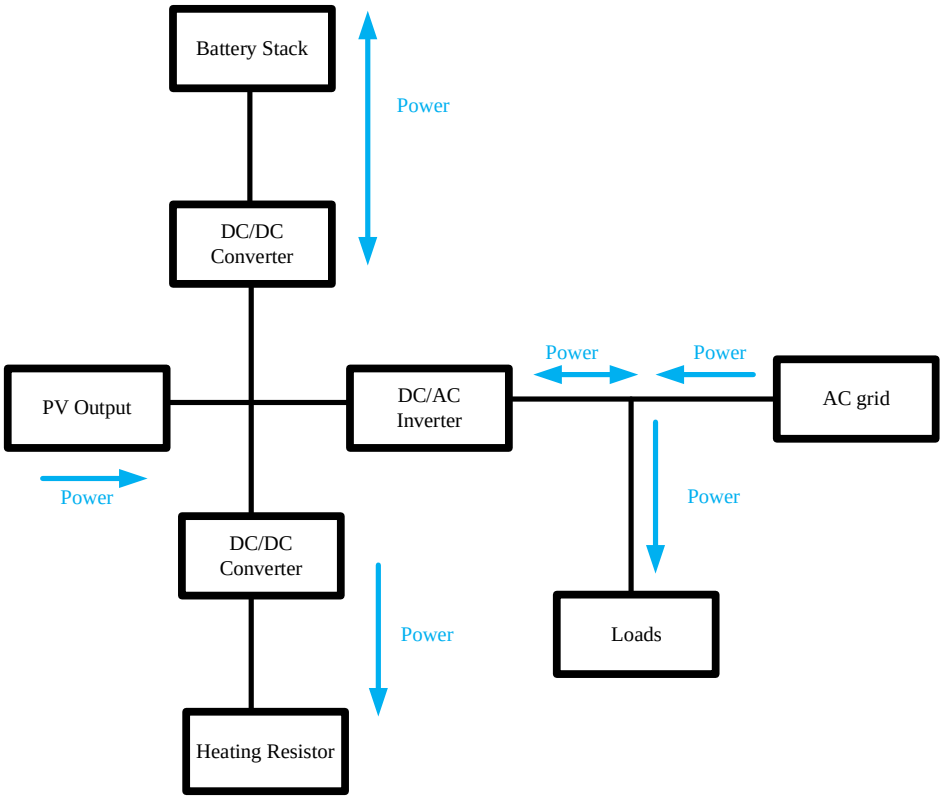

Figure 3.5. The schematic diagram of residential PV-battery and power electronic water heater system.

c) Constraints

Based on the integrated scenario described above, which combines PV generation, battery storage, and a power electronic water heater system, the specific constraints can be categorized into several key areas that build upon the constraints discussed in previous sections 3.3.1, 3.3.2, 3.3.3. More constraints are caused by the power and energy management strategies, such as the charging priority.

3.4. Input data

In this study, the optimization process for the household PV power system integrates the dataset of the PV generation, the household loads demand, the hot water consumption, and ambient temperature profiles. The aim is to demonstrate that an economically optimised system can be determined and designed by considering various factors such as grid electricity price tariffs and the unit prices of devices involved.

3.4.1. Imported PV generation, loads demand, hot water consumption and room space temperature profile

Due to uncertainty about which electric appliances are included in typical household load profiles, particularly whether an electric water heater is included and when it is on or off, the study relies on the CREST demand model version 2.2 [125] to generate realistic household electricity load demands which have been demonstrated to be relevant for this study. This model includes a separate electric water heater energy consumption and provides also PV power generation, hot water consumption, and ambient temperature profiles. For both the PV self-consumption and PV-battery scenarios, a gas boiler is assumed to be providing hot water to ensure uniformity in household load profiles across all scenarios.

The CREST model serves as a foundational tool for modelling UK domestic energy demands within the broader context of urban energy analysis. It incorporates essential components of electrical demand such as lighting and microwave ovens, integrating these in conjunction with an occupant model, PV generation model, and thermal models that include a basic building thermal model, hot water consumption patterns, and the operation of gas boilers. The reliability of the model has been confirmed through validation against three independent datasets [134]-[136].

Given that hot water consumption varies significantly based on the number of occupants in residential settings, the CREST demand model version 2.2 is employed to generate consumption profiles for houses with different occupancies (2, 3, and 5 occupants) located in the East Midlands, UK. Each dataset includes power measurements collected weekly across all seasons (January, April, July, and October), with a high-resolution sampling rate of 1 minute.

3.4.2. Grid electricity price tariffs

In this research, two distinct electricity pricing schemes are under consideration: the standard energy tariff and the Economy-7 tariff. There is a detailed explanation of each:

1. Standard Energy Tariff: Under this tariff, the price per unit of grid electricity (kWh) remains constant throughout the day. There is no differentiation between peak and off-peak hours in terms of pricing. Households pay the same rate for electricity consumed regardless of the time of day.

2. Economy-7 Tariff: This tariff offers cheaper electricity rates during a specified off-peak period, typically seven consecutive hours during the night. However, electricity prices during peak hours are generally higher compared to standard tariffs. The Economy-7 plan allows households to benefit from lower electricity costs during off-peak hours, making it advantageous for energy-intensive activities like washing, EV charging, charging battery stacks and heating the water in the hot water cylinder for next day usage. Besides, to avoid the impact of abnormal energy price increases attributed to the Ukraine war, the study utilizes electricity price tariffs from 2021 instead of 2022. Annual electricity prices from various suppliers [137]-[139] are referenced to calculate

the average electricity price specific to the East Midlands region, as detailed in Table 3.1. Economy-7 tariffs typically offer cheaper rates during off-peak hours but slightly higher rates during peak times compared to standard tariffs. Besides, in 2019, the UK government ended the feed-in tariff scheme for new installations of household PV systems. Instead, the UK government has shifted towards supporting renewable energy through other mechanisms such as smart export guarantees (SEG) or time-of-use tariffs, where homeowners can receive payments for exporting surplus electricity to the grid based on market rates or agreed tariffs with their energy suppliers [140]. However, electricity market fluctuations can impact the economic viability of selling PV energy into the grid, making returns unpredictable. Thus, the electricity sold to grid is not considered in this thesis, and more reasons can be seen in Section 3.1.

This pricing strategy allows the battery stack and water heater system to optimize energy consumption by leveraging cheaper electricity rates during off-peak periods under the Economy-7 tariff even without PV generation. This approach not only helps in reducing household electricity costs but also aligns with energy efficiency goals by encouraging consumption during periods of lower demand on the grid.

Table 3.1. The annual average electricity prices for the standard and Economy-7.

Electricity tariff	Time	2021 Price (p/kWh)	2022 Prices (p/kWh)
Standard rate	All day (0:00-24:00)	19	30
Economy-7	Day (07:00-24:00)	22	35
	Night (0:00-07:00)	11	20

3.4.3. Device price

In this thesis, the financial benefit of the household PV power system is determined by calculating the difference between the savings on electricity bills and the capital investment cost of system components over a specified operational period, which is considered as 10 years [142]. The optimal design

point for component sizing is identified where the system achieves the highest financial benefit, balancing revenue (savings) against the initial system cost. Since the fixed cost does not affect the selection of the maximum financial benefit point for each scenario, a £ 300 (like installation fee of the system, etc.) fixed cost is considered for all scenarios, which is referred from [141] and [142]. Thus, the devices installation and unit price that was used in this study is shown in Table 3.2.

Table 3.2. Device price.

Components	Price
A fixed cost [142]	£ 300
Li-lion battery storage [141]	20 p/Wh
Converter cost [141]	30 p/W
PV cost [143]	70 p/W_{pk}

3.5. Modelling for system components

To ensure optimal sizing of system components within the household PV power system, accurate modelling of each component is crucial.

3.5.1. Modelling converters

In this study, optimizing the ratings of the power electronic converters—specifically the PV inverter, the battery charger (DC/DC converter), and DC/DC converter for the power electronic water heater system—is crucial for maximizing their efficiency and performance. Here is a detailed explanation of how these converters is modelled and integrated into the optimization process:

1. **Power Converter Efficiency and Dependency of Losses with Power Rating:**

The efficiency of each converter impacts the amount of power loss during energy transmission. Power rating specifies the maximum safe power level the converter can handle. Exceeding this rating can lead to inefficiencies and potential damage [145] which means processed power will always be limited to its rating.

2. **Converter power losses**

(1) **Conduction Losses:** These losses occur due to the resistance of the power semiconductor devices (such as MOSFETs, IGBTs, diodes) when they are in their "on" state. This also includes resistive losses in passive components like resistors and wires. In the "on" state of a power semiconductor, the resistance causes power loss. Conduction losses increase with current load, but they are typically lower than switching losses at lower frequencies. (2) **Switching losses** occur during the transition periods when the semiconductor switches between on

and off states. It can be significant at high switching frequencies and during high-current transitions.

(3) **Magnetic losses** occur in inductors and transformers, which are critical components in many power converters. These losses arise due to the magnetic field created by current flowing through the coils. Magnetic losses increase with the operating frequency and size of the core, and are more significant in transformers and inductors. (4) **Copper losses** occur in the windings of inductors, transformers, and other magnetic components. These losses are a result of the resistance of copper windings. These losses are typically a significant portion of total losses in high-current converters, especially at high frequencies.

(5) **Stand-by losses** are the power consumed by the converter when it is not actively supplying power to a load, or when the converter is in an idle state. It includes power losses in the control circuitry, gate drivers, auxiliary power supplies (cooling fans or monitoring circuits), leakage currents, and parasitic elements. It is often a small fraction of the total power, ranging from a few watts in small devices to 1–5% of rated power in large industrial systems.

The total losses of a converter are the sum of all individual loss components, including switching losses, conduction losses, magnetic losses, copper losses, and standby losses [147]. Extensive research has been conducted to evaluate and analyse power losses in converters [146][147]. However, these losses are highly influenced by several factors, such as switching frequency, current magnitude, resistance, and other design and operating conditions.

Table 3.2 provides an overview of the typical percentage contributions of each type of loss in a power converter. These estimates are derived from general

assumptions, typical converter designs, publicly available materials (e.g., research from TI), and evaluations from publicly accessible research studies.

Table 3.2. Typical percentage contribution of each type of loss in a power converter.

Type	Switching losses	Conduction losses	Magnetic losses	Copper losses	Stand-by losses
Percentage of total power losses	30%-60%	10%-30%	5%-20%	5% -15%	1%-5%

3. **Cut-off Power ($P_{cut\text{-}off}$):**

The cut-off power losses in a converter refer to the threshold where power losses become substantial enough to affect the converter's efficiency, performance, or operational limits. For example, standby losses, a type of power-independent loss, become particularly significant during low-power operation, disproportionately reducing the system's overall efficiency. By implementing a cut-off power level, the converter avoids operating in these inefficient low-power conditions, thereby optimizing energy utilization.

In practice, setting an appropriate cut-off power level requires consideration of the converter's design specifications and operational requirements to achieve the best balance between efficiency and operational flexibility.

4. **Power losses model of converters**

To streamline the optimization procedure, the power loss model of the converter should be computationally efficient while accurately capturing the converter's behaviour. Konstantina Panagiotou [144] built a linear model between power losses and power processed. However, as shown in Figure 3.6 (adapted from study [145]), the converter's power loss behaviour remains flat at low power levels but increases progressively as the processed power rises. Therefore, compared with linear model, a quadratic model will have higher accuracy to describe the power losses model, as shown in Equation (3.1). In this

thesis, the converter models used for these three types of converters in this study are built using the fitting parameters a, b, and c. The main limitation of this equation is the processed power should not excess the rated power of converter.

$$y = ax^2 + bx + c \tag{3.1}$$

Where y represents the power loss in [W], x is the actual power [W] processed, and a, b are the coefficients. Especially, c accounts for the standby losses of converter which is power independently. An assumed standby losses 30W [142] is made in this section.

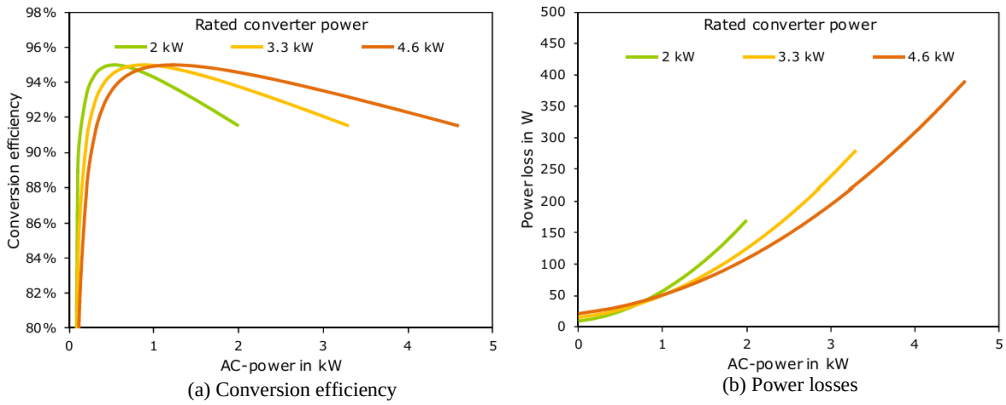

Figure 3.6. Typical efficiency characteristics of bidirectional converter. (a) converter efficiency. (b) converter power losses. (taken from [145])

To build this equation, the amount of converter power losses at different power amount processed should be firstly measured or simulated. Considering different semiconductor IGBT switches utilization in the optimization procedure, the switching power losses and conduction power losses of switches are simulated in the PLECS software for simplicity. The simulation models of these switches are derived from Infineon Technology. The power losses of magnetic device (inductors) and capacitors are directly measured from the lab test setup. The converter setup parameters can be seen in the chapter 5 in Table 5.6. Thus, switches' power losses can be simulated in the software while filter's power losses can be measured in the setup.

This type of converter power losses evaluation method is also used in another research [148]. Compared with conventional power losses calculation method [147], this type of power losses evaluation method significantly reduces the computation when processing optimization procedure in MATLAB.

Five different power sizes of converters (0.52 kW, 1.64 kW, 2.4 kW, 3.5 kW, and 6 kW) are examined to understand their respective behaviours. Based on CREST electricity demand data, the smallest size (0.52 kW) generally meets the power requirements of a single household, while the 1.64 kW converter can cover over 80% of household power needs. The 2.4 kW and 3.5 kW sizes are sufficient for nearly all household power demands (excluding peak power situations), whereas the largest size (6 kW) is deployed for highest peak power scenarios.

Thus, through the curve fitting of converter power losses (DC/DC converter, inverter, and converter for electric water heater), the coefficients (a, b, c) of the equation (3.1) are shown in Table 3.3. To validate the accuracy of this model methods, one example of 1.6 kW DC/AC inverter is analysed through the comparison between data collected (simulation and experiment) and fitting curve, as shown in Figure 3.7. At low power levels, the collected data closely matches the curve fitting results. As the processed power increases, the difference between the curve fitting and the collected data remains minimal. Therefore, when calculating the efficiency, this difference can be neglected.

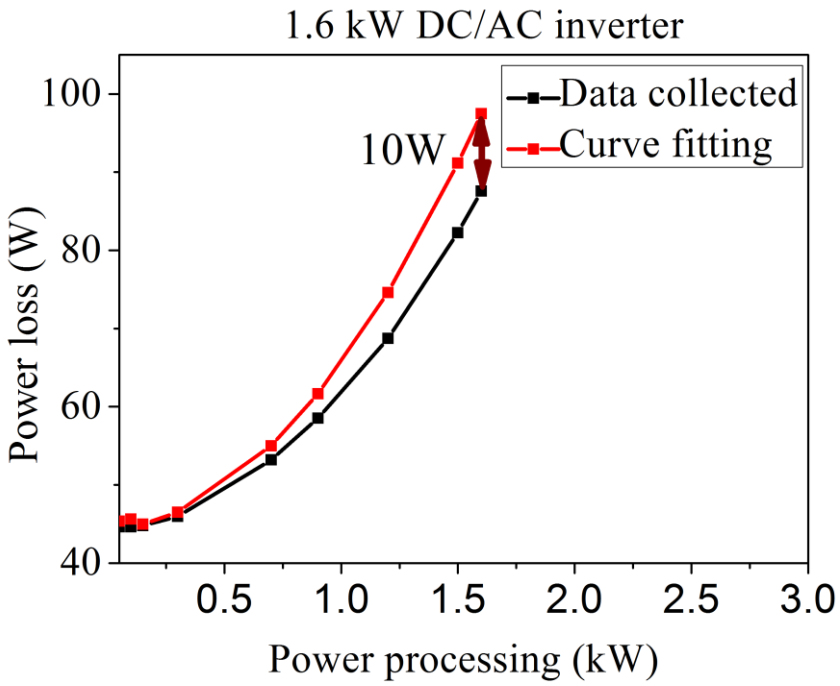

Figure 3.7. Comparison between data collected and curve fitting.

The collected data and the established relationship between power losses and power processed for three converters can be seen in Figure 3.8. And the efficiency at different power processed is shown in Figure 3.9, where the tested voltage is 400V DC bus, 240V grid and 300V battery stack. Besides, to avoid inefficiency operation of converter, the cut-off power is employed. The cut-off point is typically chosen to prevent standby losses and other inefficiencies at low power levels from becoming dominant. In this thesis, the cut-off power is set at converter efficiency over 70%. Furthermore, the impact of cut-off power on the optimization is also researched in the Section 4.3.2.

Table 3.3. The curve fitting parameters for three types of converters' power loss model.

Converter power model	DC/DC converter			DC/AC inverter			Converter for electric water heater		
0.52 kW	a	b	c	a	b	c	a	b	c
	3e-5	-5.5e-3	38.07	4e-5	-0.2e-3	45.78	8e-5	8.7e-3	33.18
1.64 kW	a	b	c	a	b	c	a	b	c
	5e-6	3.7e-3	36.14	2e-5	1.2e-3	44.35	3e-6	2.8e-2	32.03
2.4 kW	a	b	c	a	b	c	a	b	c
	4e-6	2.2e-3	36.36	7e-6	4.1e-3	44.71	2e-6	1.8e-2	33.13
3.5 kW	a	b	c	a	b	c	a	b	c
	3e-6	3.5e-3	36.03	2e-6	1.23e-2	43.71	2e-6	1.42e-2	33.52
6 kW	a	b	c	a	b	c	a	b	c
	3e-6	2.6e-3	35.97	3e-6	7.1e-3	43.71	2e-6	1.1e-2	33.91

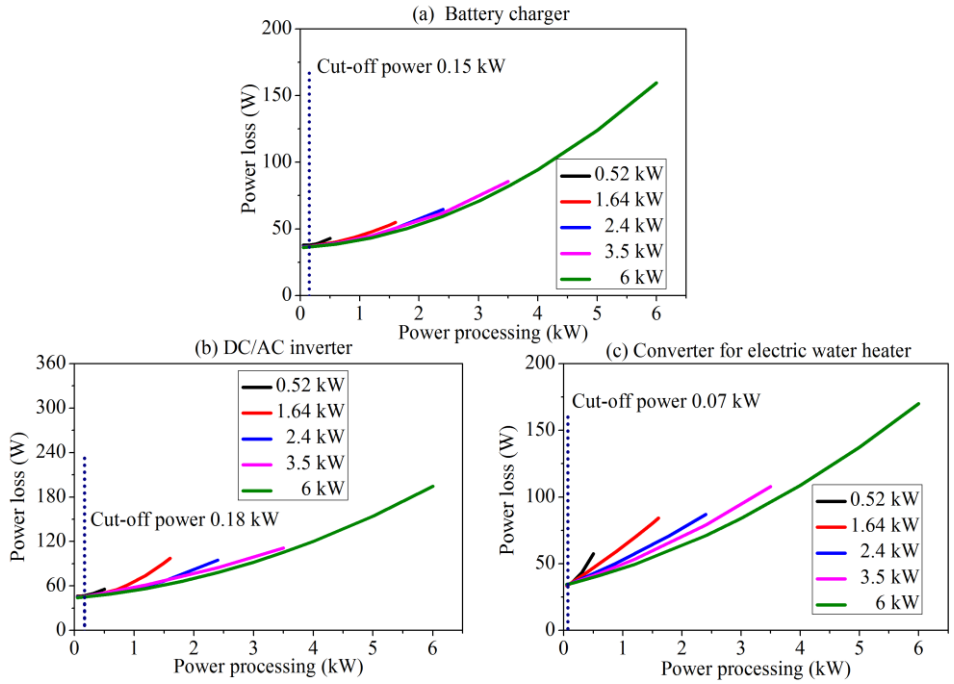

Figure 3.8. The power loss as a function of processing power level (a) Battery charger. (b) DC/AC inverter. (c) converter for electric water heater.

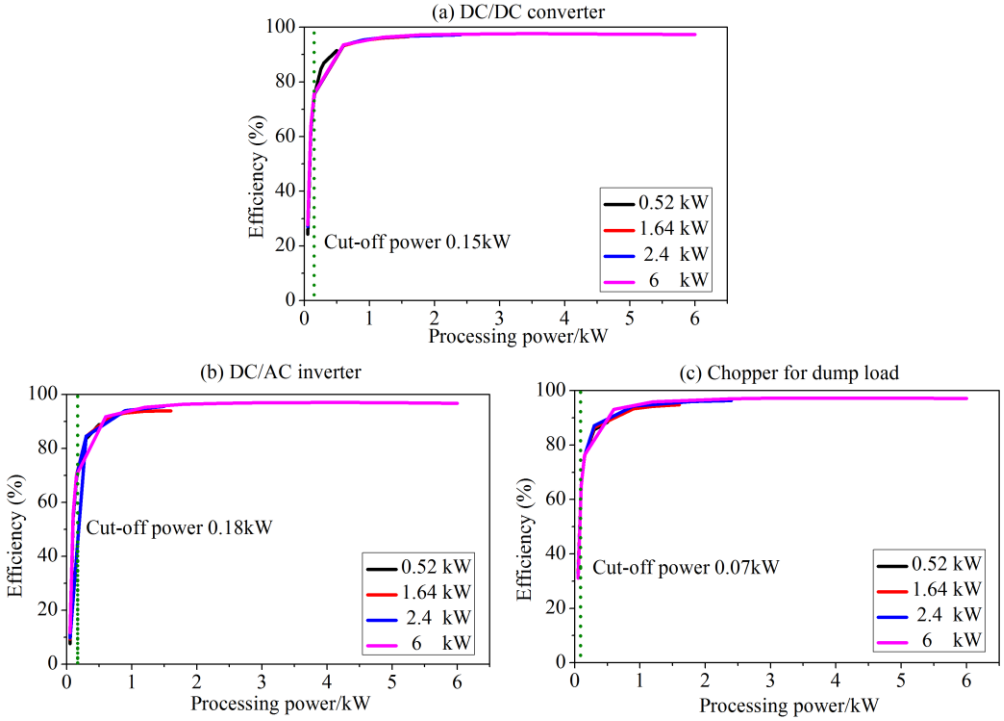

Figure 3.9. The converter efficiency as a function of processing power level charger (300V battery stack, 400V DC bus and 240V grid) (a) Battery charger. (b) DC/AC inverter. (c) converter for electric water heater.

3.5.2. Modelling battery

In this study, the modelling of the battery aims to build the function relationship between battery voltage and state of charge (SOC). Various battery

models exist, ranging from complex electrochemical models to simpler mathematical and circuit-oriented models, each offering different levels of precision and computational burden [149].

Electrochemical models are highly precise but involve solving sets of nonlinear differential equations to describe chemical reactions, making them computationally intensive [150]. Mathematical models simplify this complexity by reducing the number of equations, providing adequate accuracy suitable for specific applications [151]. Circuit-oriented models, such as voltage source-resistance models and Thevenin resistor-capacitor (RC) networks, offer a balance between accuracy and computational complexity, typically with efficiencies around 1%-5% which is use to evaluate the accuracy of the model in presenting the actual behaviour of the battery [153] [154]. 1% indicates the model has greater accuracy than the model with 5%. Combined modelling methods integrate aspects from different models to optimize parameters and improve accuracy in predicting battery lifetime, SOC (State of Charge), and response dynamics [149].

In this study, a steady state electrical equivalent model is adopted to streamline the optimization process, given the extensive real-time data from PV generation and household loads. The model focuses on key constraints like charging/discharging currents, battery voltage, and efficiency. Critical to battery safety and performance, maintaining SOC within a safe range is prioritized to prevent damage or hazardous incidents.

The chosen modified Rin model, based on the Rin model [155], consists of an ideal voltage source (V_{oc}) and an internal resistance (R_{bat}), as illustrated in Figure

3.10. This model effectively calculates the battery terminal voltage, crucial for accurately simulating its behaviour under different operational conditions.

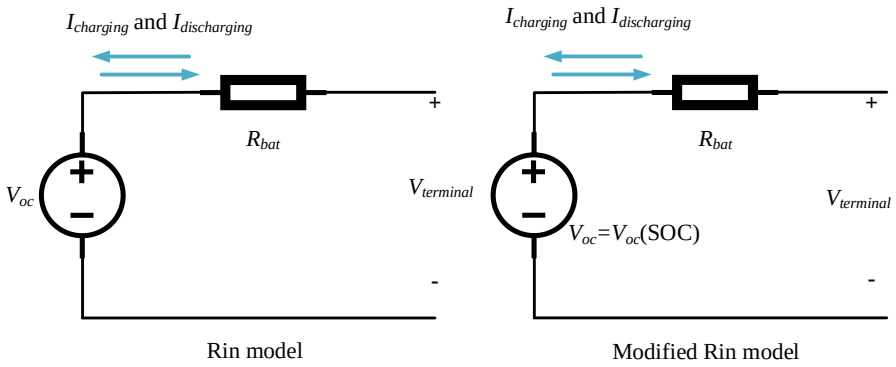

Figure 3.10. Rin model and the modified Rin model used.

The battery open circuit voltage V_{oc} can be used to estimate SOC since the electrochemical potential is closely related to the active material concentration remaining in the electrodes [156]. To keep the internal resistance constant and independent with battery SOC, the operation range of battery SOC and battery charging/discharging frequency are limited. A comparative (lithium-ion versus lead-acid battery) study [157] indicated that the lithium-ion battery has a very narrow internal resistance variation within the 0.1-0.9 SOC window. In this section, three different types of 3.6 V lithium-ions 18650 battery cell are compared where the relationship of battery open circuit voltage V_{oc} and SOC level, and the internal resistance are captured from their datasheets [158][159], as depicted in Figure 3.11. The 2Ah Molicel battery has an SOC range of 0.1 to 0.9, supporting a maximum charging rate of 1 C and a maximum discharging rate of 5 C up to SOC 0.8. The 2.8Ah Molicel battery operates within an SOC range of 0.1 to 0.8, with a maximum charging rate of 1 C and a maximum discharging rate of 3.6 C. The Panasonic 3.35Ah battery also has an SOC range of 0.1 to 0.8, with a maximum charging rate of 0.5 C and a maximum discharging rate of 2 C. Thus, the Rin model for 3.6 V lithium-ion battery cell can be built

for the optimization process as shown in orange dash short-dot line in the Figure 3.11.

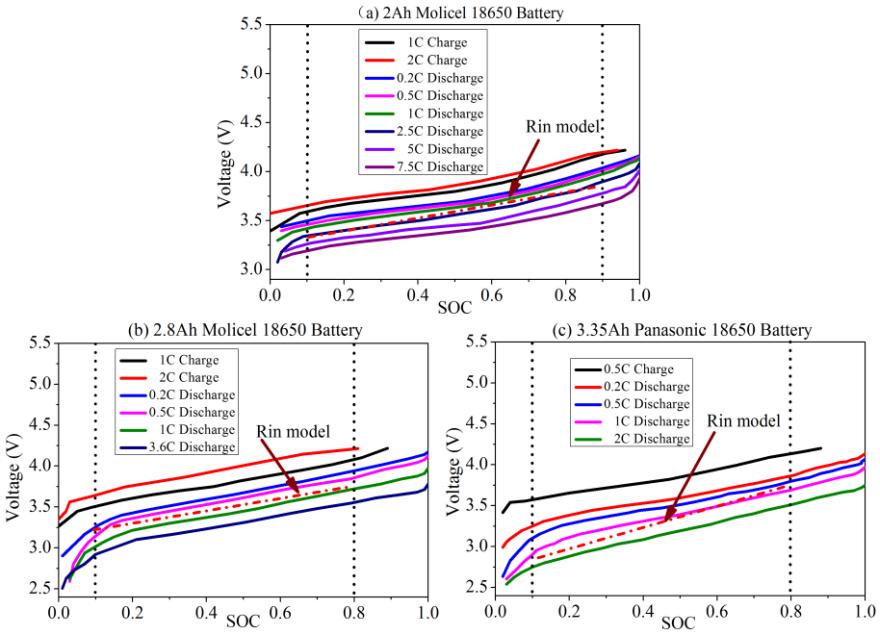

Figure 3.11. The relationships between V_{oc} and SOC for three different lithium-ion battery. (a) 2Ah battery. (b) 2.8Ah battery. (c) 3.35Ah battery.

Apparently, due to relatively higher SOC range and discharging rate of 2Ah Molicel battery cell, it is possible to install the minimal size of battery stack, compared to other two types of battery cell. Thus, the relationship of V_{oc} and SOC is built using equation (3.2).

$$V_{OC} = 0.62 * \text{SOC} + 3.18 \tag{3.2}$$

The Rin model is established based on equation (3.3) where the ohmic power loss of this battery cell can be calculated using equation (3.3).

$$V_{terminal} = V_{OC} - I_{bat} * R_{bat} \tag{3.3}$$

$$P_{bat\_los} = I_{bat}^2 * R_{bat} \tag{3.4}$$

Where $V_{terminal}$ is the battery terminal voltage, I_{bat} is the battery current, and P_{bat_los} is the battery power loss, and battery cell internal resistance R_{bat} is 20 mΩ.

Through the connection of serval battery cells in series or parallel, a 300 V battery stack that will be assumed as nominal stack voltage in all studies, is assembled.

3.5.3. Modelling water cylinder

In many countries, hot water heater storage cylinder has been widely used in residential houses and accounts for a large proportion of electricity demand. It is more advantageous to have a hot water storage than use an instant hot water tap, as the powers are significantly smaller, causing less disturbance on the local distribution system; however, hot water cylinders are subject to heat loss especially if they need to store water for long periods of times.

One approach to evaluate the potential of using the hot water cylinder for energy storage is to simulate electricity demand via a physical model of a cylinder together with assumed hot water usage patterns [160]. Approaches to physically modelling hot water tanks vary. The simplest way is to assume that the water in the cylinder is fully mixed and described by a single temperature variable. A further complexity step may assume the thermal stratification effect [161] considering one-dimensional model, two-dimensional model, and three-dimensional model, which have several temperature stratifications considered in the tank. Compared with the fully mixed model, thermal stratification models have more accuracy but require more parameters and computations along with the household hot water usage data. Typically, the self-reported usage date over a specified period or a statistical approach for longer periods is used to simulate the hot water usage [162]. In some literatures, this modelling electricity consumption approach is validated by detailed comparisons simulated and monitored electricity demand over short intervals for specific tanks.

In this literature review, the main aim of hot water tank is to consume the excess PV power to maintain constant the temperature of hot water for the household hot water usage. However, as shown in Figure 3.12 (a), the traditional modelling method assumes the temperature of hot water always fluctuates in a small hysteresis controlled range [161], such as 60℃~65℃ , where the electricity consumed to heat up the water back to maximum level is from either the grid or PV panels, which will result in expensive peak hour grid electricity consumption (assuming consumption of hot water happens during day time and immediately sensed by the temperature control) and limit the excess PV energy absorption.

To reduce the electricity cost and utilize more PV energy, the off-peak grid electricity and PV energy are taken as the hot water energy sources in this thesis. As depicted in Figure 3.12 (b), the idea is that the water in the cylinder aims to be heated up to a high temperature (at least 80℃) when the cheap off-peak grid electricity or excess PV energy is available. Then, even though there is cold water injected into the water tank, the temperature of the water in the water tank will reduce but will always have an appropriate usage temperature (at least 40℃) which satisfies the basic household hot water temperature needs especially after sunset, since the water temperature for showering or hand washing is typically among 38℃~41℃. While higher water temperatures (such as 90℃) can lead to increased tank energy dissipation compared to 60℃ water temperatures, they can also contribute to reduced costs of grid electricity purchase. This is because both cheap off-peak grid electricity and PV energy are used instead of expensive peak grid electricity as energy sources for heating hot water in the tank. The details of this process are shown as follow. Firstly, due to the cheap electricity

price, the water in the water tank will be heated to the highest allowed temperature like 90℃ (avoid boiling) during the off-peak hours, and then only the excess PV energy is employed to maintain a high temperature of hot water level like 80℃ during peak hours. After sunset, there is no energy imported from the grid to heat water in the water tank. As the hot water is used and replaced by cold-water injection, the water temperature will gradually drop but it still remains at an appropriate usable temperature (like higher than 40℃). Importantly, an assumption is made that the water in the cylinder is fully mixed which can reduce the calculations but in reality, as the hot water exits the hot water cylinder, it is expected that due to stratification, temperature of hot water exit will be higher than average model temperature.

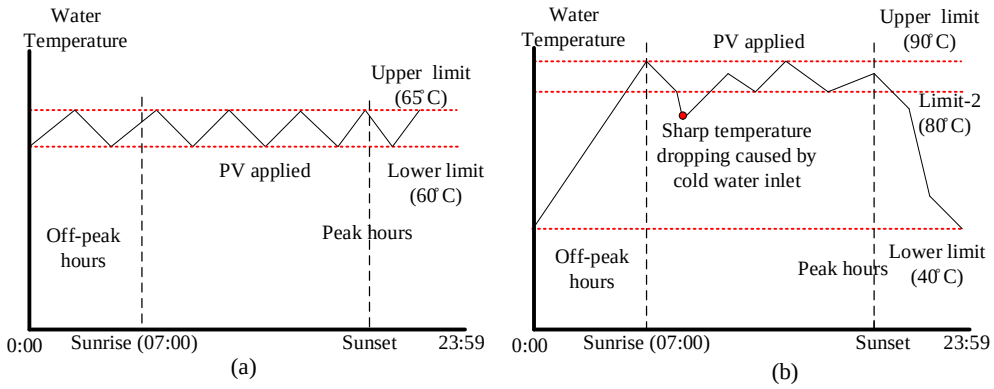

Figure 3.12. Two methods for modelling daily hot water consumption.

A BREDEM procedure [163][164] [165] was established by the Energy Saving Trust (EST) organisation to model hot water consumption (DHW) based on the analysis of collected data derived from a real pool of approximately 120 British houses. In the analysis, four key goals were identified:

1) Measure hot water usage volume and energy consumption.

2) Identify DWH heating patterns- time and temperature.

3) Comparison between the measured results with the BREDEM procedure results to validate this model appropriately.

4) Identify where in a dwelling hot water is being consumed.

In this study, in order to reduce the complexity of model and simplify computation, the BREDEM procedure and SAP procedure were used to quantify the amount of daily hot water consumption. Figure 3.13 shows the configuration for hot water cylinder used in this study. As the hot water flows out to consumer, the cold water is injected into the tank which replaces the consumed water, and the tank remains full at any time. Three temperature sensors are mounted in the primary immersion heater circuit, water inlet and outlet pipe respectively to establish the hot water energy requirement, including energy stored in outlet hot water and the energy dissipation from tank storage. Similarly, a water flow sensor is installed in the cold-water inlet to monitor the volume/flow of water fed in through the pipe. Thus, the volume of household hot water consumption and energy stored in the outlet hot water are measured respectively.

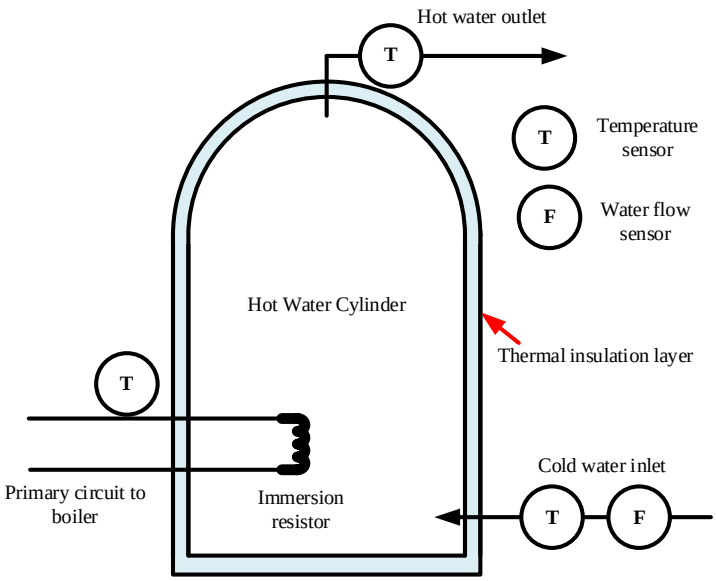

Figure 3.13. The configuration for a typical hot water cylinder.

Besides, EST analysis results also concluded that the number of occupants was the best variable to use for identifying the volume of hot water usage. The details of BREDEM procedure and tank energy dissipation quantification are shown as follow.

- **BREDEM procedure for modelling daily hot water usage amount**

1. Calculate the average litres Vol per day of hot water according to equation (3.5)

$$Vol = 36 + 25N \tag{3.5}$$

Where N is the number of occupants.

2. Calculate the average litres per day in each individual month (Vol_m) by multiplying Vol by the following factor, as shown in Table 3.4.

Table 3.4. The factor for calculating the average litres per day in each individual month and annual level.

Jan	Feb	Mar	Apr	May	Jun	Jul	Aug	Sept	Oct	Nov	Dec	Annual
1.1	1.06	1.02	0.98	0.94	0.9	0.9	0.94	0.98	1.02	1.06	1.1	1.0

3. For each month, calculate the energy content of the hot water used (E_m(kWh)) as follows

$$E_m = Vol_m N(m) \rho c_w \theta_m / 3600 \tag{3.6}$$

Where $N(m)$ is the number of days in the month. ρ is the density of water (1kg/litre), c_w is the specific heat capacity of water (4.19 kJ/kg K), and θ_m is the required temperature rise (℃) in each month, tabulated in Table 3.5.

Table 3.5. The required temperature rise (℃) in each month and annual level.

Jan	Feb	Mar	Apr	May	Jun	Jul	Aug	Sept	Oct	Nov	Dec	Annual
41.2	41.4	40.1	37.6	36.4	33.9	30.4	33.4	33.5	36.3	39.4	39.9	37

Notably, in this study, the model of daily hot water volume and energy consumption is based on the annual average level. According to the BREDEM procedure suggestion, the annual averaged water temperature rise is selected as 37 ℃ which is calculated from the difference between 15 ℃ inlet cold water to 52 ℃ outlet hot water. Hence, the daily hot water usage amount is 86, 111, and 161 litres for 2, 3, and 5 occupants house respectively, which is calculated by equation 3.6, and the energy consumption amount (heating water only) is shown in Table 3.6.

Table 3.6. Modelling results as a function of the number of occupants

The number of occupants	2	3	5
$Vol\ /L$	86	111	161
E_m/kWh	3.7	4.78	6.93

Based on the previous analysis, the off-peak (00:00-07:00) grid electricity will be the only stable source to energy to heat the water in the tank. However, the hot water consumption happens rarely during this night period. To ensure enough daily hot water supply, almost all daily hot water needs should be firstly heated to temperature during off-peak night hours, and then the intermittent excess PV energy is used to compensate the tank heat energy storage loss and the sudden water temperature dropping caused by cold water injection that replaces the hot water consumption. Therefore, the water tank size for 2, 3, and 5 occupants house should be designed equal at least to their daily hot water usage volume: 86, 111, and 161 litres respectively.

- **The converted hot water consumption profile**

To ensure an appropriate temperature of hot water for household usage, the temperature of hot water in the tank needs to be monitored. Thus, the profiles of ambient temperature and hot water usage are needed which are also produced by the CREST model. However, the CREST model exhibits different heating behaviour compared to the method considered in this thesis, as shown in Figure 3.12 (b), with hot water temperatures fluctuating within the 50℃-70℃ range. To apply the selected hot water consumption profiles in this thesis, these profiles need to be scaled to daily hot water consumption of 86, 111, and 161 Liters for different occupant numbers (2, 3, and 5, respectively). Additionally, due to the wider temperature range of 40℃-90℃ considered in this thesis, the heat energy reduction from hot water usage at each time should be equivalent to that in the scaled CREST model. To simplify the process, the annual average hot water

temperature rise of 37℃, as investigated by the BREDEM procedure, is used to calculate the heat energy reduction for each instance of hot water use in the CREST model. This approach is appropriate since the BREDEM procedure dataset is also used in the CREST model. The converted hot water consumption profile, based on this temperature rise, establishes the estimated hot water consumption amount each time, as shown in Equation (3.7).

$$Vol_{use}\rho c_w * 37 = Vol_{usenew}\rho c_w * (T_{i-1} - 15) \quad (3.7)$$

Where Vol_{use} is the hot water usage amount in scaled CREST model with annual average hot water temperature rise (37 ℃) considered, Vol_{usenew} represents the new hot water usage amount after temperature conversion, T_{i-1} represents the hot water temperature at previous "i-1" time instant, whilst the inlet cold water temperature is considered to be 15 ℃.

Thus, the produced hot water consumption profiles have the same total energy as the scaled 86 L, 111 L and 161 L hot water consumption profiles in CREST model.

- **The hot water cylinder heat dissipation model**

The schematic diagram of hot water cylinder model is shown in Figure 3.14, where $T_{win}, T_{wout}, T_{airi}$, represents the cold inlet water temperature (15 ℃), hot water outlet temperature, and internal ambient temperature of room space respectively, $\varphi_{ele}, \varphi_{PV}$ represents the power from the grid and PV panels respectively, and H_{loss} represents the cylinder heat loss coefficient which is taken as a typical value of 2.8 W/K [125] for all three different size of water cylinder (86, 111, and 161 litres). Thus, the hot water temperature of the fully mixed model can be illustrated as equation 3.8, where the temperature of hot water in the tank at each time can be calculated.

$$Vol_m \rho c_w \frac{d(T_{wouti} - T_{wouti-1})}{dt} = -(T_{wouti-1} - 15)\rho c_w * \frac{Vol_{usenew}}{\mathrm{dt}} + \varphi_{ele} + \varphi_{PV} - H_{loss}(T_{wout} - T_{airi}) \quad (3.8)$$

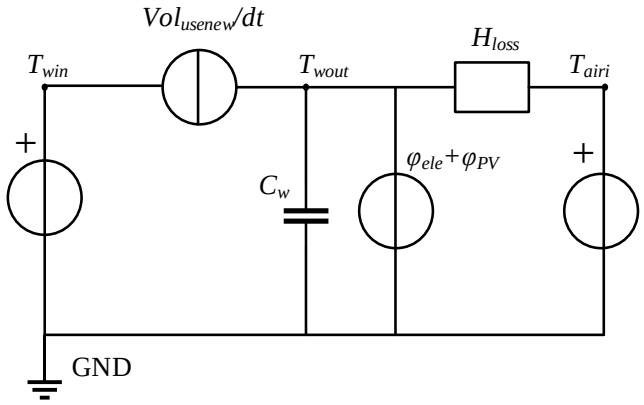

Figure 3.14. Hot water cylinder model [125].

Hence, the daily hot water consumption model, along with the cylinder heat dissipation model based on the number of occupants are established. Compared with the tank thermal stratification model, the amount of computations and model complexity in this approach are reduced sharply.

To validate the hot water cylinder thermal model, the hot water outlet temperature T_{wout}, and internal ambient temperature T_{airi} and the hot water consumption amount Vol_{usenew} is drawn as the Figure 3.15, where the data comes from the CREST model. As the hot water is consumed, the cold water is injected into the cylinder which will immediately lower the water temperature in the cylinder.

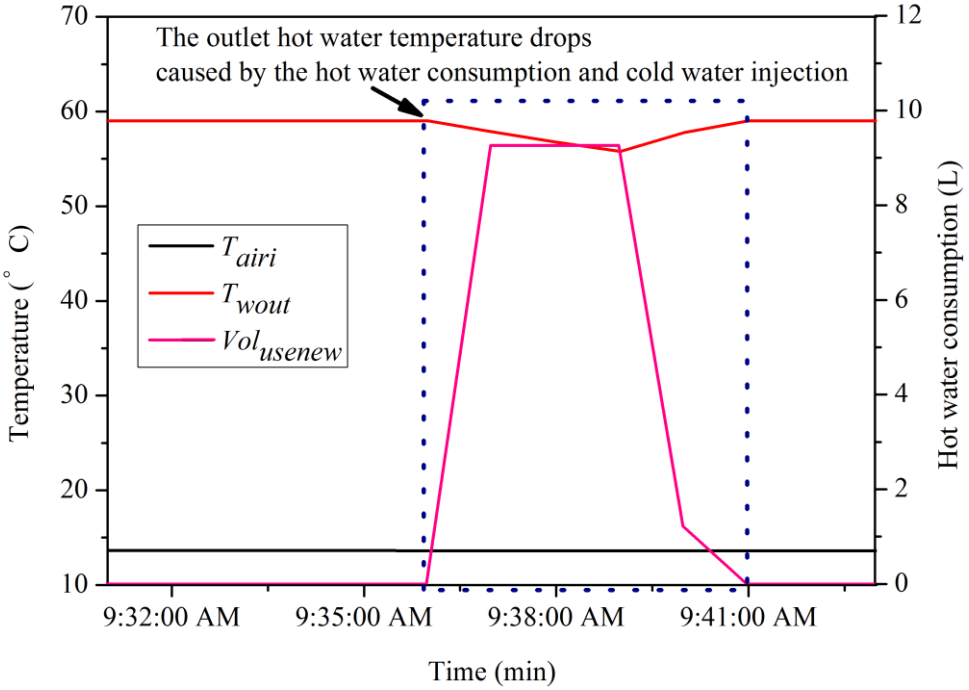

Figure 3.15. The thermal model of hot water cylinder validation.

3.6. Overnight charging algorithm

In this study, both battery storage and hot water tanks are utilized to store excess PV energy, aiming to enhance PV self-consumption rates and reduce electricity costs for end-users. However, battery energy storage presents greater complexity compared to hot water tank storage, particularly due to its capability to feed energy back into the system during peak hours to meet demand.

A crucial aspect of battery energy storage is the pre-charge level, denoted as SOC_{pre}, which significantly influences the amount of energy available for use during the next morning and start of the peak demand periods. This SOC_{pre} is managed by an overnight charging control algorithm that is adjusted based on daily weather conditions and next day predictions. For instance, when expecting clouds or rain next day, the battery may be charged to a higher SOC_{pre} overnight to ensure sufficient energy reserves. Conversely, during sunny weather, when significant amount of PV excess energy will be available, the battery might be charged to a lower SOC_{pre} or not charged at all overnight.

Various algorithms are applied to determine the optimal SOC_{pre} for battery storage, including constant full overnight charging, yearly optimized overnight charging, seasonal optimized overnight charging, and weather-predicted overnight charging. These algorithms aim to maximize the economic benefits of the system by choosing the most efficient SOC_{pre}. However, due to the unpredictable nature of weather conditions and load consumption behaviours, accurately predicting the optimal SOC_{pre} can be challenging.

In this study, the constant full overnight charge algorithm is compared with various SOC_{pre} levels ranging from no overnight charging to fully charging with

0.1 SOC intervals across four seasons where the results are researched in the next chapter.

3.7. Objective functions

This study aims to design optimally the size of key devices such as PV panels, converter power size, and battery stack, based on the maximum financial benefits of the entire system over a 10-year period. The weekly electricity costs are defined by equation 3.9.

$$C_{ele} = E_{op} * p_{op} + E_{pt} * p_{pt} \tag{3.9}$$

Where C_{ele} is the weekly electricity cost bought from grid. E_{op} and E_{pt} are the amount of electricity bought from grid at off-peak time and peak time respectively for one week. p_{op} and p_{pt} are the grid electricity unit price at off-peak time and peak time respectively.

For each scenario, to identify the most financial benefits, the electricity cost saving using Economy-7 tariffs with and without the PV power system installation is computed, and then the total financial benefit of the entire system is calculated by the total electricity cost saving minus the cost of devices installation and purchase. Therefore, the total financial benefits C_{total} for the 10-year period can be expressed as equation 3.10.

$$C_{total} = \left(E_{ln} * p_{op} + E_{ld} * p_{pt} - C_{ele}\right) * 52 * 10 - \sum_1^n PE_i * p_i - C_{fixed} \tag{3.10}$$

E_{ln} and E_{ld} are the weekly amount of household electricity consumption without PV energy applied. Importantly, if the daily hot water energy consumption is considered in the scenario, the hot water energy consumption during the off-peak hours is considered as load consumption. To optimise the devices size, the cost of the initial devices purchase, along with a fixed installation fee (C_{fixed}) should be considered which includes installation,

common components, etc. The initial capital costs include the cost for converters, PV panels, and battery stack which can be calculated by the power/energy size of device PE_i multiplied by its unit price p_i. Besides, the water tank cost can be taken as a part of fixed cost which will not affect the most financial benefit devices design, but it could also be considered that this existed at the property and therefore only a refurbishment fee could be applied.

Besides, the PV utilization rate should be also considered to sufficiently utilize PV energy as possible.

$$\delta_{PV} = \frac{E_{losses}+E_l-E_{ele}}{E_{PV}} \tag{3.11}$$

Where δ_{PV} is the PV utilization rate, E_{PV} is the total PV generated energy, E_{ele} is the total amount of electricity bought from grid, E_{losses} is the energy losses (converters and battery stack energy charging/discharging losses), and E_l is the loads demand, including the energy consumption by hot water tank during the off-peak hours if power electronic water heater system is considered.

3.8. Examining scenarios/cases and processing optimization simulation

To process the optimal procedure, each scenario/case should be examined firstly. Secondly, since the pre-charge level of battery stack significantly affects the optimization results, different pre-charge level of battery stack is compared to evaluate the impact on the whole system. Especially, the initial SOC of the battery should be equal to the SOC at the end of one week to ensure that there is zero net energy stored in the battery stack. Then, the sensitive analysis is done to explore the effects of various factors, like difference of number of occupants, input data resolution, as demonstrated later. Finally, the optimal procedure for each scenario is determined based on maximizing the financial benefits of the entire system over a 10-year operational period. This involves fine-tuning parameters, algorithms, and strategies to achieve the most cost-effective, battery storage, and other components within the household energy system.

3.9. Summary

In this chapter, the procedure and details for optimizing a household PV system with energy storage in the form of either battery storage or hot water storage, are outlined. The optimization process is structured into six key steps:

1. Identifying Different Scenarios: Begin by defining various application scenarios based on specific requirements and specifications. This includes determining component limits such as current/power capacities, as well as outlining power flow strategies and operational constraints.

2. Input Data Collection: Gather essential data required for modelling and simulation. This includes data on PV generation, household loads, hot water consumption patterns, ambient room temperatures, device prices, and grid electricity tariffs. Accurate and comprehensive data collection is crucial for realistic simulation outcomes.

3. Modelling System Components: Develop detailed models for each system component. These models should strike a balance between accuracy and computational efficiency to facilitate their integration into the optimization process. Key components typically include converters (e.g., PV inverters, DC/DC converters), battery model, and hot water tank.

4. Defining Optimization Objective Functions: Define clear optimization objectives, which often involve maximising the financial benefits (e.g., 10 years) and considering the PV utilization rate. These objectives serve as benchmarks against which different scenarios and strategies are evaluated.

5. Examining Each Scenario and Sensitivity Analysis: Evaluate each defined scenario to understand its performance under various conditions. Conduct sensitivity analyses to assess the impact of different variables such as model

choices, number of occupants, and data resolution on system performance and optimization outcomes.

6. Processing Optimization: Implement the optimization algorithms tailored to each scenario based on the defined objectives. This step involves running simulations to optimize the sizing and operation of PV systems with energy storage, considering constraints and maximizing the economic benefits.

7. Presenting Optimization Results: Finally, present the optimized results for each scenario. These results provide valuable insights and recommendations for end-users regarding the configurations, strategies, and technologies to achieve their energy goals.

By following these structured steps, the optimization process ensures a systematic approach to designing and operating household PV systems with energy storage, tailored to maximize cost-effectiveness.

Chapter 4: Single house application

Following the procedure established in Chapter 3, this chapter presents a detailed case study. Initially, each scenario is examined to ensure that the optimization process is robust, realistic, and tailored to the specific conditions and requirements of the household PV power system. Next, a sensitivity analysis is conducted to explore the impacts of various factors on the optimization results. Finally, the chapter concludes by presenting the optimization results that offer the maximum financial benefits of the case study.

4.1. Scenarios examination

This section includes the analysis of various test scenarios defined in Section 3.3, following the design and development procedures outlined in Chapter 3. Before optimally sizing the system components, each scenario must be thoroughly examined. This section focuses solely on the examination of scenarios. Thus, a case study is selected where the input data and models used are fixed, as shown in Table 4.1. The goal is to validate whether the performance and behaviour of the simulated results for each scenario meet the defined constraints and specifications.

Table 4.1. The input date and model selection for these examined scenarios ('-' means not applied).

<table>
<tr><th rowspan="2">Examined scenario</th><th colspan="6">Input data and model selection</th></tr>
<tr><th>PV generation</th><th>Loads consumption</th><th>Converters power rating</th><th>Battery stack energy rating</th><th>Hot water tank capacity</th><th>Ambient temperature and hot water consumption profiles</th></tr>
<tr><td>PV self-consumption scenario</td><td rowspan="2">1.8 kW peak output power profiles in one week for four seasons (1-minute time resolution)</td><td rowspan="4">2-person household load consumption profiles in one week for four seasons (1-minute time resolution)</td><td rowspan="4">1.64 kW power rating for the converter used</td><td>-</td><td>-</td><td>-</td></tr>
<tr><td>PV-battery scenario</td><td>5.98 kWh/20 Ah battery stack</td><td>-</td><td>-</td></tr>
<tr><td>PV-power electronic water heater scenario</td><td rowspan="2">3 kW peak output power profiles in one week for four seasons (1-minute time resolution)</td><td>-</td><td rowspan="2">86 Liters (2 persons) water tank</td><td rowspan="2">2-person household hot water consumption profiles and ambient temperature profiles in one week for four seasons (1-minute time resolution)</td></tr>
<tr><td>PV-battery-power electronic water heater scenario</td><td>5.98 kWh/20 Ah battery stack</td></tr>
</table>

4.1.1. PV self-consumption scenario

i. Specifications and requirements

This scenario represents a basic PV application where the end-users are the direct electricity consumers. There are no energy storage devices in this scenario. When the residential electricity demand exceeds the PV generation, or when the power level of the PV inverter is limited, the load power deficit is met by the grid. Additionally, when the PV power generation is larger than the loads consumption or the PV inverter power rating, the PV generation power is curtailed. The reasons for this are shown in Section 3.1.

ii. Interactions

Two different meters measure the power flow of the house: one meter (dua-rate) quantifies the electricity purchased from the grid during peak hours and off-peak hours respectively, while the other measures the PV energy consumed.

iii. Model selection

The model selection can be seen in Table 4.1 and the electricity tariffs can be seen in Section 3.4.2.

iv. Scenario validation

Table 4.2 summarises the outcomes of the PV self-consumption scenario which indicates the loads consumption (peak hours (07:00-24:00) and off-peak hours (0:00-07:00)), the PV energy calculated from the input PV profile, the PV energy used by the system, the cost of electricity purchased, and PV utilization rate for each seasonal week.

Table 4.2. Outcome of PV self-consumption with two meters scenario on one week basis.

	Spring		Summer		Autumn		Winter		Average
Loads consumption /kWh	68.25		65.91		85.29		97.65		
	Off-peak	Peak	Off-peak	Peak	Off-peak	Peak	Off-peak	Peak	
	6.09	62.16	7.37	58.54	6.85	78.45	7.37	90.28	
PV energy from the profile /kWh	64.62		68.74		48.33		27.28		
Used PV/ kWh	23.82		26.59		20.59		13.63		
PV utilization rate/%	36.86		38.68		42.6		49.96		42.03
Energy loss/ kWh	4.35		4.69		4.36		3.57		
Purchased/ kWh	48.76		43.62		68.68		87.59		62.16
	6.09	42.67	7.37	36.25	6.85	61.83	7.37	80.22	
Standard price/ £	9.26		8.29		13.05		16.64		11.81
Economy-7/£	10.06		8.79		14.36		18.46		12.92

v. Analysing the results of the process simulations

Based on Table 4.2, the mismatch between power generation and load consumption, coupled with the absence of energy storage, results in significant loads demand being sourced from the grid and substantial curtailment of PV generation to maintain grid stability. Consequently, PV utilization rate remains below 50% throughout all seasons. Furthermore, as detailed in Section 3.4.2, the standard electricity tariff generally exceeds the off-peak rate but is lower than

the peak rate. In this scenario, significantly more electricity is purchased during peak hours compared to off-peak hours, leading to higher costs under Economy-7 tariffs rather than standard tariffs.

4.1.2. PV-battery energy storage scenario

i. Specifications and requirements

To leverage the lower off-peak electricity unit price offered by the Economy-7 tariff, the battery stack can be charged from the grid during off-peak hours to a predefined State of Charge (SOC) level (SOC_{pre}). This stored energy can then be utilized during peak hours to meet the household's electricity demand when the grid electricity prices are higher. It's worth noting that electric energy consumption for hot water is not accounted for in this scenario. Additionally, the amount of PV generation curtailed can be reduced significantly by the utilization of battery energy storage. By implementing such a strategy, households can potentially reduce their electricity costs by capitalizing on the Economy-7 tariff's lower rates.

The charging of the battery stack to a predefined State of Charge (SOC_{pre}) can vary depending on the day or season. The rate at which the battery is charged is influenced by factors such as the power rating of the battery charger, the maximum charging current of the battery cells, and the available capacity of the battery itself. It's crucial to limit the charging power to prevent damage to the devices, including the battery stack and converters. This restriction ensures that the charging process remains within safe operational limits, safeguarding the longevity and performance of the battery system and associated components.

ii. Interactions

In this scenario, two meters are needed. The one is to measure the amount of PV energy utilized, and the other (dua- rate) is to record how much energy purchased from the grid (peak and off-peak period).

During peak hours, the primary goal is to prioritize the consumption of PV generated power by the household loads. Any excess PV energy beyond immediate consumption requirements will be used to charge the battery stack, provided there is available capacity. If the household demand exceeds the instantaneous PV generation, the stored energy in the battery stack is utilized. However, if the demand surpasses the maximum discharge capability of the battery stack, the remaining load power demand is sourced from the grid. When the excess PV generation cannot be absorbed by the battery stack, the PV generation will be curtailed. Therefore, the grid serves as the last resort power supply during peak demand periods.

Conversely, during off-peak hours, the grid supplies energy for household loads and pre-charging of the battery stack is needed since the energy stored in the battery stack may be used to satisfy the loads demand during the peak hours.

This systematic approach aims to minimize reliance on grid electricity during peak hours (thereby reducing costs) and manage the storage and discharge of energy using the battery system.

iii. Model selection

An overnight charging control algorithm is employed in this scenario that sets the pre-charging level SOC_{pre} of battery stack to 0.5 for the scenario examination process. The model selection can be seen in Table 4.1 and the electricity tariffs can be seen in Section 3.4.2.

iv. Scenario validation

In order to examine this scenario, the battery energy storage operation is monitored for each week of the seasons by capturing the battery stack charging patterns: SOC, voltage, charging/discharging power and current, as shown in Figure 4.1 (spring week), Figure 4.2 (summer week), Figure 4.3 (autumn week) and Figure 4.4 (winter week). The battery operation should satisfy the system constraints, such as 0.1-0.9 state of charge range, 1 C maximum charging rate and 5 C maximum discharging rate (The battery stack nominal voltage is 300 V and the 20 Ah battery stack), and the maximum converter transmission power (1.64 kW). Table 4.3 summarises loads consumption (peak hours and off-peak hours), the cost of electricity purchased, and PV utilization rate for each seasonal week.

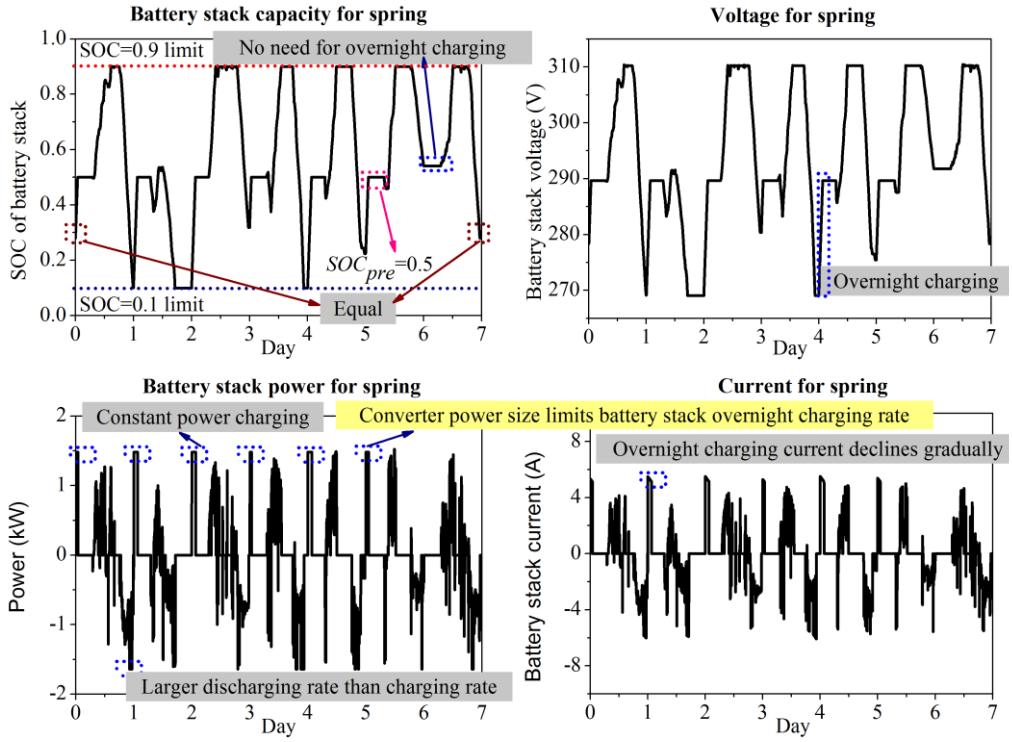

Figure 4.1. Battery energy storage operation for PV-battery & overnight charging scenario during a spring week.

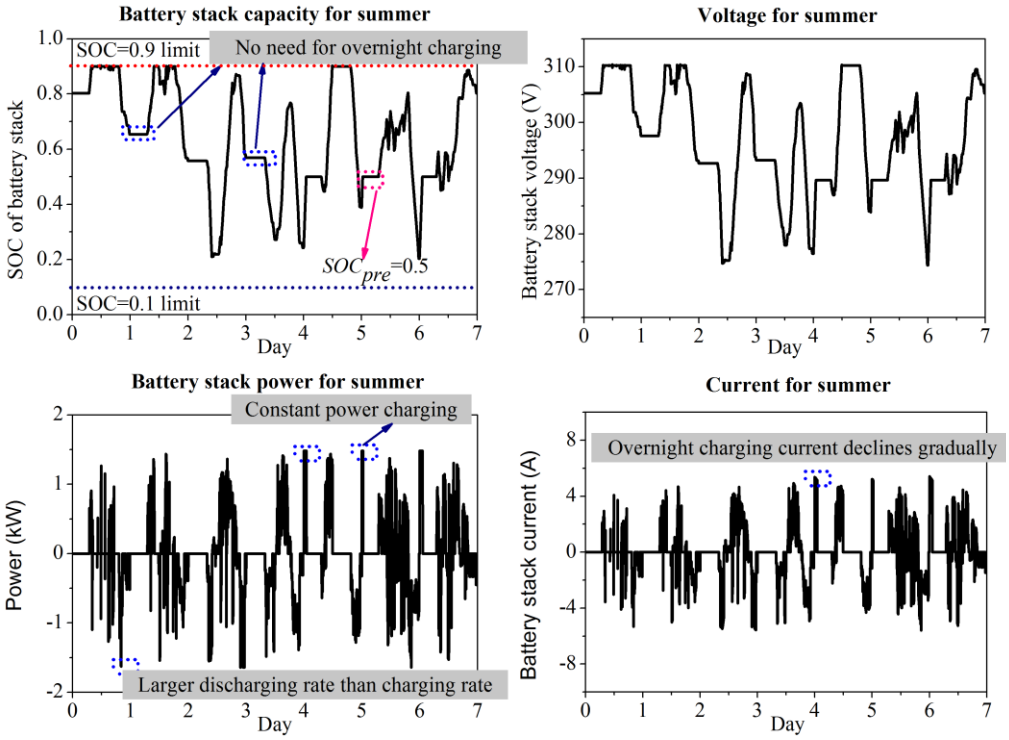

Figure 4.2. Battery energy storage operation for PV-battery & overnight charging scenario during a summer week.

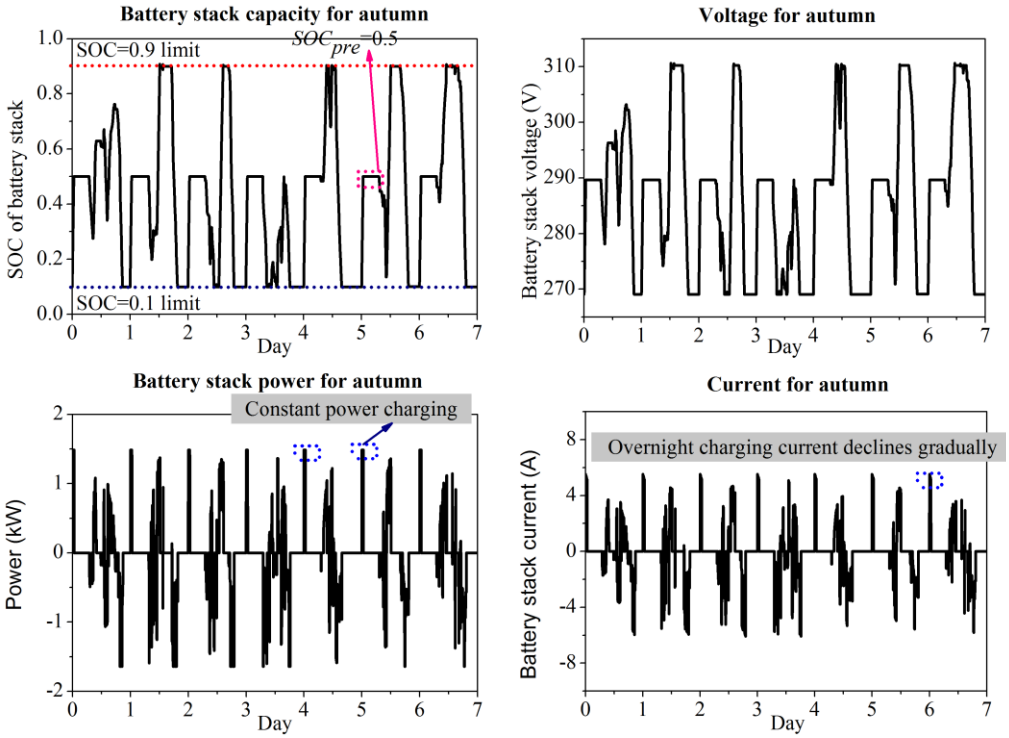

Figure 4.3. Battery energy storage operation for PV-battery & overnight charging scenario during an autumn week.

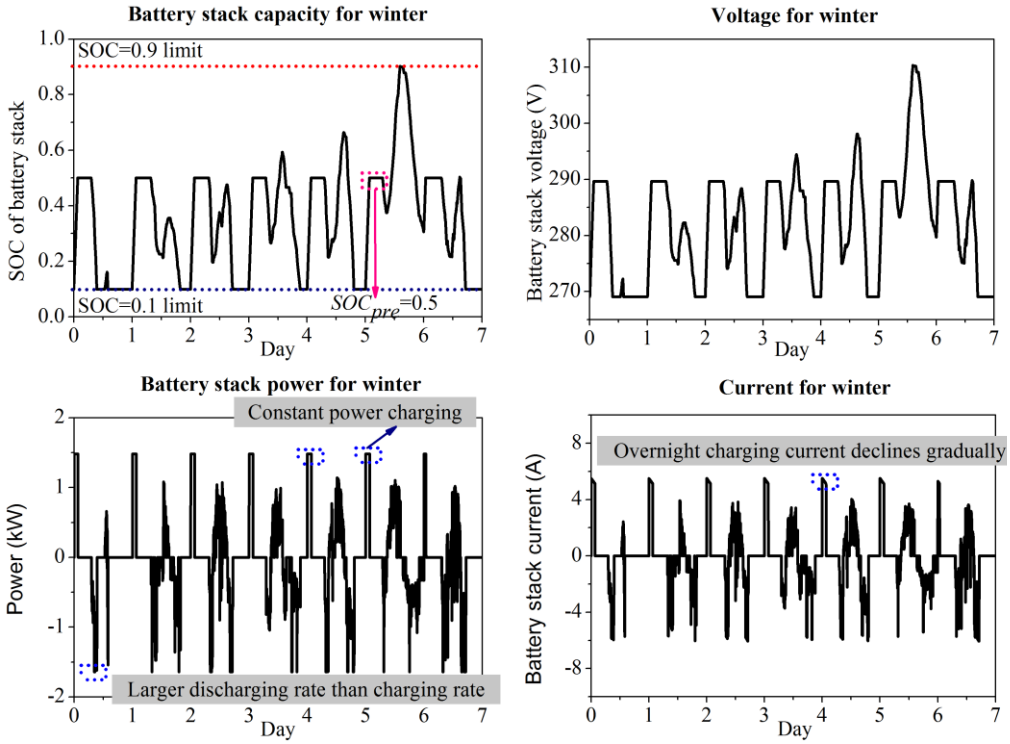

Figure 4.4. Battery energy storage operation for PV-battery & overnight charging scenario during a winter week.

Table 4.3. Outcome of PV-battery with overnighting charging with two meters scenario over a one-week basis.

	Spring		Summer		Autumn		Winter		Average
Consumption /kWh	68.25		65.91		85.29		97.65		
	Off-peak	Peak	Off-peak	Peak	Off-peak	Peak	Off-peak	Peak	
	6.09	62.16	7.37	58.54	6.85	78.45	7.37	90.28	
PV energy from the profile/ kWh	64.62		68.74		48.33		27.28		
Used PV/kWh	42.73		50.4		41.14		26.52		
η_{PV}/%	66.12		73.31		85.13		97.22		80.45
Energy loss/ kWh	12.46		10.5		13.37		11.75		
Purchased/ kWh	37.98		26.01		57.52		82.88		51.1
Standard price/£	7.22		4.94		10.93		15.75		9.71
Economy-7/£	6.02		4.31		9.81		15.19		8.83

v. Analysing the results of the process simulations

The comparison between Table 4.3 and Table 4.2 reveals significant improvements in the average utilization rate of PV-generated energy across all seasons, thanks to the implementation of a 0.5 SOC pre-charging algorithm in the battery energy storage system. Specifically, the average utilization rate of PV-generated energy increases by approximately 38% for each season. More PV

energy is consumed rather than curtailed. Compared to PV self-consumption, where load consumption remains the same, more PV energy is utilized, and more grid electricity is stored in the battery stack for daily use. This results in purchasing less expensive peak-hour electricity from the grid. Consequently, the Economy-7 tariffs are more cost-effective than the standard tariffs.

4.1.3. PV-power electronic water heater scenario

i. Specifications and requirements

In this scenario, there is no battery energy storage system, so it is not possible to store electricity for later use. Instead, the occupants directly consume the PV energy generated by the rooftop panels. During off-peak hours, the water in the tank is heated to the desired temperature of 90°C (avoiding boiling) using the lower electricity tariffs of Economy-7. During peak hours, excess PV energy is used to maintain the water temperature within the range of 80°C-90°C, compensating for temperature drops due to tank storage heat loss, hot water consumption, and cold-water injection. This ensures that the water temperature in the tank remains above the appropriate hot water usage temperature of 40°C at all times without consuming grid electricity during peak hours. More details can be found in Section 3.5.3.

ii. Interactions

Two meters are also needed to monitor the amount of both PV energy consumed and grid electricity imported. The dual-rate meter will measure grid electricity usage during both peak and off-peak hours. It is also assumed that a dedicated control system is incorporated to ensure the effective operation of the entire setup

iii. Model selection

The model used and the input data used can be seen in the Table 4.1.

iv. Scenario validation

To validate the function of the system, the power electronic water heater system operation is monitored for each season by capturing the charging power and hot water temperature in the hot water tank over one week, as shown in Figure 4.5 (spring week), Figure 4.6 (summer week, Figure 4.7 (autumn week), and Figure 4.8 (winter week). From these figures, it shows that the water temperature is always in the range of 40℃-90℃ , and the maximum power/heating rate for heating water in the tank never exceeds 1.64 kW, which indicates that the whole system satisfies the constraints.

Table *4.4* summarises the key outcomes of this scenario where the PV utilization rate, energy loss (converter energy loss), and the cost of grid electricity purchase at two electricity tariffs are shown.

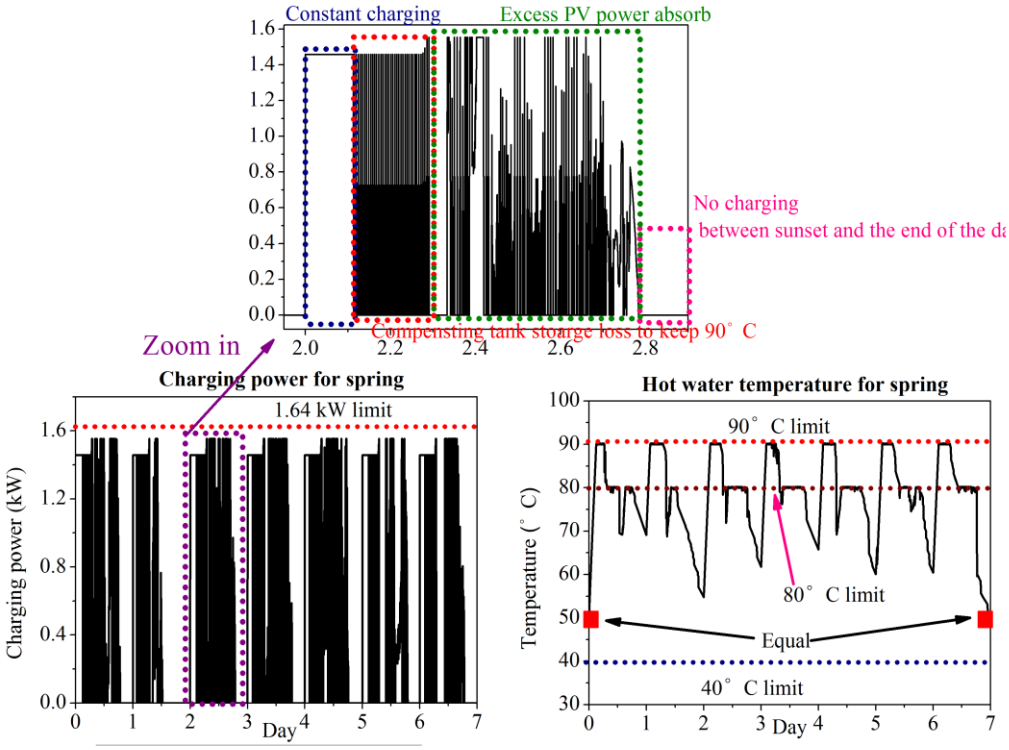

Figure 4.5. The power electronic water heater system operation for PV-power electronic water heater energy storage scenario-spring.

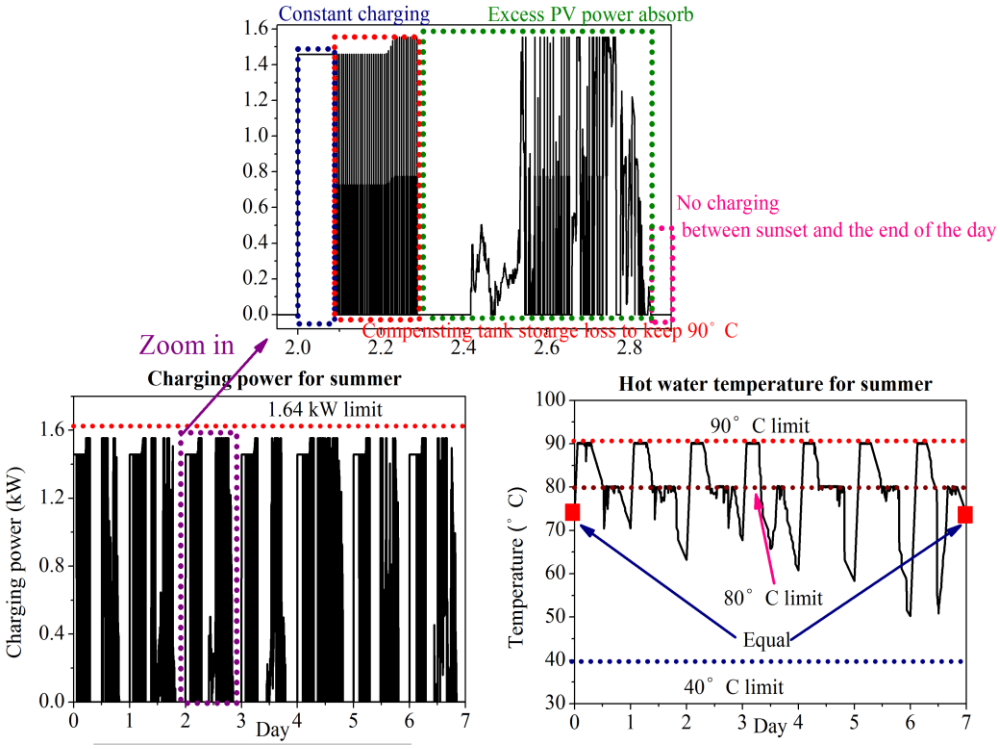

Figure 4.6. The power electronic water heater system operation for PV-power electronic water heater energy storage scenario-summer.

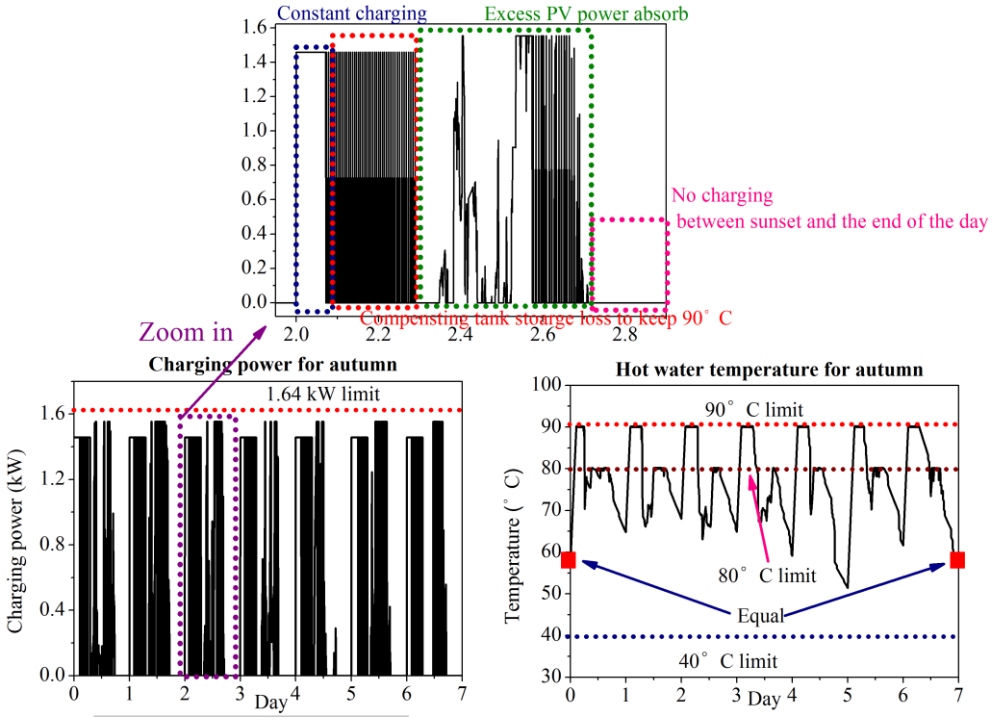

Figure 4.7. The power electronic water heater system operation for PV-power electronic water heater energy storage scenario-autumn.

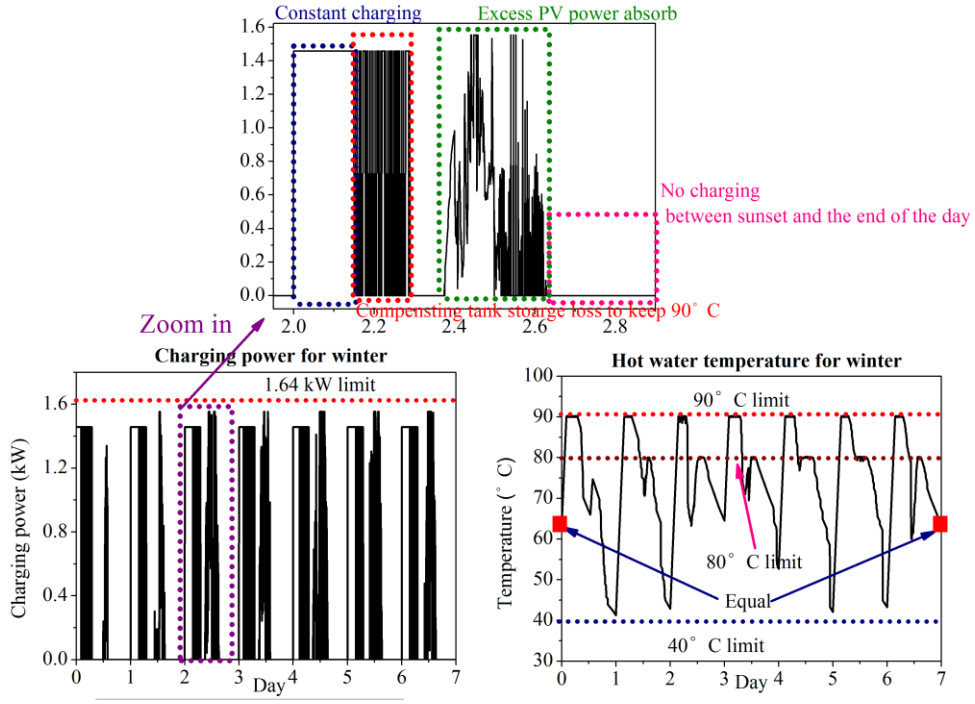

Figure 4.8. The power electronic water heater system operation for PV-power electronic water heater energy storage scenario-winter.

Table 4.4. Outcome of PV-power electronic water heater power system (2-occupant) with two meters scenario on one week basis.

	Spring		Summer		Autumn		Winter		Average
Consumption /kWh	68.25		65.91		85.29		97.65		
	Off-peak	Peak	Off-peak	Peak	Off-peak	Peak	Off-peak	Peak	
	6.09	62.16	7.37	58.54	6.85	78.45	7.37	90.28	
Energy consumption for heating water/ kWh	54.35		53.55		52.54		52.48		53.23
	33.76	20.59	29.37	24.18	31.44	21.1	38.14	14.34	
PV energy from the profile/kWh	107.71		114.57		80.56		45.46		
Used PV/kWh	49.03		59.15		48.31		31.45		
PV utilization rate/%	45.52		51.63		59.97		69.18		56.58
Energy loss/ kWh	9.45		10.11		9.56		9.18		
Purchased/ kWh	83.02		70.42		99.08		127.86		95.1
Standard price/£	15.77		13.38		18.83		22.60		17.65
Economy-7/£	13.44		11.16		17.16		24.29		16.51

v. Analysing the results of the process simulations

In this 2-occupant model, the total daily hot water consumption amount is 86 Liters, and the total energy consumption aligns with the hot water consumption profile of the scaled CREST model, which also totals 86 Liters. In this model, both cheap off-peak grid electricity and PV energy are used instead of expensive peak grid electricity as energy sources for heating hot water in the tank. However,

given the uncertainty in the amount of excess PV energy, significant amounts of cheap off-peak grid electricity are needed to heat water in the tank to a high temperature, ensuring that the water remains at an appropriate temperature for immediate usage since the cold-water injection can drop the water temperature. As indicated in Table 1.4, over 60% of the energy used for heating water comes from PV energy in spring, summer, and autumn. In winter, this percentage drops to 38% due to reduced excess PV energy and low average hot water temperatures in the tank. Therefore, if the excess PV energy is larger, such as in the spring, summer, and autumn, the energy from the grid to heat water in the tank will takes smaller proportion of the total heating water energy consumption.

Additionally, comparing the cost of grid electricity purchased at standard tariffs versus Economy-7 tariffs, an average weekly saving of £1.14 is achieved for Economy-7 tariffs.

4.1.4. PV-battery-power electronic water heater scenario

i. Specifications and requirements

In this scenario, a battery energy storage system and a power electronic water heater are integrated to more effectively utilize the PV generated energy and ensure an adequate supply of hot water for household use. During off-peak hours, when no PV is available, the water in the tank is consistently heated towards a target temperature of maximum 90°C, while the battery can also be charged to a predefined SOC level (SOC_{pre}=0.5), if feasible. Grid electricity also covers household load consumption during off-peak hours.

During peak hours, to maintain the appropriate hot water temperature (above 40°C) in the water tank for immediate usage and to avoid using expensive peak grid electricity, it is advisable to primarily use the excess PV energy to heat water

in the tank. The remaining PV energy directed to the battery storage system. Moreover, the battery can be discharged to meet household loads demand during peak times.

ii. Interactions

Two meters are essential for monitoring both PV energy export and the time dependent grid electricity consumption. It is also assumed that a dedicated control system is incorporated to ensure the effective operation of the entire setup. It regulates the energy and power flow throughout the system, which includes household loads, the battery stack, the hot water tank, PV generation, and grid electricity.

iii. Model selection

The model used and the input data used can be seen in the Table 4.1.

iv. Model validation

Based on Section 4.1.2 and Section 4.1.3, this scenario combines a battery storage system with a hot water energy storage system. To minimize redundancy, the operation of both the power electronic water heater system and the battery stack is monitored at different seasons, like spring and winter in this model, to validate the system's functionality. This monitoring captures the operational characteristics of the battery stack and the hot water tank energy storage systems over one week (Figure 4.9 and Figure 4.10 for spring, Figure 4.11 and Figure 4.12 for winter).

During off-peak hours, priority is given to the hot water tank for grid electricity charging over the battery stack. In peak hours, if the temperature of the hot water remains within the range of 80°C to 90°C, excess PV energy is stored in the battery stack, provided there is sufficient capacity available.

It can be seen that both the hot water system and the battery stack meet the specified power and capacity constraints. Table 4.5 summarizes the key outcomes of the scenario involving PV-battery integration and power electronic water heater (including overnight charging) for four seasons.

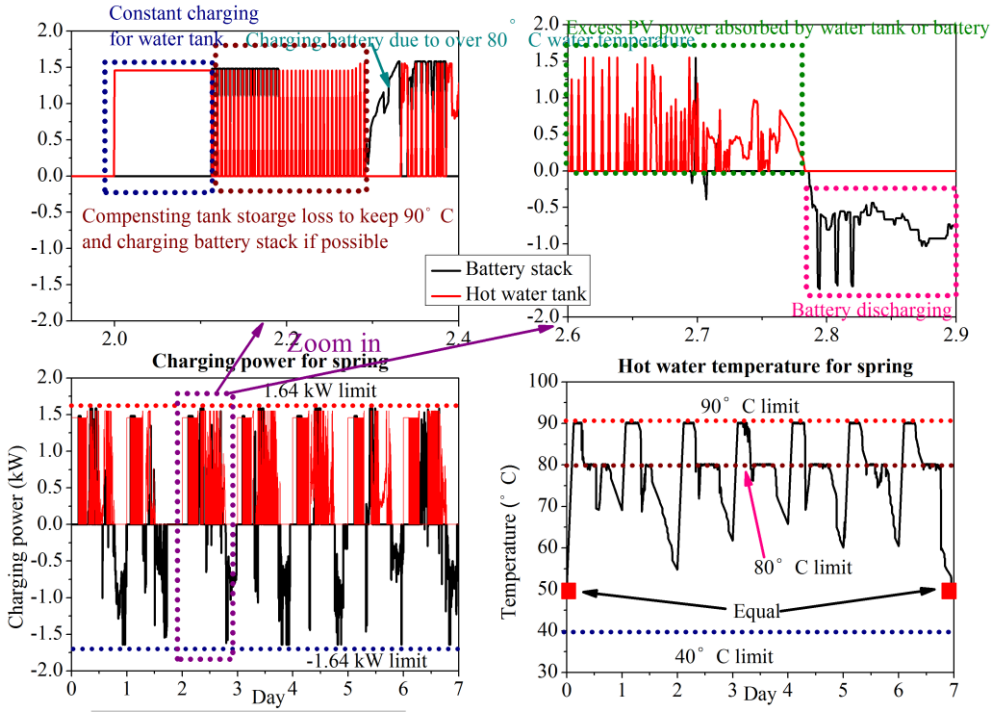

Figure 4.9. The power process of battery stack and power electronic water heater system during a spring week.

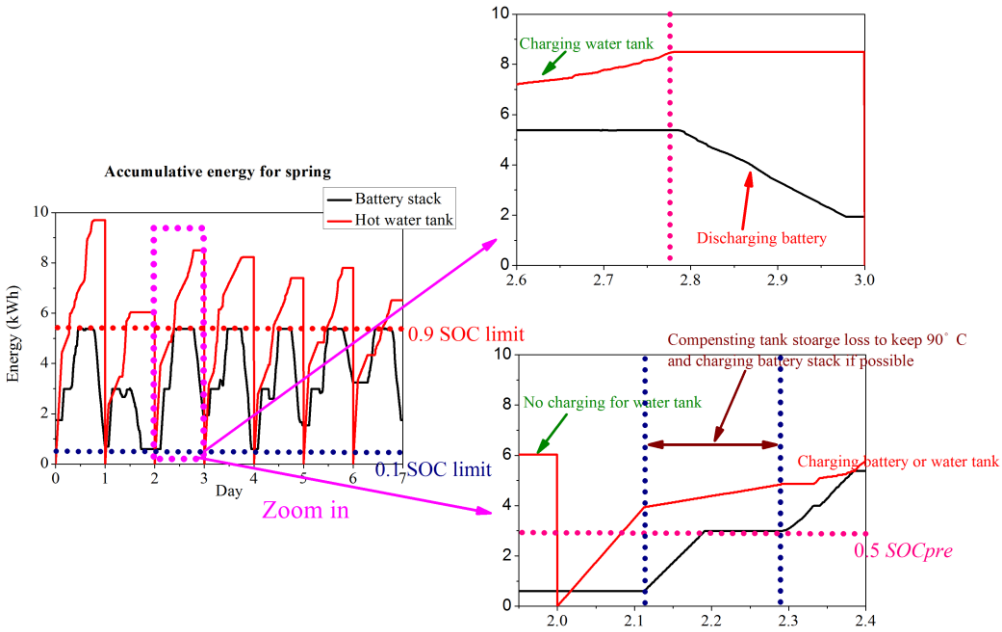

Figure 4.10. The energy process of battery stack and power electronic water heater system during a spring week.

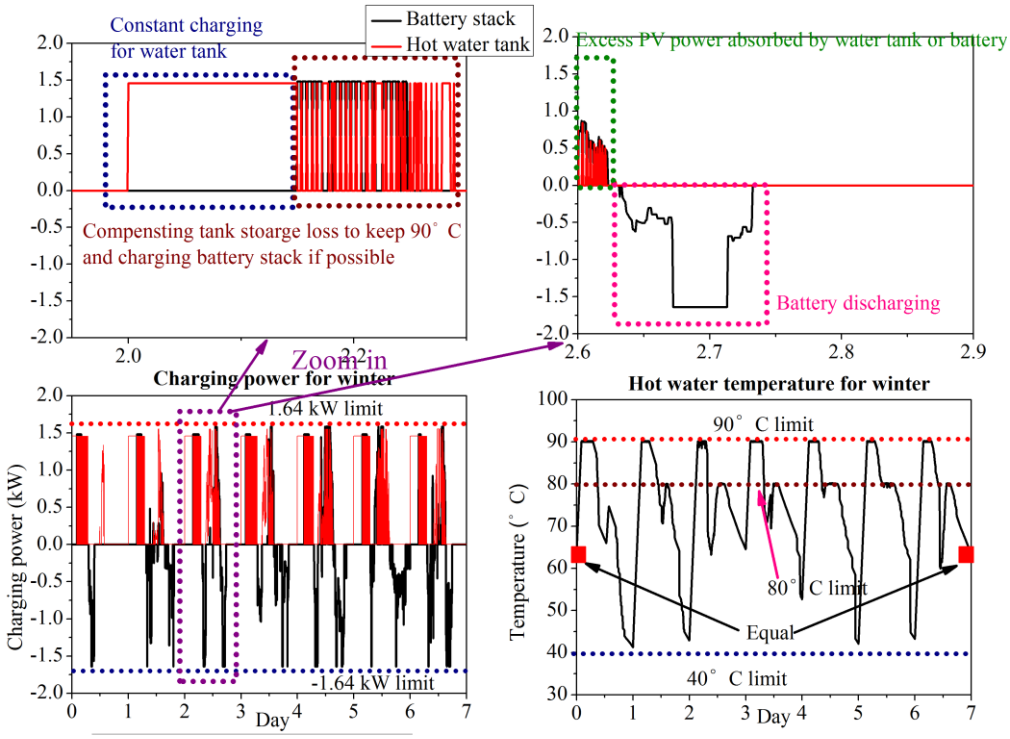

Figure 4.11. The power process of battery stack and power electronic water heater system during a winter week.

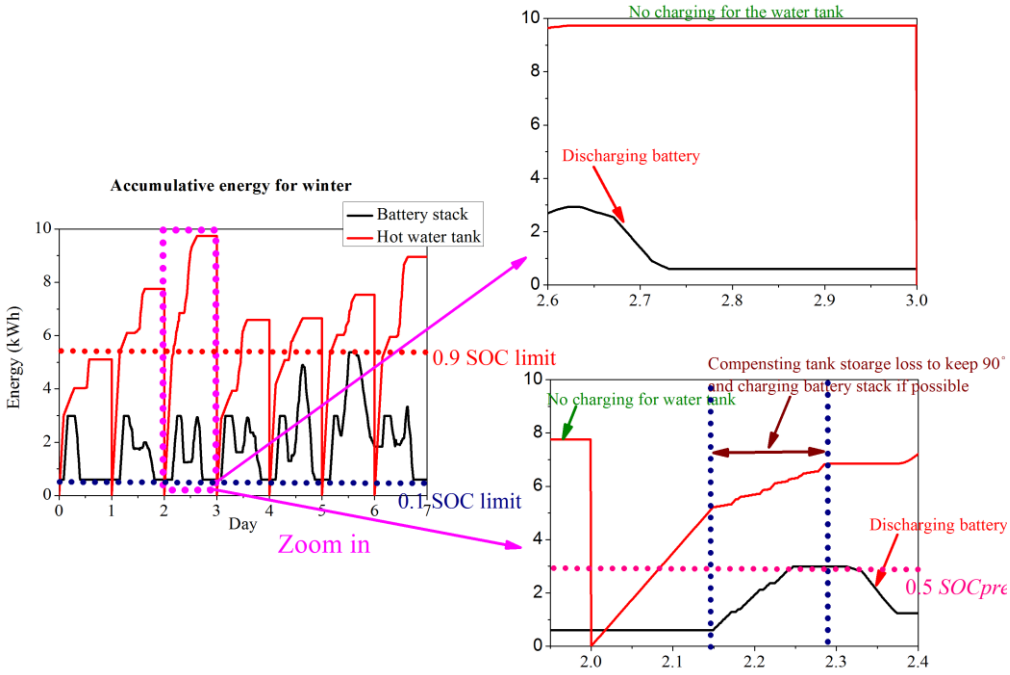

Figure 4.12. The energy process of battery stack and power electronic water heater system during a winter week.

Table 4.5. Outcome of PV-battery and power electronic water heater system (2 occupants) on a per weekly basis.

	Spring		Summer		Autumn		Winter		Average
Consumption /kWh	68.25		65.91		85.29		97.65		
	Off-peak	Peak	Off-peak	Peak	Off-peak	Peak	Off-peak	Peak	
	6.09	62.16	7.37	58.54	6.85	78.45	7.37	90.28	
Energy consumption for heating water/ kWh	54.35		53.55		52.54		52.48		53.23
	33.76	20.59	29.37	24.18	31.44	21.1	38.14	14.34	
PV energy from the profile/kWh	107.71		114.57		80.56		45.46		
Used PV/kWh	65.66		77.66		67.17		42.75		
PV utilization rate/%	60.96		67.78		83.39		94.04		76.54
Energy loss/ kWh	16.04		14.17		16.64		14.95		
Purchased/kWh	72.98		55.97		87.3		122.33		84.65
Standard price/£	13.87		10.63		16.76		23.24		16.13
Economy-7/£	9.79		7.59		12.8		19.38		12.39

v. Analysing the results of the process simulations

In this scenario, the battery stack acts as a supplementary energy storage unit to the hot water tank, enabling energy storage and release for household consumption as needed during peak time. By integrating the battery stack into the PV-battery and power electronic water heater system, the utilization of PV generation is significantly enhanced, achieving an average increase of nearly 20% compared to the PV-power electronic water heater scenario.

The installation of the battery stack offers several advantages, particularly in conjunction with an Economy-7 price tariff, which gives approximately £4 lower average cost than the standard tariffs. This cost-saving benefit is amplified by overnight charging, which optimizes energy consumption patterns. Even during winter months, when more electricity may need to be purchased from the grid, the Economy-7 tariff proves advantageous over scenarios relying solely on PV and power electronic water heater systems due to possibility to charge cheaply the battery overnight whilst during daytime very little PV excess exist during winter.

4.2. Different overnight charging level of battery stack

The pre-charge level of battery stack directly determines the amount of overnight charging energy which can impact the electricity bill significantly. Practically, there are many available control algorithms to choose the overnight charging level of battery, like constant overnight charging, yearly, and weather-based predication. However, the pre-charge level is a preset value for the battery SOC, representing the target charging level. If the charging process is restricted by factors, such as a small battery charger power rating with a large battery stack energy rating, the battery stack may not reach the preset SOC level during the 7-hour off-peak time window. In this section, it concentrates on assessing the impacts of different overnight charging level (SOC_{pre}) on the performance of the scenario, where the PV utilization rate, the amount of grid electricity purchased, and the cost of grid electricity purchased are highlighted. Thus, the PV-battery and PV-battery-power electronic water heater scenarios are selected. The model definitions can be found in Table 4.6.

Table 4.6. The input data and model selection for two examined scenarios ('-' means not applied).

Examined scenario	Input data and model selection					
	PV generation	Loads consumption	Converters power rating	Battery stack energy rating	Hot water tank capacity	Ambient temperature and hot water consumption profiles
PV-battery scenario	3 kW peak output power profiles in one week for four seasons (1-minute time resolution)	2-person household load consumption profiles in one week for four seasons (1-minute time resolution)	1.64 kW power rating for the converter used	5.98 kWh/20 Ah battery stack	-	-
PV-battery-power electronic water heater scenario					86 Liters (2 persons) water tank	2-person household hot water consumption profiles and ambient temperature profiles in one week for four seasons (1-minute time resolution)

4.2.1. Different SOC_{pre} for PV- battery energy storage scenario

i. Model validation

To show the behaviour of battery stack, the SOC of battery stack at three different SOC_{pre} levels (0.1, 0.5, 0.9) in the summer and winter are plotted in the Figure 4.13 as an example. During off-peak hours, the battery stack will be charged to the defined SOC_{pre} level. Due to different SOC_{pre} level, the charging/discharging performance of the battery stack can be varied a lot but all SOC of battery in the battery SOC limitations (0.1-0.9).

Table 4.7 summarizes the outcomes regarding PV utilization rate and the cost of grid electricity purchased at different SOC_{pre} levels across four seasons over one week. The highlighted row indicates the minimum total cost of grid electricity purchased.

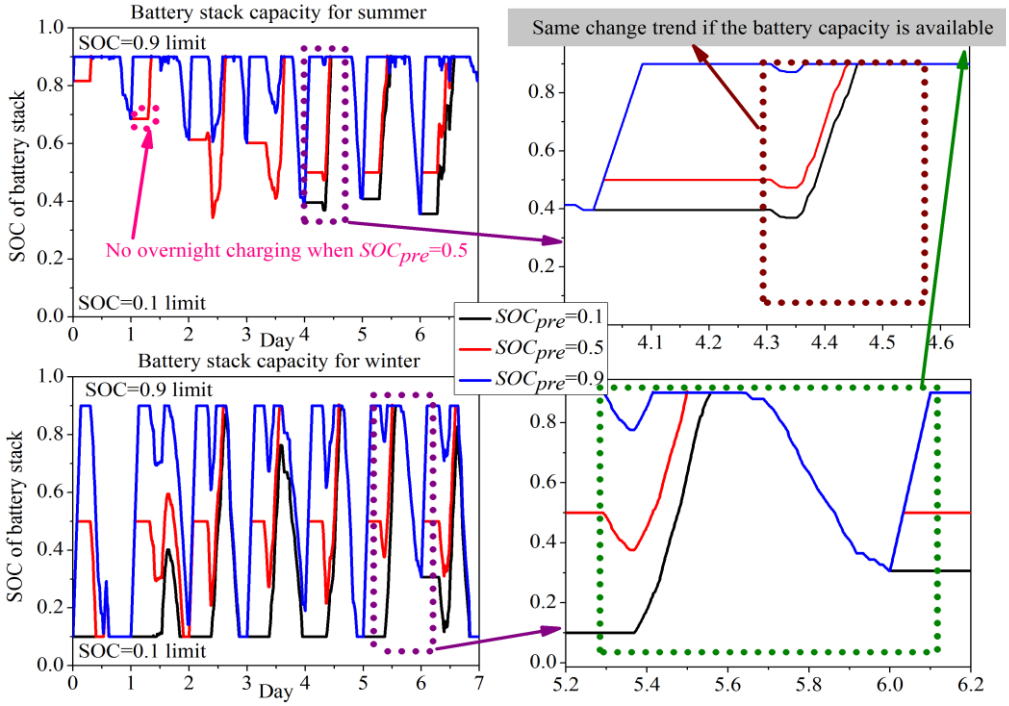

Figure 4.13. The battery capacity changing behaviour at 0.1,0.5,0.9 overnight charging level-spring and summer.

Table 4.7. Outcomes of different SOC_{pre} for PV-battery energy storage scenario (20 Ah/5.98kWh battery).

Spring					Summer				
	Electricity purchased from grid					Electricity purchased from grid			
SOC_{pre}	Off-peak/kWh	Peak/kWh	PV utilization rate/%	Total cost of grid electricity purchased (Economy-7) /£	SOC_{pre}	Off-peak/kWh	Peak/kWh	PV utilization rate/%	Total cost of grid electricity purchased (Economy-7) /£
0.1	6.09	16.17	50.7	4.95	0.1	7.37	12.99	47.05	3.67
0.2	9.47	15.38	49.95	5.13	0.2	7.37	12.99	47.05	3.67
0.3	12.17	14.82	48.6	5.4	0.3	7.37	12.99	47.05	3.67
0.4	16.87	14.29	45.87	5.74	0.4	8.51	12.99	46.8	3.8
0.5	20.65	13.78	42.94	6.02	0.5	10.78	12.99	45.21	4.04
0.6	25.28	13.78	39.11	6.4	0.6	12.67	12.99	43.57	4.25
0.7	29.69	13.78	35.07	6.75	0.7	17.11	12.99	40.86	4.74
0.8	34.1	13.78	31	7.12	0.8	20.88	12.99	37.59	5.16
0.9	38.5	13.78	26.88	7.53	0.9	25.6	12.99	33.85	5.67
Autumn					Winter				
	Electricity purchased from grid					Electricity purchased from grid			
SOC_{pre}	Off-peak/kWh	Peak/kWh	PV utilization rate/%	Total cost of grid electricity purchased (Economy-7) /£	SOC_{pre}	Off-peak/kWh	Peak/kWh	PV utilization rate/%	Total cost of grid electricity purchased (Economy-7) /£
0.1	6.85	29.42	71.96	7.23	0.1	7.37	55.58	92.06	13.04
0.2	11.63	27.94	71.16	7.43	0.2	14.55	52.51	92.12	13.15
0.3	15.85	27.36	68.14	7.76	0.3	18.33	49.69	91.18	12.95
0.4	19.63	26.81	64.3	8.06	0.4	23.09	46.81	89.39	12.84
0.5	24.42	26.28	59.88	8.47	0.5	27.1	45.58	83.78	13.01
0.6	28.83	25.74	55.26	8.83	0.6	31.51	44.47	77.03	13.25
0.7	33.23	25.5	50.12	9.27	0.7	35.92	43.37	70.21	13.49
0.8	37.64	25.5	44.72	9.75	0.8	40.09	42.51	63.3	13.76
0.9	42.05	25.5	39.25	10.24	0.9	41.96	44.47	55.1	14.12

ii. Analysing the results of the process simulations

As shown in Table 4.7, increasing the pre-charge level can indeed reduce the PV utilization rate under the model and input dataset conditions. This is because more battery space is occupied by off-peak electricity as the pre-charge level increases. During seasons with significant PV energy generation, such as spring, summer, and autumn, the battery stack is configured to avoid overnight charging to achieve the minimum cost of grid electricity purchased. Conversely, when PV generation is significantly reduced, such as in winter, the battery stack needs pre-charge (0.4 SOC) to minimize costs, as the cheap off-peak electricity can be released by the battery to meet the load demand deficit during peak times.

Table 4.8 presents the weekly average of PV utilization rate and cost of grid electricity purchased. The findings highlight that the battery stack seems to be no charge during off-peak hours to reach the minimum grid cost of grid electricity purchased in this models and input date conditions. Significantly, when the battery stack undergoes overnight charging, a portion of off-peak grid electricity is used to cover the standby losses of converters (PV inverter and battery charger). This results in a much higher amount of off-peak grid electricity purchased compared to when there is no overnight charging for the battery stack (PV inverter and battery can be shut down during 7 off-peak hours).

In conclusion, the pre-charge level significantly affects the PV utilization rate and the amount and cost of grid electricity purchased which is closely associated with the financial benefits of the PV-battery scenario. Thus, in the optimisation procedure, the SOC_{pre} needs to be considered.

Table 4.8. Weekly average outcome for different overnight charging levels.

Average				
	Electricity purchased from grid			
SOC_{pre}	Off-peak/kWh	Peak/kWh	PV usage/%	Electricity cost /£
0.1	6.92	28.54	65.44	7.22
0.2	10.76	27.21	65.07	7.35
0.3	13.43	26.22	63.74	7.45
0.4	17.03	25.23	61.59	7.61
0.5	20.74	24.66	57.95	7.89
0.6	24.57	24.25	53.74	8.18
0.7	28.99	23.91	49.07	8.56
0.8	33.18	23.7	44.15	8.95
0.9	37.03	24.19	38.77	9.39

4.2.2. Different SOC_{pre} for PV-battery-power electronic water heater energy storage scenario

In this scenario, the pre-charging level of the battery stack is influenced by the operation of the power electronic water heater system since the hot water tank has the priority to absorb energy from both excess PV energy and grid.

i. Model validation

Figure 4.14 monitors the behaviour of the battery SOC at three different SOC_{pre} levels (0.1, 0.5, 0.9) being shown in the Figure 4.14, for one week in the

summer and winter respectively. Although the pre-charge level changes, the battery SOC is still in the SOC constraints (0.1-0.9). Table 4.9 summarizes the outcomes regarding PV utilization rate and the cost of grid electricity purchased at different SOC_{pre} levels across four seasons over one week. The highlighted row indicates the minimum total cost of grid electricity purchased.

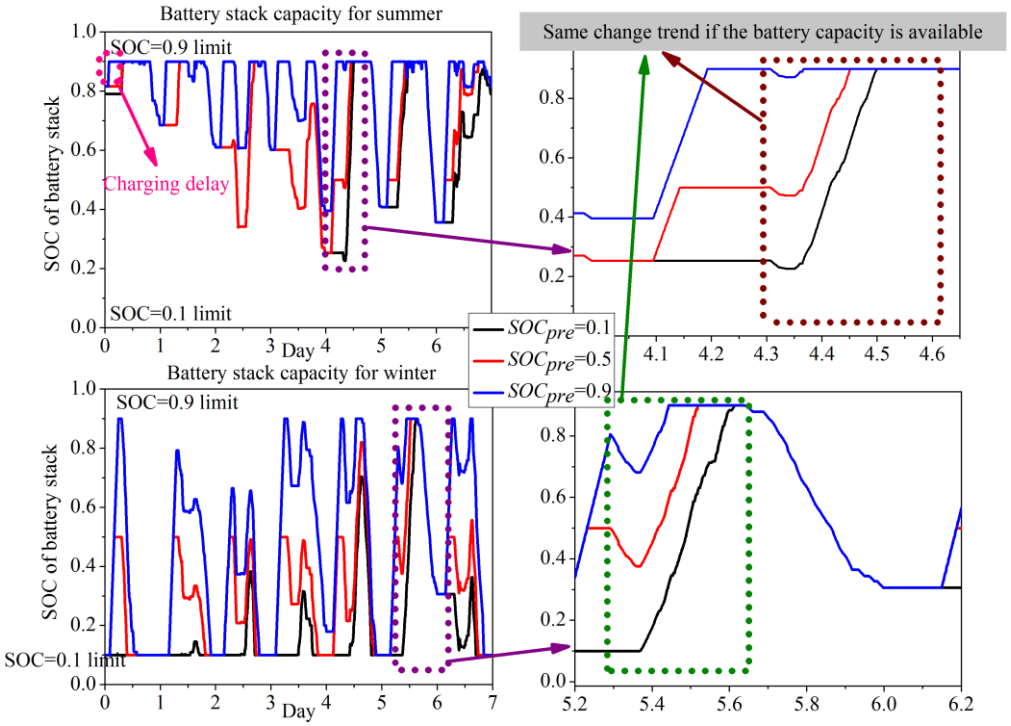

Figure 4.14. The battery capacity changing behaviour at 0.1,0.5,0.9 overnight charging level-spring and summer.

Table 4.9. Outcomes of different SOC_{pre} for PV-battery-power electronic water heater power system scenario (20 Ah/5.98kWh battery).

Spring					Summer				
	Electricity purchased from grid					Electricity purchased from grid			
SOC_{pre}	Off-peak/kWh	Peak/kWh	PV utilization rate/%	Total cost of grid electricity purchased (Economy-7) /£	SOC_{pre}	Off-peak/kWh	Peak/kWh	PV utilization rate/%	Total cost of grid electricity purchased (Economy-7) /£
0.1	43.87	18.57	68.66	8.91	0.1	39.38	12.99	70.4	7.19
0.2	46.61	17.78	67.91	9.04	0.2	39.38	12.99	70.4	7.19
0.3	49.32	17.2	66.51	9.21	0.3	39.88	12.99	70.16	7.25
0.4	53.17	16.6	63.85	9.5	0.4	40.94	12.99	69.37	7.36
0.5	56.95	16.04	60.96	9.79	0.5	42.97	12.99	67.78	7.59
0.6	61.38	15.45	57.8	10.15	0.6	44.86	12.99	66.14	7.79
0.7	65.79	14.88	54.34	10.51	0.7	48.15	12.99	63.95	8.16
0.8	70.2	14.36	50.86	10.88	0.8	51.65	12.99	60.91	8.54
0.9	74.6	13.84	47.31	11.25	0.9	56.17	12.99	57.2	9.04
Autumn					Winter				
	Electricity purchased from grid					Electricity purchased from grid			
SOC_{pre}	Off-peak/kWh	Peak/kWh	PV utilization rate/%	Total cost of grid electricity purchased (Economy-7) /£	SOC_{pre}	Off-peak/kWh	Peak/kWh	PV utilization rate/%	Total cost of grid electricity purchased (Economy-7) /£
0.1	42.19	35.86	90.38	12.53	0.1	50.26	66.07	97.42	20.06
0.2	46.85	33.22	90.49	12.46	0.2	55.65	63.01	97.49	19.98
0.3	50.76	31.48	88.63	12.51	0.3	59.43	60.19	96.54	19.78
0.4	54.27	30.11	86.31	12.59	0.4	64.03	57.02	95.31	19.59
0.5	58.26	29.04	83.39	12.8	0.5	68.44	53.89	94.04	19.38
0.6	62.49	28.33	79.2	13.11	0.6	72.84	50.85	92.5	19.2
0.7	66.89	27.81	74.57	13.48	0.7	77.03	48.41	89.81	19.12
0.8	71.23	27.28	70.02	13.84	0.8	80.77	46.31	87.06	19.07
0.9	75.01	26.76	66.13	14.14	0.9	82.82	45.45	84.84	19.11

ii. Analysing the results of the process simulations

For the selected models and input dataset, the overnight charging level that provides the lowest total cost of grid electricity for each season is found to be 0.1 for spring and summer, 0.2 for autumn, and 0.8 for winter, as shown in Table 4.9. Notably, when the battery pre-charge level is 0.1 or 0.2, the outcome results are the same, as shown in the summer data in Table 4.7. This is because excess PV energy is stored in the battery stack, causing the SOC to exceed 0.2 throughout the week and no charging for the battery during off-peak hours. This indicates that the pre-charge level is closely related to the excess PV generation

situation, and the optimal pre-charge level of the battery stack might differ depending on the season.

Table 4.10 summarizes the weekly average PV utilization rate and the cost of electricity purchased. The results show that the system achieves the minimum total cost of grid energy and the highest PV utilization rate when the battery stack overnight charging level is set to 0.1. Significantly, since the battery charger is shut down to mitigate standby losses when the battery stack has no pre-charge needs, the amount of grid electricity used at a 0.1 SOC pre-charge level is much lower than that at a 0.2 SOC pre-charge level.

Table 4.10. Average weekly outcome for different overnight charging levels.

Average				
	Electricity from grid			
SOC_{pre}	Off-peak/kWh	Peak/kWh	PV utilization rate/%	Total cost of grid electricity purchased (Economy-7) /£
0.1	43.93	33.37	81.72	12.17
0.2	47.12	31.75	81.57	12.17
0.3	49.85	30.47	80.46	12.19
0.4	53.1	29.18	78.71	12.26
0.5	56.66	27.99	76.54	12.39
0.6	60.39	26.91	73.91	12.56
0.7	64.47	26.02	70.67	12.82
0.8	68.46	25.24	67.21	13.08
0.9	72.15	24.76	63.87	13.39

4.3. Impact of complex modelling factors

To illustrate the impacts of different factors on outcomes, this thesis examines the influence of various factors, including:

- The depth of discharge (0.1-0.9 versus 0.2-0.7)
- The consideration of ohmic battery losses
- The consideration of a cut-off minimum power

4.3.1. Battery model

4.3.1.1. Different allowed DOD of battery stack applied

In Section 3.5.2, it was observed that for a given size of battery, the usable DOD directly influences the design and performance of the battery stack. Within a wider DOD range of 0.1-0.9, the behaviour of the Li-ion battery cells is typically linear and straightforward to model. However, for other types of battery models, the available SOC range may be narrower, offering less usable stored energy that is then affecting the overall performance of the system. In this section, the PV-battery-power electronic water heater scenario is selected, where the input data and models selection are shown in 3.4.

Table 4.11. The input date and model selection for researching different DOD impacts.

Examined scenario	Input data and model selection					
	PV generation	Loads consumption	Converters power rating	Battery stack energy rating	Hot water tank capacity	Ambient temperature and hot water consumption profiles
PV-battery-power electronic water heater scenario	3 kW peak output power profiles in one week for four seasons (1-minute time resolution)	2-person household load consumption profiles in one week for four seasons (1-minute time resolution)	1.64 kW power rating for the converter used	0.6 kWh/ 2Ah-17.9 kWh/60 Ah battery stack (0.5 pre-charge)	86 Liters (2 persons) water tank	2-person household hot water consumption profiles and ambient temperature profiles in one week for four seasons (1-minute time resolution)

Figure 4.15 illustrates the impact on weekly average grid electricity purchased total cost (under an Economy-7 tariff) for different battery sizes and DOD limits with 0.5 SOC overnight pre-charging. A wider available DOD range allows for

more usable energy storage of electricity, reducing cost for purchasing grid electricity. However, when the battery stack size is too small, the available battery energy storage for either 0.5 or 0.8 Depth of Discharge (DOD) has less impact on the cost of electricity purchased from the grid. Conversely, when the battery stack is too large, the available battery storage space has redundancy, reducing the impact of different DOD levels on this cost. Noticeably, the slope of both curves falls sharply at first, then begins to flatten around a 5 kWh battery stack and becomes almost flat beyond 10 kWh. This indicates that the savings in purchased grid electricity costs drop significantly after a 5 kWh battery stack.

Therefore, when considering the selection of the optimal battery stack size under these model and input data conditions, the optimum battery size can be defined as the point where any further increase in size (such as beyond 5 kWh) does not result in a substantial reduction in slope or a worsening of economic impact.

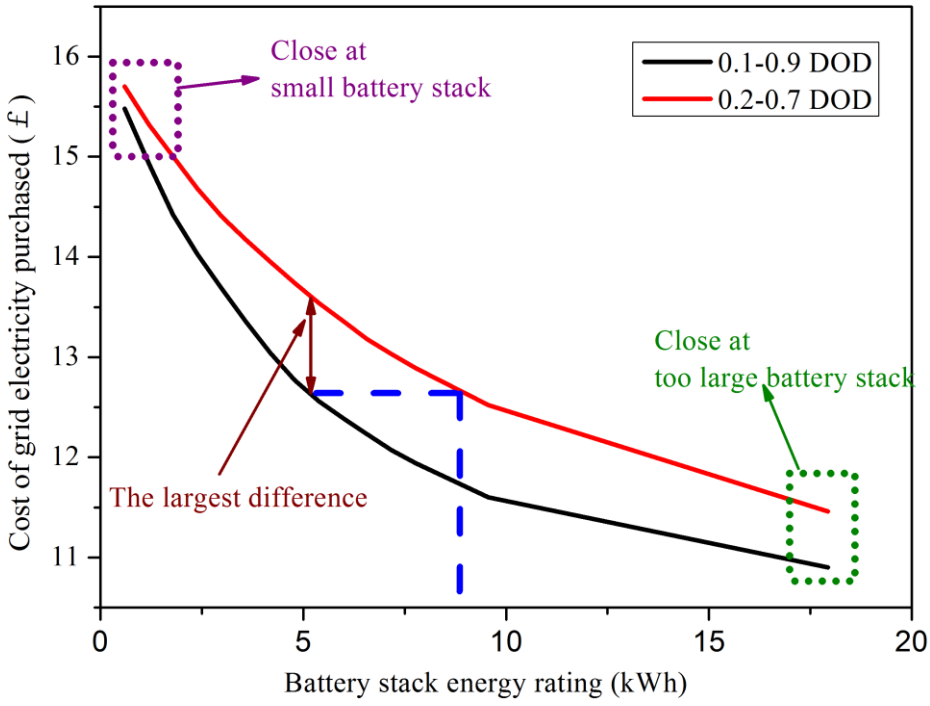

Figure 4.15. Weekly average electricity cost as the function of different battery stack.

4.3.1.2. Ohmic losses

To explore the impact of battery internal resistance on system outcomes, the PV-battery-power electronic water heater scenario is considered where the models and input data selection is seen in Table 4.12.

Table 4.12. The input date and model selection for researching Ohmic losses impacts.

Examined scenario	Input data and model selection					
	PV generation	Loads consumption	Converters power rating	Battery stack energy rating	Hot water tank capacity	Ambient temperature and hot water consumption profiles
PV-battery-power electronic water heater scenario	3 kW peak output power profiles in summer (1-minute time resolution)	2-person household load consumption profiles in summer (1-minute time resolution)	1.64 kW power rating for the converter used	1.2 kWh/ 4Ah and 20.32 kWh/68 Ah battery stack (0.5 pre-charge)	86 Liters (2 persons) water tank	2-person household hot water consumption profiles and ambient temperature profiles in summer (1-minute time resolution)

As seen in Section 3.5.2, different battery stacks are composed of multiple battery cells connected together (3.6V/2Ah/20 mΩ Molicel battery cell). For a nominal 300V battery stack (83 cells connected in series), a 1.2 kWh/4Ah battery stack has an internal resistance of 0.83 Ω, while this resistance is 0.049 Ω for a 20.32 kWh/68Ah battery stack. In this scenario, the connection resistance between each battery cell is not considered.

Figure 4.16 presents comparison results for these two types of battery stacks, depicting scenarios both with and without ohmic losses in the summer. In the case of the smaller battery stack size considered (1.2 kWh) having the higher internal resistance (0.83 Ω), the impact of ohmic losses is insignificant. This is because the battery stack's operational duration is lower and the relative ohmic energy losses which account also for operational time, remain negligible. Conversely, for the larger battery stack (20.32 kWh) with lower internal resistance (0.049 Ω), ohmic losses are also minimal due to the stack's capability to efficiently manage power flows without substantial loss effects as for a given battery stack voltage assumed constant for all, battery current is proportional

with battery power and not energy rating whilst energy losses, for same utilization time, will be dependent on battery internal resistance which is inverse proportional with energy rating.

The findings reveal that the difference between the idealized battery model (without ohmic losses) and the model incorporating ohmic losses is minimal which can be neglected.

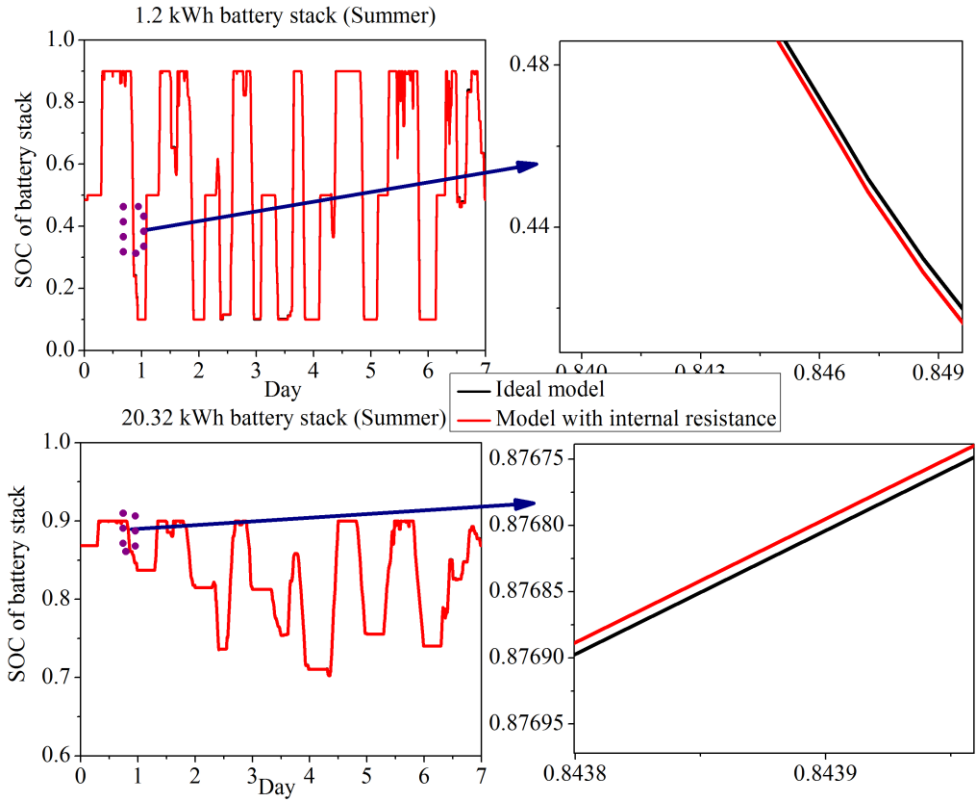

Figure 4.16. The comparison of different battery model with different battery stack size in the PV-battery-power electronic water heater scenario (summer week).

4.3.2. Cut-off power for all converters

The cut-off power ($P_{cut\text{-}off}$) level of converters plays a significant role in determining their cycle losses and efficiency, particularly at low operational power levels where the converters operate with low efficiency or be completely switched off that cancels losses but forces the system to purchase energy from grid (although the amount is very small). It has been recognized that one effective method to mitigate battery stack round-trip efficiency degradation is to

disable battery operations when the processing power falls below a specified threshold (cut-off power).

In this study, we compare converters operating with and without cut-off power limitations, for PV inverter (0.18 kW $P_{cut\text{-}off}$), battery charger (0.15 kW $P_{cut\text{-}off}$) and converter for heater (0.07 kW $P_{cut\text{-}off}$), as detailed in Section 3.5.1. This analysis focuses on the PV-battery-power electronic water heater scenario, where the input data and models definition can be seen in Table 4.13.

Table 4.13. The input data and model selection for researching cut-off power impacts.

Examined scenario	Input data and model selection					
	PV generation	Loads consumption	Converters power rating	Battery stack energy rating	Hot water tank capacity	Ambient temperature and hot water consumption profiles
PV-battery-power electronic water heater scenario	3 kW peak output power profiles in one week for four seasons (1-minute time resolution)	2-person household load consumption profiles in one week for four seasons (1-minute time resolution)	1.64 kW power rating for the converter used	5.98 kWh/ 20Ah (0.5 pre-charge)	86 Liters (2 persons) water tank	2-person household hot water consumption profiles and ambient temperature profiles in one week for four seasons (1-minute time resolution)

Figure 4.17 illustrates the comparison of battery stack charging /discharging process in the summer with and without cut-off power applied. When cut-off power is not implemented, the converter transfers and manages any power levels down to zero potentially involving unnecessary battery operations. Conversely, with cut-off power in place, battery operations are minimized unless necessary, cancelling converters standby power losses (each converter 30W stand-by losses) and optimizing efficiency.

Figure 4.18 presents the comparison of weekly average energy losses and purchased grid electricity cost with and without cut-off power for all converters. The energy losses contain battery ohmic losses, and the energy losses of PV inverter, battery charger and converter for water heater. Apparently, the total energy losses of the entire system are significantly reduced for all battery stack

energy rating when the cut-off power of converter is applied. However, compared to low energy rating battery stack, the high energy rating battery stack has larger operation duration which will cause more energy losses. Under this test conditions, incorporating cut-off power does not significantly increase the cost of grid electricity purchased, as operations below the cut-off power threshold are infrequent and typically involve minimal power levels.

Overall, this analysis underlines the importance of using cut-off power settings in converters for improving system efficiency by reducing unnecessary battery operations and associated energy losses.

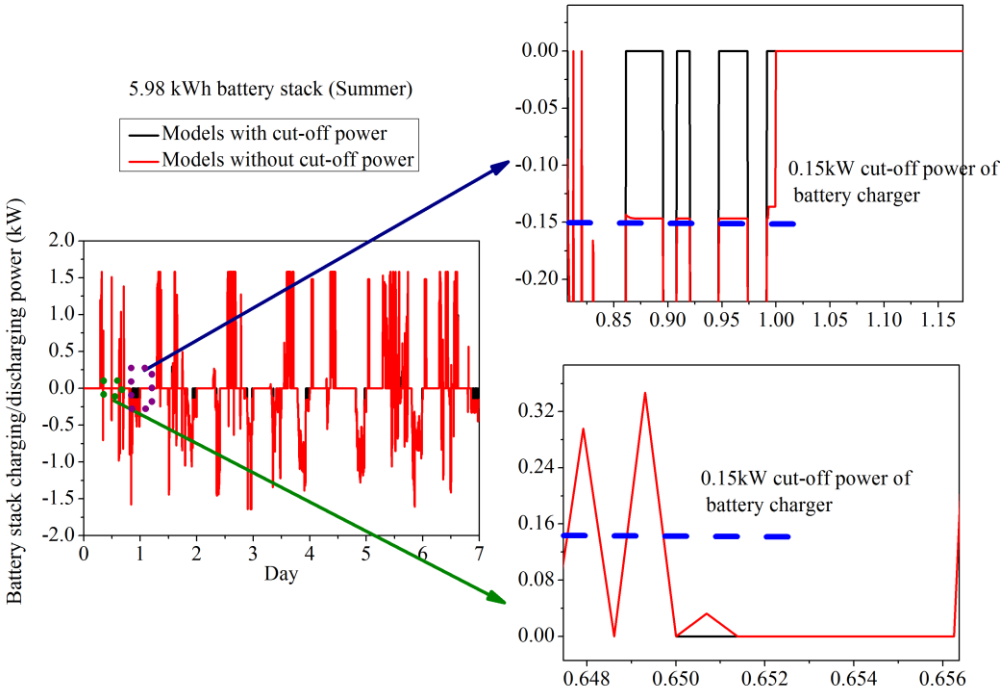

Figure 4.17. The comparison of the charging/discharging of battery stack with/without cut-off power in the summer.

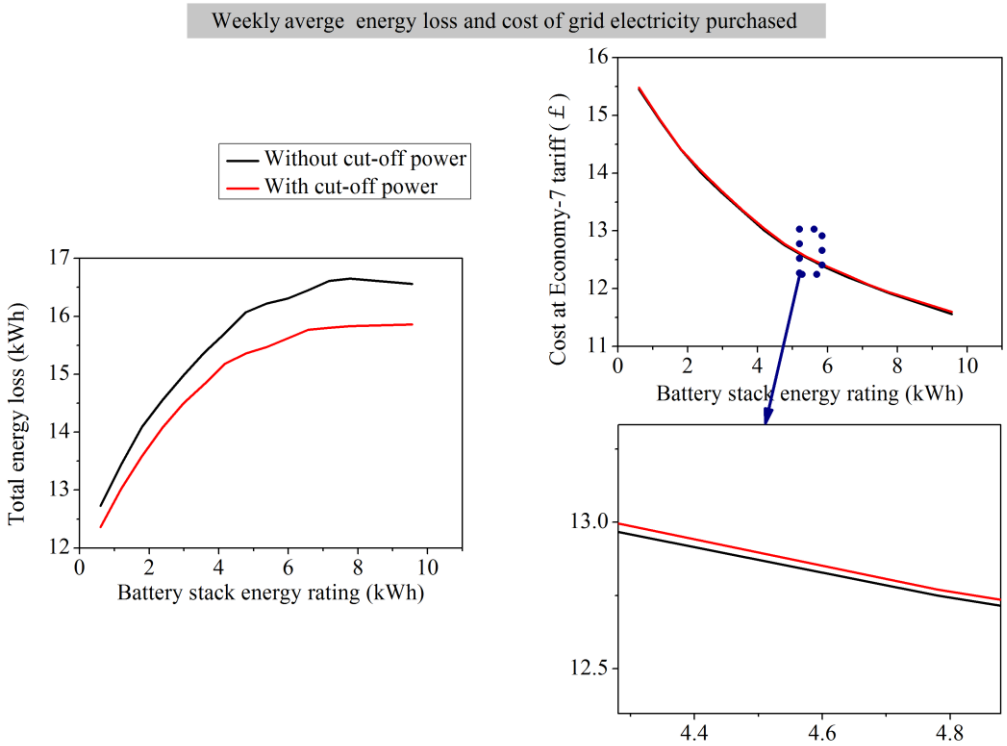

Figure 4.18. The comparison of the weekly average total energy losses and the purchased electricity cost with/without cut-off power considered for all converters.

4.4. Different input data impact

Understanding the impact of imported power profiles on outcome parameters is essential due to the variability in power generation and consumption profiles influenced by factors such as household size, daily habits, and location. In this thesis, different domestic loads consumption power profiles, hot water consumption profiles, and room space temperature profiles sourced from the CREST dataset with adjusted PV generation are examined and compared. Two primary factors are considered:

1. Number of House Occupants: Larger households typically require more room space, higher loads consumption, and increased hot water usage.

2. Sample Resolution: The resolution of input data affects the averaging of PV generation and loads consumption data, potentially introducing deviations in outcomes.

By analysing various power profiles under these conditions, the study aims to provide insights into how different household characteristics and data resolutions impact system performance, efficiency, and cost-effectiveness. This investigation is crucial for optimizing system design and operation to suit diverse residential energy needs and conditions.

4.4.1. Different house occupants

In this section, the impact of household occupancy (2, 3, or 5 occupants) on the cost of electricity purchased is examined. More residents in a household result in higher load consumption and greater hot water demand, necessitating proportionally increased PV generation. For comparison across different power profiles, the CERST model generates household load profiles with 1-minute resolution for 2, 3, and 5 occupants. The details of model and input data selection are shown in Table 4.14.

Table 4.14. The input data and model selection for researching different house occupants impacts.

Examined scenario	Input data and model selection					
	PV generation	Loads consumption	Converters power rating	Battery stack energy rating	Hot water tank capacity	Ambient temperature and hot water consumption profiles
PV-battery-power electronic water heater scenario	3 kW peak output power profiles in one week for four seasons (1-minute time resolution)	2-, 3-, and 5-person household load consumption profiles in one week for four seasons (1-minute time resolution)	1.64 kW, 2.4 kW, 3.5 kW, 6 kW, power rating for all converters used	0.6 kWh/ 2Ah-9.56 kWh/32 Ah battery stack (0.5 pre-charge)	86 Liters, 111 Liters, 161 Liters (2,3,5 persons) water tank	2-, 3-, and 5-person household hot water consumption profiles and ambient temperature profiles in one week for four seasons (1-minute time resolution)

The term "1.64 kW converters" refers to the power rating of all converters (PV inverter, battery charger, and converter for water heater) being set to 1.64 kW, with similar settings applied for 2.4 kW, 3.5 kW, and 6 kW converters. In Figure 4.19, it is evident that higher household occupancy leads to increased electricity consumption and higher grid energy purchased costs, particularly due to elevated hot water usage and overall load demand.

When a small converter power rating (1.64 kW) is applied, it significantly limits the 3 kW peak PV power output, resulting in significant curtailment of PV output and increased grid electricity purchases. Conversely, larger converters (3.5 kW and 6 kW) show minimal differences in the cost of grid electricity purchased, as they effectively handle most power conversion tasks. However, overly large converters (e.g., 6 kW) may lead to higher electricity costs due to inefficient operation at lower power processing levels.

Therefore, optimizing converter sizes tailored to the number of occupants is essential to achieve cost savings across different household configuration.

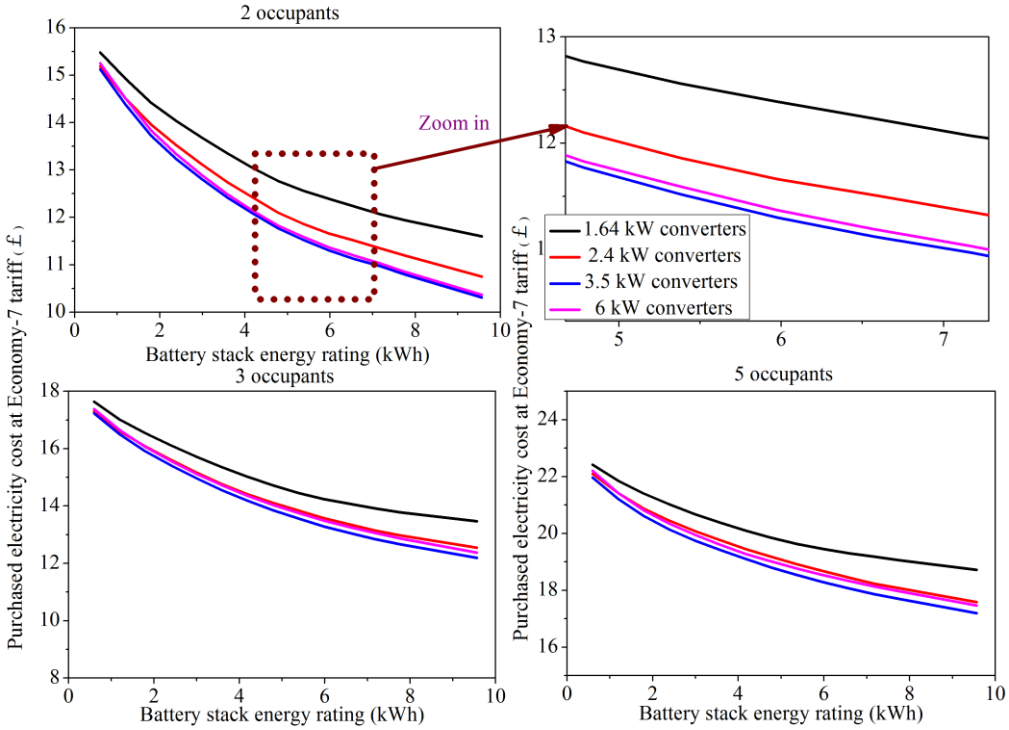

Figure 4.19. The weekly average purchased electricity cost for different house occupants at different converters power size and different battery stack energy rating.

4.4.2. Different sample resolution

In this study, two different sample resolutions of power profiles are compared: 1-minute and 5-minute intervals. To achieve the 5-minute resolution from the 1-minute dataset, the average power within each 5-minute window is calculated. The details of model and input data selection are shown in Table 4.5.

Table 4.15. The input data and model selection for researching different sample resolution impacts.

Examined scenario	Input data and model selection					
	PV generation	Loads consumption	Converters power rating	Battery stack energy rating	Hot water tank capacity	Ambient temperature and hot water consumption profiles
PV-battery-power electronic water heater scenario	3 kW peak output power profiles in one week for four seasons (1-minute time resolution)	2-, 3-, and 5-person household load consumption profiles in one week for four seasons (1- and 5-minute time resolution)	1.64 kW power rating for all converters used	0.6 kWh/ 2Ah-9.56 kWh/32 Ah battery stack (0.5 pre-charge)	86 Liters, 111 Liters, 161 Liters (2,3,5 persons) water tank	2-, 3-, and 5-person household hot water consumption profiles and ambient temperature profiles in one week for four seasons (1- and 5-minute time resolution)

Figure 4.20 illustrates that the battery stack charging patterns are very similar for both 1-minute and 5-minute resolutions across different household occupancies. Any differences observed are primarily due to the lower peak values in the 5-minute input dataset.

Figure 4.21 presents the weekly average cost of grid electricity purchased under an Economy-7 tariff for both 1-minute and 5-minute input data resolutions. It consistently shows that the electricity costs are higher for the 1-minute resolution compared to the 5-minute resolution. The higher costs associated with the 1-minute resolution are attributed to two factors:

1. Efficiency Impact: The system experiences higher losses with 1-minute data due to higher peak power ripples contained within this dataset. These additional power losses add up to noticeable energy losses that must be compensated by purchasing extra electricity from the grid.

2. Power Restrictions: Small and medium-sized power converters may struggle to handle the peak powers present in the 1-minute dataset, necessitating additional energy purchased from the grid to meet power demands due to power limitations.

Therefore, the choice of input power resolution significantly affects the purchased grid energy cost. Opting for a 5-minute resolution reduces costs by

smoothing out extreme current and power peaks and improving power losses, thereby minimizing additional energy purchases from the grid.

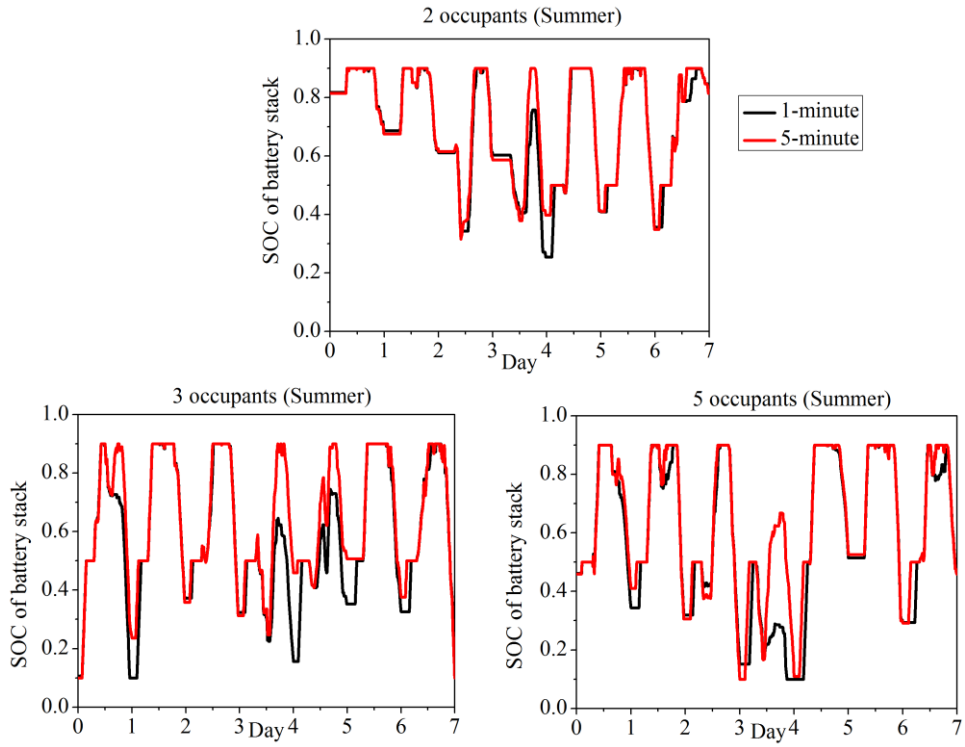

Figure 4.20. The battery stack charging pattern for different occupants at different input datasets sample resolution in summer.

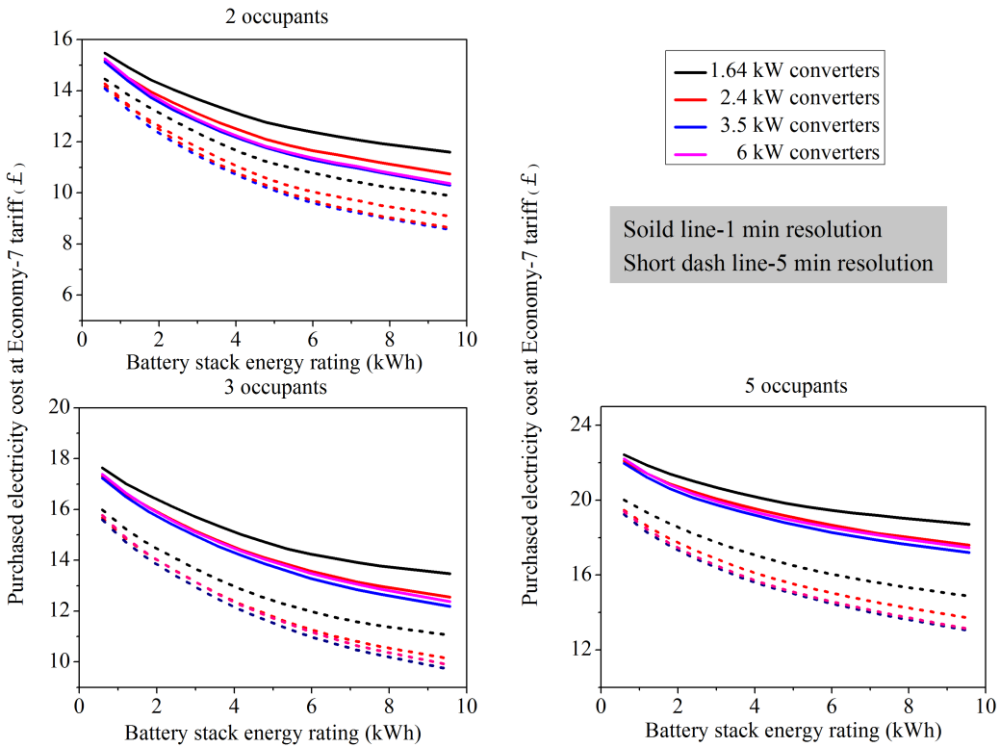

Figure 4.21. The weekly average purchased grid energy for different house occupants for 1-minute (solid) and 5-minute (dash) power sample resolution.

4.5. Optimal sizing

The size of system components such as PV generation, battery stack energy rating, and power converters power rating plays a crucial role in determining energy and power flows, thereby influencing the economic viability of the system.

PV generation (indicated by peak power) directly impacts self-consumed energy and the amount of energy imported from the grid. However, when PV generated power exceeds load consumption and energy storage is unavailable, the excess energy may be exported or curtailed (as considered in this thesis), reducing self-consumption. Similarly, the energy rating of the battery stack affects peak power purchases and the ability to store and use excess energy. A properly sized battery stack can optimize energy utilization and further reduce grid dependence.

Additionally, the power converter size determines the efficiency of power transfer within the system, influences power losses, and restricts the power transfer rating. This means that the choice of power converter size is crucial for balancing system efficiency, minimizing power losses, and ensuring adequate power transfer capabilities to meet household demand.

Oversizing components like PV generation, converters, and battery stacks may enhance the benefits of PV energy by reducing electricity costs. However, this approach also escalates initial purchase and installation costs.

Choosing the optimal size for each component involves balancing these factors. It requires evaluating the financial benefits derived from the reduced cost of electricity purchased under Economy-7 tariffs against the upfront costs of system installation and purchase, which can be seen in Section 3.4. This assessment

typically considers a 10-year operational period, factoring in the cost savings from electricity purchased and subtracting the initial system costs. Therefore, this section researches the study case for each scenario to find the optimal sizing scheme that achieves the maximum financial benefits over a 10-year operational period.

4.5.1. Sizing for PV self -consumption scenario

In this scenario, no energy storage device is utilized. Thus, only the PV generation (indicated by PV peak output power) and PV inverter power rating need to be optimised. The details of model and input data selection for the study case are shown in Table 4.16. Based on CREST electricity demand data, the smallest size (0.52 kW) generally meets the power requirements of a single household, while the 1.64 kW converter can cover over 80% of household power needs. The 2.4 kW and 3.5 kW sizes are sufficient for nearly all household power demands (excluding peak power situations), whereas the largest size (6 kW) is deployed for highest peak power scenarios.

Table 4.16. The input data and model selection in the PV self-consumption scenario optimization ('-' means not applied).

Examined scenario	Input data and model selection					
	PV generation	Loads consumption	Converters power rating	Battery stack energy rating	Hot water tank capacity	Ambient temperature and hot water consumption profiles
PV self-consumption scenario	Adjusted peak output power profiles (0.6 kW to 7.2 kW at intervals of 0.6 kW) in one week for four seasons (1-minute time resolution)	2-, 3-, and 5-person household load consumption profiles in one week for four seasons (1-minute time resolution)	0.52 kW, 1.64 kW, 2.4 kW, 3.5 kW, 6 kW, power rating for all converters used	-	-	-

Figure 4.22 illustrates the maximum financial benefits over a 10-year period for PV self-consumption systems across different sizes of PV generation and inverters. It demonstrates that installing a PV system can reduce the cost of

purchased grid electricity for residents compared to solely importing electricity from the grid. Notably, due to the higher demand for loads in a 5-occupant house, more PV energy can be consumed rather than curtailed, resulting in greater financial benefits compared to a 2-occupant house.

Furthermore, larger PV panels and converter power sizes do not necessarily yield the highest financial benefits due to mismatches between PV generation and household load consumption, which cause significant PV energy curtailment. Instead, optimal benefits in terms of maximum financial reward with minimum investment are achieved with specific PV and inverter installations, such as 1.2 kW peak power PV panels paired with 0.52 kW inverters across various household sizes (2, 3, or 5 occupants).

Nevertheless, the absence of energy storage devices limits the PV utilization rate in this scenario, as highlighted in Table 4.17, where the optimal installations result in approximately 50% PV utilization rate across all household types. This suggests that even with increased household loads consumption, PV panel and inverter sizes remain small in this scenario. Thus, it needs to install energy storage solutions to further enhance PV utilization rates and increases the financial benefits.

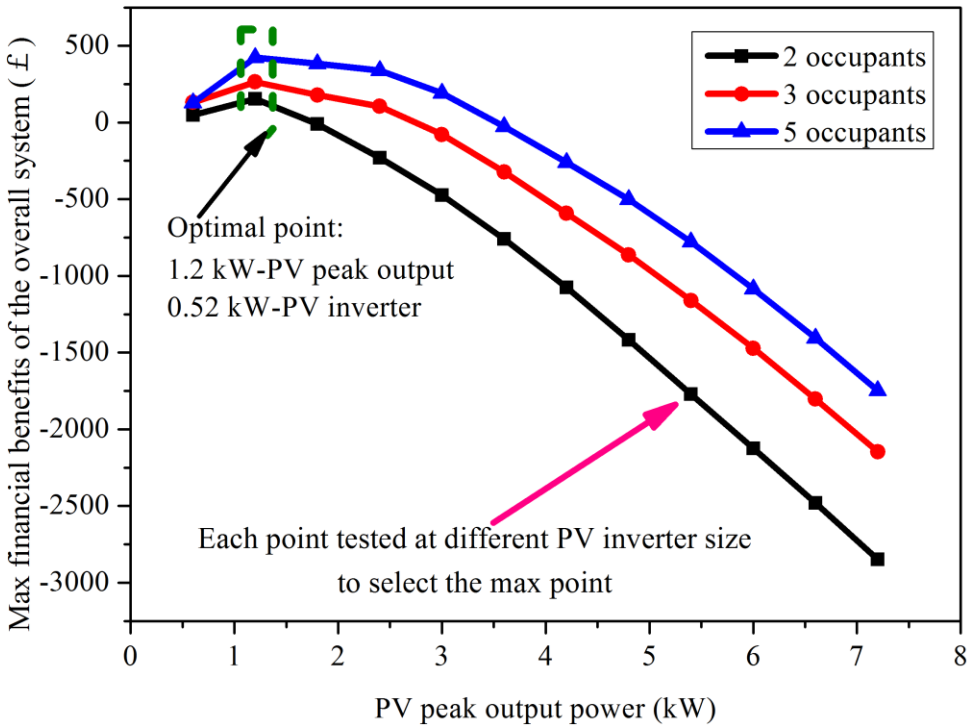

Figure 4.22. Financial benefits of the overall system for 10-year period at different PV peak power and PV inverter size.

Table 4.17. Financial benefits and PV utilization rate at optimal point for different occupants applications for 10-year period.

Number of occupants	2		3		5	
Optimal devices design	PV peak/kW	PV inverter/kW	PV peak/kW	PV inverter/kW	PV peak/kW	PV inverter/kW
	1.2	0.52	1.2	0.52	1.2	0.52
Electricity cost without PV installation /£	8673.4		9880.1		11893	
Financial benefits of optimal point/£	159.77		264.12		417.89	
PV utilization rate/%	46.35		42.4		52.64	

4.5.2. Sizing for PV-battery energy storage scenario

To store and utilize the excess PV energy, a battery stack energy storage system is utilized in this scenario. In this scenario,0.6 kW- 7.2 kW peak output generation power PV string is considered, along with a 0.6 kW interval, and 14 types of battery stack capacity (0.598 kWh-9.56 kWh) and 15 types of the power size combination of PV inverter and battery charger which are shown in Figure 4.23. Besides, to compare with the PV self-consumption, the energy consumption associated with producing hot water is not considered in this

scenario. More details of models and input data selection for the study case are shown in Table 4.18.

Table 4.18. Input data and model selection in the PV-battery scenario optimization ('-' means not applied).

Examined scenario	Input data and model selection					
	PV generation	Loads consumption	Converters power rating	Battery stack energy rating	Hot water tank capacity	Ambient temperature and hot water consumption profiles
PV self-consumption scenario	Adjusted peak output power profiles (0.6 kW to 7.2 kW at intervals of 0.6 kW) in one week for four seasons (1-minute time resolution)	2-, 3-, and 5-person household load consumption profiles in one week for four seasons (1-minute time resolution)	15 types of converters combinations	0.6 kWh/ 2Ah-9.56 kWh/32 Ah battery stack (SOC 0.1-0.9 with 0.1 interval pre-charge)	-	-

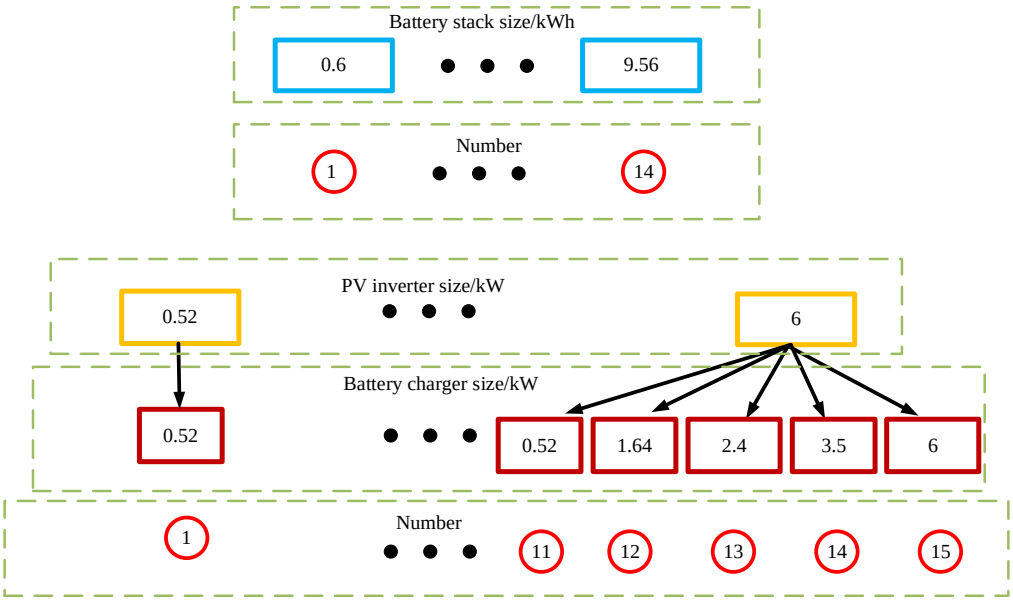

Figure 4.23. Series number of the battery stack and the combination of PV inverter and battery charger.

In this study, the pre-charge level of the battery stack is crucially influenced by seasons and household load consumption, as detailed in Section 4.2. To determine optimal device sizes, different pre-charge levels during night/off peak charging of the battery stack SOC (0.1-0.9 with 0.1 intervals) are employed. This approach aims to identify the best combinations of PV installation, battery stack

size, and converter power rating over a 10-year period for varying numbers of occupants in residential settings.

Figure 4.24 illustrates an example of the financial benefits of a PV-battery energy storage system over 10 years for a 2-occupant household, considering different device sizes with 0.1 pre-charge level of the battery during off peak time. The yellow bars highlight instances where financial benefits exceed £500. The results emphasize that simply scaling up device sizes does not necessarily lead to higher financial gains, indicating that an optimal configuration exists.

Table 4.19 summarizes the optimal device sizes for different household occupancies. Notably, smaller PV panel installations and converter combinations, along with a 5.98 kWh battery stack with 0.1 pre-charge level of battery stack, prove most economical for 2-occupant households. In contrast, for 3 or 5 occupants, increasing the peak power of the PV string to 3 kW is beneficial, in conjunction with using a larger 5.98 kWh battery stack required for 5 occupants. Interestingly, it appears that a 0.1 pre-charge level for the battery stack during off-peak hours maximizes financial returns (financial benefits). This implies that there is no need for overnight charging for battery stack in all houses (2, 3, and 5 occupant), as the available SOC stars at 0.1. Moreover, PV self-utilization rates exceed 70% across all houses, highlighting the efficacy of the PV-battery system configuration.

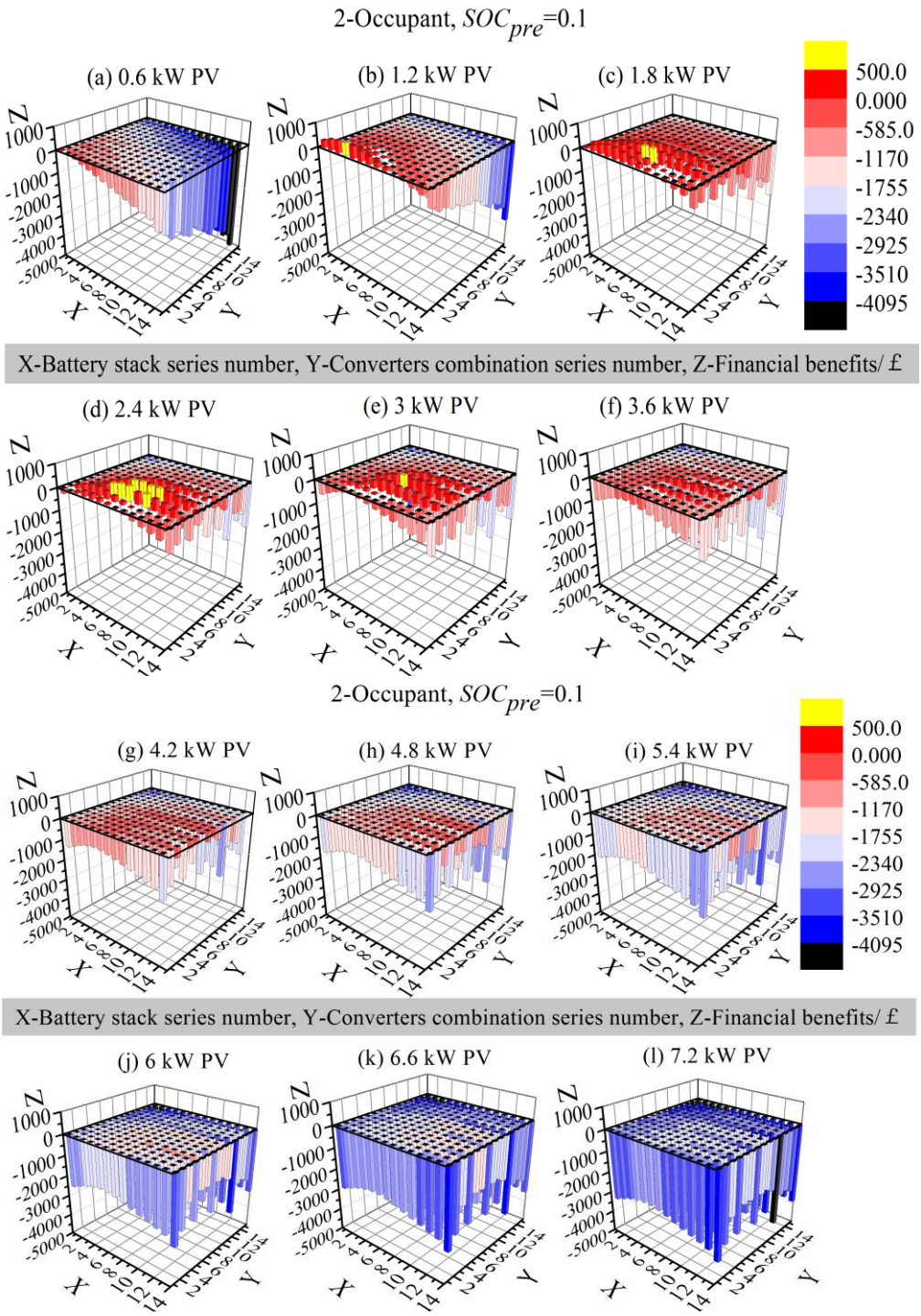

Figure 4.24. Financial benefits of PV-battery energy storage scenario for 10-year period at 0.1 pre-charge.

Table 4.19. Optimal devices design for PV-battery energy storage scenario for different house applications for 10-year period.

Number of occupants	2			3			5		
Optimal devices design	PV peak/ kW	Inverter-Battery charger combination/kW	Battery stack/kWh - SOC_{pre}	PV peak/ kW	Inverter-Battery charger combination/kW	Battery stack/kWh -SOC_{pre}	PV peak/ kW	Inverter-Battery charger combination/kW	Battery stack/kWh - SOC_{pre}
	2.4	1.64-1.64-×	4.78-0.1	3	2.4-1.64-×	4.78-0.1	3	2.4-1.64-×	5.98-0.1
Electricity cost without PV installation /£	8673.4			9880.1			11893		
Financial benefits of optimal point/£	620.51			1278.1			1467.1		
PV utilization rate/%	72.6			73.41			76.9		

4.5.3. Sizing for PV-power electronic water heater scenario

In this scenario, the excess PV energy and grid electricity are the only sources to heat water in a hot water tank, and the excess PV energy stored in the eater tank is explored as an alternative to battery energy storage. Based on the models, devices, and electricity tariff outlined in Chapter 3, the optimal configurations for the PV-power electronic water heater system are determined for households with 2, 3, and 5 occupants. As detailed in Section 3.5.3, the water in the tank is initially heated to 90°C using inexpensive grid electricity during off-peak hours. Excess PV energy is then used to compensate for storage losses and to maintain a operating water temperature of at least 40°C despite fluctuations caused by hot water usage and cold-water input during peak hours. This ensures a continuous availability of supply of hot water for household needs at any time. More details of models and input data selection for the study case are shown in Table 4.20.

Table 4.20. Input data and model selection in the PV-power electronic water heater scenario optimization ('-' means not applied).

Examined scenario	Input data and model selection					
	PV generation	Loads consumption	Converters power rating	Battery stack energy rating	Hot water tank capacity	Ambient temperature and hot water consumption profiles
PV self-consumption scenario	Adjusted peak output power profiles (0.6 kW to 7.2 kW at intervals of 0.6 kW) in one week for four seasons (1-minute time resolution)	2-, 3-, and 5-person household load consumption profiles in one week for four seasons (1- minute time resolution)	15 types of converters combinations (similar with the converter combination in PV-battery scenario where the difference is the battery charger is changed to the converter for water heater)	-	86 L for 2-occupant, 111 L for 3-occupant, and 161 L for 5-occupant	2, 3, 5-person household hot water consumption profiles and ambient temperature profiles in one week for four seasons (1-minute time resolution)

Table 4.21 presents the results of the optimization algorithm for the study case. Due to the intermittent nature of PV generation, the grid electricity is used to heat water in the water tank during off-peak hours which is essential to ensure adequate water temperature in the tank all day. Consequently, certain PV panel and converter combinations are deemed unsuitable for all three household sizes. For instance, a 0.52 kW PV inverter or a 0.52 kW converter for the electric water heater is insufficient for all household situations (2, 3, 5-occupant). The small power rating of the PV inverter and the converter for the water heater restricts the ability to absorb excess PV energy to heat water during peak hours. Compared to larger converters, this results in a relatively lower water temperature, which may drop below the appropriate hot water usage temperature (40°C) when hot water is consumed, and cold water is injected.

In the 5-occupant household with a larger water tank (161 L) installed, smaller PV panel installations (e.g., 1.2 kW) suffice because a significant portion of energy is sourced from the grid during off-peak periods. As a result, the average hot water temperature in the water tank remains higher and is more robust against temperature drops when hot water is consumed and cold water is injected.

Conversely, with a small water tank size installation, the robustness against temperature drops caused by cold water injection is poor. Therefore, smaller PV installations, such as 1.2 kW and 2.4 kW for a 3-occupant house, are inadequate to satisfy the hot water usage temperature energy demand, as no peak grid electricity is consumed.

Moreover, the 5-occupant household exhibits higher electric energy demand for both household loads and hot water energy demand. Therefore, with the same PV panel installation and converter power rating utilization for both 2-occupant

and 5-occupant households, more excess PV energy can be consumed rather than curtailed in the 5-occupant household. This results in less grid electricity purchased and higher financial benefits achieved compared to the 2-occupant household.

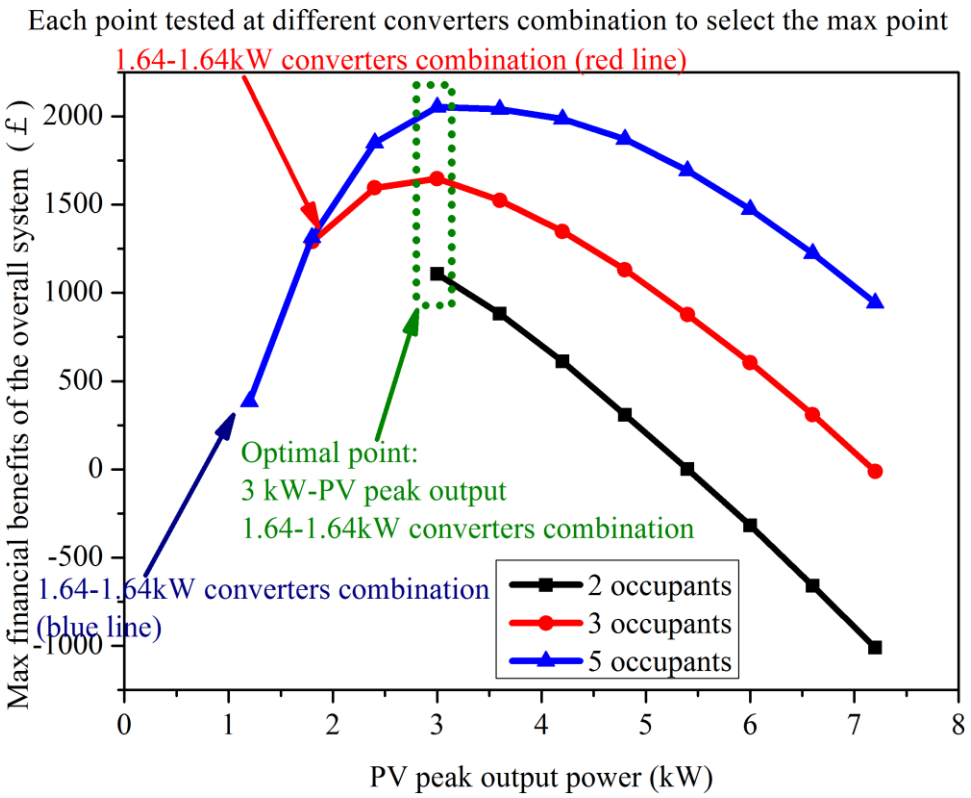

Figure 4.25. Financial benefits of PV-power electronic water heater scenario at different PV and converters combination installation for 10-year period.

Table 4.21. Optimal devices design for PV-power electronic water heater scenario for different house applications for 10-year period.

Number of occupants	2		3		5	
Optimal devices design	PV panels/ kW	Inverter-electric water heater converter/kW	PV panels/ kW	Inverter-electric water heater converter/kW	PV panels/ kW	Inverter-electric water heater converter/kW
	3	1.64-1.64	3	1.64-1.64	3	1.64-1.64
Electricity cost without PV installation /£	12865		14579		17508	
Financial benefits of optimal point/£	111.05		1647.5		2061.7	
PV utilization rate/%	56.83		63.46		67.17	
Energy consumption for heating water in the tank (weekly average)						
Off-peak & peak energy consumption /kWh	33.18&20.05		38.76&21.69		51.01&23.58	

4.5.4. Sizing for PV-battery-power electronic water heater scenario

In this scenario, surplus PV energy is stored in both a hot water tank and a battery stack to enhance PV utilization and achieve financial benefits. Various sizes of PV panels (peak power: 0.6 kW to 7.2 kW), combinations of converters (PV inverter, battery charger, and converter for electric water heater), and battery stack capacities (0.598 kWh to 9.56 kWh) are evaluated to determine the optimal device selection.

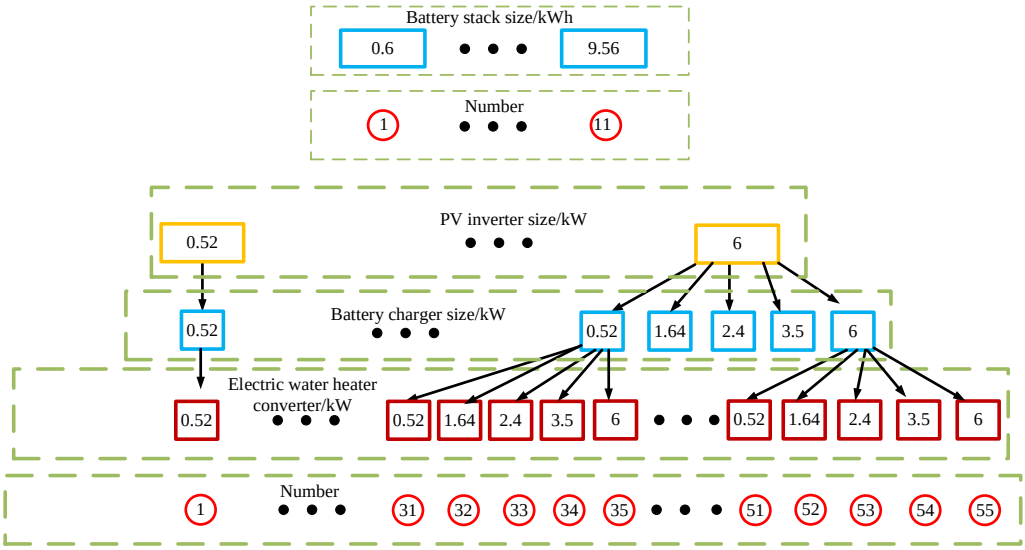

Figure *4.26* illustrates the diverse combinations of converters and battery stacks, encompassing of 55 converter configurations and 11 battery capacities. More details of models and input data selection for the study case are shown in Table 4.22.

Table 4.22. Input data and model selection in the PV-battery-power electronic water heater scenario optimization.

Examined scenario	Input data and model selection					
	PV generation	Loads consumption	Converters power rating	Battery stack energy rating	Hot water tank capacity	Ambient temperature and hot water consumption profiles
PV self-consumption scenario	Adjusted peak output power profiles (0.6 kW to 7.2 kW at intervals of 0.6 kW) in one week for four seasons (1-minute time resolution)	2-, 3-, and 5-person household load consumption profiles in one week for four seasons (1-minute time resolution)	55 types of converters combinations	0.6 kWh/ 2Ah-9.56 kWh/32 Ah battery stack (SOC 0.1-0.9 with 0.1 interval pre-charge)	86 L for 2-occupant, 111 L for 3-occupant, and 161 L for 5-occupant	2, 3, 5-person household hot water consumption profiles and ambient temperature profiles in one week for four seasons (1-minute time resolution)

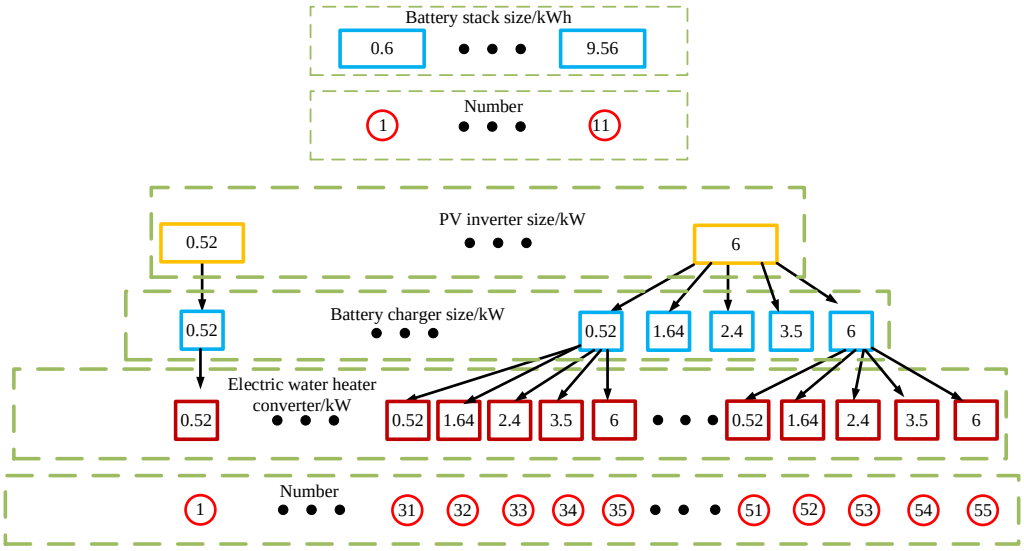

Figure 4.26. Series number of the battery stack and the combination of PV inverter, battery charger, and electric water heater converter.

Figure 4.27 illustrates the financial benefits example at a 0.2 SOC_{pre} level for the battery stack in the PV-battery-power electronic water heater scenario over a 10-year period. Like the PV-power electronic water heater scenario, configurations with PV panel installations below 2.4 kW peak power cannot meet the household's hot water energy consumption needs. It was found that starting from 3 kW peak power generation, the system can consistently provide hot water at a minimum of 40°C for household use. Therefore, PV installations

smaller than 2.4 kW are unsuitable for households with 2, 3, and 5 occupants using the PV/battery/power electronic water heater scenario.

It is found that as the sizes of system components (PV panels, converter power rating, and battery stack capacity) increase, initial investment costs rise, thereby reducing overall financial benefits. To determine the optimal device sizes and optimal SOC_{pre} level for the battery, various combinations of battery stack capacities, converter configurations, and PV panel sizes are evaluated across applications with 2, 3, and 5 occupants. The optimal configurations for the study case are summarized in Table 4.23. Apparently, the PV utilization rate exceeds 74% for all households (2, 3, and 5 occupants) while achieving maximum financial benefits with this optimal selection. Additionally, the pre-charge level (SOC_{pre}) of the battery stack significantly impacts the economic viability of the entire system. For households with 3 and 5 occupants, setting the battery stack pre-charge level to 0.3 SOC_{pre} maximizes financial benefits, while a 0.2 SOC_{pre} level is optimal for 2 occupants.

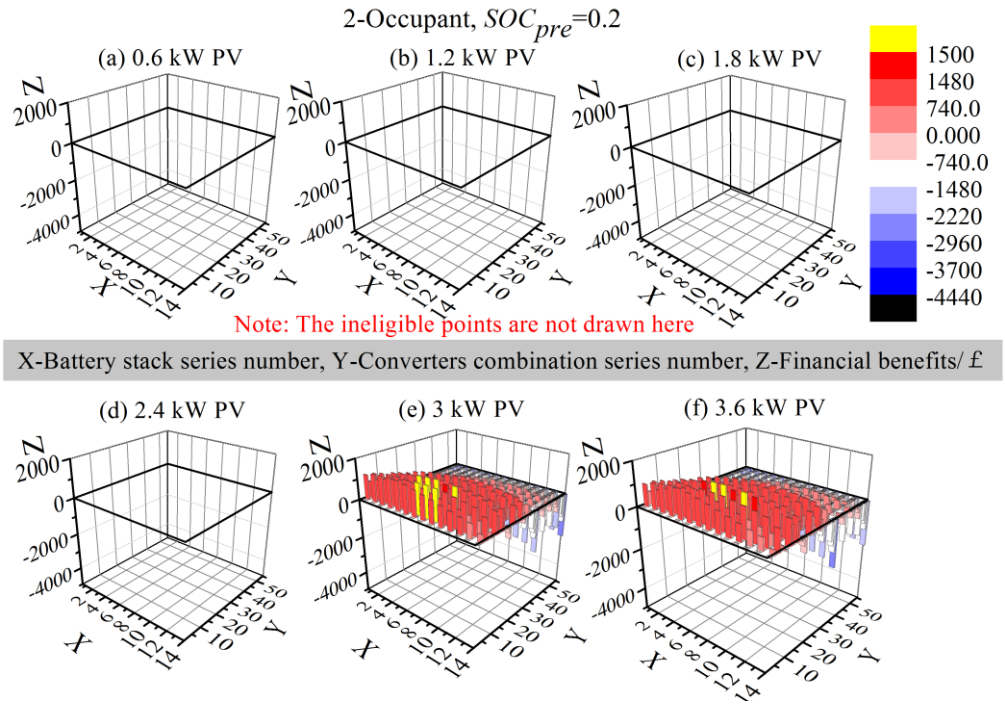

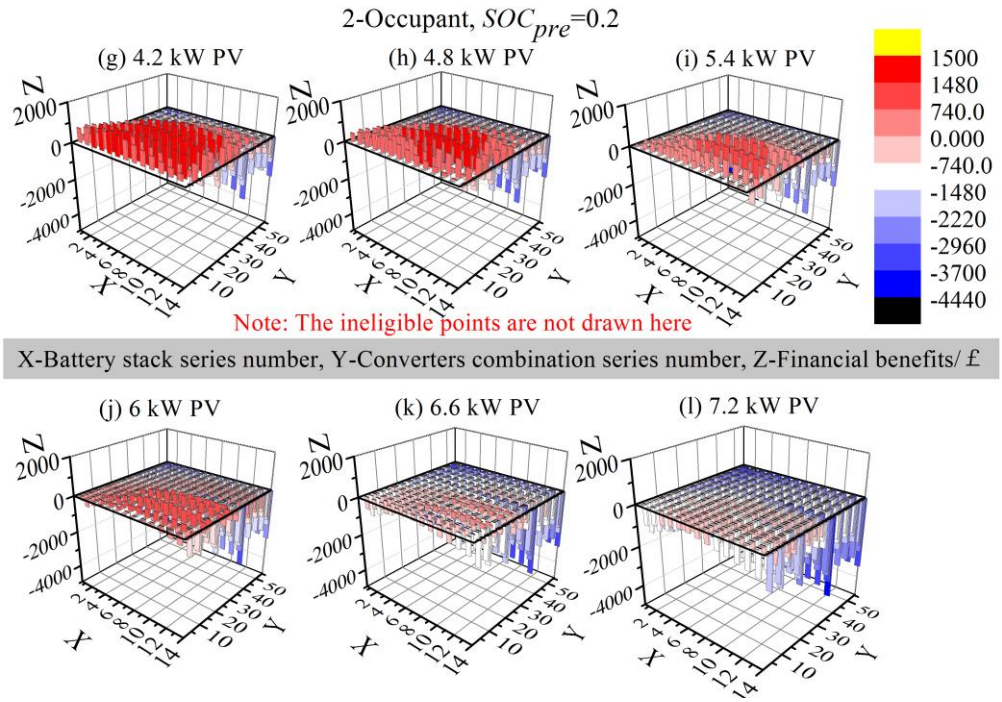

Figure 4.27. Financial benefits of PV-battery-power electronic water heater scenario for 10-year period at 0.2 pre-charge.

Table 4.23. Optimal devices design for PV-battery-power electronic water heater scenario for different house applications for 10-year period.

Number of occupants	2			3			5		
Optimal devices design	PV panels/kW	Inverter-Battery charger-electric water heater converter combination/kW	Battery stack/kWh - SOC_{pre}	PV panels/kW	Inverter-Battery charger-electric water heater converter combination/kW	Battery stack/kWh - SOC_{pre}	PV panels/kW	Inverter-Battery charger-electric water heater converter combination/kW	Battery stack/kWh - SOC_{pre}
	3	2.4-1.64-1.64	4.78-0.2	4.2	2.4-1.64-1.64	5.98-0.3	4.8	3.5-2.4-1.64	7.17-0.3
Electricity cost without PV installation /£	12863			14680			17772		
Financial benefits of optimal point/£	1599.4			2449.8			3006		
PV utilization rate/%	80.56			74.26			75.74		

4.5.5. Comparison of these four scenarios

Table 4.24 presents a comparison of optimal design outcomes based on financial benefits over a 10-year period for various scenarios. Addressing the challenge of mismatch between PV generation and household consumption, it is

found that integrating energy storage devices into PV systems proves advantageous following the optimization analyses.

Comparing scenarios, employing energy storage systems—specifically battery storage—enhances system economics and supports larger PV panel installations, particularly as household electrical device usage increases. This thesis considers two types of energy storage systems: battery storage and thermal storage in the form of the hot water tank found in most households. Due to the difficulty in replicating hot water consumption patterns in PV self-consumption scenarios and PV-battery energy storage scenarios, comparisons are made between PV self-consumption versus PV-battery energy storage, and PV-power electronic water heater versus PV-battery-power electronic water heater scenarios.

Notably, compared to scenarios without PV systems or with PV panels alone, integrating energy storage devices allows for larger PV panel installations, thereby increasing the financial benefits. The PV-battery-power electronic water heater scenario emerges as the most profitable approach for utilizing PV energy. It not only provides household with hot water but also delivers substantial financial benefits while achieving a high PV utilization rate (over 74%).

Table 4.24. The comparison between financial benefits and PV utilization rate for different scenario for different occupants applications ('×' represents the stuff is not applied).

Scenario		2			3			5		
	Devices type	PV panels/kW	Inverter-Battery charger-electric water heater converter combination/kW	Battery stack/kWh - SOC_{pre}	PV panels/kW	Inverter-Battery charger-electric water heater converter combination/kW	Battery stack/kWh - SOC_{pre}	PV panels/kW	Inverter-Battery charger-electric water heater converter combination/kW	Battery stack/kWh - SOC_{pre}
PV self-consumption scenario	Optimal design	1.2	0.52-×-×	×-×	1.2	0.52-×-×	×-×	1.2	0.52-×-×	×-×
	Financial benefits/£	159.77			264.12			417.89		
	PV utilization rate/%	46.35			42.4			52.64		
PV-battery energy storage scenario	Optimal design	2.4	1.64-1.64-×	4.78-0.1	3	2.4-1.64-×	4.78-0.1	3	2.4-1.64-×	5.98-0.1
	Financial benefits/£	620.51			1278.1			1467.1		
	PV utilization rate/%	72.6			73.41			76.9		
PV-power electronic water heater scenario	Optimal design	3	1.64-×-1.64	×-×	3	1.64-×-1.64	×-×	3	1.64-×-1.64	×-×
	Financial benefits/£	111.05			1647.5			2061.7		
	PV utilization rate/%	56.83			63.46			67.17		
PV-battery power electronic water heater scenario	Optimal design	3	2.4-1.64-1.64	4.78-0.2	4.2	2.4-1.64-1.64	5.98-0.3	4.8	3.5-2.4-1.64	7.17-0.3
	Financial benefits/£	1599.4			2449.8			3006		
	PV utilization rate/%	80.56			74.26			75.74		

4.6. Summary

Followed the optimization procedure outlined in Chapter 3, this chapter aims to determine the most profitable device sizes (PV panels, converters, and battery stack energy rating) for each given study case. While the input data originates from England, the optimization methodology (a rule-based approach integrated with numerical data) can be adapted for use in other regions.

Initially, each scenario undergoes validation to ensure simulation results adhere to defined constraints. Given the sensitivity of costs of purchased electricity to the pre-charge level of battery stack, the analysis explores the impact of different SOC preset levels (ranging from 0.1 to 0.9 at 0.1 intervals) on both PV-battery energy storage and PV-battery with power electronic scenarios. Varying SOC preset levels influence battery stack operation, affecting electricity costs and PV utilization rates. Consequently, flexible adjustment of battery stack pre-charge levels is essential to maximize economic returns based on different PV generation and household consumption patterns.

Next, a sensitivity analysis is conducted to examine how various model parameters and input data factors impact energy and financial outcomes. Parameters such as DOD range directly influence the available battery energy, while factors like internal resistance, cut-off power, and standby losses affect system efficiency. Lower input data resolution diminishes optimization result accuracy. Finally, after the optimization procedure is proposed for each study case, the most economically efficient combination of devices and designs are shown for different household occupancies across various test scenarios.

The results highlight the importance of optimizing the different device sizes to achieve maximum financial benefits and self-consumption of PV generated

energy rather than simply installing the largest devices without considering costs. Compared to other PV utilization scenarios, the PV-battery-power electronic water heater scenario emerges as the most profitable option, offering a high PV self-utilization rate of approximately 74% for all 2, 3, and 5 occupants houses at highest financial benefits while simultaneously providing hot water for household consumption.

Chapter 5: Modelling PV-battery-novel power electronic water heater power system

In this chapter, the circuit topology, modelling method, harmonics compensation capability, and control algorithm of the proposed power electronic water heater will be demonstrated, as well as the control algorithms for the PV inverter and battery DC/DC converter. Subsequently, the proposed power electronic water heater and its control methods are simulated using PLECS. To explore different types of PV applications, the performance of the PV inverter and battery charger is also simulated. Figure 5.1 shows the schematic diagram of the established PV power system, including battery energy storage system (battery stack and bidirectional DC/DC converter), PV input, PV inverter, power electronic water heater system, and autotransformer (used in the experimental setup for safety operation). Significantly, the power electronic water heater can be interfaced with either the DC bus or the AC grid. In the optimization chapter, the topology of the power electronic water heater connected to the DC bus is examined. Meanwhile, the topology of the power electronic water heater connected to the AC grid is also identified and evaluated for further study.

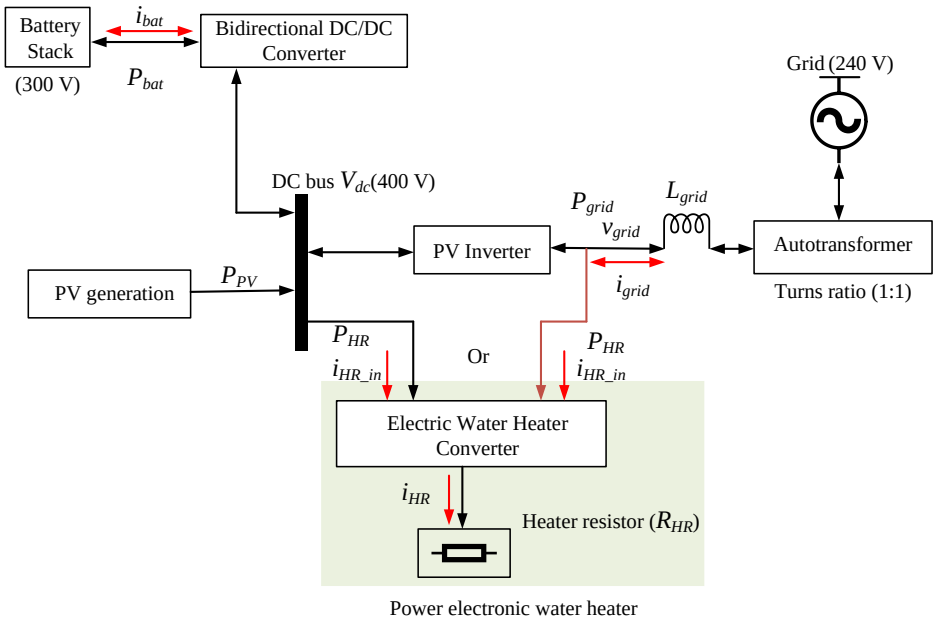

Figure 5.1. Schematic diagram of PV-battery-novel power electronic water heater integrated system.

5.1. The proposed power electronic water heater

5.1.1. The topology of the power electronic water heater

The proposed power electronic water heater is illustrated in Figure 5.2 (a) when it is connected to the AC grid. It comprises an input *LC* filter, a diode rectifier bridge, one IGBT (S_4), and three immersion heater loads. To widen the power consumption range of the water heater, three individual immersion heating loads are controlled by three cheaper relays switches (S_1, S_2, S_3). Since the heating element is constructed using wound resistive wire, which may be inductive, a parasitic inductor (L_{HR}) will be present in each heating element. Therefore, a freewheeling diode must be mounted in parallel with the heating element to eliminate any overvoltage caused during the turn-off transient of the corresponding switch. Besides, the i_{HR_in} is the input current of the power electronic water heater and the i_{HR} is the current flowing through the heater resistor.

To accurately consume excess PV power and broaden the power consumption range, IGBT, S_4 is PWM-controlled, while the rest of the relays (S_1, S_2, S_3) are used to control the heating load resistance. The LC filter (L_{HR_in}, C_{HR_in}) is designed to reduce the switching current ripple fed into the power grid. The diode bridge converts AC voltage to DC voltage.

The circuit can be also simplified as shown in Figure 5.2 (b), with just one heater.

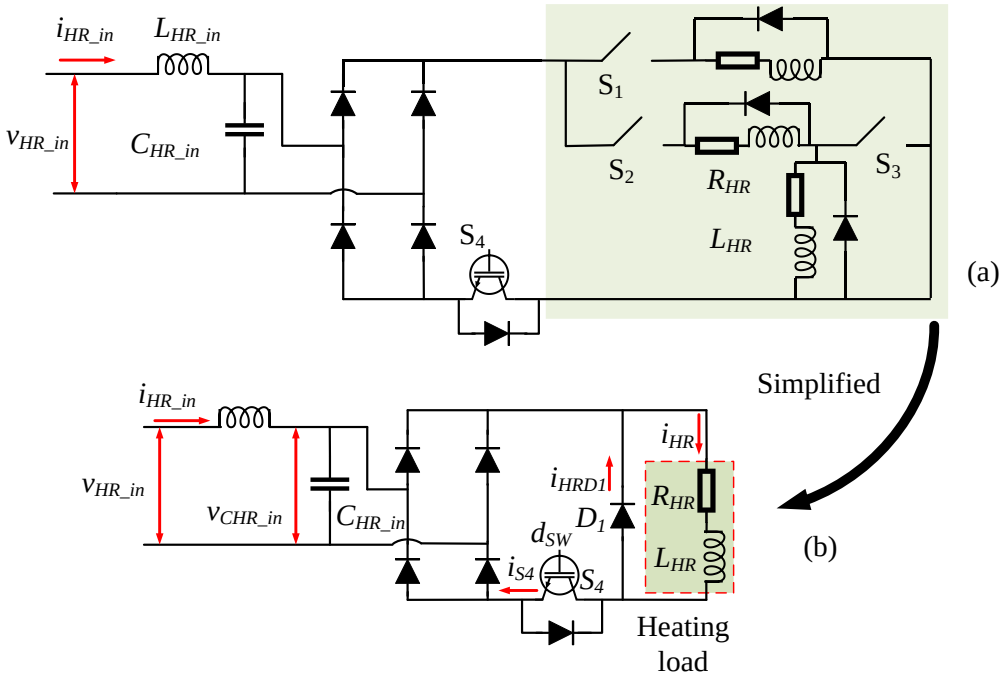

Figure 5.2. Topology of the proposed power electronic water heater.

It takes significant time for traditional electric water heaters with relays to adjust to match the amount of surplus PV power, with relay reaction times of around 50 ms. This delay can result in a mismatch between PV power generation and power consumption. However, the proposed power electronic water heater demonstrates better transient performance, as validated by simulation.

First, a simulation model of the proposed power electronic water heater, shown in Figure 5.2 (a), is built using PLECS software. By controlling the three relay switches (S_1, S_2, S_3), five different heating resistive loads can be achieved, as illustrated in Table 5.1. When this power electronic water heater is connected to a 400 V DC input or a 240 V AC input with a 0.5 duty cycle for switch S4, the input voltage v_{HR_in} and input current i_{HR_in} for different switching combinations are shown in Figure 5.3 (a) and Figure 5.3 (b), respectively.

The simulation results reveal that the proposed power electronic water heater exhibits varying input currents in response to switching combinations. This

indicates that the heater has a broader power consumption range without requiring extreme duty cycle utilization for S_4.

Table 5.1. 5 types of heating resistance at different switching combinations (0-switching off, 1-swicthing on).

Stage	S_1	S_2	S_3	Equivalent resistance
1	0	0	0	0
2	0	1	0	$2R_{HR}$
3	1	0	0	R_{HR}
	0	1	1	R_{HR}
4	1	1	0	$2/3R_{HR}$
5	1	1	1	$1/2R_{HR}$

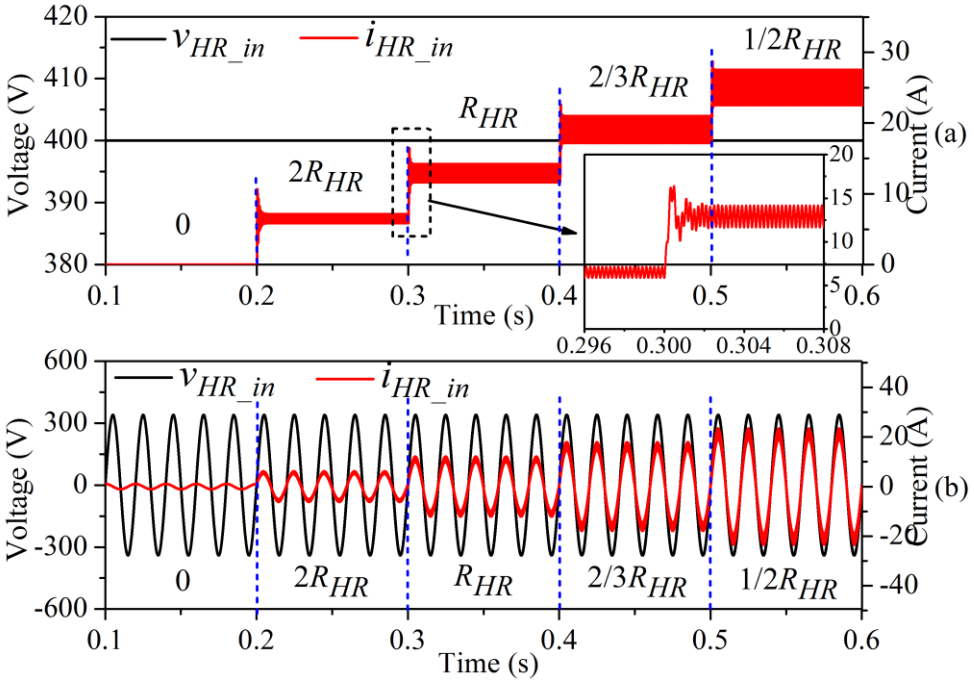

Figure 5.3. Simulation results of input voltage and current at different switch combinations with (a) DC input voltage and (b) AC input voltage.

To validate the functionality of harmonics compensation capability and power consumption of the power electronic water heater, the simplified circuit as shown in Figure 5.2 (b) is used in the later theoretical waveforms analysis, experimental and simulation validation. In this topology, the relays (S_1, S_2, S_3) controlled resistors are simplified to one resistor.

5.1.2. Switching patterns of simplified circuit.

The theoretical waveforms are depicted in Figure 5.4, which includes the gate drive signals v_{Gs4}, input voltage and current, v_{CHR_in} and i_{HR_in}, switching current

i_{S4}, freewheeling diode current i_{HRD1} and the load current i_{HR}. The proposed power electronic water heater features a buck converter to transform the energy to the heating load and a shunt filter to eliminate the harmonic generated from household non-linear loads. The duty cycle D_{sw} is calculated by the amount of excess PV power and grid harmonics, which can be seen in the later section. There are three work modes in each period. Due to the high switching frequency in the proposed system, the input grid voltage and current are regarded as a constant value during a switching period. Before interval 1, the switch S_4 is off and no current flows into the load.

Interval 1 (t_0, t_1): When the switch S_4 turns on, the filter capacitor C_{HR_in} is discharged while the input grid current i_{HR_in} flows into the heating load through the diode rectifier bridge. The load current starts to increase because of the existence of parasitic inductor L_{HR} (32.34 uH). Due to the discontinuous current mode, there are no switching losses generated in the switch, S_4.

Interval 2 (t_1, t_2): S_4 turns off at start of this interval. The system is in a freewheeling state due to the diode D_1. The load inductor current decreases to zero rapidly due to very small parasitic inductance. As the diode turns off at zero current, the reverse recovery losses of the diode are eliminated.

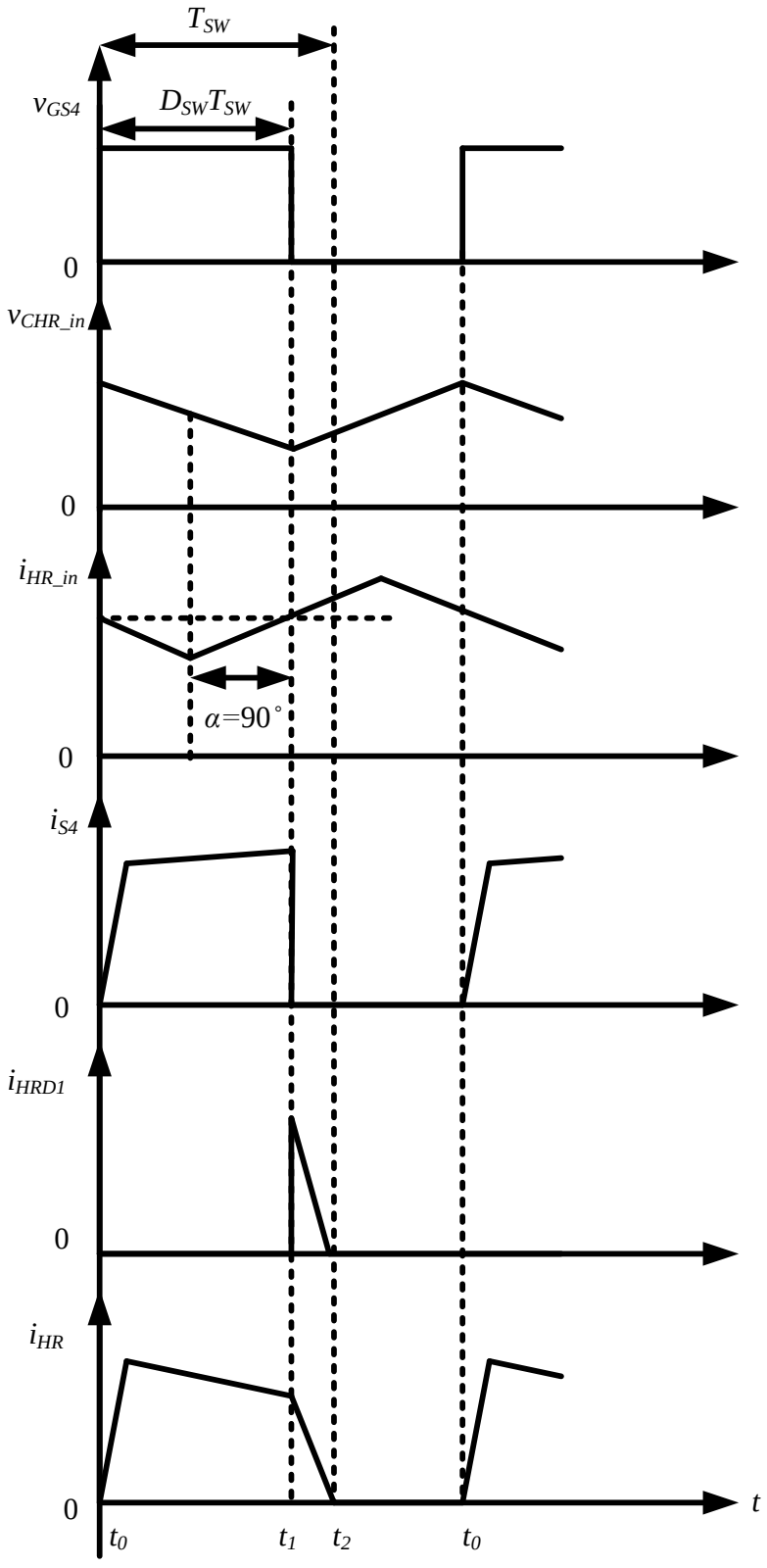

Figure 5.4. Theory waveform of proposed system.

Interval 3 (t_2, t_0): In this interval, no current flows in the circuit until the next gate signal comes. The input filter capacitor is charged.

Also, the power consumption P_{HR} of the power electronic water heater can be given by the work done by i_{HR_in} over one fundamental period T_f which is expressed as equation (5.1).

$$P_{HR} = \frac{\int_0^{T_f} i_{HR\_in}^2 * R_{HR} dt}{T_f} \tag{5.1}$$

Since the power electronic water heater is connected with grid, the power consumption P_{HR} can be transformed into equation (5.2), where $V_{HR\_in\_RMS}$ is the rated grid voltage of v_{grid}.

$$P_{HR} = \frac{V_{HR\_in\_RMS}^2}{R_{HR}} D \tag{5.2}$$

5.1.3. Harmonics compensation capability limitations exploration

Rather than keeping the duty cycle of the switch constant over the fundamental grid voltage period, it is possible to add a modulating component that can create an additional harmonic current, which will superimpose the fundamental current caused by the constant duty-cycle component. This feature can then be used to generate desired harmonic currents which will be in antiphase to the background harmonics produced by nonlinear loads of the household. Since the current absorbed from the grid can never exceed $v_{grid}(t)/R_{HR}$, the limitations of the power electronic water heater's harmonics compensation capability can be identified.

The grid voltage v_{grid} is expressed as equation (5.3) where V_{gridm} is the peak of grid voltage.

$$v_{grid}(t) = V_{gridm} \sin(\omega t) \tag{5.3}$$

The main assumption in this analysis is that a typical nonlinear household load consists of a diode rectifier front end with a capacitive DC side for smoothing and some inductance either on the DC or the AC side. This will cause a quasi-

square wave shaped grid current waveform with the quasi-square wave pulses synchronized with the sinewave voltage peaks. Since the current absorbed by the heating resistor becomes maximum around the same voltage peak, for simplicity of the analysis, it is assumed a simplified square wave pulse shape as depicted by i_{non_in} waveform in Figure 5.5 (a) where m_{wid} (rad) is the pulse width which is in the range of [0, π] and $I_{non\_in\_max}$ is the peak of the waveform. The Fourier series expansion of i_{non_in} can be represented as equation (5.4), where n is the order of harmonic components.

$$i_{non\_in}(t) = \frac{4}{\pi} I_{non\_in\_max} \sum_{n=1,3,5}^{\infty} \frac{(-1)^{\frac{n-1}{2}}}{n} \times \sin(\frac{n}{2} m_{wid}) \times \sin(n\omega t) \quad (5.4)$$

This waveform can be decomposed into a fundamental current component $i_{non\_in\_fund}$ and the residual harmonic current $i_{non\_in\_har}$, as shown in Figure 5.5 (a), which can be estimated from equation (5.5) and equation (5.6), respectively.

$$i_{non\_in\_fund}(t) = \frac{4}{\pi} I_{non\_in\_max} \sin(\frac{m_{wid}}{2}) \sin(\omega t) \quad (5.5)$$

$$i_{non\_in\_har}(t) = i_{non\_in}(t) - i_{non\_in\_fund}(t) \quad (5.6)$$

If all harmonics can be compensated, the constraint is that i_{HR_in} after harmonics compensation (red line in Figure 5.5 (b)) should always be within the zone constructed by the upper limit of i_{HR_in} (bule dot line in Figure 5.5 (b)) and the zero line (horizontal axis in Figure 5.5 (b)). Thus, due to the symmetrical characteristics of $i_{non\_in\_har}$, few special points on $i_{non\_in\_har}$ (*A, B, C* in Figure 5.5 (a)) can be used to judge if the harmonic current is fully compensated. Point *C* is located at the one-quarter of the fundamental period (T) of grid voltage and both points *A* and *B* are located at $(\pi\text{-}m_{wid})/(2\omega)$. $I_{non\_in\_harA}$, $I_{non\_in\_harB}$, and $I_{non\_in\_harC}$ represent the magnitude of residual harmonic current at these three points, respectively, as expressed by equation (5.7).

$$\begin{cases} I_{non\_in\_harA} = \frac{-2}{\pi} I_{non\_in\_max} \sin m_{wid} \\ I_{non\_in\_harB} = I_{non\_in\_max}(1 + \frac{2}{\pi} \sin m_{wid}) \\ I_{non\_in\_harC} = I_{non\_in\_max}(1 - \frac{4}{\pi} \sin \frac{m_{wid}}{2}) \end{cases} \quad (5.7)$$

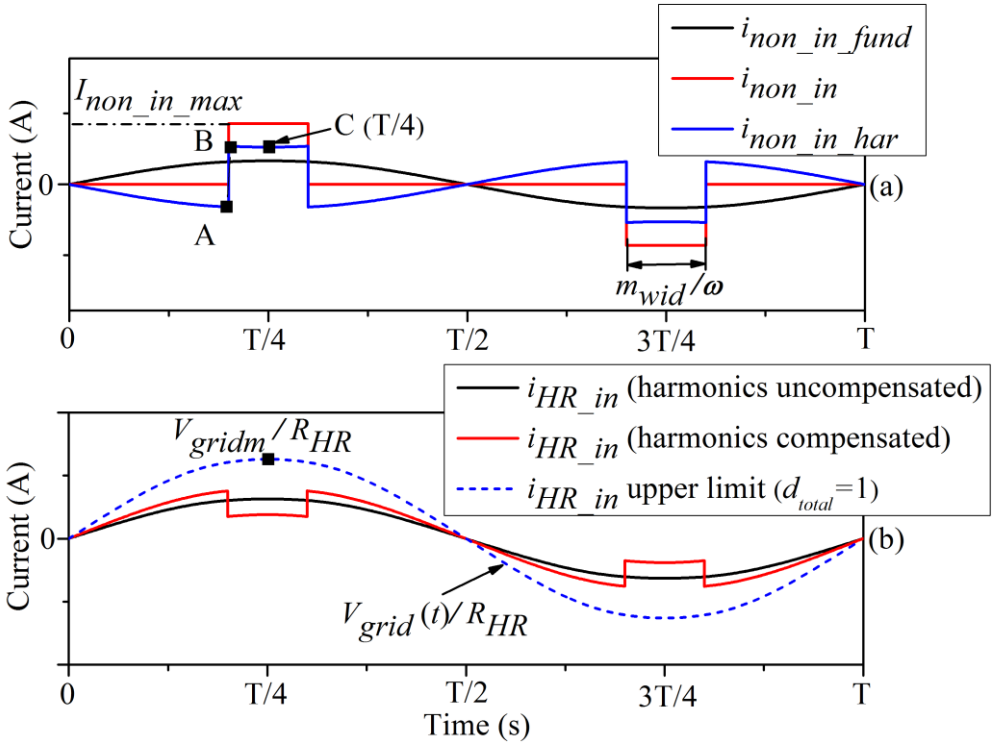

Figure 5.5. Demonstration of limitations of the power electronic water heater used for grid harmonics compensation. (a) Overall household nonlinear input current i_{non_in}, which is a sum of its fundamental current $i_{non\_in\_fund}$ and all current harmonics $i_{non\_in\_har}$. (b) Harmonics compensated and uncompensated power electronic water heater input current i_{HR_in}.

The harmonics control duty cycle d_{har} (S_4)used for harmonics compensation can be calculated from equation (5.8).

$$d_{har} = -\frac{i_{non\_in\_har}}{V_{gridm} \sin(\omega t)} R_{HR} \quad (5.8)$$

Substitute (5.7) into (5.8) we get (5.9). Here d_{har_A}, d_{har_B}, and d_{har_c} represent the duty cycle used for harmonics compensation at A, B and C, respectively.

$$\begin{cases} d_{har\_A} = \frac{\frac{2}{\pi} I_{non\_in\_max} \sin m_{wid}}{V_{gridm} \cos \frac{m_{wid}}{2}} R_{HR} \\ d_{har\_B} = -\frac{I_{non\_in\_max}(1 + \frac{2}{\pi} \sin m_{wid})}{V_{gridm} \cos \frac{m_{wid}}{2}} R_{HR} \\ d_{har\_C} = -\frac{I_{non\_in\_max}(1 - \frac{4}{\pi} \sin \frac{m_{wid}}{2})}{V_{gridm}} R_{HR} \end{cases} \quad (5.9)$$

d_{har} for these three points is decided by the non-linear current pulse width m_{wid} , magnitude $I_{non\_in\_max}$, grid voltage peak V_{gridm} and the heating resistor, R_{HR}. G_{non_har} is expressed as a common gain for d_{har} at these three points, as depicted as (5.10). Equation (5.11) explores the range of these three points which are as the function of m_{wid} .

$$G_{non\_har} = (I_{non\_in\_max} \times R_{HR})/V_{gridm} > 0 \tag{5.10}$$

$$\begin{cases} A: f_A(m_{wid}) = \frac{4}{\pi}\sin\frac{m_{wid}}{2} \\ B: f_B(m_{wid}) = -\frac{(1+\frac{2}{\pi}\sin m_{wid})}{\cos\frac{m_{wid}}{2}} \\ C: f_C(m_{wid}) = -(1-\frac{4}{\pi}\sin\frac{m_{wid}}{2}) \end{cases} \tag{5.11}$$

As shown in Figure 5.6, when m_{wid} is selected within the range of [0, π], $f_A(m_{wid})$ and $f_C(m_{wid})$ are monotonically increasing functions while $f_B(m_{wid})$ is a monotonically decreasing function which gradually closes to negative infinity at m_{wid}=π, as seen the asymptote line in Figure 5.6. Therefore, the maximum and minimum values of functions (5.11) are either at m_{wid}=0 or m_{wid}=π, as tabulated in Table 5.2.

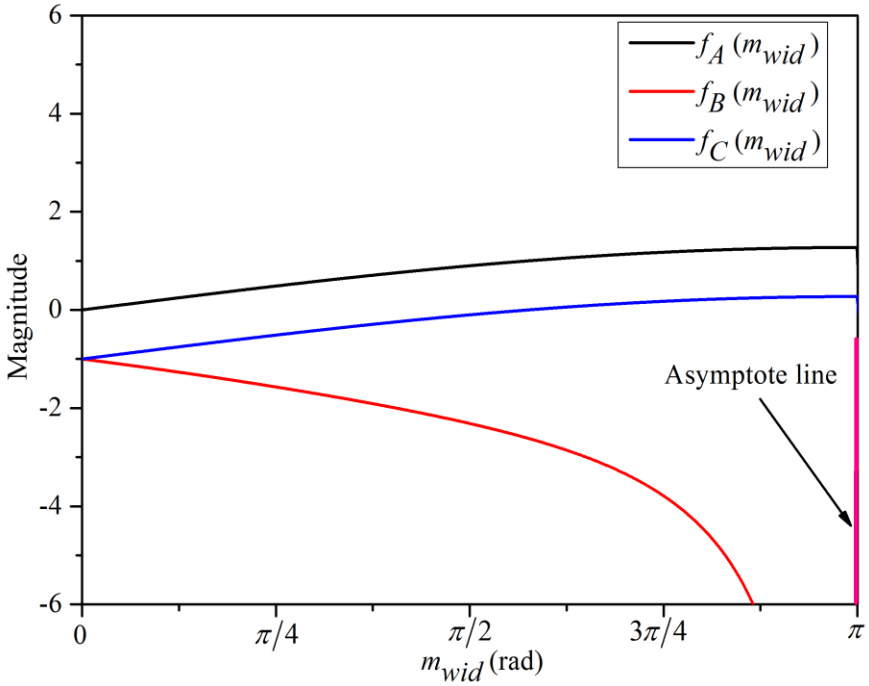

Figure 5.6. The curves of $f_A(m_{wid})$, $f_B(m_{wid})$, and $f_C(m_{wid})$ as the function of m_{wid}.

Table 5.2 The maximum and minimum values of $f_A(m_{wid})$, $f_B(m_{wid})$, $f_C(m_{wid})$.

m_{wid}	0	π
$f_A(m_{wid})$	0	1.273
$f_B(m_{wid})$	-1	$-\infty$

Due to various non-linear electrical appliances at home, both m_{wid} and $I_{non\_in\_max}$ vary a lot. To fully compensate harmonics, the total duty cycle d_{total} for the switch should be in the range of [0,1], as depicted in (5.12), where the duty cycle d_{act} is used for controlling the amount of power consumption because the power electronic water heater input current is distorted after harmonics compensation function applied as seen in Figure 5.5 (b). Thus, the limitation can be described as equation (5.13).

$$0 \le d_{har} + d_{act} \le 1 \tag{5.12}$$

$$\begin{cases} \frac{\frac{2}{\pi} I_{non\_in\_max} \sin m_{wid}}{V_{gridm} \cos\frac{m_{wid}}{2}} R_{HR} + d_{act} \le 1 \\ d_{act} - \frac{I_{non\_in\_max}(1+\frac{2}{\pi}\sin m_{wid})}{V_{gridm} \cos\frac{m_{wid}}{2}} R_{HR} \ge 0 \\ d_{act} - \frac{I_{non\_in\_max}(1-\frac{4}{\pi}\sin\frac{m_{wid}}{2})}{V_{gridm}} R_{HR} \ge 0 \end{cases} \tag{5.13}$$

5.1.4. Comparison with conventional electric water heater and another filter respectively

5.1.4.1. Comparison with conventional electric water heater

This section outlines the advantages of the proposed power electronic water heater in utilizing excess PV power and compensating for grid harmonics. These benefits are demonstrated through two comparisons with both conventional electric water heaters and shunt filters.

To evaluate the performance of the proposed power electronic water heater utilized in PV power consumption, the comparison considers factors such as switch lifetime, switching frequency, compatibility with excess PV power, and harmonics injection into the grid, as summarized Table 5.3. Compared to relays or triacs [92][93][94], the IGBT's longer lifetime significantly reduces

maintenance costs and enhances reliability. Furthermore, the application of PWM technology and the high switching frequency of the IGBT enable the proposed water heater to respond quickly and accurately to fluctuations in excess PV power generation. Additionally, the implementation of an input filter minimizes harmonics injection into the grid, ensuring improved power quality in the proposed power electronic water heater.

Table 5.3 Comparison with conventional electric water heater.

Features	Conventional electric water heater	Proposed power electronic water heater
Switch lifetime	Relay: 100,000 to 10 million operations Traics: 100,000 to several million cycles	Reliable for 10-20 years or billions of switching cycles
Switching frequency	Relay: 0.1~ up to 100 Hz Traics: 1~2 kHz	1 kHz~100 kHz
Capability with PV power	Hard match with excess PV	Easy
Harmonics injection to the grid	Spike produced at non-zero-crossing switching point	Minimized by input filter

5.1.4.2. Comparison with passive and shunt active filter

The proposed power electronic water heater can also function as a shunt filter, enhancing the power quality of the residential grid. A comparison between the proposed system and typical shunt filters is presented in Table 5.4. A shunt *LC* filter [166], composed of capacitors and inductors, is designed to target specific harmonic frequencies by providing a low-impedance path for those harmonics. In contrast, eliminating harmonics of varying orders requires active filters [167][168], which utilize advanced control algorithms, such as those implemented in multilevel shunt active filters [169]. However, the extensive use of power electronics and the complexity of these control systems significantly increase the overall system cost. In comparison to a basic H-bridge active filter [170], the proposed system employs only a single IGBT for control. This design

choice reduces both the cost and the complexity of the control system, making it a more efficient and economical solution.

Table 5.4 Comparison with another filters.

Type (single phase)	Passive components number	IGBT number	Diodes number	Filtering frequency range	Control	Cost
Shunt *LC* filter [166]	Capacitor: 1 Inductor: 1	0	0	Narrow	No control	Low
H-bridge active filter [170]	Capacitor: 1 Inductor: 1	4	0	Wide	Complex	High
Proposed power electronic water heater	Capacitor: 1 Inductor: 1	1	5	Wide	Simple	Medium

5.1.5. Harmonics compensation control schemes

In this paper, there are two harmonics compensation methods compared: Direct harmonics compensation versus PI control harmonics compensation. Besides, due to the need of harmonics extraction, the phase-locked-loop (PLL) control is also utilized.

5.1.5.1. Single phase PLL

The main task of the PLL is to provide a synchronized phase reference θ of grid voltage v_{grid} to extract current harmonics. A general structure of the single-phase PLL is established as shown in Figure 5.7 (a), where an orthogonal voltage generation system (Figure 5.7 (b)) is deployed to create a virtual signal v_{grid_β}. Compared with other complicated technologies [171], like Hilbert transform and inverse Park transform, the second order generalized integrator (SOGI) approach [172] used to create a virtual quadrature signal of v_{grid} is easier to be implemented. Significantly, the factor k affects the bandwidth of the closed loop

system. Thus, a couple of quadrature signals $v_{grid_\alpha}$and v_{grid_β} can be used for the phase locked control.

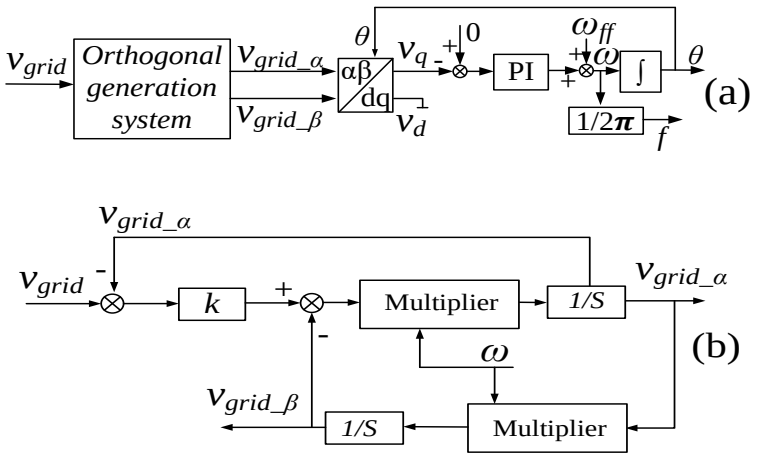

Figure 5.7. Control diagrams. (a) General PLL control diagram. (b) Orthogonal generation system of grid voltage.

5.1.5.2. Direct harmonics compensation method

Figure 5.8 shows the diagram of direct harmonics compensation method. The non-linear load input current i_{non} is firstly sampled and delayed with T/4 to produce a quadrature component. After the αβ/dq transform, the signal is filtered by the second-order low pass filter (LFP) to extract the DC component. This DC component is transformed into the fundamental component of i_{non_har} through the inverse transform which is then subtracted by i_{non} to extract all non-linear load harmonics i_{non_har}. To calculate the duty cycle d_{har} used for harmonics compensation, the extracted i_{non_har} is multiplied by R_{HR} and divided by v_{grid}. Significantly, the zero-crossing points of grid voltage should be excluded and replaced by a small value in this calculation to avoid the infinite values. Besides, a negative gain should be added to d_{har} to produce a reverse control signal to compensate these harmonics current. Consequently, the total duty cycle d_{total} (d_{total}=d_{act}+d_{har}) is used for the switch modulation, where the duty cycle d_{act} is used to consume the excess PV power exactly.

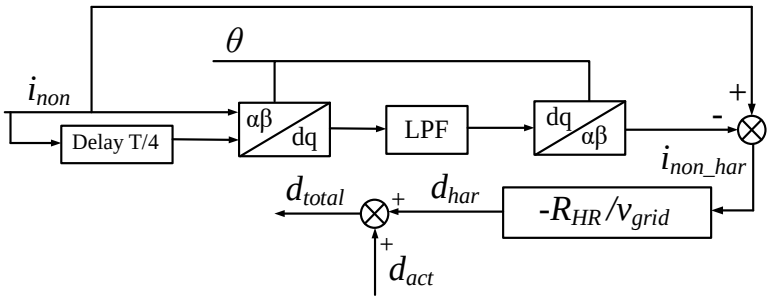

Figure 5.8. Direct harmonics compensation method.

5.1.5.3. PI control harmonics compensation method

Distinguished from direct harmonics compensation method, the PI control harmonics compensation method is based on the selective harmonic detection method [173] to compensate grid harmonics. As more power electronic appliances utilized in the household level, while each individual appliance may contribute a negligible amount of harmonic current to the network, the cumulative effect of numerous such devices could lead to significant harmonic distortion. In this paper, the 3rd, 5th, 7th, and 9th order harmonic are compensated for example. The control diagram is depicted in Figure 5.9.

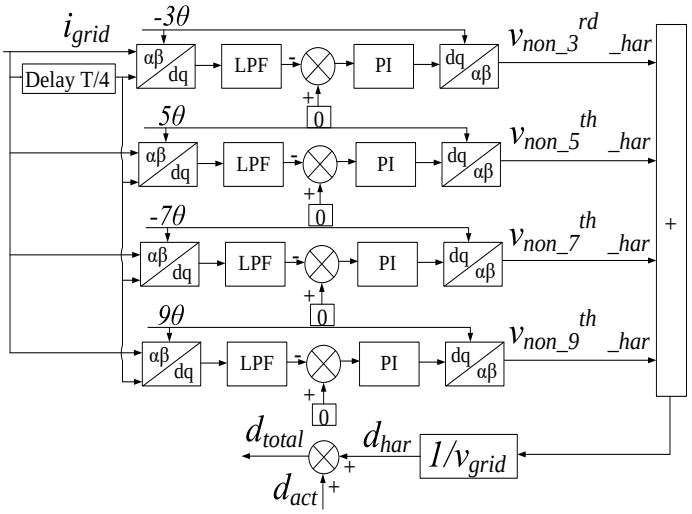

Figure 5.9. The diagram of PI control harmonics compensation method.

To extract these harmonics from the grid current i_{grid}, 3, 5, 7, and 9 times of fundamental grid voltage phase angle θ are utilized respectively. A negative sign is needed in the phase angle used in both 3rd and 7th αβ/dq and dq/αβ transform,

since the time delay T/4 for producing the orthogonal signal of grid current can cause a $3\pi/2$ and $7\pi/2$ phase shift respectively. Similar to the direct harmonics compensation method, the second order low pass filter (LFP) is also utilized in the control loop. After the PI control and dq/αβ transform, the reference signals ($v_{non\_3^{rd}\_har}$, $v_{non\_5^{th}\_har}$, $v_{non\_7^{th}\_har}$, $v_{non\_9^{th}\_har}$) are divided by the grid voltage v_{grid} and then added together to generate d_{har} which is then combined with d_{act}. The control signal d_{har} has small-valued unwanted higher order components produced from these reference signals divided by v_{grid}, leading to some higher order current harmonic injected into grid. Thus, no any other feedback loop is needed. For example, $v_{non\_9^{th}\_har}/v_{grid}$ produces small 10^{th}, 12^{th} …. order components in d_{act}, resulting in the 11^{th}, 13^{th}, order harmonics produced by the power electronic water heater at the input current. However, these small components can be neglected practically.

5.2. PV inverter

5.2.1. Topology of PV inverter

The purpose of the PV inverter in this thesis is to convert the DC current from the PV panels into AC for the grid or transfer power from the AC grid to the DC side for charging the battery stack. Figure 5.10 illustrates the topology of the PV inverter used in the experimental setup. It includes a DC bus capacitor C_{dc_bus}, IGBT switches in an H-bridge configuration, a geometrically symmetrical *LCL* filter (L_{boost}, L_{ac}, R_{LCL}, C_{LCL}), an inductor L_{grid} simulating the impedance of the distribution grid and an autotransformer, which was added for safe experimental operations.

Significantly, for harmonics filtering, the *LCL* filter is widely used in single-phase grid-connected converters due to its superior suppression capability of high-frequency harmonics and the smaller inductance when compared to an L filter. However, traditional asymmetrical *LCL* filters can create an imbalance in impedance between the L-line and N-line, causing common mode (CM) noise to convert into differential mode (DM) noise [174]. To address this issue, a symmetrical *LCL* filter is employed in this thesis. P_{grid} in used to indicate the power of PV inverter output or the power imported from the grid.

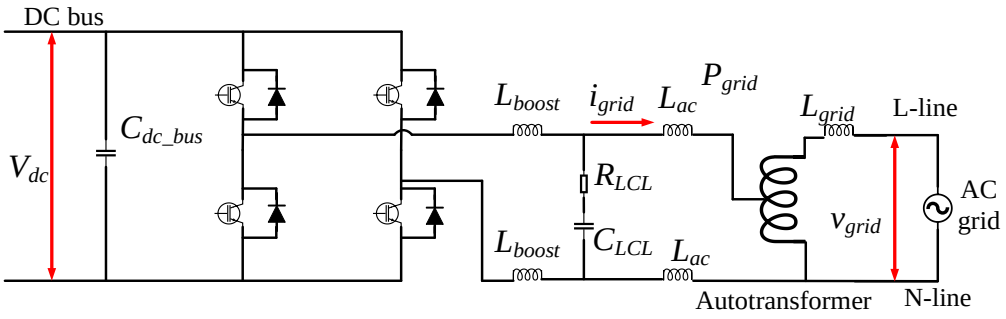

Figure 5.10. PV inverter topology.

5.2.2. Control schemes of PV inverter

A well-known proportional -resonant (PR) controller suitable for single-phase inverter operation, which avoids the challenging stationary frame to synchronous frame transformation in the single-phase system. The PR controller transfer function defined as equation (5.14) has been validated as it can track the current reference with zero steady state error [175]. However, equation (5.18) represents the ideal PR controller which can cause stability problems due to the infinite gain. Thus, a damping is introduced to make a non-ideal PR controller as shown in equation (5.15).

$$G_{PR}(s) = K_P + K_r \frac{s}{s^2+\omega_0^2} \tag{5.14}$$

$$G_{PR}(s) = K_P + K_r \frac{s}{s^2+2\omega_{PRc}s+\omega_0^2} \tag{5.15}$$

Where K_P is the proportional gain, K_r is the integral gain, ω_0 is the resonant frequency (grid frequency 50Hz) and ω_{PRc} is the bandwidth around the frequency of ω_0.

Ideally, the system shown in Figure 5.1 will not have any low order harmonics. However, the distorted magnetizing current drawn by the transformer due to the non-linearity in the B-H curve of the magnetic core, the dead time of the switches, and the distortion of grid voltage can result in the low order harmonics in the system [176]. According to the IEEE 519-2022 standard, 5 % for the current total harmonic distortion (THD) factor with individual limits of 4 % for each odd order harmonic from 3rd to 9th and 2 % for 11th to 15th. To satisfy the IEEE standards, the PR controller method is applied for suppressing low order harmonics in the grid current. Figure 5.11 shows the control scheme of the PV inverter. 3rd, 5th, and 7th order harmonics PR controllers are applied which are

combined with the fundamental PR controller to realize the grid current i_{grid} control and the low order harmonics elimination.

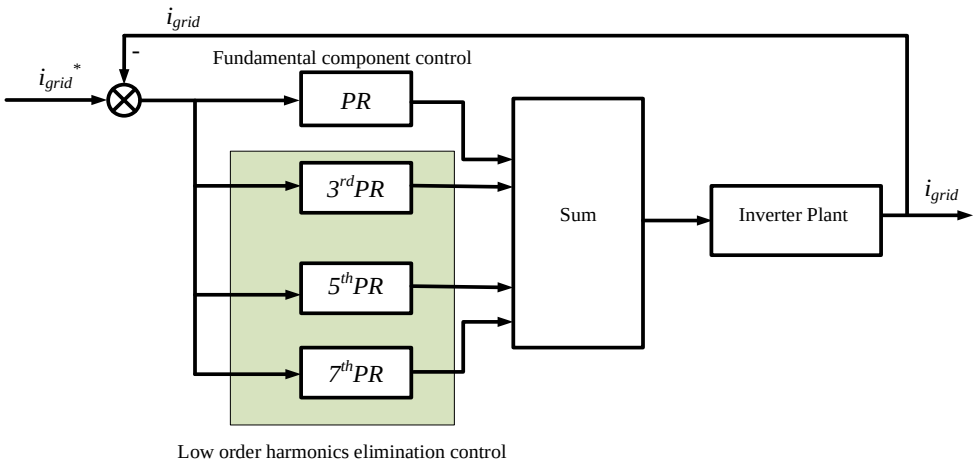

Figure 5.11. The control scheme of the PV inverter.

5.2.3. PR controllers design for PV inverter

The current reference is sinusoidal: since a PI controller is unable to track a sinusoidal reference without steady-state errors, the PR controller has been adopted. The PR controller tracks the current introducing an infinite gain at a certain frequency. In this section, the PR controllers used for fundamental and 3^{rd}, 5^{th}, and 7^{th} selective harmonic compensation are designed.

As shown in Figure 5.10, the inductance is evenly distributed on both sides of the capacitor, which helps maintain balanced current sharing between the inverter and the grid. Compared with asymmetric LCL filter, the symmetric LCL filter can a symmetric LCL filter can help suppress common-mode (CM) to differential-mode (DM) noise conversion more effectively than an asymmetric LCL filter. Thus, in the symmetric LCL filter, the equivalent inductance on each side of the capacitor is halved compared to the asymmetric LCL filter.

Firstly, the PR controller for the fundamental component is illustrated. Since the resistor R_{LCL} (2Ω) works as the passive damping to smooth the resonance

peak of the filter, the capacitor current is not sampled and not used in the loop for active damping.

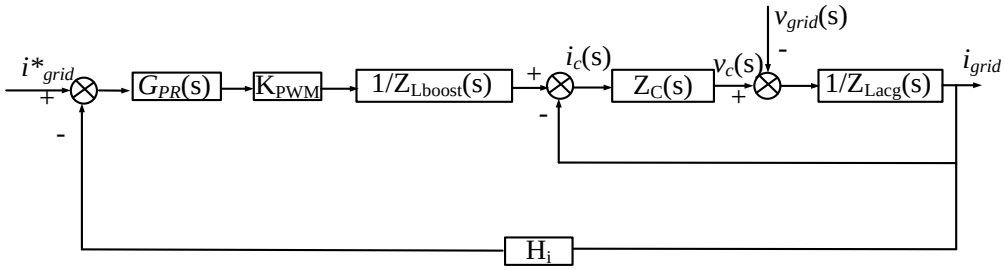

Figure 5.12.Control loop for fundamental PR controller design.

Figure 5.12 illustrates the PR control loop for the fundamental component. Z_{Lboost}(s), Z_C (s), and Z_{Lac}(s), is the impedance equation of inductor L_{boost}, capacitor C_{LCL}, and AC side inductance (L_{ac}+L_{grid}) respectively, as shown in equation (5.16).

$$Z_{Lboost} = 2sL_{boost},\ Z_C(s) = \frac{1}{sC_{LCL}} + R_{LCL},\ Z_{Lacg} = s(2L_{ac} + L_{grid}) \qquad (5.16)$$

Thus, the equivalent control diagram can be seen in Figure 5.18.

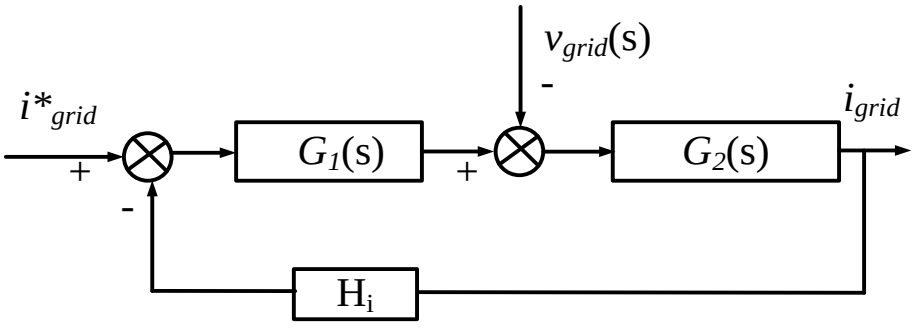

Figure 5.13.Equivalent control diagram.

Where:

$$G_1(s) = \frac{G_{PR}(s)K_{PWM}(sC_{LCL}R_{LCL}+1)}{2s^2L_{boost}C_{LCL}} \qquad (5.17)$$

$$G_2(s) = \frac{sC_{LCL}}{s^2(2L_{ac}+L_{grid})C_{LCL}+sC_{LCL}R_{LCL}+1} \qquad (5.18)$$

The open loop transfer function can be expressed as:

$$G(s) = G_1(s)G_2(s)H_i \qquad (5.19)$$

$$G(s) = \frac{K_{PWM}(sC_{LCL}R_{LCL}+1)H_i}{s^3 2L_{boost}C_{LCL}(2L_{ac}+ L_{grid})+s^2 2L_{boost}C_{LCL}R_{LCL}+2sL_{boost}} G_{PR}(s) \quad (5.20)$$

The bandwidth of the resonance which is typically around 10-20 rad/s, assuming that the bandwidth of the PR controller ω_{PRc} :

$$\omega_{PRc} = 2\pi \quad (5.21)$$

The relationship between the system cut-off frequency f_c, the sampling frequency f_s, and the resonant frequency f_{res} [177]:

$$f_c \leq \frac{1}{10} f_s, and\ \frac{1}{4} f_s < f_{res} < \frac{1}{2} f_s \quad (5.22)$$

The cutoff frequency f_c of the system is usually designed to be far lower than the sampling frequency f_s, and much smaller than the resonant frequency f_{res} of LCL filter. The Laplace transfer function of this symmetric LCL filter can be seen as:

$$G_{LCL}(s) = \frac{sC_{LCL}R_{LCL}+1}{s^3(2L_{ac}+ L_{grid})(2L_{boost})+s^2(2L_{ac}+ L_{grid})(2L_{boost})C_{LCL}R_{LCL}+s(2L_{ac}+ L_{grid}+2L_{boost})} \quad (5.23)$$

Where the resonant frequency of this symmetric LCL filter with a series damping resistor R_{LCL} in the capacitor branch is nearly the same as the undamped resonance frequency:

$$f_{res} \approx \frac{1}{2\pi}\sqrt{\frac{1}{L_{eq}C_{LCL}}} \quad (5.24)$$

$$L_{eq} = \frac{4L_{boost}(2L_{ac}+ L_{grid})}{2L_{boost}+2L_{ac}+ L_{grid}} \quad (5.25)$$

The components parameters can be seen in Table 5.6. In this thesis, the sampling frequency f_s is 5kHz, and the calculated resonance frequency f_{res} is around 2.1kHz, which satisfy the limitations shown in equation (5.22).

Therefore, considering the frequency response of the system lower than the cut-off frequency, the capacitor of LCL filter can be omitted [178]. The equation (5.19) can be rewritten as:

$$G(s) \approx \frac{K_{PWM}H_i}{2sL_{boost}}G_{PR}(s) \tag{5.26}$$

The simplified transfer function can be used to design the PR controller parameters, where the inverter gain can be chosen as $K_{PWM} = V_{dc}/V_{tri}$, V_{dc} is the DC bus voltage (400V), and V_{tri} is the magnitude of the carrier wave, which is typically set to a value of 1. Ideally when the current sampling has no delay or filtering, the transfer function of $H_i(s) = 1$.

To validate this, the bode diagram of the original (equation (5.20)) and simplified (equation (5.26)) converter plant ($G(s)/G_{PR}(s)$) is compared, as shown in Figure 5.14. Apparently, the bode diagram performance of the original and simplified inverter plan at low frequency (before cut off frequency 500Hz) is the identical. Thus, the simplified inverter transfer function (5.26) can be used for PR controller design.

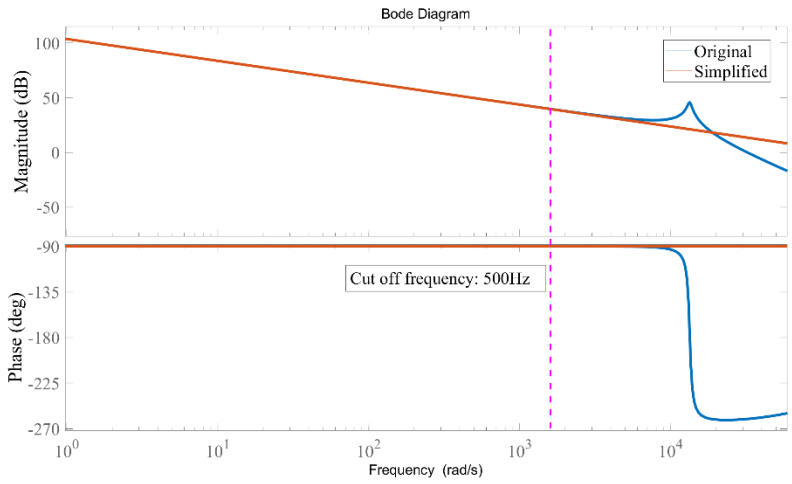

Figure 5.14.Bode diagram of the original and simplified inverter plant.

The cut-off frequency f_c is selected as 500Hz, which is higher than the fundamental frequency (f_{fund}=50Hz) and the highest selective harmonic (350Hz) which needs to be compensated. At cutoff frequency f_c, the open loop system should have unity gain and a specified phase margin $\emptyset_m$, as shown in (5.27) and (5.28).

$$|G(j\omega_C)| = 1 \tag{5.27}$$

$$\angle G(j\omega_C) = -\pi + \emptyset_m \tag{5.28}$$

Substitute equation (5.26) into (5.27) and (5.28). Due to the cut-off frequency f_c is higher than the fundamental frequency (50Hz), it is easily to calculate the $K_P = 0.02$, and $K_P = 8.6$ with phase margin $\emptyset_m = 82^\circ$. To validate the controller design, the open loop bode diagram is drawn in Figure 5.15. And for the system performance verification, the bode diagram and step response of the closed loop can be seen in Figure 5.16 and Figure 5.17 respectively. Apparently, the PR controller designed for fundamental component can keep the system stable (around 500Hz bandwidth) with 0.0104s setting time.

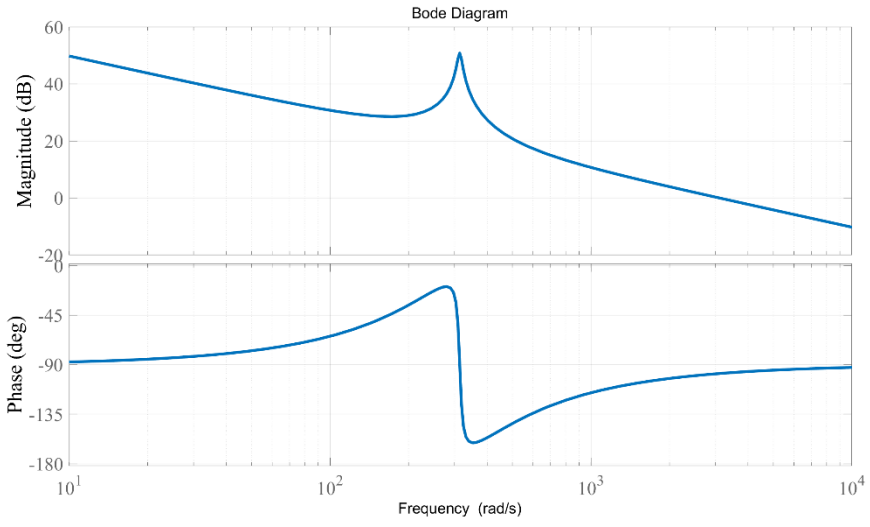

Figure 5.15.Bode diagram of the open loop.

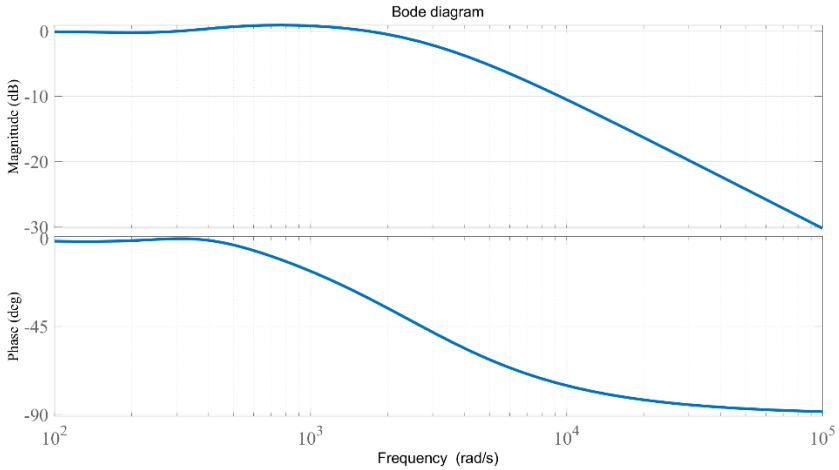

Figure 5.16.Bode diagram of the closed loop.

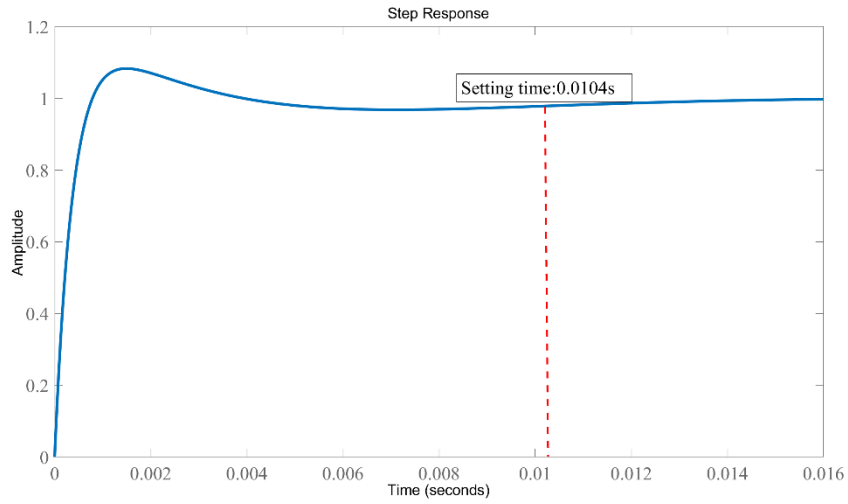

Figure 5.17.Step response diagram.

For multiple harmonic compensations (e.g., 3rd, 5th, and 7th), three PR controllers can be implemented in parallel as shown in (5.29), where the n presents the order of harmonic which needs to be compensated and ω_{PRch} represents the bandwidth of the resonance which is typically around 10-20 rad/s, where $\omega_{PRch} = 10\ rad/s$ is selected in this thesis.

$$G_{PR}(s) = \sum_{n=3,5,7} K_{nr} \frac{s}{s^2+2\omega_{PRch}s+(n\omega_0)^2} \tag{5.29}$$

K_{nr} should be high enough to provide significant gain at the harmonic order but not so high as to cause instability or excessive noise amplification. Similar with the design of the fundamental PR controller, the bode diagram is used to

tune K_{nr}. Thus, the value of K_{nr}, along with the phase margin can be seen in Table 5.5.

Table 5.5. K_{nr} for different harmonic PR controller.

Harmonic order	K_{nr}	Phase margin
3rd	26.26	65.8°
5th	44	48.7°
7th	61.8	30.6°

Thus, the fundamental PR controller, along with the PR controllers for multiple harmonic compensations (e.g., 3rd, 5th, and 7th) are designed.

5.3. Battery DC/DC converter

5.3.1. Topology of battery DC/DC converter

In this research, the battery energy storage system is designed to store surplus PV energy during the day and use low-cost grid electricity at night, while simultaneously maintaining DC bus voltage stability. A bidirectional DC/DC converter for the battery charger is shown in Figure 5.18 which includes an inductive filter L_{bat}, an IGBT switch leg, and a 300 V battery stack simulated by a bidirectional DC power supply (SM1500-CP-30) in the experimental setup. The DC/DC converter maintains a constant DC bus voltage, V_{dc}, at a high-enough level to avoid over-modulation of the PV inverter. The battery stack voltage is V_{bat}, and R_{bat} represents the internal resistance of the battery stack. i_{dch} represents the total current flows into the battery system.

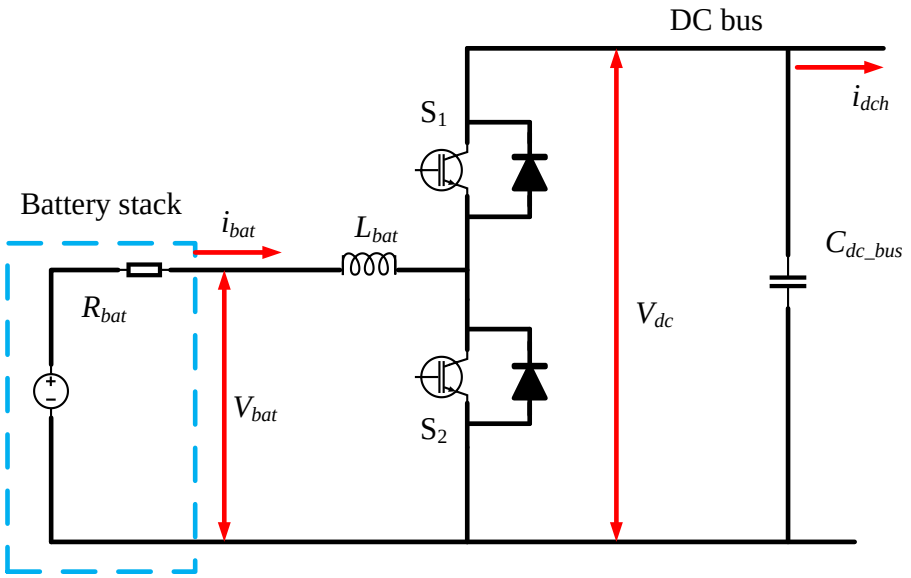

Figure 5.18. The topology of the battery stack charger.

5.3.2. The control scheme of the battery DC/DC converter

Thera are only two subintervals of this bidirectional DC/DC converter.

In the first subinterval, during $0 \sim DT_s$, when the switch S_1 is on, and the S_2 is off.

$$\begin{cases} L_{bat}\frac{di_{bat}}{dt} = v_{dc} - v_{bat} \\ C_{dc\_bus}\frac{dv_{dc}}{dt} = i_{bat} - i_{dch} \end{cases} \tag{5.30}$$

In the first subinterval, during $DT_s \sim T_s$, when the switch S_1 is off, and the S_2 is on.

$$\begin{cases} L_{bat}\frac{di_{bat}}{dt} = -v_{bat} \\ C_{dc\_bus}\frac{dv_{dc}}{dt} = -i_{dch} \end{cases} \tag{5.31}$$

Thus, during one switching period T_s, the averaged dc model can be expressed as:

$$\begin{cases} L_{bat}\frac{di_{bat}}{dt} = Dv_{dc} - v_{bat} \\ C_{dc\_bus}\frac{dv_{dc}}{dt} = Di_{bat} - i_{dch} \end{cases} \tag{5.32}$$

Considering ac perturbation: $i_{bat} = I_{bat} + \hat{\imath}_{bat}$, $v_{dc} = V_{dc} + \hat{v}_{dc}$, and $d = D + \hat{d}$. The equation (5.32) can be transferred into (5.33).

$$\begin{cases} L_{bat}\frac{d\hat{\imath}_{bat}}{dt} = (D+\hat{d})(V_{dc}+\hat{v}_{dc}) - v_{bat} \\ C_{dc\_bus}\frac{d\hat{v}_{dc}}{dt} = (D+\hat{d})(I_{bat}+\hat{\imath}_{bat}) - i_{dch} \end{cases} \quad (5.33)$$

Thus, the state space ac model is shown in (5.34).

$$\begin{cases} L_{bat}\frac{d\hat{\imath}_{bat}}{dt} = \hat{d}V_{dc} + D\hat{v}_{dc} + \hat{d}\hat{v}_{dc} - v_{bat} \\ C_{dc\_bus}\frac{d\hat{v}_{dc}}{dt} = \hat{d}I_{bat} + D\hat{\imath}_{bat} + \hat{d}\hat{\imath}_{bat} - i_{dch} \end{cases} \quad (5.34)$$

$\hat{d}\hat{v}_{dc}$ and $\hat{d}\hat{\imath}_{bat}$ can be omitted. Through Laplace Transform of equation (5.34), it can be expressed as:

$$\begin{cases} sL_{bat}i_{bat}(s) = d(s)V_{dc} + Dv_{dc}(s) - v_{bat} \\ sC_{dc\_bus}v_{dc}(s) = d(s)I_{bat} + D\ i_{bat}(s) - i_{dch} \end{cases} \quad (5.35)$$

Thus, the transfer function of i_{bat} against duty cycle d and DC bus voltage against i_{dch} can be respectively expressed as:

$$G_3(s) = \frac{i_{bat}(s)}{d(s)} = \frac{V_{dc}}{sL_{bat}} \quad (5.36)$$

$$G_3(s) = \frac{v_{dc}(s)}{d(s)} = \frac{1}{sC_{dc\_bus}}I_{bat} \quad (5.37)$$

Thus, the DC/DC converter's closed-loop control diagram is shown in Figure 5.19.

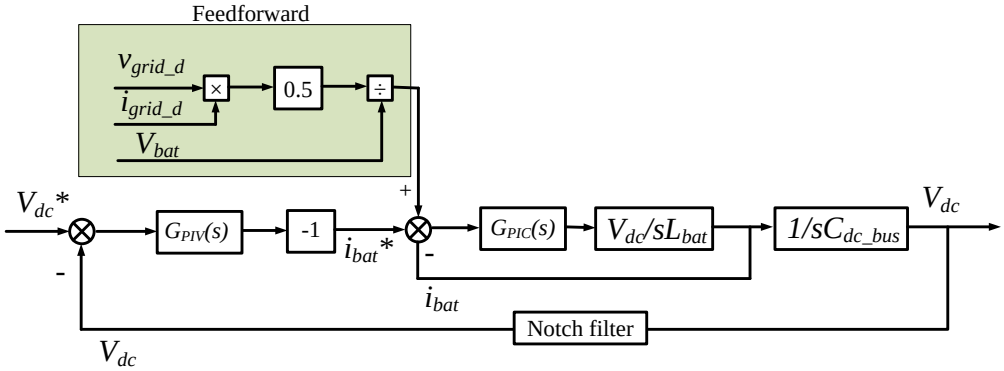

Figure 5.19. Control diagram of the battery DC/DC converter.

Two loops are employed in this control scheme: an outer slow voltage (V_{dc}) loop and an inner fast loop (i_{bat}). In the outer loop, a notch filter as shown in equation (5.38) is applied to reject the 100 Hz ripple which typically exists in

the single-phase AC system. $G_{PIC}(s)$ represents the PI controller for inner current loop and $G_{PIV}(s)$ represents the PI controller for voltage loop.

$$G(s) = A_0 \frac{s^2+\omega_n^2}{s^2+\frac{\omega_n s}{Q}+\omega_n^2} \tag{5.38}$$

Where, A_0 is the gain of the filter (1 applied); ω_n is the characteristic angular frequency which is 200π rad/s (f_n=100 Hz); and Q is the equivalent quality factor which represents the performance of the notch filter. When higher Q is applied, narrow bandwidth is achieved. In this thesis, Q=100.

The actual 100 Hz ripple will be seen by the C_{DC_bus}. Thus, through the voltage loop's PI controller, the DC bus voltage can be maintained at 400 V. Besides, during the power reversal from the charging to the discharging of the battery stack, there are typically under/overshoots of the DC bus voltage V_{dc}, which is controlled by a fast voltage controller. A feedforward loop is deployed which aims to produce a reference signal for the battery charger's inner PI current controller. The feedforward signal is produced by the grid power ($0.5\times v_{grid\_d}\times i_{grid\_d}$) divided by the battery stack voltage [179].

For inner current loop, the switching frequency is 5kHz and filter inductor L_{bat} is 3.3mH. Current can change much more rapidly, as it is directly influenced by the switching actions of the converter and inductive elements. The cutoff frequency ω_{cuc} of the inner current loop (equation (5.39)) is design at around 500Hz.

$$G_i(s) = \frac{V_{dc}}{sL_{bat}} G_{PIC}(s) \tag{5.39}$$

$$G_{PIC}(s) = k_{pc} + \frac{k_{ic}}{s} \tag{5.40}$$

At the crossover frequency ω_{cuc}, the open loop system should have unity gain and a specified phase margin $\emptyset_{cuc}$.

$$|G_i(j\omega_{cuc})| = 1 \tag{5.40}$$

$$\angle G_i(j\omega_{cuc}) = -\pi + \emptyset_{cuc} \tag{5.41}$$

Thus, through the assistance of MATLAB SISOTOOL software, the k_{pc} is designed as a value of 0.032, and k_{ic} is designed as a value of 40.58 which causes and $\emptyset_{cuc} = 72.8^{\circ}$, as shown in Figure 5.20. The bandwidth of the closed loop is 488Hz, with 0.0022s setting time, as shown in Figure 5.21 and Figure 5.22. It indicates the designed current PI controller can keep the current loop stable and fast response.

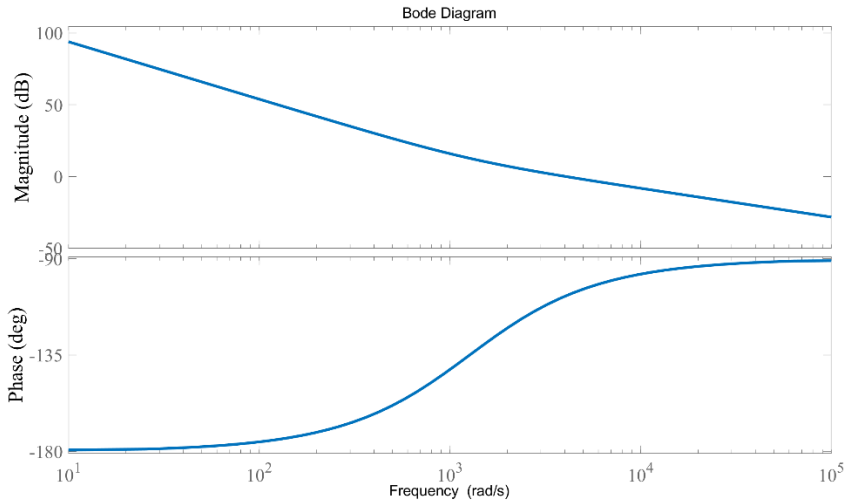

Figure 5.20. Bode diagram of the current open loop.

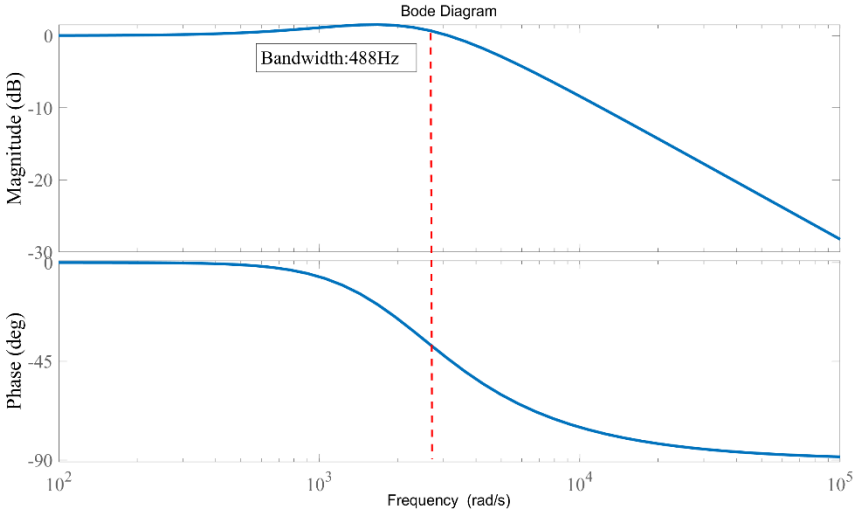

Figure 5.21. Bode diagram of the current closed loop.

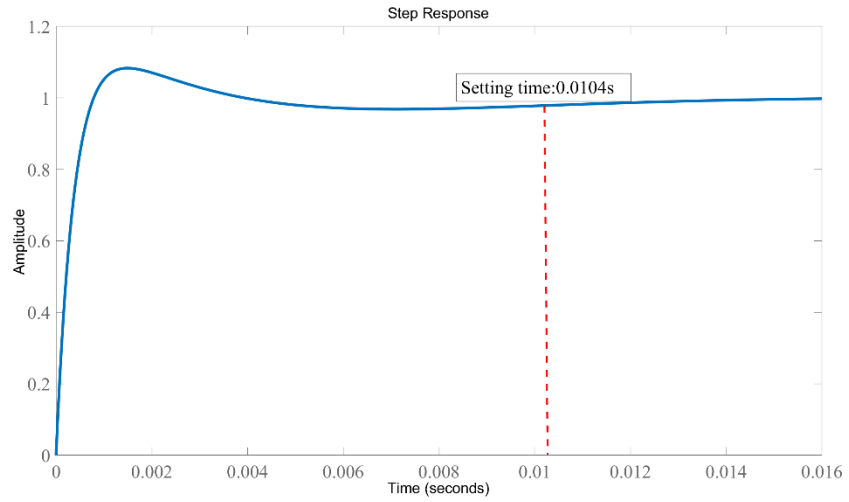

Figure 5.22. Step response diagram of the current closed loop.

For the outer voltage control loop, voltage in the system often changes more slowly since it is influenced by the DC side capacitor (1800uF). This voltage loop is used to stabilize the DC bus voltage at 400V. The cutoff frequency ω_{cuc} of the voltage loop (equation (5.42)) is design at around 50Hz. Notably, during 0-50Hz, the inner current closed loop provides 1 gain as shown in Figure 5.21. Thus, the transfer function of outer open loop can be simplified as:

$$G_v(s) = \frac{1}{sC_{dc\_bus}} G_{PIV}(s) \tag{5.42}$$

$$G_{PIV}(s) = k_{pv} + \frac{k_{iv}}{s} \tag{5.43}$$

At the crossover frequency ω_{voc}, the open loop system should have unity gain and a specified phase margin $\emptyset_{voc}$.

$$|G_v(j\omega_{voc})| = 1 \tag{5.44}$$

$$\angle G_i(j\omega_{voc}) = -\pi + \emptyset_{voc} \tag{5.45}$$

Thus, through the assistance of MATLAB SISOTOOL software, the k_{pv} is designed as a value of 0.71, and k_{iv} is designed as a value of 107.2 which causes and $\emptyset_{voc} = 69.4^{\circ}$, as shown in Figure 5.23. The bandwidth of the closed loop is 55Hz, with 0.022s setting time, as shown in Figure 5.24 and Figure 5.25. It indicates the designed current PI controller can keep the voltage loop stable and good response speed. Beside, the 100Hz resonant frequency of notch filter is out of this bandwidth.

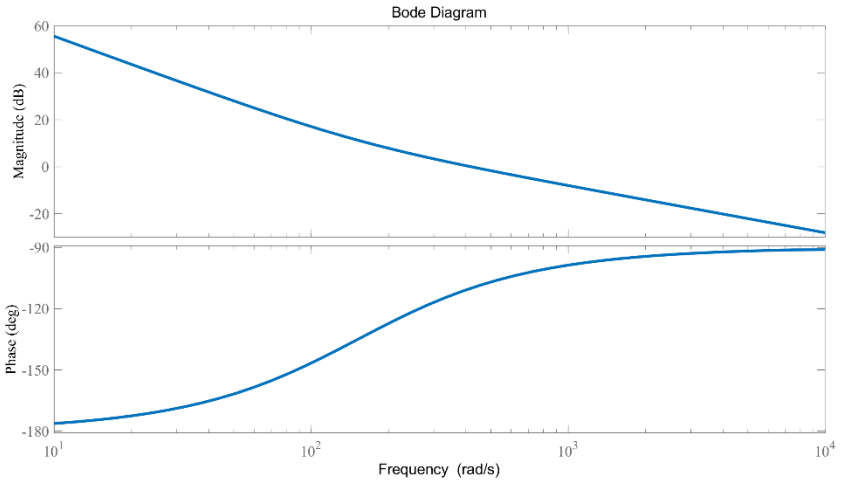

Figure 5.23. Bode diagram of the voltage open loop.

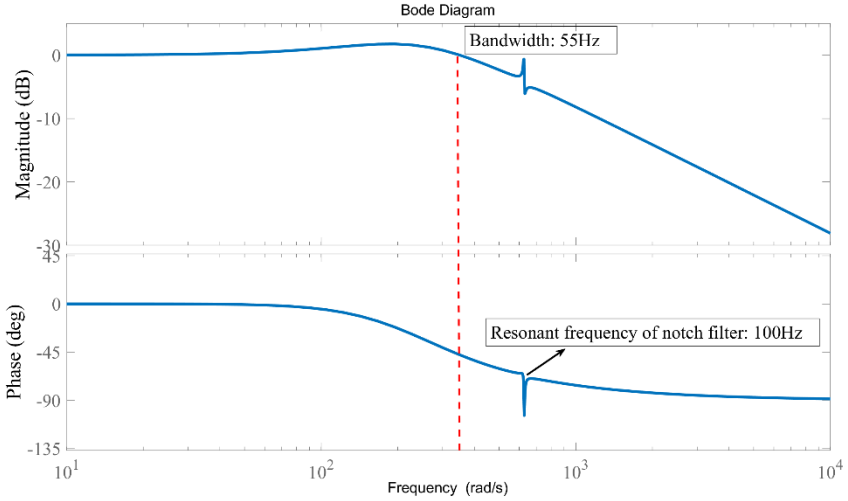

Figure 5.24. Bode diagram of the voltage closed loop.

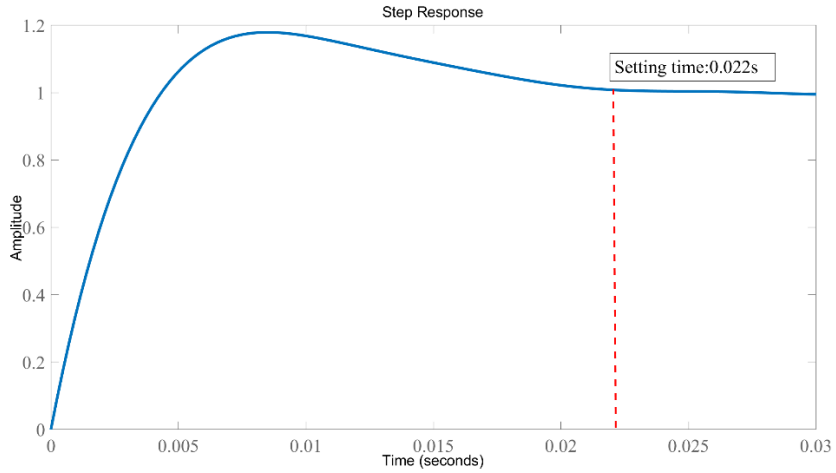

Figure 5.25. Step response diagram of the voltage closed loop.

5.4. Excess PV power consumption demonstration

In some household PV application scenarios [180], the generated PV power P_{PV} firstly is used to supply with household loads P_{loads}. Then, the surplus PV power P_{PVsur} which equals (P_{PV}-P_{loads}), can be sold to grid or stored in the battery stacks. In this paper, instead of battery energy storage, a cheaper hot water energy storage is applied. As shown in Figure 5.26, the surplus PV power is sensed by the grid side high precision energy meter. Through the communication ports (like RS485 port), the excess PV power information is sent to the micro controller (like DSP), and then the duty cycle d_{act} is calculated to control the switch S_4 of the power electronic water heater. However, when the heating hot water power needs exceeds PV power generation, the power electronic water heater can also absorb power P_g from grid.

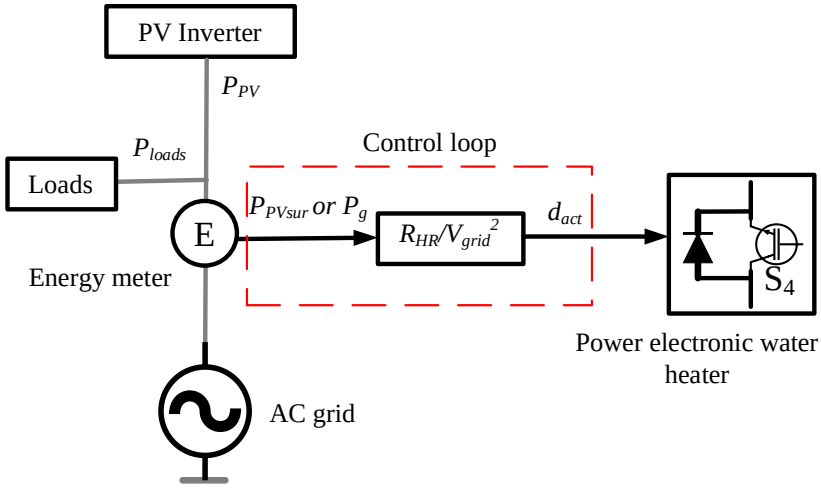

Figure 5.26. The diagram of surplus PV consumed by the power electronic water heater.

5.5. Simulation

In this section, the harmonics compensation capability is validated in the simulation using PLECS software. Additionally, the PV inverter, battery charger, and proposed power electronic water heater are simulated separately to validate their stability and transient performance. Since PV inverter and battery DC/DC converter were built by another person before, and I am not fully aware of their

component power losses, my work involves configuring the software and designing control parameters to make these two converters function effectively. Consequently, it is challenging to match the power dispatch between simulations and experimental results when validating the performance of the entire system. Therefore, the performance validation of the PV-battery-power electronic water heater power system is conducted solely through experimental setup.

Table 5.6 shows the different parameters used in the simulation models and the experimental setup. R_{non}, C_{non}, R_{non_in}, and L_{non_in} are used to build the nonlinear loads which are used to validate the grid harmonics compensation capability of power electronic water heater, as seen in section 5.5.1.

Table 5.6. Parameters used in the simulation and experimental setup.

Component Parameters	Value
Nonlinear load resistor R_{non}	458 Ω
Nonlinear load capacitor C_{non}	480 uF
Nonlinear load input resistor $R_{non\ in}$	20 Ω
Nonlinear load input inductor $L_{non\ in}$	0.05 mH
Grid side inductor L_{grid}	0.15 mH
Power electronic water heater input inductor $L_{HR\ in}$	1.4 mH
Power electronic water heater input capacitor $C_{HR\ in}$	10 uF
Heating resistor R_{HR}	15 Ω
Parasitic inductance of heating resistor L_{HR}	32.34 uH
Grid voltage v_{grid}	240 V_{RMS}
Switching frequency f_{sw}	5 kHz
Grid voltage fundamental period T	0.02 s
DC bus voltage V_{dc}	400 V
DC link capacitor $C_{DC\ bus}$	1800 uF
Inverter side inductor L_{boost}	1.3 mH
Grid side inductor L_{ac}	1.2 mH
Damping resistor R_{LCL}	2 Ω
LCL filter capacitor C_{LCL}	2.2 uF
Household Load resistors R_{loads}	30 Ω
DC bus voltage V_{dc}	400 V
Battery stack voltage V_{bat}	300 V
Battery side inductor L_{bat}	3.3 mH
DC link capacitor C_{DC_bus}	1800 uF
Inverter side inductor L_{boost}	1.3 mH
Grid side inductor L_{ac}	1.2 mH
Dumping resistor R_{LCL}	2 Ω

5.5.1. Harmonics compensation capability simulation validation

As demonstrated in the Section 5.1.5, two harmonics compensation methods are utilized in this thesis: direct harmonics compensation method and the PI

control-based harmonics compensation method (3rd, 5th, 7th, and 9th harmonics as examples). This section aims to validate the capability limitations of the proposed power electronic water heater for grid harmonics compensation. The simulation model is shown in Figure 5.27. It is composed of an adjustable non-linear load producing a similar harmonic profile as found in most household consumers, the proposed power electronic water heater, and an inductor (L_{grid} = 0.15 mH) is added to emulate the "weakness" AC grid.

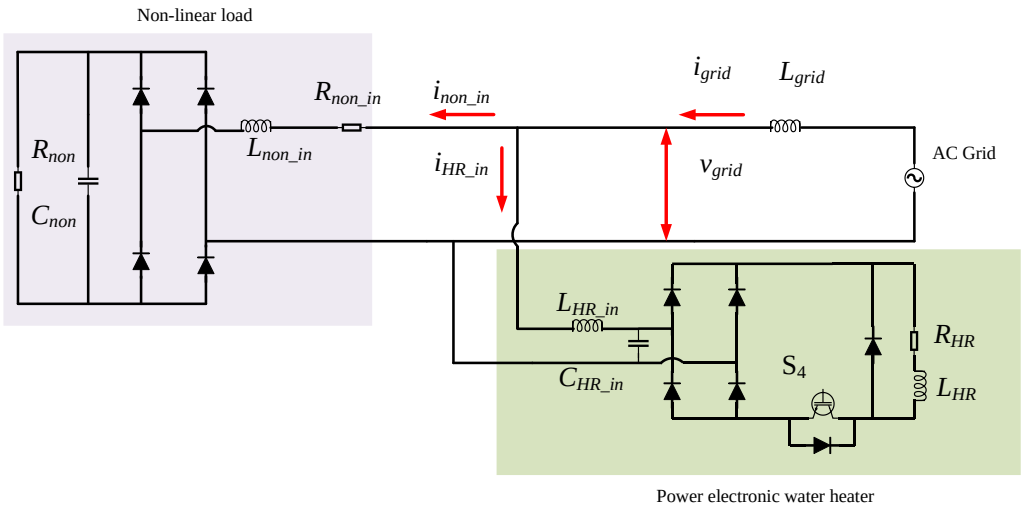

Figure 5.27. The grid harmonics compensation simulation validation topology.

As analysed in Section 5.1.3, there are limitations to using a power electronic water heater for harmonic compensation. Specifically, the duty cycle (d_{har}) allocated for harmonic compensation is restricted to the range (−1,1). To achieve complete harmonic compensation, an additional duty cycle (d_{act}) is required. This ensures that the combined duty cycle (d_{act}+d_{har}) for the switch S_4 remains within the valid range of (0,1). Through the equation (5.13), a demonstration example of this limitation is drawn as Figure 5.28, where the tested setup is shown in Figure 5.27, and the parameters can be seen in Table 5.6. In the Figure 5.28, the red areas indicate regions where the proposed power electronic water heater can fully compensate the grid harmonics. Outside these regions, full compensation of

grid harmonics is not achievable. The compensation capability (highlighted by the red area in Figure 5.28) varies significantly with different d_{act} values (e.g., 0.35 versus 0.05). For a given d_{act}, the compensation effectiveness is influenced by the pulse width m_{wid} and the peak of the harmonic current, $I_{non\_in\_max}$. Therefore, after residential harmonics are sampled, an appropriate d_{act} can be selected to fully compensate for these harmonics effectively. However, the implementation of d_{act} can cause active power consumption, but this power consumption can be stored in hot water by heating resistor R_{HR}.

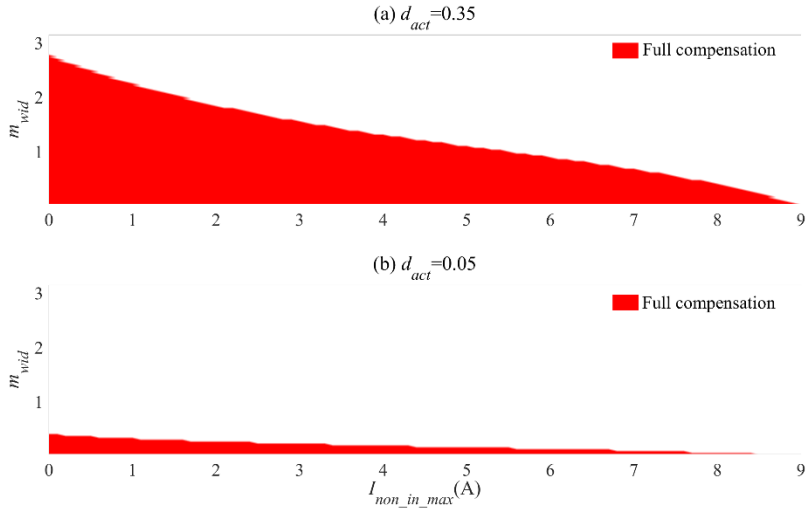

Figure 5.28. An example of harmonics compensation capability limitation. (a) d_{act} =0.35. (b) d_{act} =0.05.

(1) Harmonics compensation capability limitation validation- full harmonics compensation.

In this sector, a large extra duty cycle $d_{act} = 0.35$ is utilized, as shown in Figure 5.28 (a). The nonlinear load current should be in the red region of this figure. Thus, R_{non_in} is set to 20 Ω to decrease the peak of non-linear current i_{non_in}. The rest setup parameters can be seen in Table 5.6. Two different harmonics compensation methods are employed respectively: direct harmonics compensation and PI harmonics compensation.

Initially, the simulation results of these two harmonics compensation methods are shown in Figure 5.29 and Figure 5.30 respectively. Before 0.1s, there is no harmonics compensation. both two methods can be used to compensate the grid harmonics which make the total harmonic distortion (THD) of the grid current drop from 13.6 % to 4.3 % of direct control, and 2.1 % of PI control. However, it takes 0.12 s response time for the PI control method to realize the system stable.

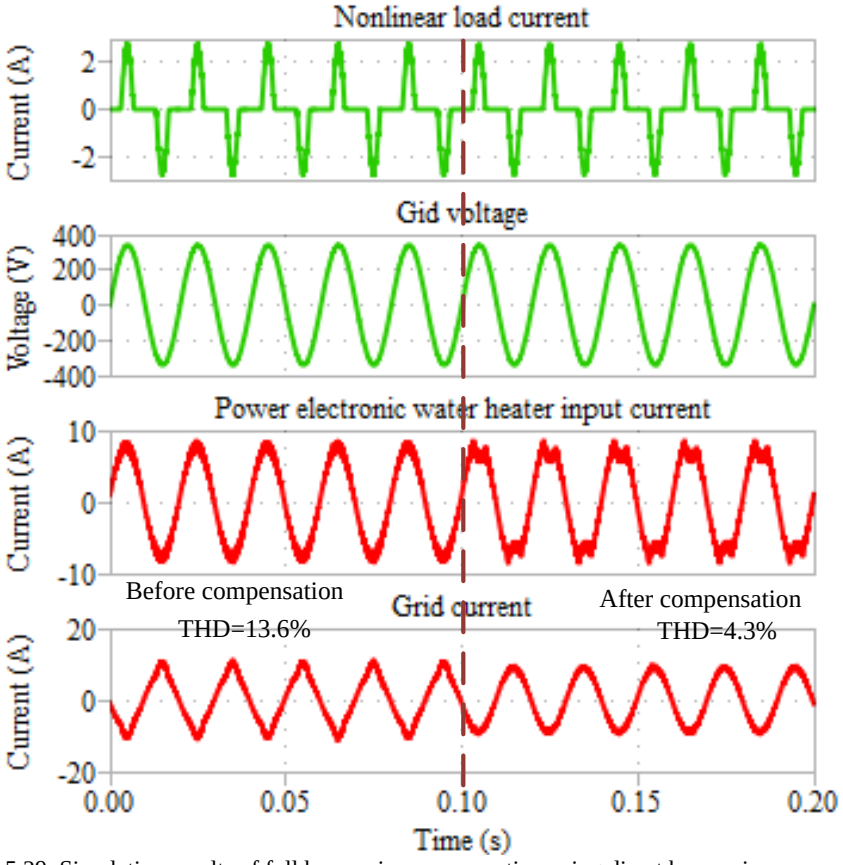

Figure 5.29. Simulation results of full harmonics compensation using direct harmonics compensation method.

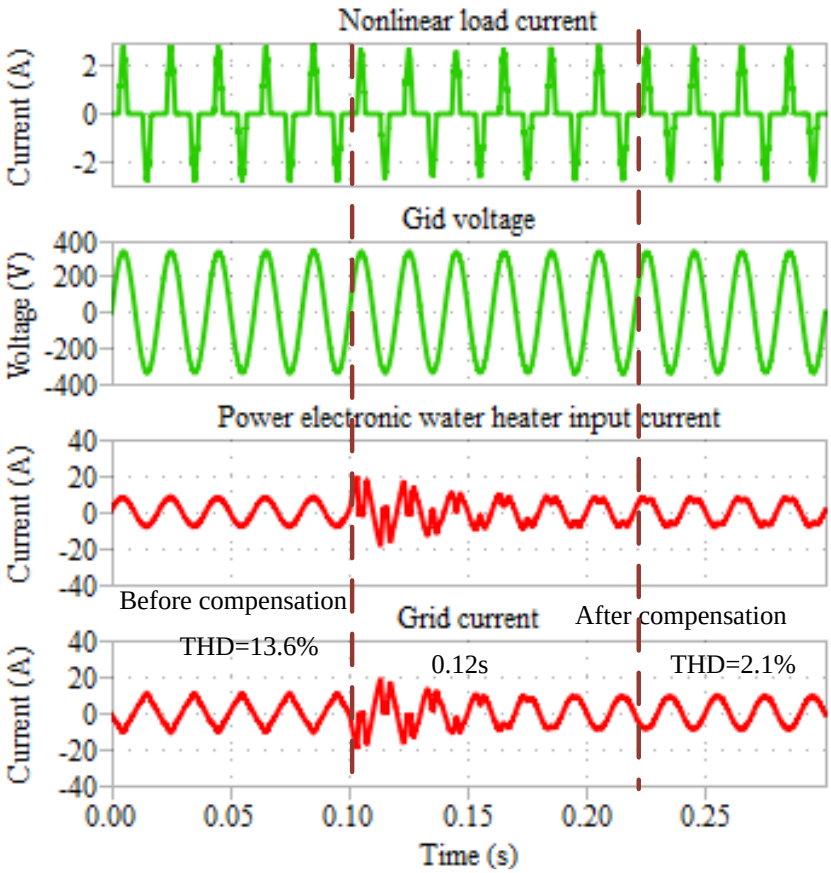

Figure 5.30. Simulation results of full harmonics compensation using PI control-based harmonics compensation method.

(2) Harmonics compensation capability limitation validation- out of harmonic compensation capability.

In this sector, a small extra duty cycle $d_{act} = 0.05$ is utilized, as shown in Figure 5.28 (b). The nonlinear load current should be out of the red region of this figure. Thus, R_{non_in} is set to 0 Ω to increase the peak of non-linear current i_{non_in}. The rest setup parameters can be seen in Table 5.6. Two different harmonics compensation methods are employed respectively: direct harmonics compensation and PI harmonics compensation.

As shown in Figure 5.31 and Figure 5.32, the THD of grid harmonics drops from 126% to 86% for direct harmonics compensation method and 76% for the PI-based harmonics compensation method, respectively. Only a part of

harmonics can be compensated, it indicates a sufficient extra duty cycle d_{act} is needed to fully compensate grid harmonics caused by nonlinear loads.

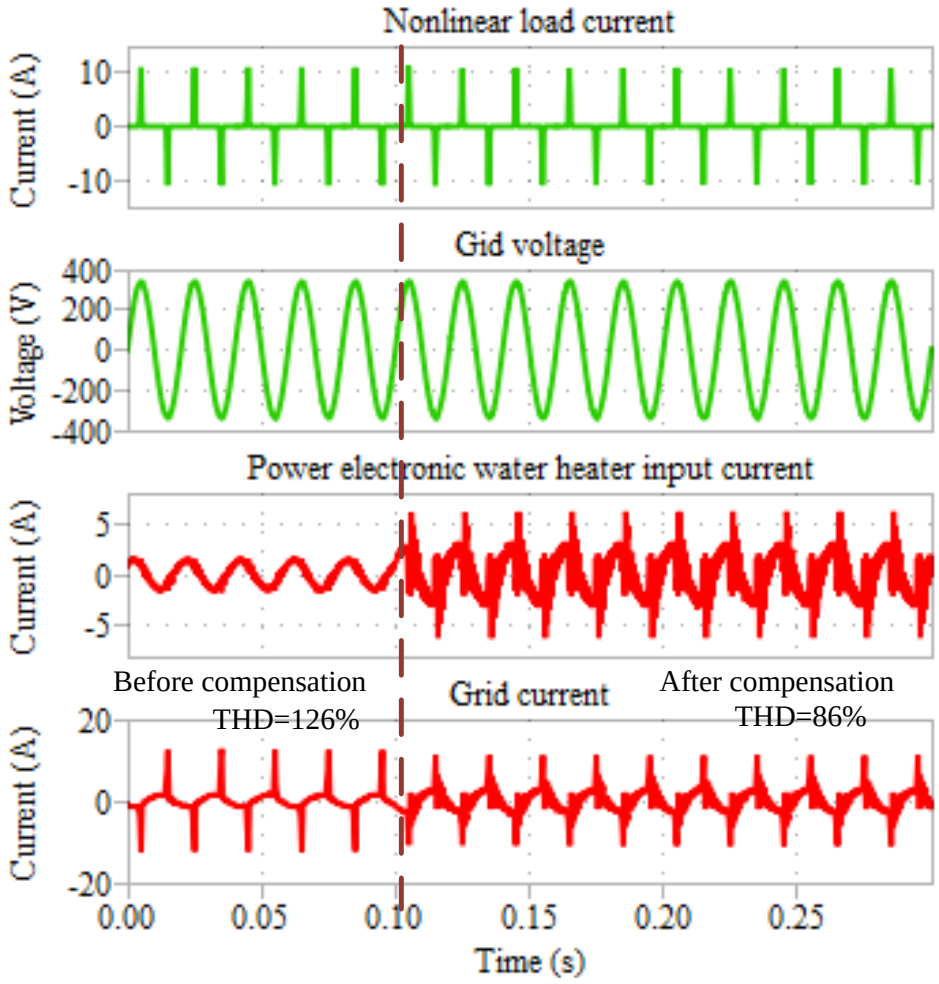

Figure 5.31. Simulation results of a part of harmonics compensation using direct harmonics compensation method.

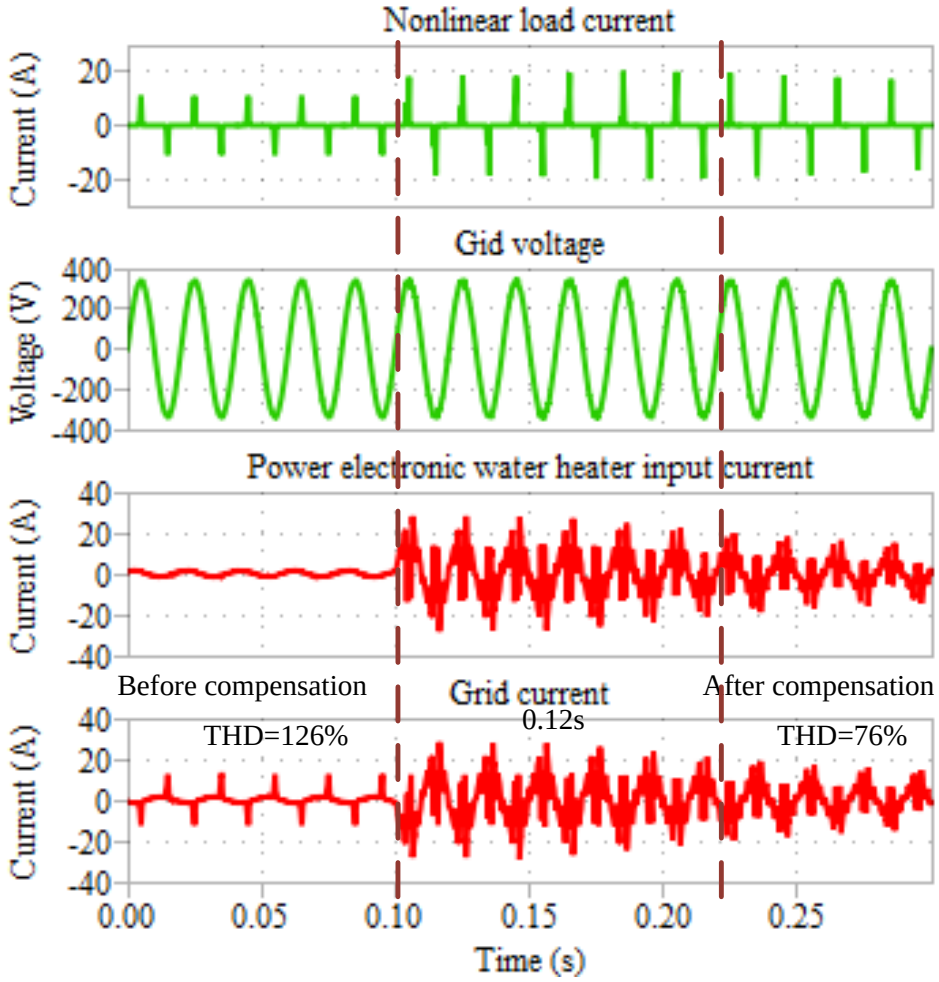

Figure 5.32. Simulation results of a part of harmonics compensation using PI-based harmonics compensation method.

5.5.2. PV inverter and battery charging system performance

A battery stack is employed to maintain a stable DC bus voltage while the PV inverter interfaces with the grid. Using PLECS, simulation models for the PV inverter and battery charger are constructed and simulated to validate their individual performances. This process ensures that each component functions correctly before integration into the overall PV power system.

Figure 5.33 illustrates the performance of the PV inverter across different output power levels, demonstrating the effective operation of the PR (proportional-resonant) controller. Grid voltage and DC bus voltage remain stable during PV power variation.

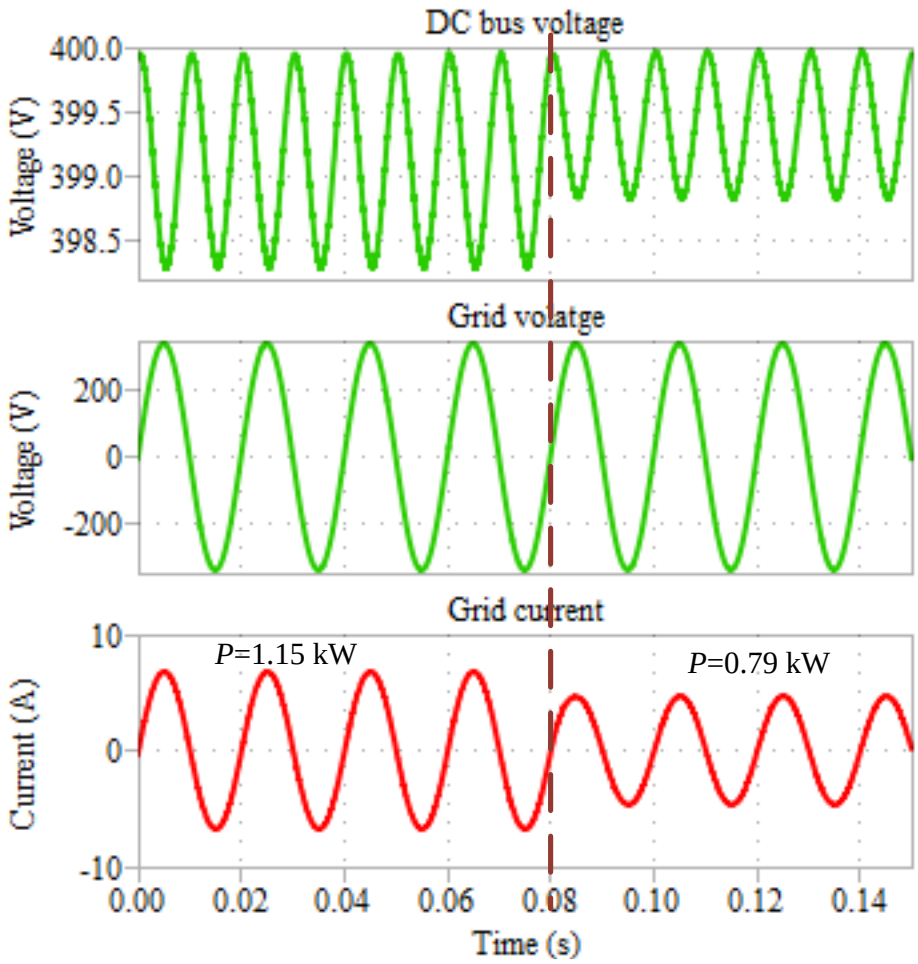

Figure 5.33. Performance of PV inverter at different output power with the PR controller.

Figure 5.34 and Figure 5.35 depict the transient performance of the battery DC/DC converter 's current control loop and double-loop control (including a voltage loop), respectively. In this simulation, the transient process of battery stack voltage and current, and DC bus voltage are shown. These simulations aim to validate the battery DC/DC converter control design detailed in Section 5.3. The results demonstrate that the battery stack effectively tracks changes in the DC bus voltage. This allows the battery DC/DC converter to either absorb or release power as needed to maintain the stability of the DC bus voltage (400 V).

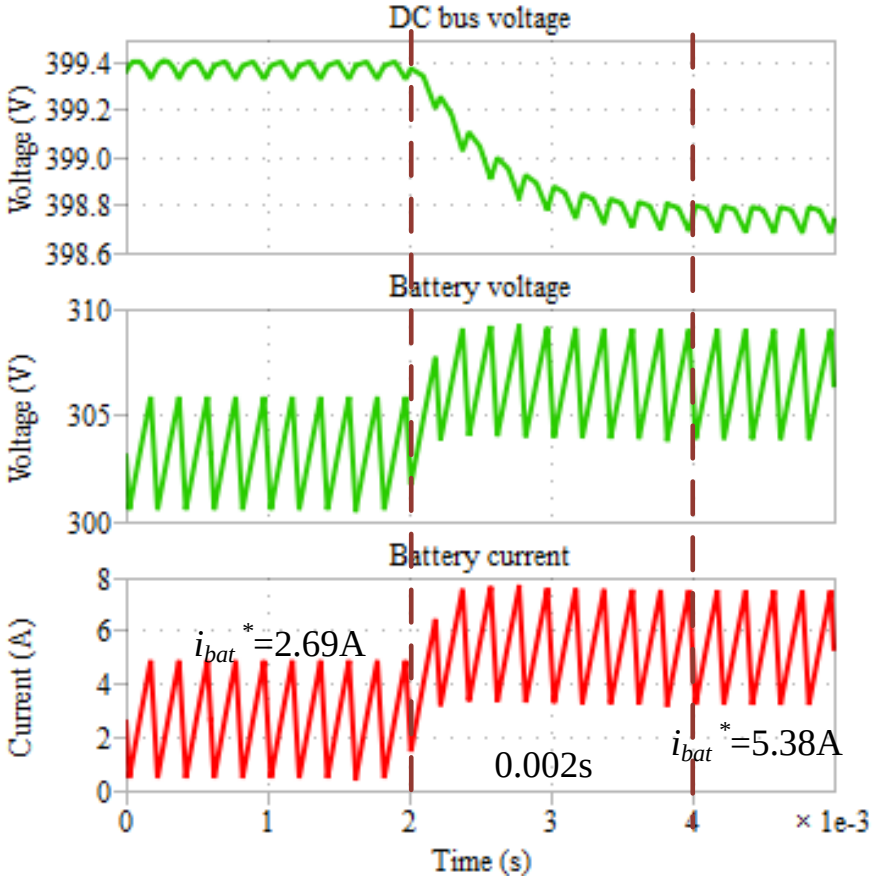

Figure 5.34. Transient performance of battery charger's current loop.

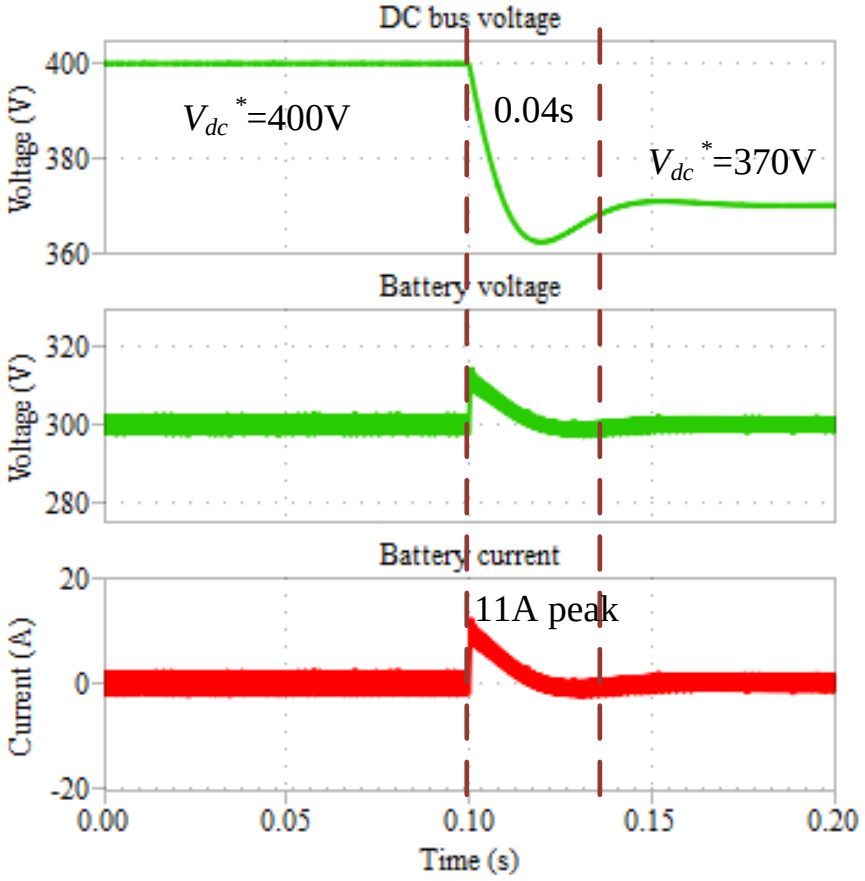

Figure 5.35. Transient performance of battery charger's double loop controller (current and voltage loop).

5.6. Summary

This chapter details the topology and control algorithms of the PV inverter, battery DC/DC converter, and power electronic water heater, which can be integrated to form various PV power system configurations. Unlike conventional relay-based electric water heaters, this thesis introduces a novel power electronic water heater that not only consumes exact surplus PV energy but also compensates for grid harmonics caused by household non-linear loads.

In addition to conventional power consumption control methods, auxiliary control schemes are implemented to meet relevant grid standards and enhance system performance. These include low-order harmonics compensation controllers for the PV inverter and feedforward control for the battery charger.

Furthermore, a simulation model of the proposed power electronic water heater is developed in PLECS to validate its harmonics compensation and precise excess PV power consumption capabilities. Simulations of the PV inverter and battery DC/DC converter are also conducted. The results confirm that the proposed power electronic water heater effectively addresses both harmonics compensation and excess PV power consumption requirements, while demonstrating robust performance of the PV inverter and battery DC/DC converter control algorithms.

Chapter 6: Experimental results

In this chapter, two main experimental validation tasks will be performed. The first task is to verify the capability of the proposed power electronic water heater to dissipate the exact amount of excess PV power available and to facilitate harmonic compensation for current distortion produced by household appliances, typically those fed by diode rectifiers. The second task is to evaluate the performance of the PV-battery-power electronic water heater system prototype and validate the stability and transient performance of the power system under varying PV generation and load demands. Additionally, practical issues such as eliminating low-order grid current harmonics caused by grid voltage distortion are addressed.

The control algorithms are implemented on a digital signal processor (DSP C6713), and the drive signals for the IGBT switches are generated by a field-programmable gate array (FPGA), which produces timings according to duty cycle references from the DSP. The PV array is emulated by a DC power supply (EA-PSI 9750-20) with a maximum voltage rating of 750 V and a current rating of 20 A. The battery stack is emulated by a bidirectional DC power supply (SM1500-CP-30) with a maximum voltage rating of 1500 V and a current rating of ±30 A. Additionally, a AC power supply (model 61705) (0-300 V , 15-1200 Hz, Max 32A and 12 kVA) is used in the power electronic water heater for grid harmonics compensation experiments. An autotransformer is used in the rest experiments as it allows the bidirectional power flow and safety operation. The established test bench of the experimental prototype is shown in Figure 6.1, with detailed hardware figures of each subsystem provided in later sections. And the components parameters can be seen in Table 5.6.

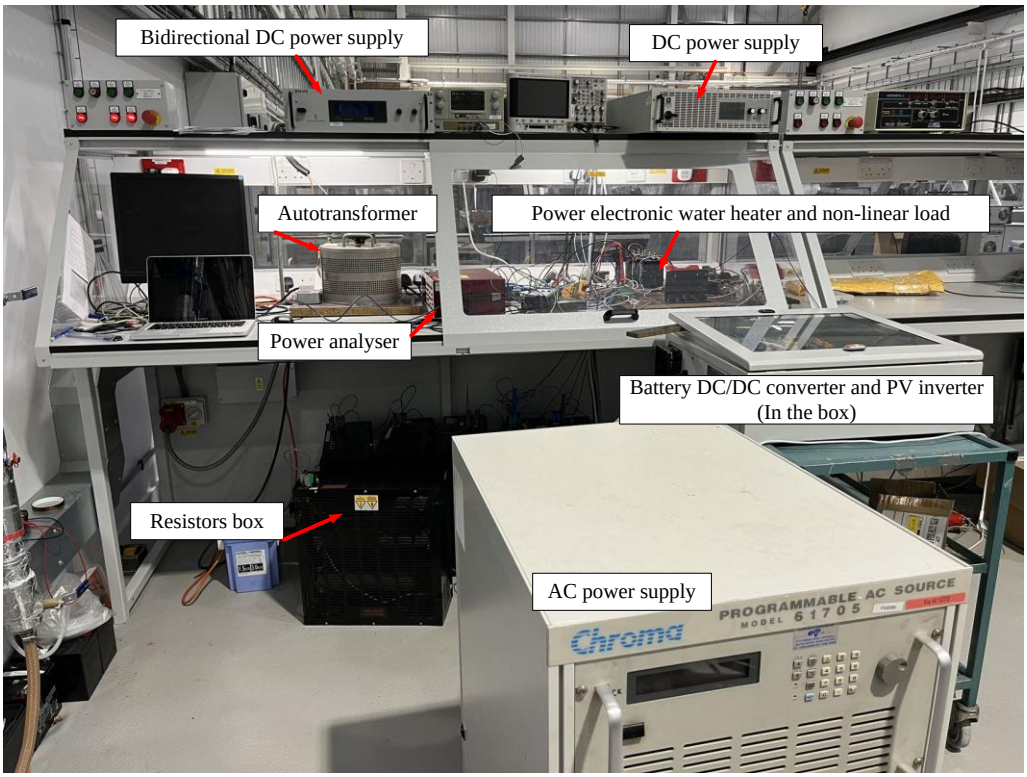

Figure 6.1. The entire established experimental prototype.

6.1. Experimental evaluation of the power electronic water heater

Following the harmonics compensation control schemes outlined in Section 5.1.5, the next step is to validate the precise power consumption and capability of the proposed electric water heater for grid current harmonics compensation in the experimental setup.

To emulate a non-linear load, a diode rectifier is used to feed a smoothing capacitor and load resistor (R_{non} and C_{non}). Additionally, to control input current surges of the non-linear load, an extra input resistor R_{non_in} and an inductor L_{non_in} are added in series on the AC side of the non-linear load.

To replicate realistic grid conditions and challenge the harmonic compensation capabilities of the proposed circuit, an AC electronic voltage source (model 61705) was utilized as the grid simulator. The voltage of this AC source is setting

as 240Vrms and an inductor $L_{grid} = 0.15$ mH is connected in series with the AC power supply to emulate the grid impedance.

The experimental hardware setup of the proposed power electronic water heater and non-linear load is depicted in Figure 6.2.

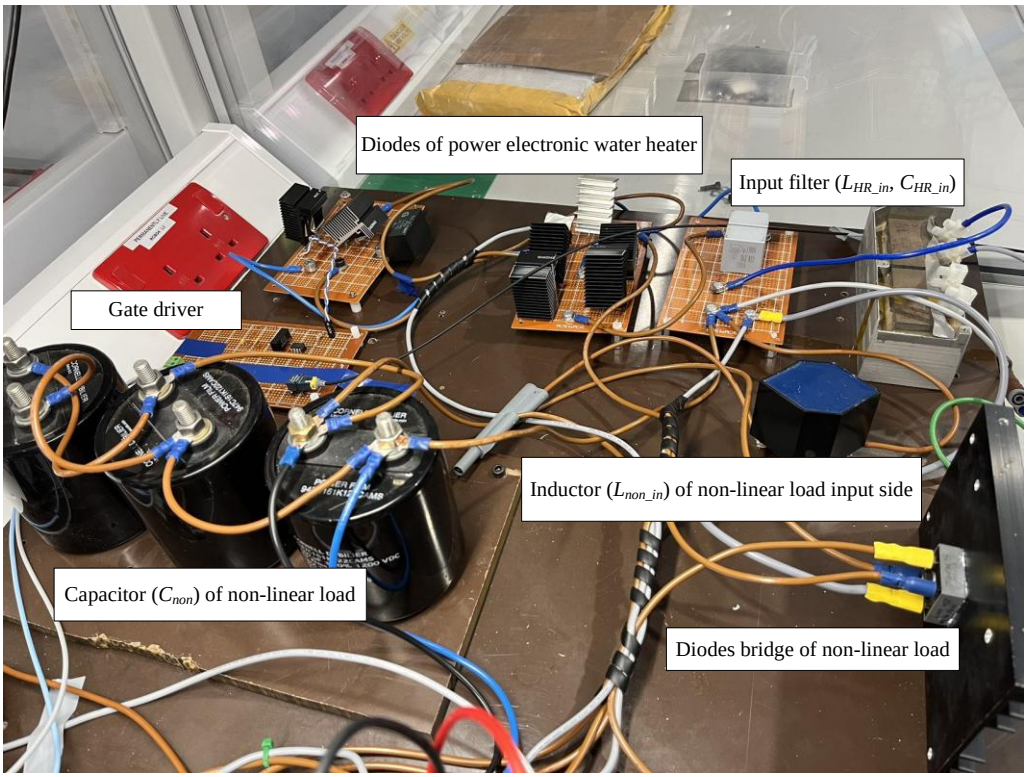

Figure 6.2. The hardware figure of the proposed power electronic water heater and non-linear load.

Due to safety regulations in the laboratory environment, a water tank and immersion heater resistor could not be directly used. Instead, they were substituted with a similar air-cooled resistor with comparable power dissipation and parasitic inductance, as depicted in Figure 6.3. This substitution ensures that the experimental setup closely approximates the operational conditions of the proposed power electronic water heater in a real-world scenario.

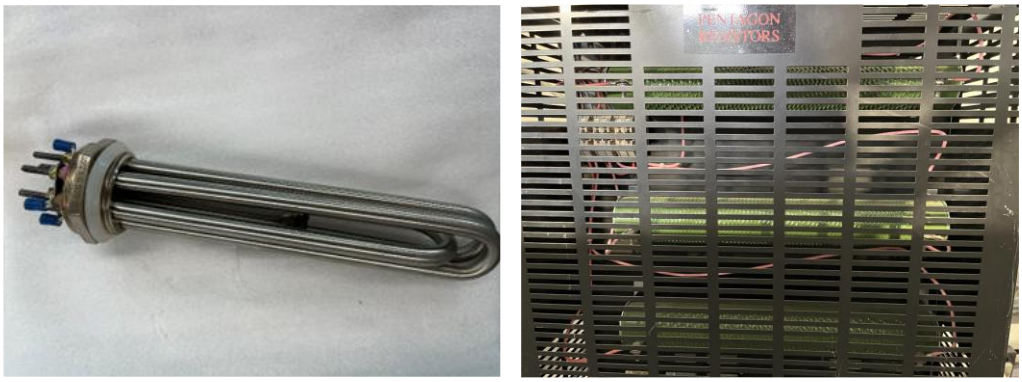

(a) Practical immersion heater (b) Coil winding resistors

Figure 6.3. The pictures of the practical immersion heater and coil winding resistors. (a) Practical immersion heater which has three individual resistors. (b) Coil winding resistors used in the experiment.

To ensure that this is a reasonable replacement from the point of view of parasitic, the parasitic inductance of the real immersion heater and of the wound air-cooled tor were measured with an impedance analyzer (KEYSIGHT E4990A). Table 6.1 shows the parasitic inductance of one immersion heater (5Ω) and one coil winding resistor (10Ω) (TE 1500B 10RJ) at few relevant frequencies. To construct 15Ω heating load, three individual immersed heaters, each with a resistance of 5 Ω, are connected in series, resulting in a total parasitic inductance of 26.67 μH. For lab testing, a load is constructed using two coil resistors (each 10 Ω) connected in parallel, followed by a series connection with a third 10 Ω resistor. This configuration achieves a total resistance of 15 Ω and a parasitic inductance of 32.34 μH. The difference in total inductance between the two configurations is minimal. Furthermore, compared to the load resistance (15 Ω), the parasitic inductance is insignificant. As discussed previously, due to the discontinuous current in the heating load, the parasitic inductance can be effectively ignored.

Table 6.1. The measurement inductance of one immersed heater and one coil winding resistor.

Component	Frequency (Hz)				
	50	5 k	10 k	20 k	50 k
	Inductance (uH)				
Heater	10.26	8.89	8.77	8.6	8.42
Coil winding resistor	21.56	20.15	19	19.76	19.51

6.1.1. Power consumption tests

Due to the needs of active power consumption for grid harmonics compensation test, power electronic water heater is connected to AC grid to facilitate the simple power consumption test. In the experimental test, the topology of the proposed power electronic water heater shown in Figure 5.2 (b) is used. When the duty cycle of the switch drops from the 0.4 to 0.21, the experimental results of v_{grid}, i_{HR_in}, i_{HR} is shown in Figure 6.4 (a). It takes around 2.5 ms to settle the current dropping from 6.2A to 3.2 A. Thus, compared to the conventional relay-based electric water heater, the proposed power electronic water heater can quickly adjust power consumption using PWM technology. This allows for more accurate and rapid consumption of excess PV energy. Besides, from the current i_{HR} flowing through the tested resistor, it also indicates that the impacts of parasitic inductance (32.34 μH) on this process can be negligible, since the extended current is quickly down to zero (about 0.02 ms) during the IGBT is turned off.

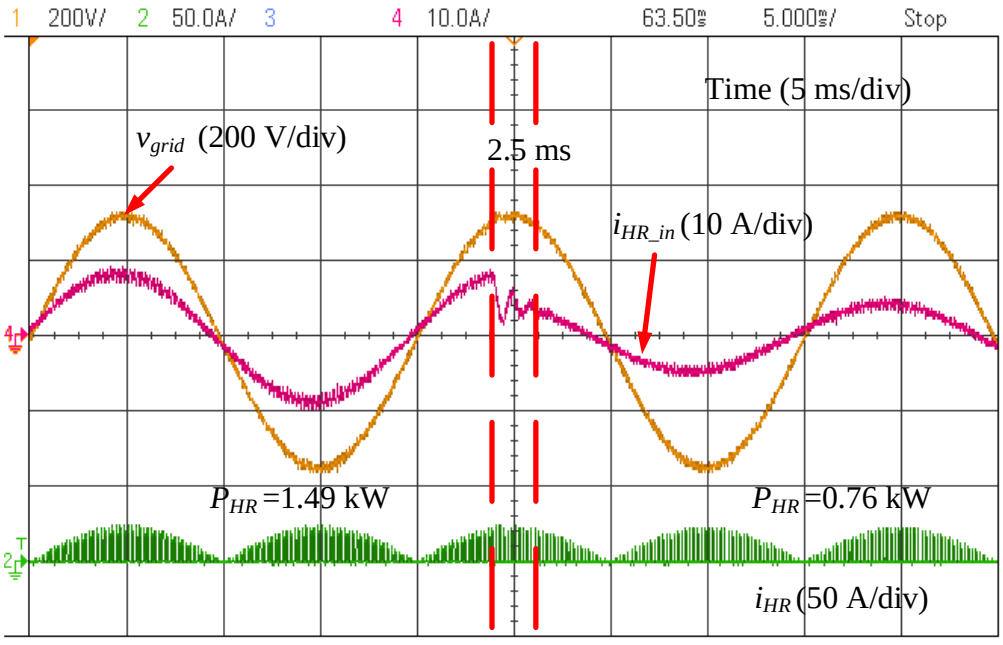

Figure 6.4. Experimental results (v_{grid}, i_{HR_in}, and i_{HR}) with sudden duty cycle change. Yellow-grid voltage, purple-grid current, and green-heater resistor current.

6.1.2. Harmonics compensation capability tests

6.1.2.1. Harmonics compensation transient tests

The schematic diagram of harmonics compensation capability test is shown in Figure 5.27. d_{act} is set to 0.18, resulting in a power consumption of 0.69 kW. Additionally, $R_{non_{in}}$ is fixed at 20 Ω. The transient performance of two harmonics compensation methods is examined: the direct harmonics compensation method and the PI control harmonics compensation method. The transient experimental results of the grid voltage v_{grid}, grid current i_{grid}, non-linear load input current i_{non_in}, and the power electronic water heater input current i_{HR_in} for these two methods are shown in Figure 6.5 (a) and (b) respectively. It is evident that the power electronic water heater can compensate the grid current harmonics no matter which type of compensation method is utilized. However, compared with direct compensation method, the response speed of the PI control method is much lower, taking 0.12 s to reach the stability in this experiment since a low pass filter is employed to extract the selected order harmonic in the PI control scheme.

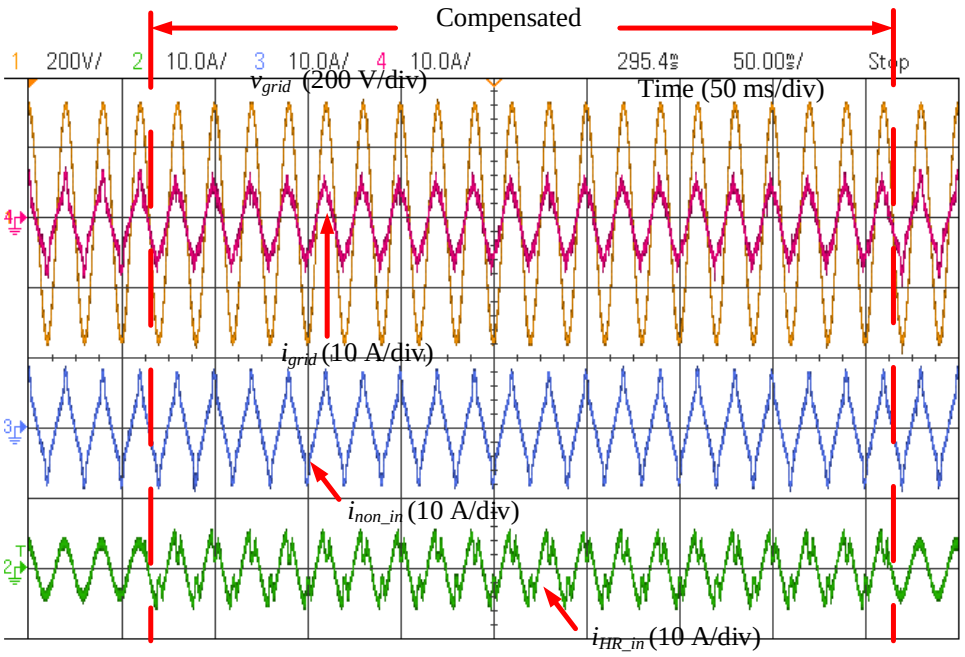

(a)

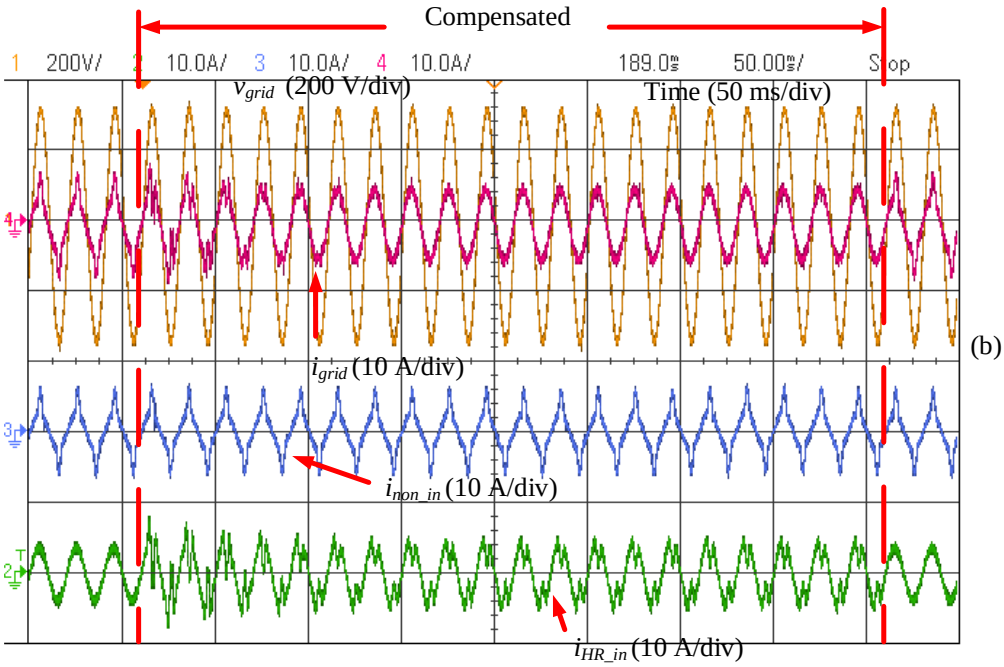

Figure 6.5. Experimental results of respond speed for two harmonics compensation methods. (a) The direct harmonics compensation method. (b) The PI control harmonics compensation method. Grid voltage v_{grid} (yellow line), grid current i_{grid} (purple line), non-linear load input current i_{non_in} (blue line), and power electronic water heater input current i_{HR_in} (green line).

6.1.2.2. Steady state tests

To ensure there is sufficient margin for the control action to manage distorted current without exceeding the maximum current absorption capability of the resistor (v_{grid}/R_{HR}), d_{act}=0.35 is utilized for switch which causes about 1.3 kW power consumption and R_{non_in} is set as 20 Ω to limit non-linear load input current i_{non_in}. The capability of power electronic water heater used for harmonics compensation was tested in direct harmonics compensation method and PI control harmonics compensation method respectively.

Figure 6.6 shows the experimental results of grid voltage v_{grid}, grid current i_{grid}, non-linear load input current i_{non_in}, and the power electronic water heater input current i_{HR_in} at uncompensated Figure 6.6 (a), direct harmonics compensation Figure 6.6 (b), and PI control harmonics compensation method Figure 6.6 (c). The proposed power electronic water heater can remove the grid harmonics caused by the household nonlinear load when the heater consumes

enough power to heat water. Figure 6.7 shows the fast Fourier transform (FFT) analysis of grid current i_{grid} which is done by power analyser (KinetiQ PPA2530) where the value of each order of harmonic current is shown in Figure 6.7 (a) and their magnitude compared to the grid fundamental current is shown in Figure 6.7 (b). It is evident that the selected order of harmonic current (3^{rd}, 5^{th}, 7^{th}, 9^{th}) is almost compensated after the harmonic compensation control applied. However, compared with the direct compensation method, PI harmonics compensation method has higher accuracy on the capability of harmonics compensation. Through the THD (total harmonic distortion) analysis of i_{grid} depicted in Table 6.2, the harmonics compensation capability of PI control method almost doubles than that of direct method.

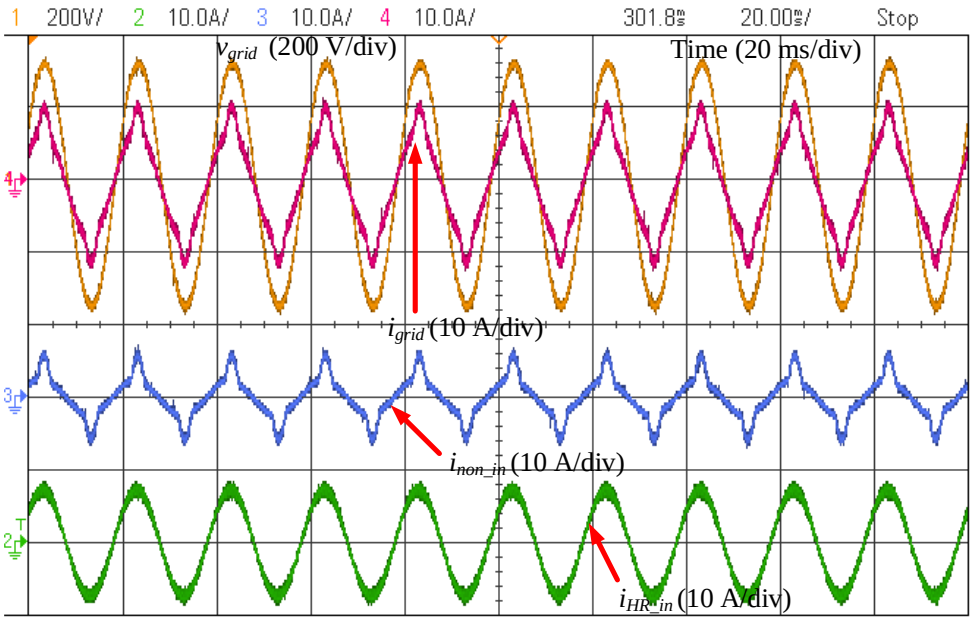

(a)

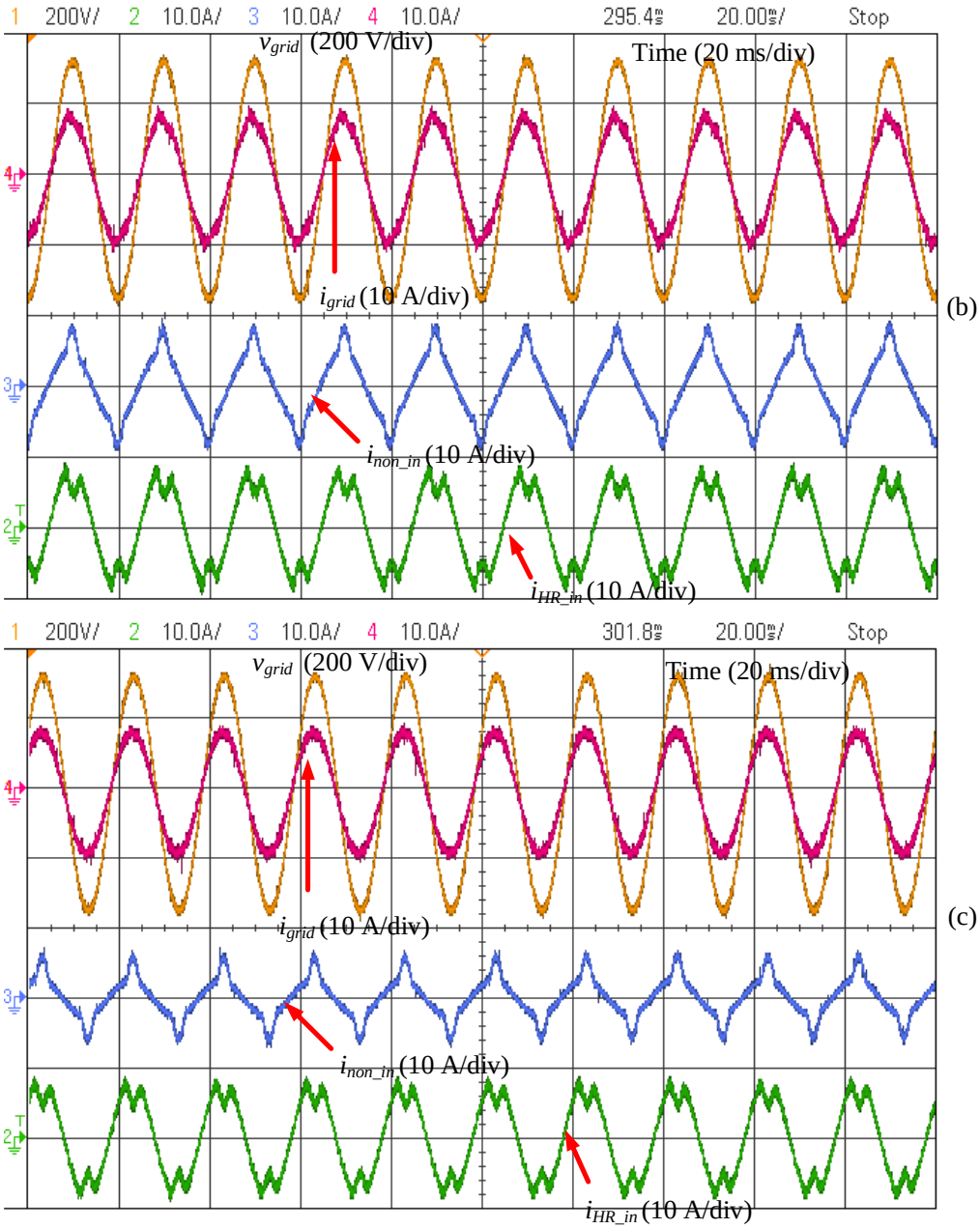

Figure 6.6. Experiment validation results at full harmonics compensation condition. (a) Uncompensated. (b) Direct harmonics compensation method. (c) PI control harmonics compensation method. Grid voltage v_{grid} (yellow line), grid current i_{grid} (purple line), non-linear load input current i_{non_in} (blue line), and power electronic water heater input current i_{HR_in} (green line).

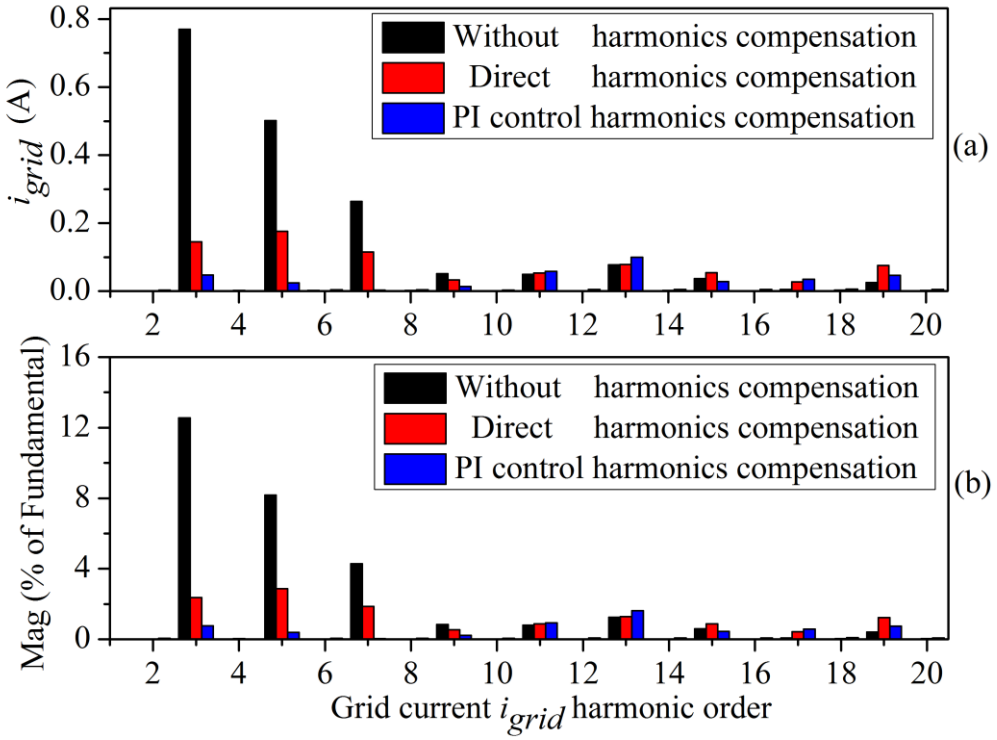

Figure 6.7. FFT analysis of grid current i_{grid} at full harmonics compensation. (a) The value of each harmonic order. (2) The magnitude of each harmonic order compared with grid current fundamental component.

Table 6.2. THD of grid current i_{grid} at full harmonics compensation.

Methods	Uncompensated	Direct compensation	PI control compensation
THD %	15.71	4.75	2.53

4.2.1 Determining the limitations of the harmonics compensation capability

In this section, the limitations of the proposed power electronic water heater used for grid harmonics compensation are discussed. From the analysis of Section 5.1.3, the power electronic water heater input current i_{HR_in} after harmonics compensation should be always inside the envelop of the upper limit of i_{HR_in} (switch constantly conducted). Thus, the power electronic water heater should consume a proper amount of power which cannot be too small or large to satisfy the full harmonics compensation condition.

To validate this analysis, a small duty cycle d_{act}=0.05 is utilized for switch S_4 which causes 0.19 kW power consumption and the R_{non_in} is removed to create large peaks in non-linear load input current i_{non_in}. Thus, compared with full

harmonics compensation situation, the smaller i_{HR_in} and larger i_{non_in} are used to examine the power electronic water heater used for grid harmonics compensation. Similarly, Figure 6.8 and Figure 6.9 show the experimental results of part harmonics compensation in the grid current and the FFT of the grid current respectively. Clearly, both direct and PI control method can only compensate a part of grid current harmonics as seen by the THD in Table 6.3, but PI control harmonics compensation method performs better than direct compensation method at 3rd, 5th, 7th, and 9th order harmonic.

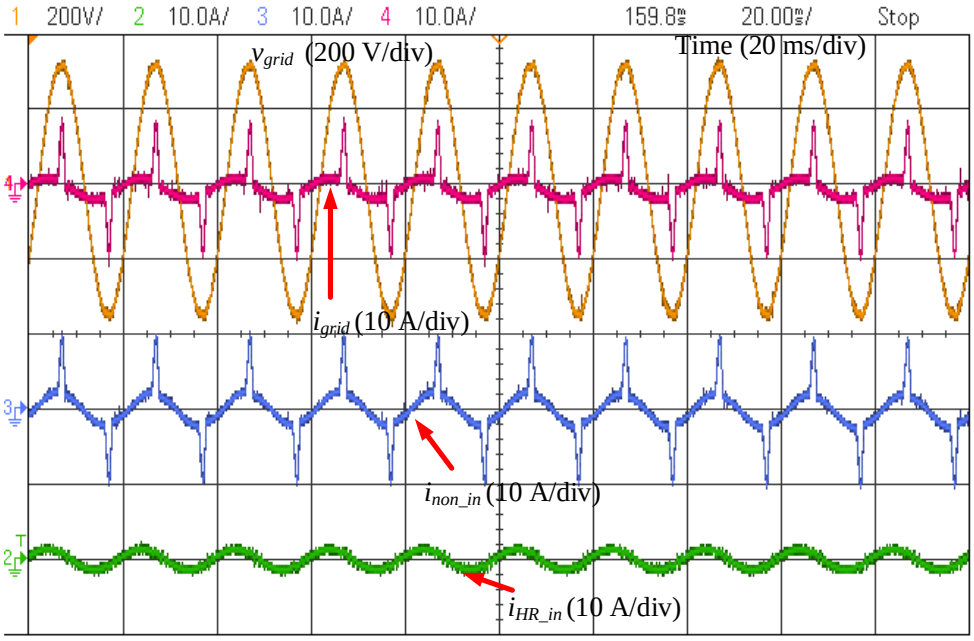

(a)

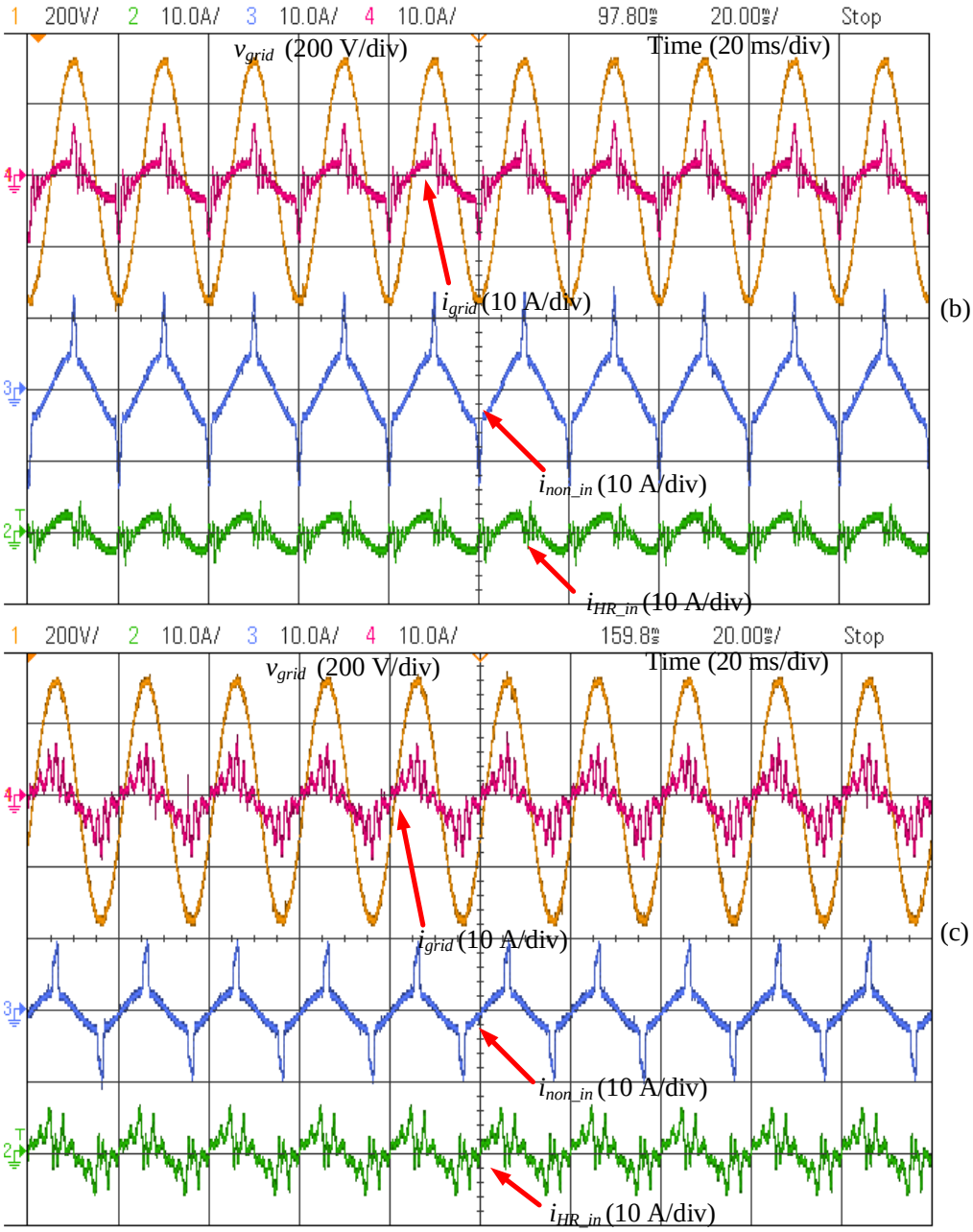

Figure 6.8. Experiment validation results at part harmonics compensation condition. (a) Uncompensated. (b) Direct harmonics compensation method. (c) PI control harmonics compensation method. Grid voltage v_{grid} (yellow line), grid current i_{grid} (purple line), non-linear load input current i_{non_in} (blue line), and power electronic water heater input current i_{HR_in} (green line).

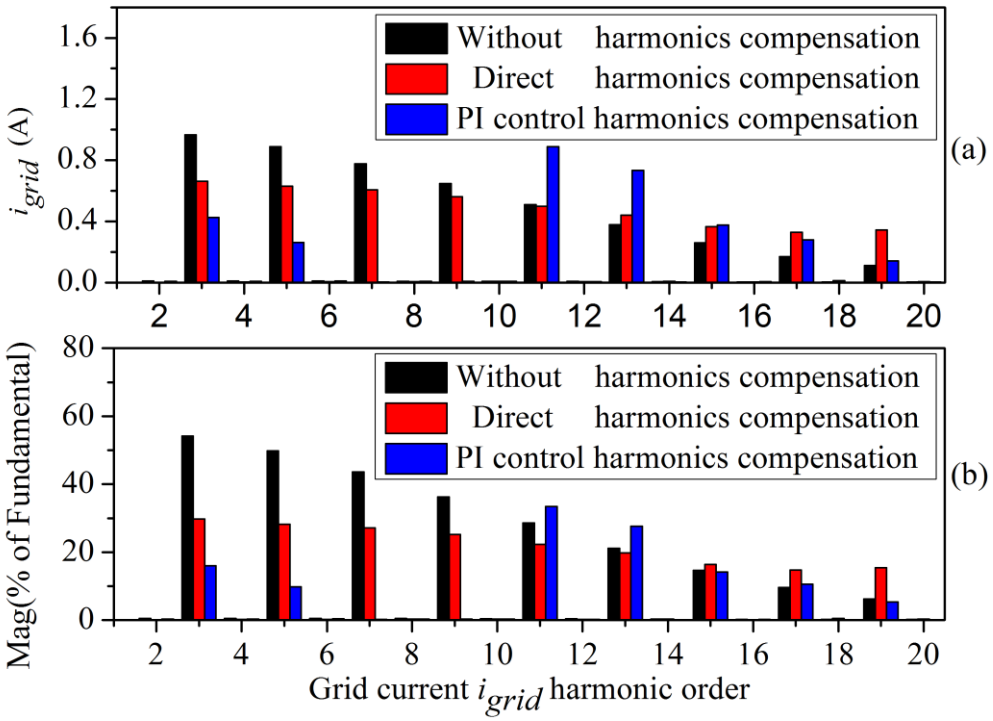

Figure 6.9. FFT analysis of grid current i_{grid} at part harmonics compensation. (a) The value of each harmonic order. (2) The magnitude of each harmonic order compared with grid current fundamental component.

However, through the comparison of Figure 6.7 and Figure 6.9, it is evident that there is a little increase of harmonic amount in high order harmonics like 17^{th} and 19^{th} when the direct harmonics compensation method is applied. The time delay caused by the digital DSP control affects more in higher order harmonic compensation, which leads to an increase in higher order harmonics (17^{th} and 19^{th}). Besides, due to the uncompensated harmonics, especially 11^{th} and 13^{th} order harmonic, they increase a little in PI control harmonics compensation method since the power electronic water heater produces little compensating harmonics into grid in PI control method (seen in Figure 6.7 and Figure 6.9) which is analysed in Section 5.1.5.

Table 6.3. THD of grid current i_{grid} when the harmonics compensation capability is limited by the current envelope (v_{grid}/R_{HR}).

Methods	Uncompensated	Direct compensation	PI control compensation
THD %	113	78.81	62.69

6.2. Experimental tests of PV inverter and battery DC/DC converter

In this section, to validate the performance of the PV-battery-novel power electronic water heater power system, each subsystem (PV inverter, battery energy storage system, and power electronic water heater) needs to be tested separately. Figure 6.10 shows the hardware setup of the battery DC/DC converter and PV inverter, while Figure 6.2 illustrates the hardware setup of the power electronic water heater. Significantly, the hardware in Figure 6.10 was not built by myself, and my work is to fix the control codes to make the system work.

Apart from the conventional tests to validate stability and transient performance of the battery DC/DC converter and PV inverter, this section addresses practical issues such as grid harmonics arising from grid voltage distortion. Besides, as shown in Section 5.3.2, a notch filter is used to 100 Hz to reject the 100 Hz ripple in the DC bus voltage V_{dc}. These challenges are tackled to ensure robust performance and functionality of the integrated PV-battery-power electronic water heater system.

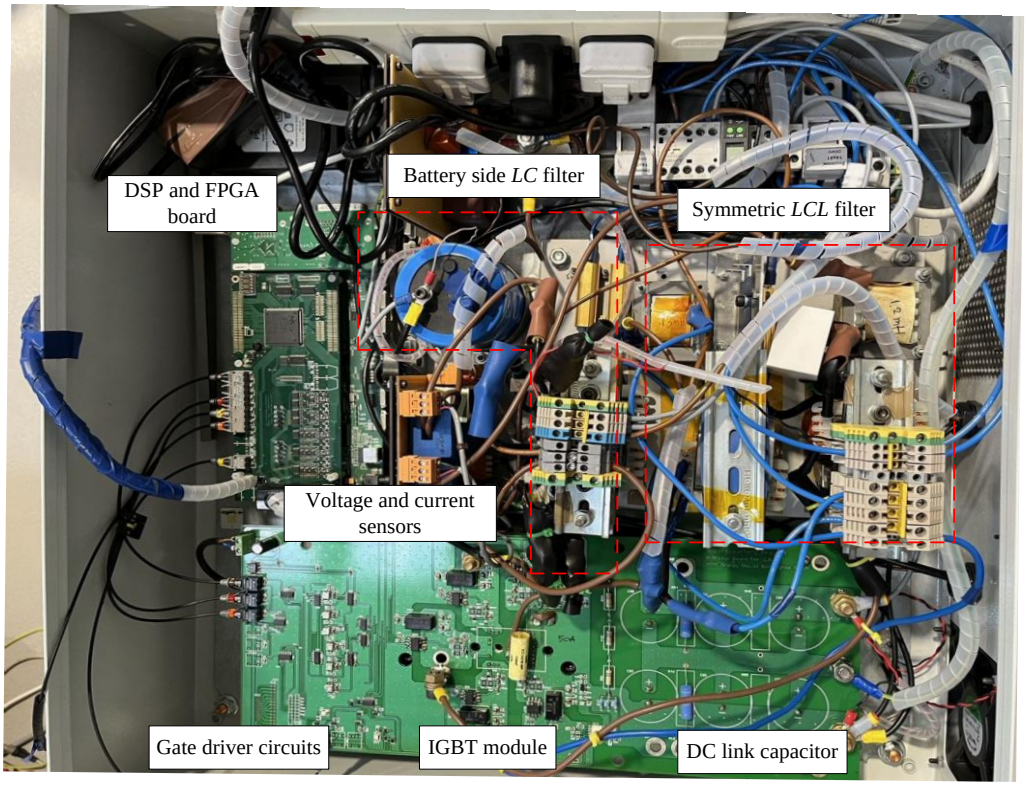

Figure 6.10. Battery DC/DC converter and PV inverter hardware figure.

6.2.1. Grid-connected PV inverter experimental tests

As shown in Figure 5.1, an autotransformer is utilized for the experimental safety operation. However, due to the distortion caused by the autotransformer, the grid voltage exhibits low-order harmonics, leading to much grid current produced, as shown in Figure 6.11. To address this issue, harmonics compensation proportional-resonant (PR) controllers targeting the (3^{rd},5^{th}, 7^{th}) harmonics are implemented in this experiment, as described in Section 5.2.2. The experimental results of grid current i_{grid}, grid voltage v_{grid} and DC bus voltage V_{dc} with and without harmonics compensation are illustrated in Figure 6.12. Additionally, Figure 6.13 presents the FFT analysis of grid current harmonics.

Before compensation, THD of the grid current is 7%, which is reduced to 3.32% after applying low-order harmonics compensation. This reduction confirms that

the harmonics compensation PR controllers effectively, demonstrating their robust performance in mitigating grid harmonic distortions.

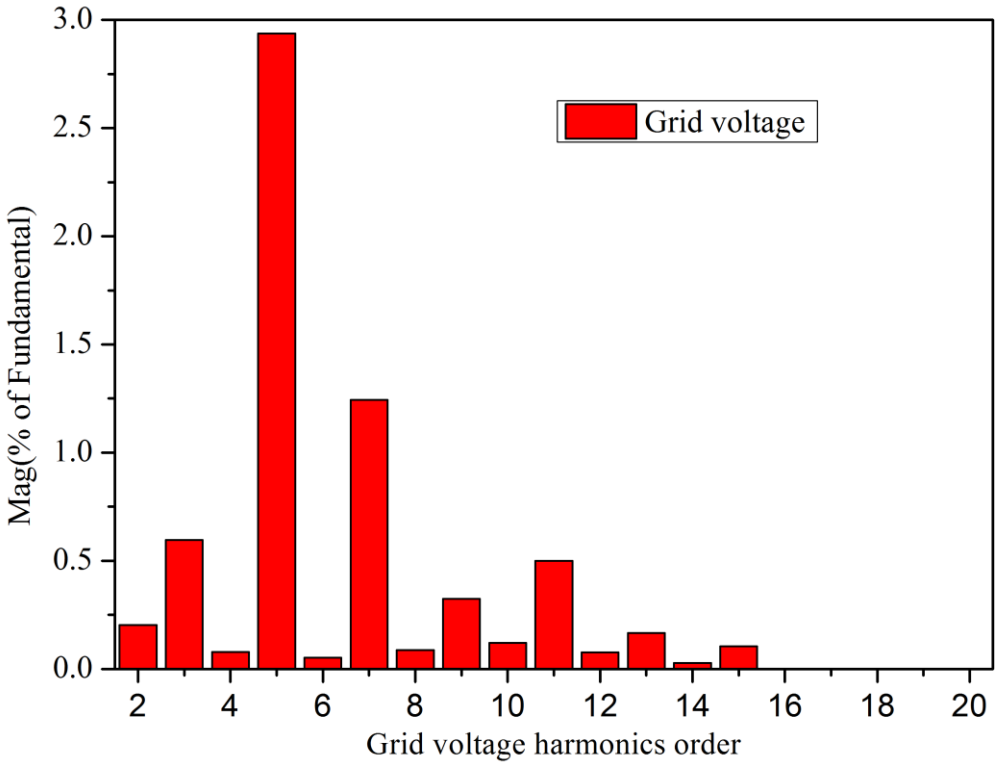

Figure 6.11. FFT of output voltage of autotransformer.

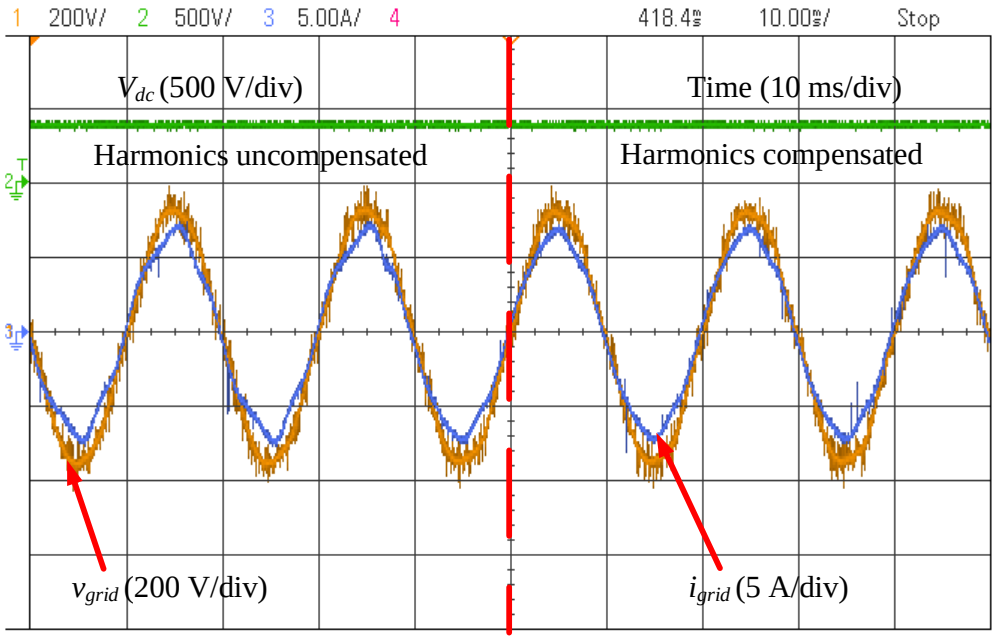

Figure 6.12. Experimental results of PV inverter grid connection test with/without low order harmonics compensation. Yellow-grid voltage, blue-grid current, and green-DC bus voltage.

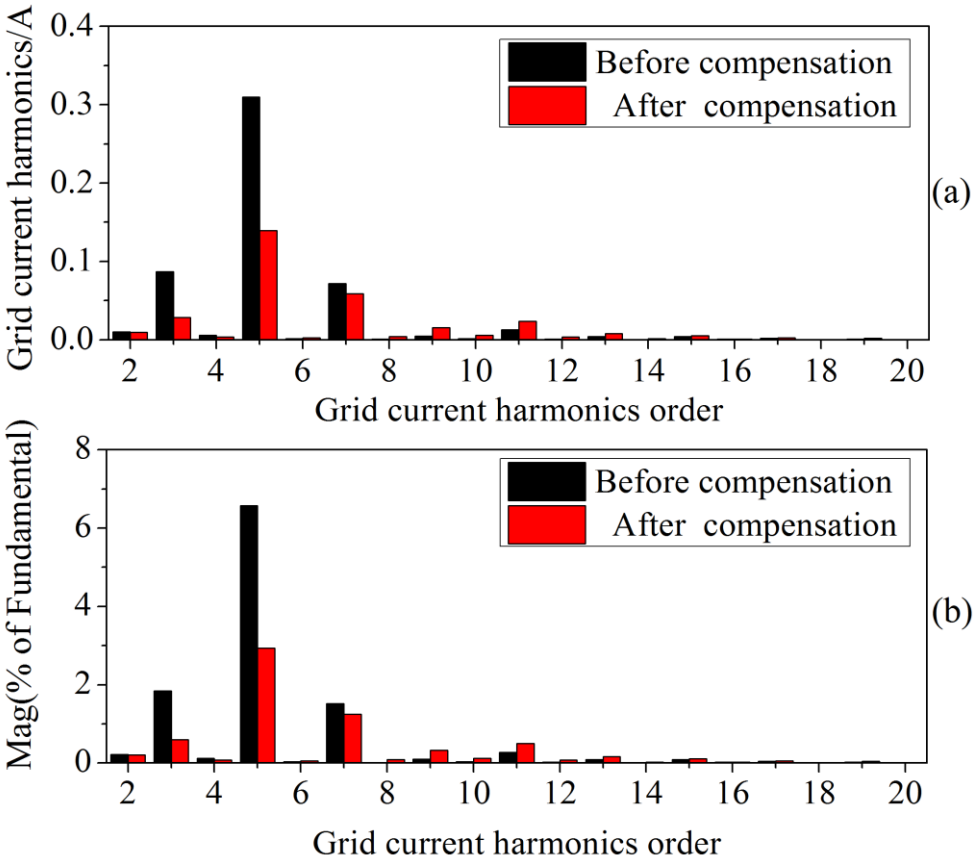

Figure 6.13. FFT analysis of grid current.

Figure 6.14 shows the experimental results of DC bus voltage (400 V), grid voltage (240 V), and grid current when the power transferred by PV inverter dropping from 1.15 kW to 0.79 kW which indicates the good transient performance the PR controller.

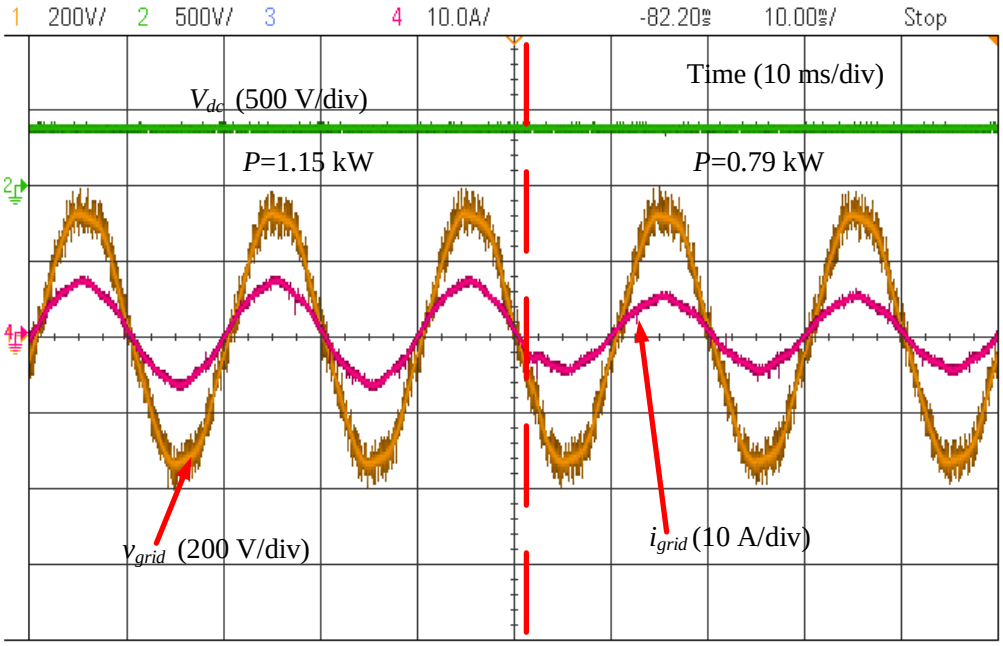

Figure 6.14. Experimental results of the power transferred changing. Yellow-grid voltage, purple-grid current, and green-DC bus voltage.

6.2.2. Battery DC/DC converter experimental tests

The battery stack is designed to absorb surplus PV energy, store grid electricity during off-peak hours, and release stored energy during peak demand periods. Figure 6.15 depicts the experimental test of the inner current loop of the battery DC/DC converter, specifically demonstrating constant current charging of the battery which can be seen in 5.3.2.

In the experiment, when the battery charging current reference i_{bat}^{*} increases from 2.69 A to 5.38 A, the battery DC/DC converter successfully adjusts to follow the new current reference within 2 ms. This rapid response time highlights the efficient performance of the battery DC/DC converter in maintaining precise control over charging currents, crucial for optimizing battery charging efficiency and stability in varying load conditions.

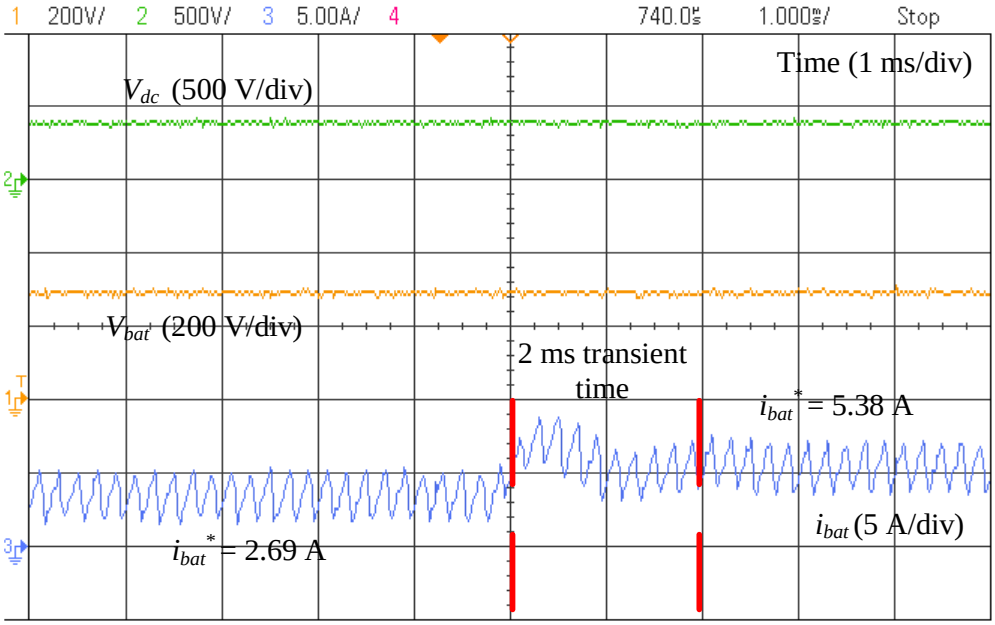

Figure 6.15. The inner current loop experimental test of battery DC/DC converter during a battery current step experimental test. Yellow-battery voltage, blue battery current, and green-DC bus voltage.

Following the control scheme detailed in Section 5.3.2, the experimental test results of the battery DC/DC converter with double-loop PI control are presented in Figure 6.16. This setup is designed to maintain stability in the DC bus voltage when the DC bus voltage fluctuates.

Therefore, to test the performance of the double-loop in the experiment, the DC bus voltage reference V_{dc}^* drops from 400 V to 370 V, simulating a scenario where the DC bus voltage is fluctuated. It is observed that the battery DC/DC converter adjusts to follow the new DC bus voltage reference within 40 ms. This response time indicates the performance of the double-loop PI control in effectively regulating the DC bus voltage, ensuring stable operation of the battery DC/DC converter under dynamic operating conditions.

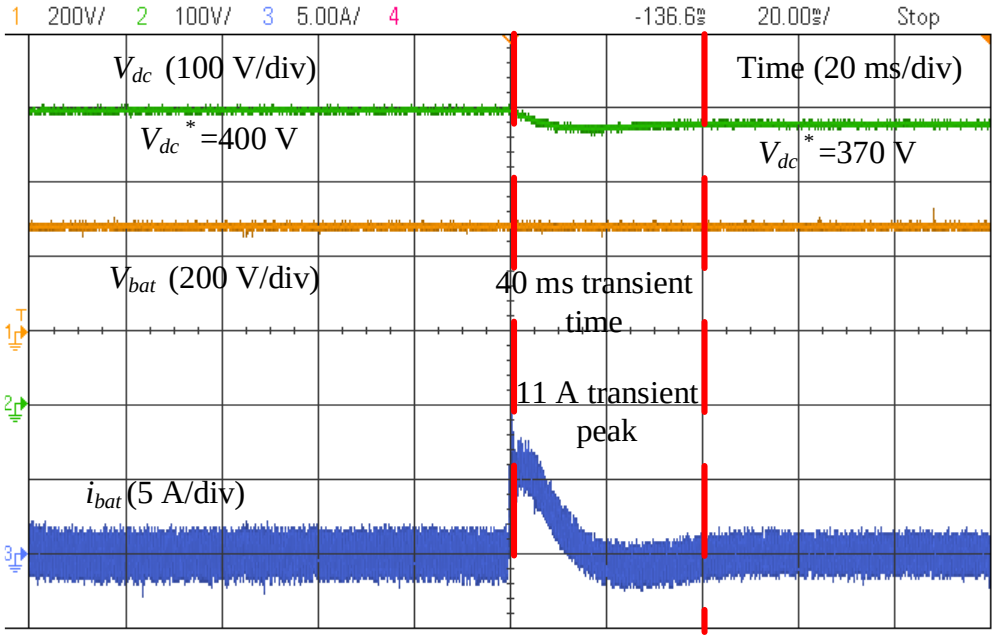

Figure 6.16. The double loops experimental tests of the battery DC/DC converter nested controller test to a DC-link reference voltage step change from 400 V to 370V. Yellow-battery voltage, blue-battery current, and green-DC bus voltage.

6.3. The performance of PV-battery-power electronic water heater power system

Given the variability inherent in PV generation and household load consumption, which can significantly impact the stability of power systems, particularly in distributed setups, it is crucial to evaluate the PV-battery-power electronic water heater power system. This section presents experimental examples under varying PV generation or household load consumption conditions to validate the stability and transient performance of the power system.

6.3.1. Performance of PV-battery power system

AS the important subsystem of PV-power electronic water heater system, the performance of PV-battery power system is firstly validated. The topology of PV-battery power system is shown in Figure 6.17. When the PV generation/loads demand changes, the experimental results of grid voltage v_{grid}, grid current i_{grid}, DC bus voltage V_{dc}, battery stack current i_{bat} at different system operation situations are shown. Since no loads are implemented in the experimental setup,

the grid power P_{grid} is used to indicate the power output of PV inverter or the power imported from grid.

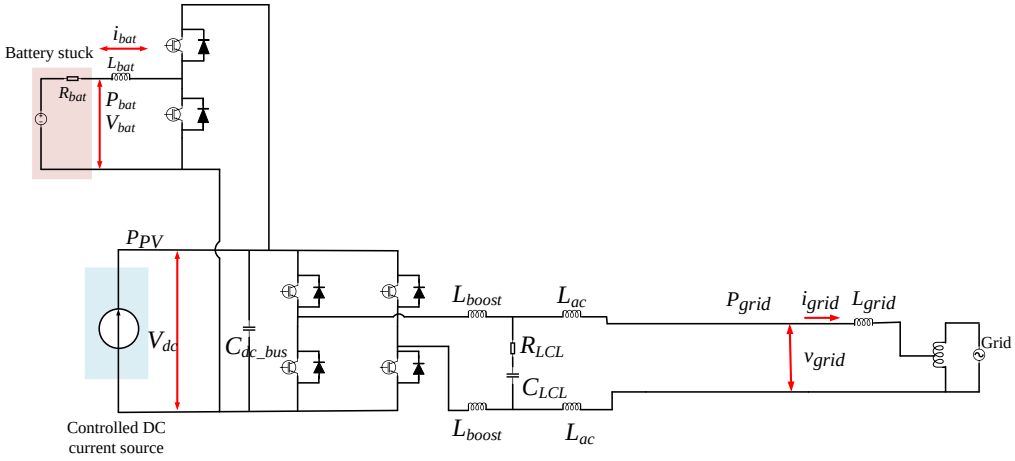

Figure 6.17. Topology of PV-battery power system.

Figure 6.18 is to emulate the situation where the battery is charged by grid electricity and then discharged to satisfy the household loads demand, and PV generation is zero. When the grid power P_{grid} commutates at ±0.42 kW ('positive' means power output from the PV inverter, 'negative' means grid power imported), battery stack can be charged/discharged quickly to keep the system power balance.

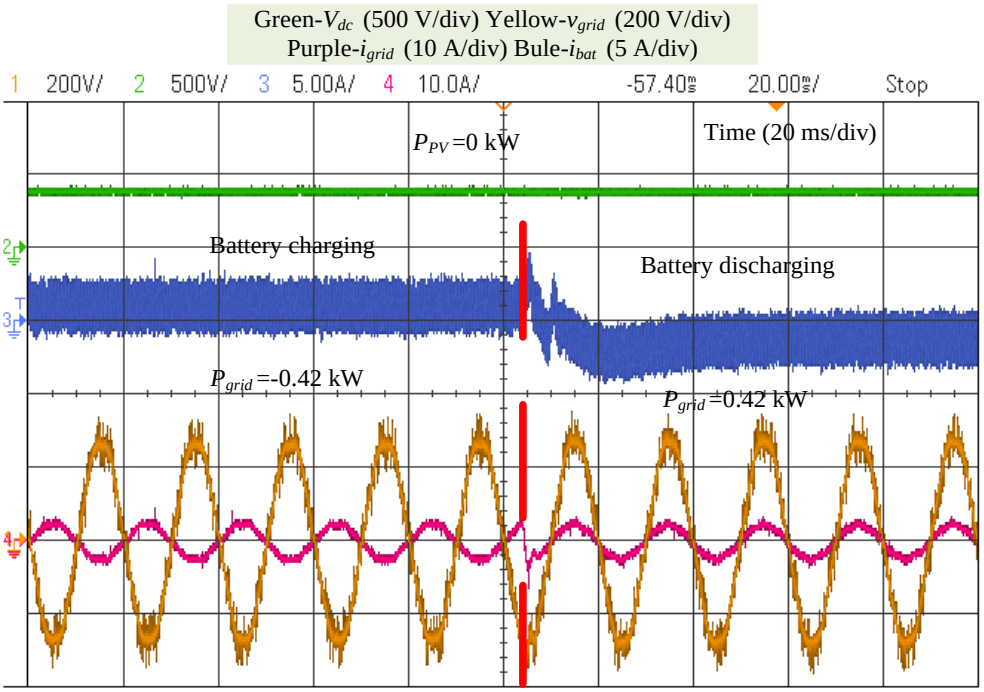

Figure 6.18. Experimental results of battery charging/discharging process from the grid. Green-DC bus voltage, yellow-grid voltage, purple-grid current, blue battery current.

Figure 6.19 is to emulate the situation that when the PV generation changes and loads demand changes at short time interval, the battery stack can absorb the excess PV energy or release energy to keep the system stable. In this situation, the PV output power firstly increases from 0.57 kW to 1.3 kW, followed by the loads demand quickly decreasing from 1.2 kW to 0.64 kW.

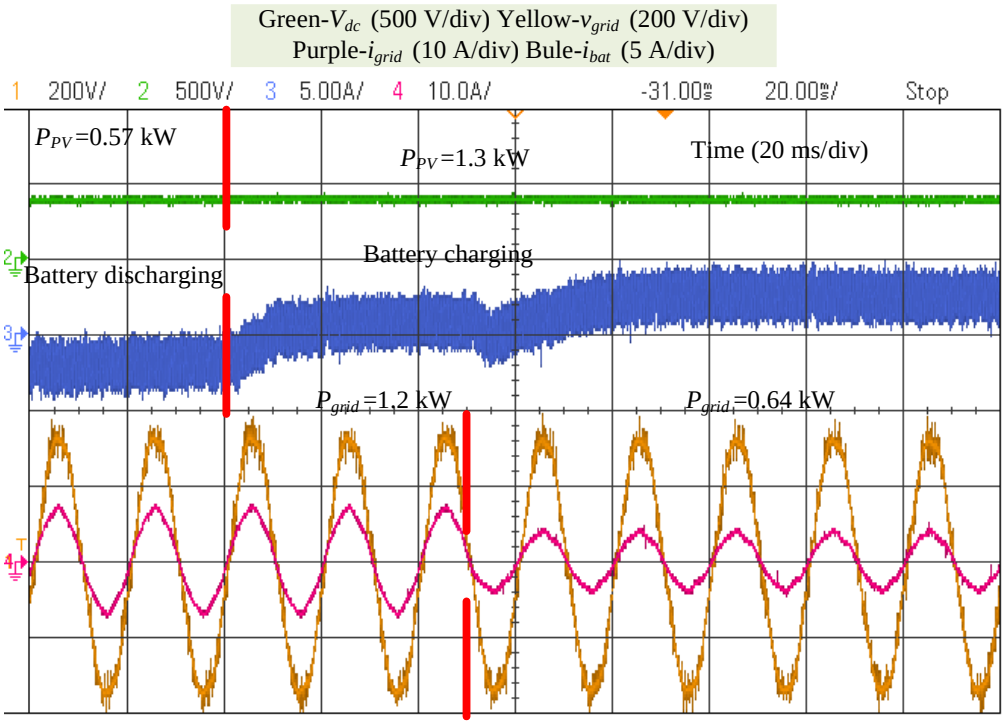

Figure 6.19. Experimental results of battery charging/discharging process from the grid under varying PV generation and loads consumption. Green-DC bus voltage, yellow-grid voltage, purple-grid current, blue battery current.

6.3.2. Performance of the entire PV-battery-power electronic water heater power system

In the optimization chapter (Chapter 3), only the power electronic water heater operating with DC input is considered, to absorb excess PV energy without incurring PV inverter energy losses. However, practically, the proposed power electronic water heater can also operate with AC voltage input. The system performance is also evaluated for the further study when the power electronic water heater is connected to AC grid. Therefore, in this section, the performance of the entire power system is evaluated under either DC input or AC input conditions for the power electronic water heater. Figure 6.20 shows the entire system topology when the power electronic water heater is connected to DC bus, while Figure 6.21 shows the entire system topology when the power electronic water heater is connected to AC grid.

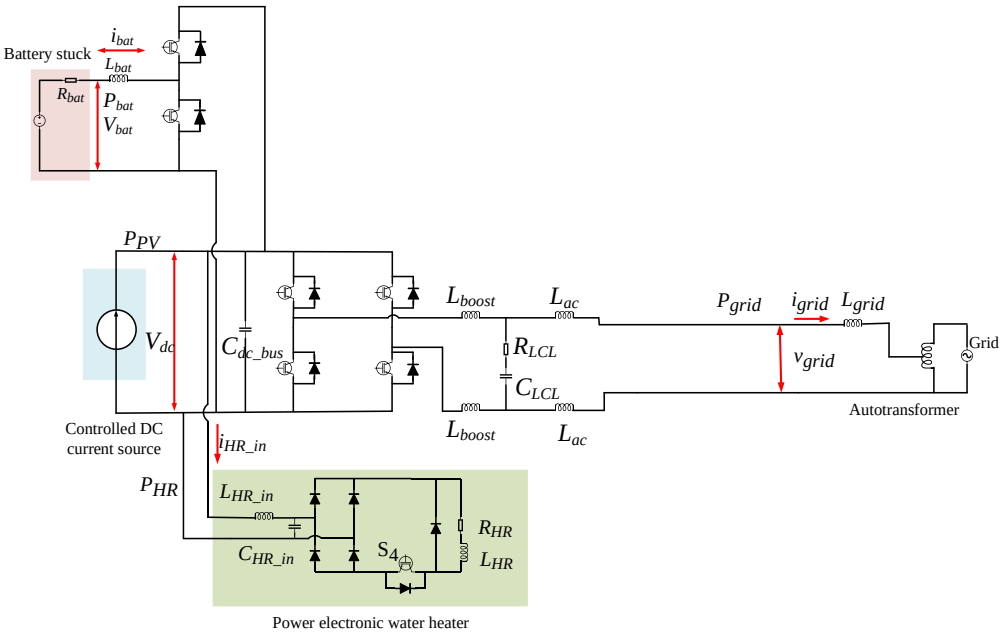

Figure 6.20. Topology of the entire PV-battery-power electronic water heater system when power electronic water heater is connected to AC grid.

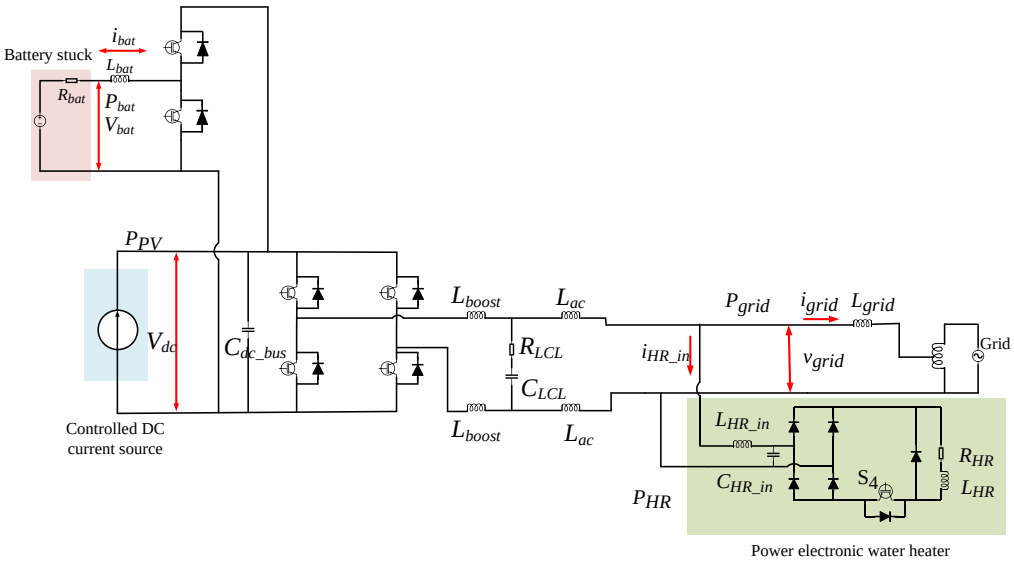

Figure 6.21. Topology of the entire PV-battery-power electronic water heater system when power electronic water heater is connected to AC grid.

6.3.2.1. DC input of power electronic water heater

Due to the maximum current limitation of the experimental setup, the 71 Ω heating resistors is used in this situation. Figure 6.22 is to emulate the situation when the entire system is under varying household loads demand and PV generation. When the household loads demand P_{grid} increases from 0.55 kW to 1.15 kW, and PV generation drops from 1.1 kW to 0.64 kW, both power

electronic water heater and battery stack can be used to absorb the excess PV energy initially, and then the battery stack is discharged to satisfy the loads demand and the water heater stops working when the PV generation is deficit. It validates the stability and transient performance of power system when the power electronic water heater is connected to the DC bus.

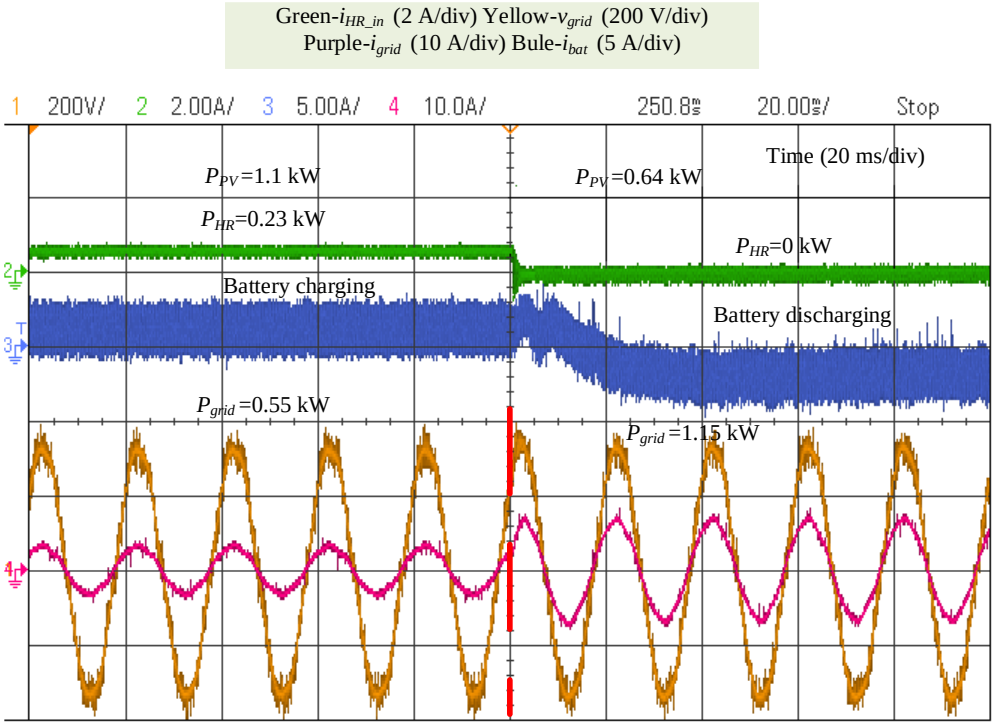

Figure 6.22. Experimental results of power electronic water heater and battery under varying loads demand and PV generation. Green-input current of power electronic water heater, yellow-grid voltage, purple-grid current, blue battery current.

6.3.2.2. AC input of power electronic water heater

For the further study, the power system stability and transient performance is validated when the power electronic water heater is connected in AC grid. In this situation, 15 Ω heat resistor is used to increase the power consumption compared to 71 Ω heat resistor. Figure 6.23 is to emulate the situation when both grid electricity and PV energy is used to heat water and charge the battery stack under varying PV generation. When the power of heating water is constant at 0.78 kW, the battery stack can quickly match the excess PV power which increases from 0.35 kW to 1.1 kW, to keep the system stable. It validates the

power system stability and transient performance when the power electronic water heater is connected to the AC grid. Importantly, the presence of low-order grid harmonics in the grid current, attributed to grid voltage distortion from the autotransformer magnetic core (as shown the schematic diagram in Figure 5.1), is noted.

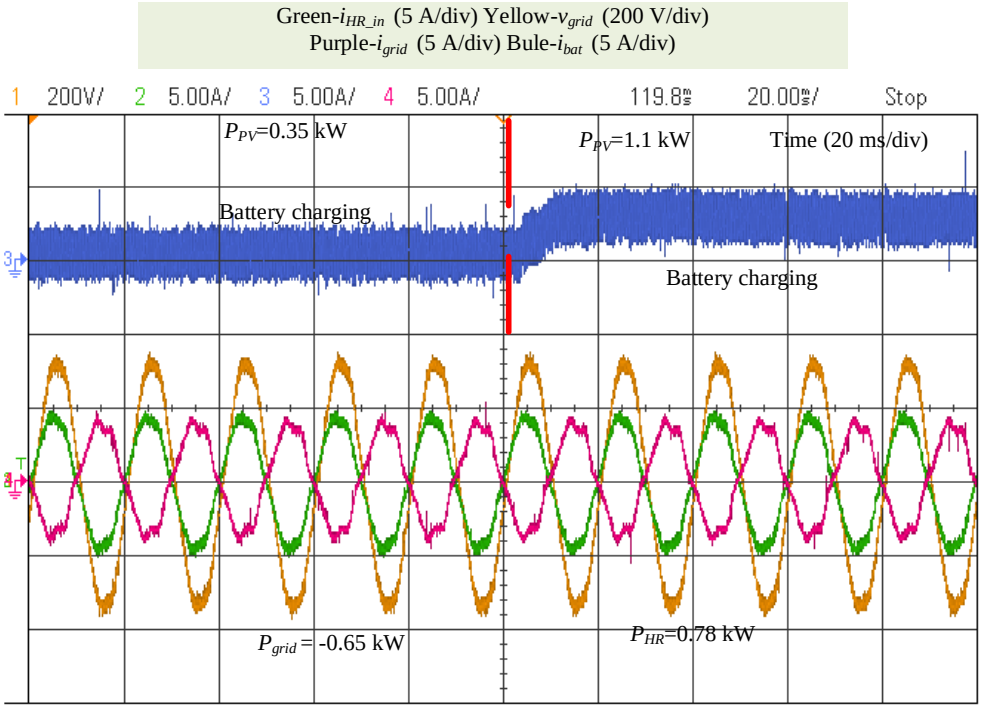

Figure 6.23. Experimental results of power electronic water heater and battery under varying PV generation. Green-input current of power electronic water heater, yellow-grid voltage, purple-grid current, blue battery current.

These experimental findings validate the flexibility and effectiveness of the proposed power electronic water heater in interfacing with either DC bus or AC grid, maintaining system stability under varying operational conditions.

6.4. Summary

In the chapter, there are two main experimental validation tasks: the proposed power electronic water heater used for grid harmonics compensation capability and the performance (stability and transient) of PV-battery-power electronic water heater power system.

Compared to the existent products, this power electronic water heater can consume an exact amount of excess PV power (PWM technology) and has the capability to compensate grid harmonics when it is interfaced with an AC grid.

1) The capability to cancel grid current harmonics depends on the amount of excess PV power processed by the domestic power electronic water heater and the shape of non-linear load current, especially its width and the peak value.

2) Compared with direct harmonics compensation control method, PI control harmonics compensation method has better harmonics compensation capability but lower dynamic response speed.

The distributed nature of power systems poses inherent challenges to stability, primarily due to the unpredictability and fluctuation of PV generation and loads consumption. Additionally, some practical issues such as the grid current harmonics caused by grid voltage distortion, are addressed.

To address these challenges, a PV-battery-power electronic water heater power system was established and rigorously tested under varying conditions of PV generation and loads consumption. The experimental findings underscored the good performance of the whole power system.

Especially, the proposed power electronic water heater can integrate into both DC bus and AC grid configurations. Although only DC input for the power

electronic water heater is considered in the optimization process, the performance validation can be also used for the further optimization study (different power system topology) where the power electronic water heater is connected to the grid.

Chapter 7: Conclusion and future work

7.1. Conclusion

In recent years, there has been a notable increase in residential PV system installations driven by high energy process and the move towards sustainability. Traditionally, the surplus PV generation was often fed back to the grid, initially due to the high financial rewards provided by the feed in tariffs but this approach is no longer appealing due to the removal of PV energy export subsidies and low energy prices offered by electricity suppliers. To further enhance PV penetration, a more viable strategy needs to be used which involves maximizing self-consumption of generated energy that would replace electricity consumption during peak energy prices. This is achieved by integrating energy storage systems that store excess PV energy for later use. Two prominent methods for energy storage in residential PV applications are battery energy storage and thermal storage, particularly using existing hot water tanks.

Given the high costs associated with installing the PV panels and the batteries, it is crucial to optimize the sizing of system components to avoid unnecessary oversizing that produces little financial benefits whilst increasing overall system costs. This research addresses this challenge by focusing on developing an economically efficient residential PV power system integrated with energy storage. Through an optimization process, the system components are sized optimally, ensuring a cost-effective design scheme calculated over a 10-year period.

One key innovation of this research is the development of a novel power electronic water heater with precise dissipation of excess PV power. This device not only enhances self-consumption by precisely utilizing only the excess PV

power available at any time but also reduces grid harmonics produced by other household appliances through its integrated compensation capability, which means a more grid friendly interface of household that would increase the capacity of the distribution grid to handle more power and reduce its associated losses caused by current harmonics. By mitigating grid harmonics and maximizing the utilization of surplus PV energy, the proposed power electronic water heater contributes significantly to the efficiency and sustainability of residential PV systems and the associated distribution grids.

Overall, this research aims to build a cost-effective residential PV system through optimized component sizing and innovative technology, thereby promoting greater adoption of renewable energy solutions in residential settings.

7.2. Contributions

The scientific contributions of this PhD thesis are found in the following chapters:

Chapter 4 details the optimization procedure for the case study to determine the optimal sizing for four types of PV applications: 1) PV self-consumption, 2) PV-battery energy storage, 3) PV-power electronic water heater, and 4) PV-battery-power electronic water heater scenarios. Initially, each scenario is examined to validate if the results obey the defined constraints. Followed by the sensitive analysis, including different level of overnight battery charge to a predefined state of charge SOC_{pre} of the battery stack, different converter models and battery models applied, and different input dataset (occupants versus time resolution), the impacts of these factors on the optimization results are analysed. Besides, Electricity sold back to the grid is not considered, as the UK government decided in 2019 that feed-in tariffs should be market-driven, making them more unpredictable. The impact of feed-in tariff fluctuations on the results is mitigated in this thesis. Lastly, the optimal sizing results are presented and compared across these four PV application scenarios. The findings indicate that maximum financial benefits can be achieved by integrating both hot water energy storage and a battery stack, while maintaining a high PV utilization rate (over 74%) for different household sizes (2, 3, and 5 occupants) over a 10-year period.

Chapter 5, the PV-battery-power electronic water heater power system with the topology and control schemes are depicted. Especially, a novel power electronic water heater is proposed which can be used for grid harmonics compensation and consume the excess PV energy exactly. Except for the

topology, modelling and control methods, the harmonics compensation capability limitations of the power electronic water heater is also analysed by the mathematical method. Moreover, to eliminate the grid harmonics caused by the distorted grid voltage, harmonics compensation PR controllers for PV inverter is implemented.

Chapter 6, there are two main experimental results shown in this chapter: the power electronic water heater used for grid harmonics compensation, along with its harmonics compensation capability limitations validation, and the stability and transient performance of PV-battery-power electronic water heater power system under various PV generation/loads consumption. The results indicate that the proposed power electronic water heater has the expected performance of grid harmonics compensation with simulations. In addition, the performance of PV-battery-power electronic water heater power system is also evaluated where the proposed power electronic water heater can be interfaced with DC bus or AC grid.

7.3. Future work

There are a few points which can be investigated further.

- **Different system validation required**: In this research, the PV generation/loads consumption input dataset is from the single house located in the East Midlands of UK which is produced by CREST model. It might be difference of the optimal design results for another region since the PV generation and the custom of the loads consumption may be different.
- **More system requirements and specifications considered:** To close to the real system operation condition, more requirements and requirements should be considered. For instance, in this research, the maintenance fees of system components are not included. Besides, when the models applied change or another energy storage device added, the energy loss or power flow will be modified.
- **Commercialising a design and sizing software:** The optimization procedure in this study is based on the MATLAB platform. Step further, these codes can be made into a software with visible window where the users can input their location typical PV generation/load consumption, choose different models they preferred, and select the energy storage type they wanted. After processing the optimization procedure, the optimal sizing scheme is provided for the users.
- **Commercialising the proposed power electronic water heater:** The performance of the proposed power electronic water heater has been validated in the simulation and experimental prototype. The

next step is to introduce this power electronic water heater into the market product.

7.4. Publication

[1] Shangkun Li, Christian Klumpner, and Rishad Ahmed. ‘‘Implementation of a Power Electronic Water Heater to Dissipate the Exact Excess of PV Power With Harmonic Compensation Capability,’’ in IEEE Journal of Emerging and Selected Topics in Power Electronics. (Under review)

Reference

[1] Singh, Piyush Pratap, et al. "Green hydrogen production from biomass–A thermodynamic assessment of the potential of conventional and advanced bio-oil steam reforming processes." International Journal of Hydrogen Energy 50 (2024): 627-639.

[2] Wang, Jiannan, and Waseem Azam. "Natural resource scarcity, fossil fuel energy consumption, and total greenhouse gas emissions in top emitting countries." Geoscience Frontiers 15.2 (2024): 101757.

[3] Dhyani, Vaibhav, and Thallada Bhaskar. "A comprehensive review on the pyrolysis of lignocellulosic biomass." Renewable energy 129 (2018): 695-716.

[4] Ashok, Jangam, et al. "Recent progress in the development of catalysts for steam reforming of biomass tar model reaction." Fuel Processing Technology 199 (2020): 106252.

[5] Jaswal, Anurag, Piyush Pratap Singh, and Tarak Mondal. "Furfural–a versatile, biomass-derived platform chemical for the production of renewable chemicals." Green Chemistry 24.2 (2022): 510-551.

[6] Shah, Wasi Ul Hassan, et al. "Energy efficiency evaluation, technology gap ratio, and determinants of energy productivity change in developed and developing G20 economies: DEA super-SBM and MLI approaches." Gondwana Research 125 (2024): 70-81.

[7] Energy Institute, "Statistical Review of World Energy (2023) – with major processing by Our World in Data": Available: https://ember-climate.org/data-catalogue/yearly-electricity-data/. 2024.

[8] Tugcu, Can Tansel, and Angeliki N. Menegaki. "The impact of renewable energy generation on energy security: Evidence from the G7 countries." Gondwana Research 125 (2024): 253-265.

[9] Gov.uk, "UK Energy In Brief,'' 2023.

[10] Gov.uk, "the ten-point plan for a green industrial revolution,'' updated 18 November 2020.

[11] Department for Business, Energy & Industrial Strategy, "Energy Consumption in the UK (ECUK)", updated in 2023.

[12] Williams, Christopher JC, Jann O. Binder, and Tobias Kelm. "Demand side management through heat pumps, thermal storage and battery storage to increase local self-consumption and grid compatibility of PV systems." 2012 3rd IEEE PES Innovative Smart Grid Technologies Europe (ISGT Europe). IEEE, 2012.

[13] Gov.uk, "United Kingdom housing energy fact file,'' 2013.

[14] Electricity Supply in the UK: A chronology, Electricity Council, UK, 1987.

[15] D. Plessis, S. Vincent, and J. J. Roetker, "Energy management system with solar water heater," U.S. Patent Application, no. 13/046,870, Mar. 2012.

[16] R. A. Chaudhry, A. Y. Hinton, and J. Boros, "Water heater having a supplemental photovoltaic heating arrangement," U.S. Patent Application, no. 10,072,853. 11, Sep. 2018.

[17] H. A. Attia, M. El-Metwally, and O. M. Fahmy. "Harmonic distortion effects and mitigation in distribution systems," Journal of American Science, vol. 6, no. 10, pp. 173-183, Oct. 2010.

[18] S. Anwar, A. Elrayyah, and Y. Sozer, "Efficient single-phase harmonics elimination method for microgrid operations," IEEE Trans. Ind. Electron., vol. 51, no. 4, pp. 3394-3403, Jan. 2015.

[19] T. F. Wu, H. S. Nien, C. L. Shen, and T. M. Chen, "A single-phase inverter system for PV power injection and active power filtering with nonlinear inductor consideration," IEEE Trans. Ind. Electron., vol. 41, no. 4, pp. 1075-1083, Jul. 2005.

[20] J. M. S. Callegari, A. L. P. Oliveira, L. S. Xavier, A. F. Cupertino, D. I. Brandao, and H. A. Prerira, "Voltage Detection-Based Selective Harmonic Current Compensation Strategies for Photovoltaic Inverters," IEEE Trans. Energy Conversion, vol. 38, no. 3, pp. 7046-7051, Jan. 2023.

[21] T. f. Wu, M. Misra, l. C. Lin, and C. W. Hsu, "An improved resonant frequency based systematic LCL filter design method for grid-connected inverter," IEEE Trans. Ind. Electron., vol. 64, no. 8, pp. 6412-6421, Mar. 2017.

[22] Khatib, Tamer, Ibrahim A. Ibrahim, and Azah Mohamed. "A review on sizing methodologies of photovoltaic array and storage battery in a standalone photovoltaic system." Energy Conversion and Management 120 (2016): 430-448.

[23] Khezri, Rahmat, Amin Mahmoudi, and Hirohisa Aki. "Optimal planning of solar photovoltaic and battery storage systems for grid-connected residential sector: Review, challenges and new perspectives." Renewable and Sustainable Energy Reviews 153 (2022): 111763.

[24] Zammit, Daniel, Maurice Apap, and Cyril Spiteri Staines. "Comparison between PI and PR current controllers in grid connected PV inverters." (2014).

[25] Shair, Jan, et al. "Power system stability issues, classifications and research prospects in the context of high penetration of renewables and power electronics." Renewable and Sustainable Energy Reviews 145 (2021): 111111.

[26] Kavlak, Goksin, James McNerney, and Jessika E. Trancik. "Evaluating the causes of cost reduction in photovoltaic modules." Energy policy 123 (2018): 700-710.

[27] Mohammed, Abdalla Y., Farog I. Mohammed, and Mamoun Y. Ibrahim. "Grid connected Photovoltaic system." 2017 international conference on communication, control, computing and electronics engineering (ICCCCEE). IEEE, 2017.

[28] Prabaharan, N., and K. Palanisamy. "Analysis and integration of multilevel inverter configuration with boost converters in a photovoltaic system." Energy Conversion and Management 128 (2016): 327-342.

[29] Weniger, Johannes, et al. "Dynamic mismatch losses of grid-connected PV-battery systems in residential buildings." Journal of Energy Storage 13 (2017): 244-254.

[30] Nehrir, Mohammad Hashem, and Caisheng Wang. Modeling and control of fuel cells: distributed generation applications. Vol. 41. John Wiley & Sons, 2009.

[31] Vosoughi, Naser, Seyed Hossein Hosseini, and Mehran Sabahi. "A new transformer-less five-level grid-tied inverter for photovoltaic applications." IEEE Transactions on Energy Conversion 35.1 (2019): 106-118.

[32] Boumaaraf, Houria, Abdelaziz Talha, and Omar Bouhali. "A three-phase NPC grid-connected inverter for photovoltaic applications using neural network MPPT." Renewable and Sustainable Energy Reviews 49 (2015): 1171-1179.

[33] Sandelic, Monika, Ariya Sangwongwanich, and Frede Blaabjerg. "Reliability evaluation of PV systems with integrated battery energy storage systems: DC-coupled and AC-coupled configurations." Electronics 8.9 (2019): 1059.

[34] Tan, Nadia Mei Lin, Takahiro Abe, and Hirofumi Akagi. "Design and performance of a bidirectional isolated DC–DC converter for a battery energy storage system." IEEE Transactions on Power Electronics 27.3 (2011): 1237-1248.

[35] Huff, Georgianne. DOE Global Energy Storage Database. No. SAND2015-1450PE. Sandia National Lab.(SNL-NM), Albuquerque, NM (United States), 2015.

[36] Molina, Marcelo Gustavo. "Dynamic modelling and control design of advanced energy storage for power system applications." Dynamic Modelling 300 (2010).

[37] Zhao, Haoran, et al. "Review of energy storage system for wind power integration support." Applied energy 137 (2015): 545-553.

[38] Evans, Annette, Vladimir Strezov, and Tim J. Evans. "Assessment of utility energy storage options for increased renewable energy penetration." Renewable and Sustainable Energy Reviews 16.6 (2012): 4141-4147.

[39] DOE Global Energy Storage Database, 2020. [online]. Available: http://www.energystorageexchange.org/projects/data_visualization/

[40] Wang, Jidai, et al. "Overview of compressed air energy storage and technology development." Energies 10.7 (2017): 991.

[41] Züttel, Andreas, et al. "Hydrogen: the future energy carrier." Philosophical Transactions of the Royal Society A: Mathematical, Physical and Engineering Sciences 368.1923 (2010): 3329-3342.

[42] Armaroli, Nicola, and Vincenzo Balzani. "The hydrogen issue." *ChemSusChem* 4.1 (2011): 21-36.

[43] Najjar, Yousef SH. "Hydrogen safety: The road toward green technology." International Journal of Hydrogen Energy 38.25 (2013): 10716-10728.

[44] Liu, Ming, Wasim Saman, and Frank Bruno. "Review on storage materials and thermal performance enhancement techniques for high temperature phase change thermal storage systems." Renewable and Sustainable Energy Reviews 16.4 (2012): 2118-2132.

[45] H Abedin, Ali, and Marc A Rosen. "A critical review of thermochemical energy storage systems." The open renewable energy journal 4.1 (2011).

[46] Prasad, J. Sunku, et al. "A critical review of high-temperature reversible thermochemical energy storage systems." Applied Energy 254 (2019): 113733.

[47] Dubey, Richa, and Velmathi Guruviah. "Review of carbon-based electrode materials for supercapacitor energy storage." Ionics 25 (2019): 1419-1445.

[48] Iro, Zaharaddeen S., C. Subramani, and S. S. Dash. "A brief review on electrode materials for supercapacitor." Int. J. Electrochem. Sci 11.12 (2016): 10628-10643.

[49] Häggström, Fredrik, and Jerker Delsing. "Iot energy storage-a forecast." Energy Harvesting and Systems 5.3-4 (2018): 43-51.

[50] Tehrani, Z., et al. "Large-area printed supercapacitor technology for low-cost domestic green energy storage." Energy 118 (2017): 1313-1321.

[51] Krichen, Moez, et al. "A Survey on energy storage: Techniques and challenges." Energies 16.5 (2023): 2271.

[52] Zhang, Yong, et al. "Advances and challenges in improvement of the electrochemical performance for lead-acid batteries: A comprehensive review." Journal of Power Sources 520 (2022): 230800.

[53] Beaudin, Marc, et al. "Energy storage for mitigating the variability of renewable electricity sources: An updated review." Energy for sustainable development 14.4 (2010): 302-314.

[54] Wen, Jianping, Dan Zhao, and Chuanwei Zhang. "An overview of electricity powered vehicles: Lithium-ion battery energy storage density and energy conversion efficiency." Renewable Energy 162 (2020): 1629-1648.

[55] Wen, Zhaoyin, et al. "Main challenges for high performance NAS battery: materials and interfaces." Advanced functional materials 23.8 (2013): 1005-1018.

[56] Blumbergs, Ervins, et al. "Cadmium recovery from spent Ni-Cd batteries: a brief review." Metals 11.11 (2021): 1714.

[57] Skyllas-Kazacos, Maria, et al. "Progress in flow battery research and development." Journal of the electrochemical society 158.8 (2011): R55.

[58] Liu, Tiefeng, et al. "Bipolar electrodes for next-generation rechargeable batteries." Advanced Science 7.17 (2020): 2001207.

[59] Kouro, Samir, et al. "Grid-connected photovoltaic systems: An overview of recent research and emerging PV converter technology." IEEE Industrial Electronics Magazine 9.1 (2015): 47-61.

[60] Bletterie, B., R. Bründlinger, and G. Lauss. "On the characterisation of PV inverters' efficiency—introduction to the concept of achievable efficiency." Progress in Photovoltaics: Research and Applications 19.4 (2011): 423-435.

[61] Burger, Bruno, and Dirk Kranzer. "Extreme high efficiency PV-power converters." *2009 13th European Conference on Power Electronics and Applications*. IEEE, 2009.

[62] Naveed, Muhammad Mohsin, and Alberto Castellazzi. "A Single Phase GaN GITs-Based Bidirectional Multilevel Inverter for High Voltage Grid Tied Photovoltaic Power System." Electric Power Components and Systems 51.8 (2023): 769-784.

[63] Yafaoui, Ahmad, Bin Wu, and Samir Kouro. "Improved active frequency drift anti-islanding detection method for grid connected photovoltaic systems." IEEE transactions on power electronics 27.5 (2011): 2367-2375.

[64] Dong, Dong, et al. "Leakage current reduction in a single-phase bidirectional AC–DC full-bridge inverter." IEEE Transactions on Power Electronics 27.10 (2012): 4281-4291.

[65] Jung, Youngseok, et al. "High-frequency DC link inverter for grid-connected photovoltaic system." Conference Record of the Twenty-Ninth IEEE Photovoltaic Specialists Conference, 2002.. IEEE, 2002.

[66] Kolantla, Dharani, et al. "Critical review on various inverter topologies for PV system architectures." IET Renewable Power Generation 14.17 (2020): 3418-3438.

[67] Burger, Bruno, and Dirk Kranzer. "Extreme high efficiency PV-power converters." 2009 13th European Conference on Power Electronics and Applications. IEEE, 2009.

[68] Kumar, Rahul, and Prerna Gau. "Comparative Study of THD in 5-level Neutral Point Clamped Multilevel Converter Using Multicarrier PWM and SHEPWM Techniques." International Journal of Electronic and Electrical Engineering 7.4 (2014): 373-378.

[69] Meinhardt, Mike. "Multi-string-converter: The next step in evolution of string-converter technology." Proc. 9th Eur. Power Electronics and Applications Conf., 2001. 2001.

[70] P. Garrity, "Solar photovoltaic power conditioning unit," U.S. patent 8,391,031B2, 2013.

[71] Fornage, Martin. "Method and apparatus for converting direct current to alternating current." U.S. Patent No. 7,796,412. 14 Sep. 2010.

[72] Kebede, Abraham Alem, et al. "A comprehensive review of stationary energy storage devices for large scale renewable energy sources grid integration." Renewable and Sustainable Energy Reviews 159 (2022): 112213

[73] Karshenas, Hamid R., et al. "Bidirectional dc-dc converters for energy storage systems." Energy storage in the emerging era of smart grids 18 (2011).

[74] Tytelmaier, Kostiantyn, et al. "A review of non-isolated bidirectional dc-dc converters for energy storage systems." 2016 II International Young Scientists Forum on Applied Physics and Engineering (YSF). IEEE, 2016.

[75] Kang, Taewon, et al. "A design and control of bi-directional non-isolated DC-DC converter for rapid electric vehicle charging system." 2012 Twenty-Seventh Annual IEEE Applied Power Electronics Conference and Exposition (APEC). IEEE, 2012.

[76] Odo, Polycarp. "A Comparative Study of Single-phase Non-isolated Bidirectional dc-dc Converters Suitability for Energy Storage Application in a dc Microgrid." 2020 IEEE 11th

International Symposium on Power Electronics for Distributed Generation Systems (PEDG). IEEE, 2020.

[77] Lin, Weiming, et al. "A novel tapped inductor bi-directional buck-boost topology." INTELEC 2008-2008 IEEE 30th International Telecommunications Energy Conference. IEEE, 2008.

[78] Das, Pritam, S. Ahmad Mousavi, and Gerry Moschopoulos. "Analysis and design of a non-isolated bidirectional ZVS-PWM DC–DC converter with coupled inductors." IEEE Transactions on Power Electronics 25.10 (2010): 2630-2641.

[79] Fritz, Niklas, Mohamed Rashed, and Christian Klumpner. "Power density optimization of a dc/dc converter for an aircraft supercapacitors energy storage." 2018 IEEE International Conference on Electrical Systems for Aircraft, Railway, Ship Propulsion and Road Vehicles & International Transportation Electrification Conference (ESARS-ITEC). IEEE, 2018.

[80] De, Dipankar, et al. "Modelling and control of a multi-stage interleaved DC–DC converter with coupled inductors for super-capacitor energy storage system." IET Power Electronics 6.7 (2013): 1360-1375.

[81] Zhao, Biao, et al. "Overview of dual-active-bridge isolated bidirectional DC–DC converter for high-frequency-link power-conversion system." IEEE Transactions on power electronics 29.8 (2013): 4091-4106.

[82] Chung, HS-H., Wai-Leung Cheung, and K. S. Tang. "A ZCS bidirectional flyback dc/dc converter." IEEE Transactions on Power Electronics 19.6 (2004): 1426-1434.

[83] Zhang, Zhe, Ole C. Thomsen, and Michael AE Andersen. "Optimal design of a push-pull-forward half-bridge (PPFHB) bidirectional DC–DC converter with variable input voltage." IEEE Transactions on Industrial Electronics 59.7 (2011): 2761-2771.

[84] Roggia, Leandro, et al. "Integrated full-bridge-forward DC–DC converter for a residential microgrid application." IEEE Transactions on Power Electronics 28.4 (2012): 1728-1740.

[85] Wang, Kunrong, et al. "Bi-directional DC to DC converters for fuel cell systems." Power electronics in transportation (Cat. No. 98TH8349). IEEE, 1998.

[86] Hirose, Toshiro, and Hirofumi Matsuo. "A consideration of bidirectional superposed dual active bridge dc-dc converter." The 2nd International Symposium on Power Electronics for Distributed Generation Systems. IEEE, 2010.

[87] Zhu, Lizhi. "A novel soft-commutating isolated boost full-bridge ZVS-PWM DC–DC converter for bidirectional high-power applications." IEEE Transactions on Power Electronics 21.2 (2006): 422-429.

[88] Gitau, Michael N., Gerhard Ebersohn, and John G. Kettleborough. "Power processor for interfacing battery storage system to 725 V DC bus." *Energy Conversion and Management* 48.3 (2007): 871-881.

[89] Hillers, André, Daniel Christen, and Juergen Biela. "Design of a highly efficient bidirectional isolated LLC resonant converter." *2012 15th International Power Electronics and Motion Control Conference (EPE/PEMC)*. IEEE, 2012.

[90] Yang, Bo, et al. "LLC resonant converter for front end DC/DC conversion." *APEC. Seventeenth Annual IEEE Applied Power Electronics Conference and Exposition (Cat. No. 02CH37335)*. Vol. 2. IEEE, 2002.

[91] The Association of Plumbing& Heating contractors, "Understanding hot water systems in the home," 2019. [online]. Available: https://www.aphc.co.uk/wp-content/uploads/2019/07/UNDERSTANDING-HOT-WATER-SYSTEMS-IN-THE-HOME-Dec13.pdf

[92] D. Plessis, S. Vincent, and J. J. Roetker, "Energy management system with solar water heater," U.S. Patent Application, no. 13/046,870, Mar. 2012

[93] R. A. Chaudhry, A. Y. Hinton, and J. Boros, "Water heater having a supplemental photovoltaic heating arrangement," U.S. Patent Application, no. 10,072,853. 11, Sep. 2018.

[94] T. J. Carlisle, "Electric water heater," U.S. Patent Application, no. 6,080,973. 27, Jun. 2000.

[95] M.A. Murphy, and J. R. Baxter, "Water heater and method of customizing the water heater," U.S. Patent Application, no. 7,822,325. 26, Oct. 2010.

[96] A. S. Hasirumane, T. J. S. Toussaint, and B. J. Buniak, "Variable power water heater," U.S. Patent Application, no. 11,215,381. 4, Jan. 2022.

[97] Erdinc, Ozan, and Mehmet Uzunoglu. "Optimum design of hybrid renewable energy systems: Overview of different approaches." Renewable and Sustainable Energy Reviews 16.3 (2012): 1412-1425.

[98] Khezri, Rahmat, Amin Mahmoudi, and Hirohisa Aki. "Optimal planning of solar photovoltaic and battery storage systems for grid-connected residential sector: Review, challenges and new perspectives." Renewable and Sustainable Energy Reviews 153 (2022): 111763.

[99] Khatib, Tamer, Ibrahim A. Ibrahim, and Azah Mohamed. "A review on sizing methodologies of photovoltaic array and storage battery in a standalone photovoltaic system." Energy Conversion and Management 120 (2016): 430-448.

[100] Mohamed, Sayed, et al. "An efficient planning algorithm for hybrid remote microgrids." IEEE transactions on sustainable energy 10.1 (2018): 257-267.

[101] Katsigiannis, Yiannis A., Pavlos S. Georgilakis, and Emmanuel S. Karapidakis. "Hybrid simulated annealing–tabu search method for optimal sizing of autonomous power systems with renewables." IEEE Transactions on Sustainable Energy 3.3 (2012): 330-338.

[102] Spertino, Filippo, Paolo Di Leo, and Valeria Cocina. "Economic analysis of investment in the rooftop photovoltaic systems: A long-term research in the two main markets." Renewable and Sustainable Energy Reviews 28 (2013): 531-540.

[103] Khan, Muhammad Waseem, et al. "Optimal energy management and control aspects of distributed microgrid using multi-agent systems." Sustainable Cities and Society 44 (2019): 855-870.

[104] Wang, Caisheng, and M. Hashem Nehrir. "Power management of a stand-alone wind/photovoltaic/fuel cell energy system." IEEE transactions on energy conversion 23.3 (2008): 957-967.

[105] Kaur, Amandeep, Jitender Kaushal, and Prasenjit Basak. "A review on microgrid central controller." Renewable and Sustainable Energy Reviews 55 (2016): 338-345.

[106] Espina, Enrique, et al. "Distributed control strategies for microgrids: An overview." IEEE Access 8 (2020): 193412-193448.

[107] Antonelli, Gianluca. "Interconnected dynamic systems: An overview on distributed control." IEEE Control Systems Magazine 33.1 (2013): 76-88.

[108] Vandoorn, Tine L., et al. "Microgrids: Hierarchical control and an overview of the control and reserve management strategies." IEEE industrial electronics magazine 7.4 (2013): 42-55.

[109] Ceglia, F., et al. "From smart energy community to smart energy municipalities: Literature review, agendas and pathways." Journal of Cleaner Production 254 (2020): 120118.

[110] Mahmoud, Fayza S., et al. "Optimal sizing of smart hybrid renewable energy system using different optimization algorithms." Energy Reports 8 (2022): 4935-4956.

[111] Khatib, Tamer, Azah Mohamed, and Kamaruzzaman Sopian. "A review of photovoltaic systems size optimization techniques." Renewable and Sustainable Energy Reviews 22 (2013): 454-465.

[112] Kazem, Hussein A., Tamer Khatib, and Kamaruzzaman Sopian. "Sizing of a standalone photovoltaic/battery system at minimum cost for remote housing electrification in Sohar, Oman." Energy and Buildings 61 (2013): 108-115.

[113] Rawat, Rahul, S. C. Kaushik, and Ravita Lamba. "A review on modeling, design methodology and size optimization of photovoltaic based water pumping, standalone and grid connected system." Renewable and Sustainable Energy Reviews 57 (2016): 1506-1519.

[114] Arun, P., Rangan Banerjee, and Santanu Bandyopadhyay. "Optimum sizing of photovoltaic battery systems incorporating uncertainty through design space approach." Solar Energy 83.7 (2009): 1013-1025.

[115] Kaplani, Eleni, and Socrates Kaplanis. "A stochastic simulation model for reliable PV system sizing providing for solar radiation fluctuations." Applied Energy 97 (2012): 970-981.

[116] Markvart, T., A. Fragaki, and J. N. Ross. "PV system sizing using observed time series of solar radiation." Solar energy 80.1 (2006): 46-50.

[117] Posadillo, R., and R. López Luque. "A sizing method for stand-alone PV installations with variable demand." Renewable Energy 33.5 (2008): 1049-1055.

[118] G ó mez - Gonz á lez, Manuel, Francisco Javier Ruiz - Rodriguez, and Francisco Jurado. "Metaheuristic and probabilistic techniques for optimal allocation and size of biomass distributed generation in unbalanced radial systems." IET Renewable Power Generation 9.6 (2015): 653-659.

[119] Yang, Hongxing, et al. "Optimal sizing method for stand-alone hybrid solar–wind system with LPSP technology by using genetic algorithm." Solar energy 82.4 (2008): 354-367.

[120] Sinha, Sunanda, and S. S. Chandel. "Review of software tools for hybrid renewable energy systems." Renewable and sustainable energy reviews 32 (2014): 192-205.

[121] Molina, Marcelo Gustavo, and Emmanuel Jesús Espejo. "Modeling and simulation of grid-connected photovoltaic energy conversion systems." International journal of hydrogen energy 39.16 (2014): 8702-8707.

[122] Ashtiani, Mina Najafi, et al. "Techno-economic analysis of a grid-connected PV/battery system using the teaching-learning-based optimization algorithm." Solar Energy 203 (2020): 69-82.

[123] Kaur, Rajvir, Vijayakumar Krishnasamy, and Nandha Kumar Kandasamy. "Optimal sizing of wind–PV-based DC microgrid for telecom power supply in remote areas." IET Renewable Power Generation 12.7 (2018): 859-866.

[124] Shabani, Masoume, et al. "Techno-economic impacts of battery performance models and control strategies on optimal design of a grid-connected PV system." Energy Conversion and Management 245 (2021): 114617.

[125] McKenna, Eoghan, and Murray Thomson. "High-resolution stochastic integrated thermal–electrical domestic demand model." Applied Energy 165 (2016): 445-461.

[126] Ofgem, a non-ministerial government department, "Feed-in Tariffs,'' 2020. Available:https://www.ofgem.gov.uk/sites/default/files/docs/2020/09/scheme_closure_v4.pdf

[127] Ofgem. 2024. Available: https://www.ofgem.gov.uk/

[128] Urtasun, Andoni, Pablo Sanchis, and Luis Marroyo. "Adaptive voltage control of the DC/DC boost stage in PV converters with small input capacitor." IEEE Transactions on Power Electronics 28.11 (2013): 5038-5048.

[129] De Brito, Moacyr Aureliano Gomes, et al. "Evaluation of the main MPPT techniques for photovoltaic applications." IEEE transactions on industrial electronics 60.3 (2012): 1156-1167.

[130] Luthander, Rasmus, et al. "Photovoltaic self-consumption in buildings: A review." Applied energy 142 (2015): 80-94.

[131] Hawkes, Adam, and Matthew Leach. "Impacts of temporal precision in optimisation modelling of micro-Combined Heat and Power." Energy 30.10 (2005): 1759-1779.

[132] Stan, Ana-Irina, et al. "A comparative study of lithium ion to lead acid batteries for use in UPS applications." 2014 IEEE 36th international telecommunications energy conference (INTELEC). IEEE, 2014.

[133] Armstrong, P., et al. "Improving the energy storage capability of hot water tanks through wall material specification." Energy 78 (2014): 128-140.

[134] Department of Energy and Climate Change, Smart Metering Implementation Programme, Energy Demand Research Project: Early Smart Meter Trials, 2007–2010 [computer file]. Colchester, Essex: UK Data Archive [distributor], November 2014. SN: 7591, 2010.

[135] Carbon Trust, Micro-CHP Accelerator. Carbon Trust. 2011. Available: https://www.carbontrust.com/resources/reports/technology/micro-chp-accelerator

[136] Energy Saving Trust. Measurement of domestic hot water consumption in dwellings; 2008.

[137] Budget energy company, '' our tariff table''. [online]. Available: https://budgetenergy.co.uk/help/tarifftable

[138] Eon company, '' our variable tariff prices''. [online]. Available: https://www.eonnext.com/tariffs

[139] Powerni company, '' unit rates'' 2023. [online]. Available: https://powerni.co.uk/compare-electricity-ni/unit-rates/

[140] Gov.uk, "The Feed-In Tariffs scheme: closure of the scheme to new applications after 31 March 2019, and administrative measures: government response,'' December 2018.

[141] Mariaud, Arthur, et al. "Integrated optimisation of photovoltaic and battery storage systems for UK commercial buildings." Applied energy 199 (2017): 466-478.

[142] Panagiotou, Konstantina, Christian Klumpner, and Mark Sumner. "Sizing guidelines for grid-connected decentralised energy storage systems: single house application." The Journal of Engineering 2019.17 (2019): 3802-3806.

[143] Evro, Solomon, C. Wade, and O. Tomomewo. "Solar PV technology cost dynamics and challenges for US new entrants." *American Journal of Energy Research* 11.1 (2023): 15-26.

[144] Panagiotou, Konstantina, Christian Klumpner, and Mark Sumner. "Sizing guidelines for grid-connected decentralised energy storage systems: single house application." *The Journal of Engineering* 2019.17 (2019): 3802-3806.

[145] Weniger, Johannes, et al. "Sizing of battery converters for residential PV storage systems." Energy Procedia 99 (2016): 3-10.

[146] Piris-Botalla, Laureano, et al. "Power losses evaluation of a bidirectional three-port DC–DC converter for hybrid electric system." *International Journal of Electrical Power & Energy Systems* 58 (2014): 1-8.

[147] Dieckerhoff, Sibylle, Steffen Bernet, and Dietmar Krug. "Power loss-oriented evaluation of high voltage IGBTs and multilevel converters in transformerless traction applications." *IEEE Transactions on Power Electronics* 20.6 (2005): 1328-1336.

[148] Kulsangcharoen, Ponggorn, et al. "Experimental evaluation and efficiency optimisation of a grid-connected converter for household energy storage applications." (2014): 1-2.

[149] Tamilselvi, S., et al. "A review on battery modelling techniques." Sustainability 13.18 (2021): 10042.

[150] Moura, Scott J., Nalin A. Chaturvedi, and Miroslav Krstić. "Adaptive partial differential equation observer for battery state-of-charge/state-of-health estimation via an electrochemical model." Journal of Dynamic Systems, Measurement, and Control 136.1 (2014): 011015.

[151] Hu, Tingshu, Brian Zanchi, and Jianping Zhao. "Simple analytical method for determining parameters of discharging batteries." IEEE Transactions on Energy Conversion 26.3 (2011): 787-798.

[152] Li, Shuhui, and Bao Ke. "Study of battery modeling using mathematical and circuit-oriented approaches." 2011 IEEE Power and Energy Society General Meeting. IEEE, 2011.

[153] Saxena, Saurabh, et al. "A novel approach for electrical circuit modeling of Li-ion battery for predicting the steady-state and dynamic I–V characteristics." Sādhanā 41 (2016): 479-487.

[154] Rao, Ravishankar, Sarma Vrudhula, and Daler N. Rakhmatov. "Battery modeling for energy aware system design." Computer 36.12 (2003): 77-87.

[155] Campagna, Nicola, et al. "Battery models for battery powered applications: A comparative study." Energies 13.16 (2020): 4085.

[156] Sun, Li, Guanru Li, and Fengqi You. "Combined internal resistance and state-of-charge estimation of lithium-ion battery based on extended state observer." Renewable and Sustainable Energy Reviews 131 (2020): 109994.

[157] Stan, Ana-Irina, et al. "A comparative study of lithium ion to lead acid batteries for use in UPS applications." 2014 IEEE 36th international telecommunications energy conference (INTELEC). IEEE, 2014.

[158] Molicel, "Molicel lithium-ion battery datasheets", [online]. Available: https://www.molicel.com/products-applications/explore-by-product/

[159] Panasonic, "Panasonic NCR 18650B lithium-ion battery datasheets", [online]. Available: https://industrial.panasonic.com/ww/products/pt/lithium-ion/models/NCR18650BD

[160] Jack, M. W., et al. "A minimal simulation of the electricity demand of a power electronic water heater cylinder for smart control." Applied Energy 211 (2018): 104-112.

[161] Han, Y. M., R. Z. Wang, and Y. J. Dai. "Thermal stratification within the water tank." Renewable and Sustainable Energy Reviews 13.5 (2009): 1014-1026.

[162] Widén, Joakim, et al. "Constructing load profiles for household electricity and hot water from time-use data—Modelling approach and validation." Energy and buildings 41.7 (2009): 753-768.

[163] Energy Saving Trust organisation, "Analysis of the EST's power electronic water heater trials and their implications for amendments to BREDEM and SAP.'' 2009, [online]. Available: https://files.bregroup.com/bre-co-uk-file-library-copy/filelibrary/SAP/2012/STP09-DHW01_Analysis_of_EST_DHW_data.pdf

[164] Energy Saving Trust organisation, "Measurement of power electronic water heater consumption in dwellings.'' 2008, [online]. Available: https://www.gov.uk/government/publications/measurement-of-domestic-hot-water-consumption-in-dwellings

[165] UK government, "The Government's Standard Assessment Procedure for Energy Rating of Dwellings.'' 2012, [online]. Available: https://www.gov.uk/guidance/standard-assessment-procedure

[166] A.F. Zobaa, F. Ahmed, M. M. Abdel Aziz, and S. H. E., "Comparison of shunt-passive and series-passive filters for DC drive loads," Electric Power Components and Systems, pp. 275-29, Oct. 2010.

[167] L. H. Tey, P. L. So, and Y. C. Chu, "Improvement of power quality using adaptive shunt active filter," IEEE transactions on power delivery 20., no.2, pp. 1558-1568, Apr. 2005.

[168] F. T. Ghetti, A. A. Ferreira, H. A. Braga, and P. G. Barbosa, "A study of shunt active power filter based on modular multilevel converter (MMC)," 2012 10th IEEE/IAS International Conference on Industry Applications. pp. 1-6, Nov. 2012.

[169] B. Sangeetha, and K. Geetha, "Performance of multilevel shunt active filter for smart grid applications." International Journal of Electrical Power & Energy Systems. pp.927-932, Dec. 2014.

[170] H. Fujita, "A single-phase active filter using an H-bridge PWM converter with a sampling frequency quadruple of the switching frequency." IEEE Transactions on Power Electronics. vol.24, no.4, pp. 934-941, Apr. 2009.

[171] Feola, Luigi, Roberto Langella, and Alfredo Testa. "On the effects of unbalances, harmonics and interharmonics on PLL systems." IEEE Transactions on Instrumentation and Measurement 62.9 (2013): 2399-2409.

[172] Ciobotaru, Mihai, Remus Teodorescu, and Frede Blaabjerg. "A new single-phase PLL structure based on second order generalized integrator." 2006 37th IEEE Power Electronics Specialists Conference. IEEE, 2006.

[173] Qian, Lewei, David Cartes, and Hui Li. "Experimental verification and comparison of MAFC method and DQ method for selective harmonic detection." IECON 2006-32nd Annual Conference on IEEE Industrial Electronics. IEEE, 2006.

[174] Li, Xiaoqiang, et al. "Decoupled Magnetic Integration of Symmetrical LCL Filter With a Common-Mode Inductor for Single-Phase Grid-Connected Converters." IEEE Journal of Emerging and Selected Topics in Industrial Electronics 3.4 (2021): 966-977.

[175] Gao, Feng, et al. "Indirect dc-link voltage control of two-stage single-phase PV inverter." 2009 IEEE energy conversion congress and exposition. IEEE, 2009.

[176] Kulkarni, Abhijit, and Vinod John. "Mitigation of lower order harmonics in a grid-connected single-phase PV inverter." IEEE transactions on power electronics 28.11 (2013): 5024-5037.

[177] Zhang, Ningyun, Houjun Tang, and Chen Yao. "A systematic method for designing a PR controller and active damping of the LCL filter for single-phase grid-connected PV inverters." *Energies* 7.6 (2014): 3934-3954.

[178] Bao, Chenlei, et al. "Design of injected grid current regulator and capacitor-current-feedback active-damping for LCL-type grid-connected inverter." 2012 IEEE Energy Conversion Congress and Exposition (ECCE). IEEE, 2012.

[179] Kulsangcharoen, Ponggorn, et al. "Experimental evaluation and efficiency optimisation of a grid-connected converter for household energy storage applications." (2014): 1-2.

[180] Hanser, Philip, et al. "The practicality of distributed PV-battery systems to reduce household grid reliance." Utilities Policy 46 (2017): 22-32.

[181] Department of Energy and Climate Change, Smart Metering Implementation Programme, Energy Demand Research Project: Early Smart Meter Trials, 2007– 2010 [computer file]. Colchester, Essex: UK Data Archive [distributor], November 2014. SN: 7591, 2010

[182] Carbon Trust, Micro-CHP Accelerator. Carbon Trust. 2011.

[183] Energy Saving Trust. Measurement of domestic hot water consumption in dwellings; 2008

Appendix A: CREST model demonstration

The CREST (centre for renewable energy system technology) demand model (domestic model) is an open-source software built by Loughborough University. It is an integrated thermal-electrical demand model based on a bottom-up activity-based structure, using stochastic programming techniques to represent dwelling diversity, producing calibrated and validated output at high-resolution, based on reduced-order thermal-electrical networks to represent thermal dynamics, and developed as free open-source software to promote transparency and further research.

Figure A 1 shows the overall architecture of the integrated thermal-electrical demand model. This model contains electrical demand and generation (appliances, lighting, and photovoltaics) and integrates these with an updated occupancy model, a solar thermal collector model, and new thermal models including a low order building thermal model, domestic hot water consumption, thermostat and timer controls and gas boilers. The occupancy model generates stochastic sequences of occupancy for each dwelling, which form a basis for the calculation of appliance, lighting, and water-fixture switch-on events. These are aggregated to determine the dwelling's electricity and hot water demands. The thermal demand model simulates the dwelling's thermal dynamics and gas demands given the climate data, internal heat gains, and dwelling-specific building fabric data. The occupancy, irradiance and external temperature models are the principle means of ensuring the integrated model has appropriately correlated output variables. The integrated model retains several sub-models from the previously published model: the irradiance model, the PV model, and the appliance and lighting models (which are part of the electrical demand

model). While the new model includes more input data than previously, it remains self-contained, and does not require any further data from the user to run.

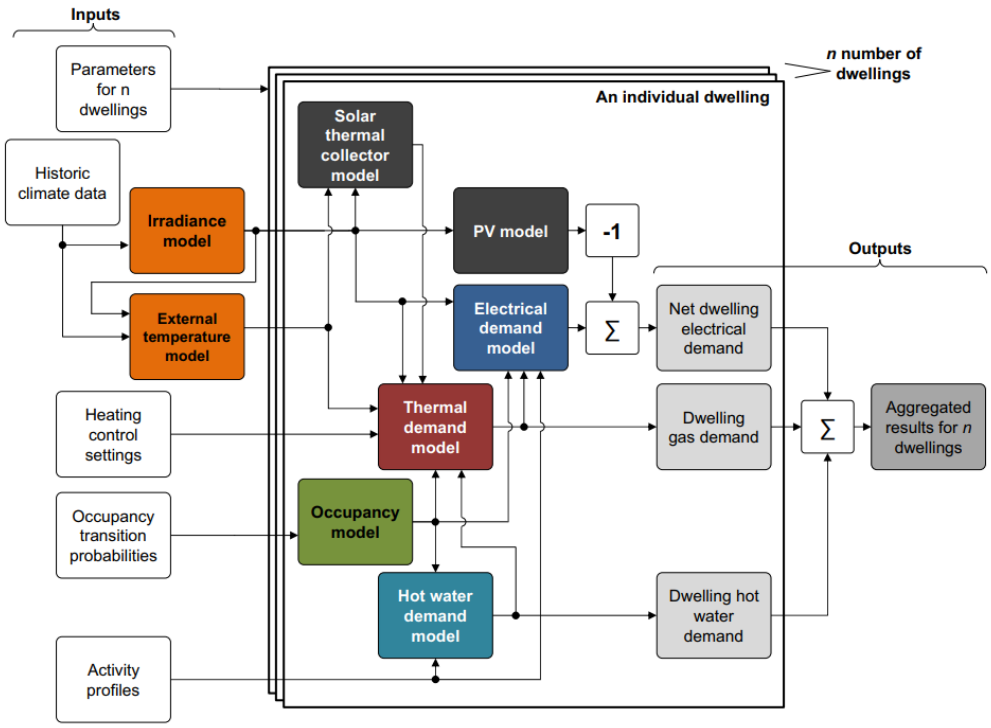

Figure A 1. Overall architecture of the integrated thermal-electrical demand model [125].

Through the definition of date (day of month and weekday or weekend), location (latitude and longitude), as shown in Figure A 2, and the number of occupants, this CREST model (version 2.2) can be used to produce the data profiles needed in this thesis, like the PV generation data profiles, domestic loads consumption data profiles without electric water heater energy consumption, room space temperature profiles, and the hot water consumption profiles.

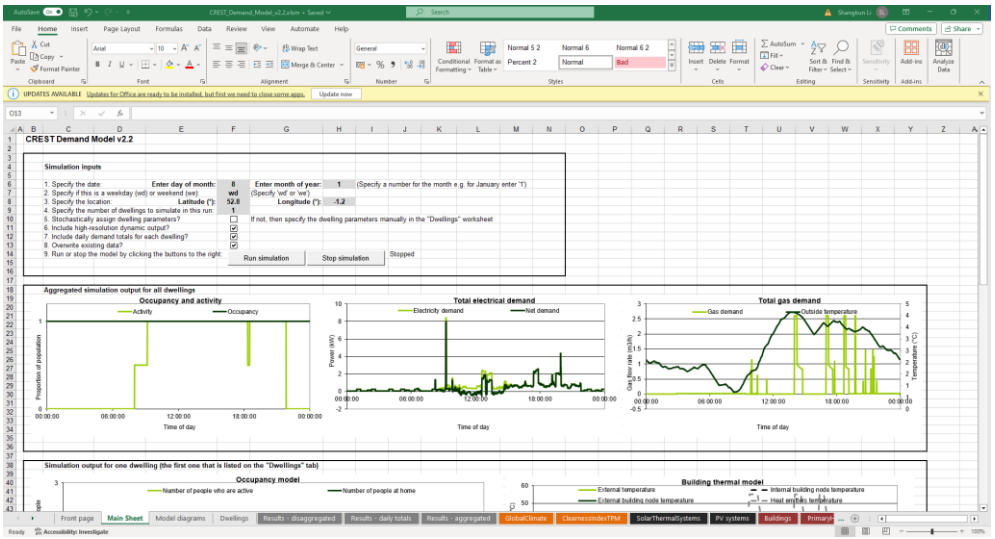

Figure A 2. The main operation window (Excel software) of the CREST model to produce various data profiles.

Lastly, to validate the model, the output of the thermal and hot water sub-models are compared against independent data sets which were not used in their calibration. Simulated gas demands are compared with data from the Energy Demand Research Project Early Smart Meter Trials [181]. and the gas-boiler control group of the Carbon Trust Micro-CHP Accelerator [182]. Hot water demands are compared with the data from the Energy Saving Trust Measurement of Domestic Hot Water Consumption in Dwellings [183].

Appendix B: DSP controlling platform

In this thesis, to control the PV-battery-power electronic water heater power system, a fast and effective control platform is achieved by implementing a Texas Instrument C6713 floating point DSP and the DSP starter kit which, with its on USB port, allows the user to fulfil the specific application and connect the controller to the host computer for development and control purposes.

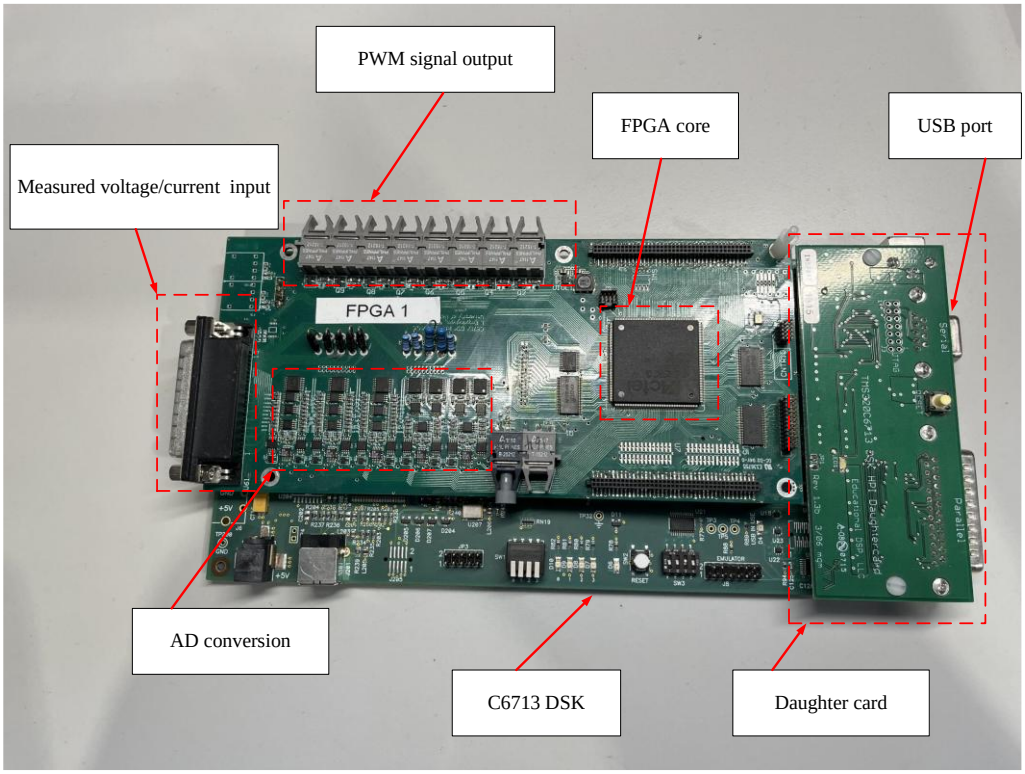

Figure B 1. The DSP controlling platform.

Figure B 1 shows the DSP controller platform which mainly includes C6713 DSK board, FPGA board integrated with AD conversion and PWM generation, and daughter card. The C6713 is a high-speed floating-point processor which runs at 225MHz and can perform up to eight operations per cycle. One of the major advantages of employing the C6713 DSK is linked to its peripherals and the ability to add external peripherals. The FPGA essentially “sits” in the memory map of the 6713DSK. It is connected using the External Memory

Interface (EMIF) of the DSK board. The FPGA is programmed with an interface to the address and data buses of the DSK. Besides, the AD conversion and PWM output ports (optical) are also mounted in the FPGA board. A daughter card is employed in this platform which aims to use the host port interface (HPI) of the C6713 where the HPI port allows a host to access the internal memory of the C6713 without interrupting the central processing unit (CPU) of the DSP. It allows a bi-directional data transfer between the host PC and the DSP and to download sampled variables. Thus, the variables operated in the program can be monitored at real time through the PC in the MATLAB software, as shown in Figure B 2.

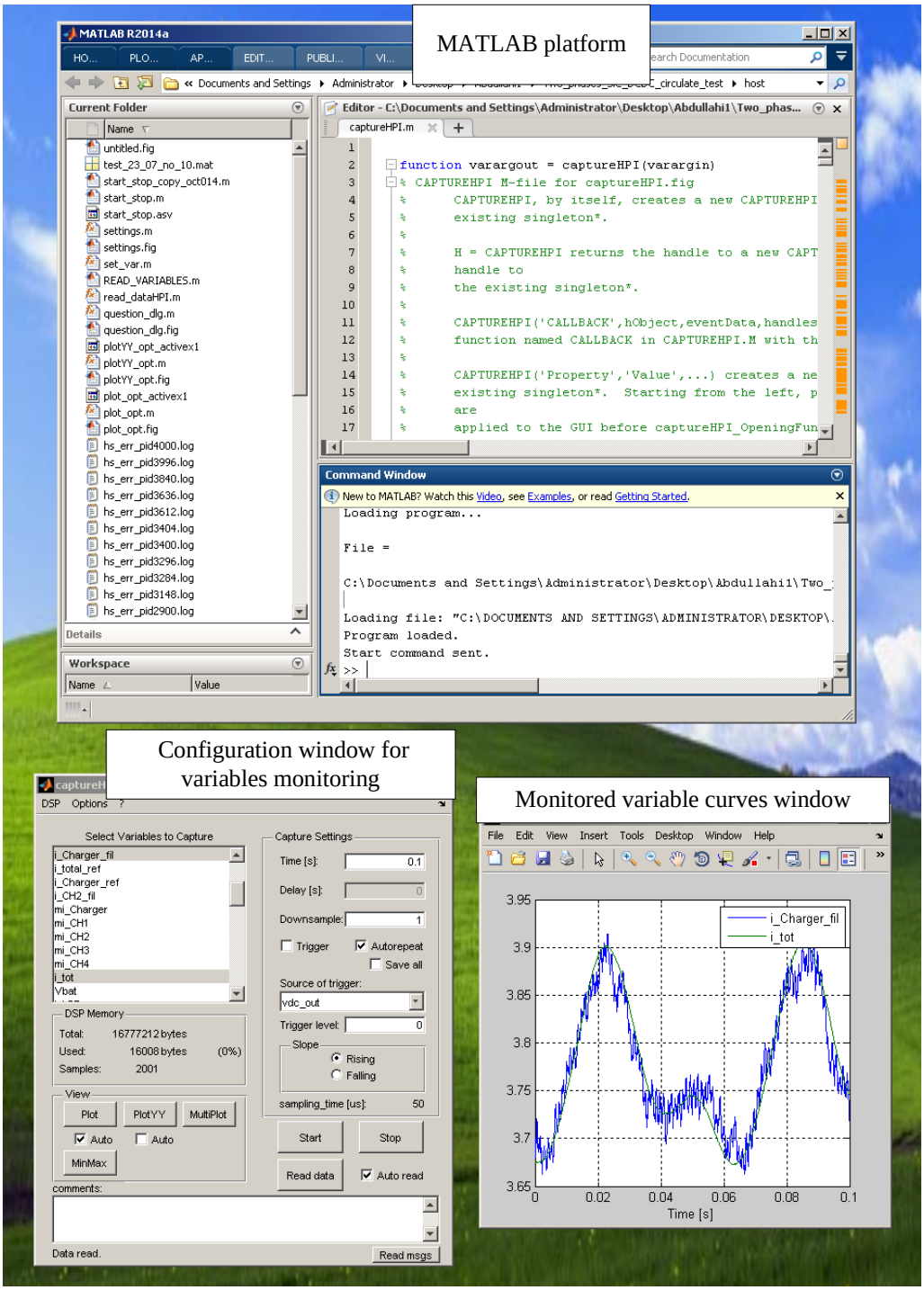

Figure B 2. The MATLAB platform used for monitoring variables at real time.